



**UNIVERSIDAD NACIONAL AUTÓNOMA DE MÉXICO**

**PROGRAMA DE POSGRADO EN CIENCIAS DE LA TIERRA**

**"IMPACTO DE LA VARIABILIDAD DE LA CIRCULACIÓN ATMOSFÉRICA  
EN LA GESTIÓN DEL RECURSO EÓLICO EN MÉXICO"**

**TESIS**

QUE PARA OPTAR POR EL GRADO DE:

**DOCTORA EN CIENCIAS DE LA TIERRA**

PRESENTA:

**Karla Pereyra Castro**

**TUTOR**

Dr. Ernesto dos Santos Caetano Neto (Instituto de Geografía, UNAM)

**MIEMBROS DEL COMITÉ TUTOR**

Dra. Ana Luz Quintanilla Montoya (Facultad de Ingeniería Civil, U. de C.)

Dr. Oscar Martínez Alvarado (National Centre for Atmospheric Science, UK)

**Ciudad Universitaria, CD.MX.**

**Agosto, 2022**



Universidad Nacional  
Autónoma de México



**UNAM – Dirección General de Bibliotecas**  
**Tesis Digitales**  
**Restricciones de uso**

**DERECHOS RESERVADOS ©**  
**PROHIBIDA SU REPRODUCCIÓN TOTAL O PARCIAL**

Todo el material contenido en esta tesis esta protegido por la Ley Federal del Derecho de Autor (LFDA) de los Estados Unidos Mexicanos (México).

El uso de imágenes, fragmentos de videos, y demás material que sea objeto de protección de los derechos de autor, será exclusivamente para fines educativos e informativos y deberá citar la fuente donde la obtuvo mencionando el autor o autores. Cualquier uso distinto como el lucro, reproducción, edición o modificación, será perseguido y sancionado por el respectivo titular de los Derechos de Autor.

Declaro conocer el Código de Ética de la Universidad Nacional Autónoma de México, plasmado en la Legislación Universitaria. Con base en las definiciones de integridad y honestidad ahí especificadas, aseguro mediante mi firma al calce que el presente trabajo es original y enteramente de mi autoría.

Todas las citas de, o referencias a la obra de otros autores aparecen debida y adecuadamente señaladas, así como acreditadas mediante los recursos editoriales convencionales.



Karla Pereyra Castro

## Dedicatoria

*A mi hermosa familia,  
por su amor y compañía.*



## **Agradecimientos**

*A mis padres, por el amor y la compañía en esta etapa de mi vida. Gracias por la comida, los abrazos y las palabras de aliento. Mamá, gracias por confiar en mí y escucharme. Papá, gracias por enseñarme que trabajo y descanso son igualmente necesarios.*

*A mis hermanas, por su amor, por cuidarme desde que era una niña y permitirme ser tan yo... la que dibujaba arañas patonas. Kary, gracias por tu compañía a la distancia, tienes un corazón hermoso y admiro tu bondad. Silvia, gracias por ser mi compañera de estudio, la espectadora de mis bailes y mi porrista personal.*

*A Emmanuel, por brindarme una felicidad que desconocía. Encuentro enorme dicha en ser tu tía y verte sonreír.*

*A Irving (mi compañero en esta gran ciudad), gracias por la paciencia, por apoyarme en cada paso, por escucharme cuando el trabajo agobiaba, por distraerme con comida japonesa...gracias por seguir bailando conmigo...*

*Y en la calle codo a codo somos mucho más que dos.*

*A mi tía Lupe, por tenerme siempre en sus oraciones y reconfortarme con sus palabras.*

*A Gemma, mi amiga de la infancia (apenas ayer), por estar a una llamada o mensaje de distancia aunque pasemos días sin platicar. Tu carácter ha hecho mi vida más ligera y luminosa.*

*A Dolores, por las palabras de aliento. Agradezco que estés aquí para reír juntas de las alegrías y penas de la adultez. Te quiero mucho.*

*A Tania, por ser mi compañera de doctorado, aunque no estuviéramos inscritas en el mismo. Gracias por acompañarme en las buenas y en las malas. Platicar contigo ha sido catártico y reconfortante, desde aquél taller que tomamos en la UV. Las horas de papiroflexia juntas hicieron la pandemia menos estresante.*

*A Rosita, ¿en qué nos quedamos ayer? Gracias por estar ahí cuando hay una crisis. Te quiero. Nuestras pláticas sobre temas académicos me motivan y sin duda fueron clave en la época universitaria.*

*A Ruben, eres un amigo tan querido... agradezco tu escucha y tu inteligencia emocional. Gracias por las palabras adecuadas para incitarme a reflexionar.*

*A Arendy, por enseñarme que la risa es terapéutica, más aún si te ríes de los problemas de la vida. Gracias por escucharme y aceptar pequeñas dosis de abrazos.*

*A Edgar, honorable miembro ovejuno, por presentarme a Arendy jajaja... no es cierto. Gracias por tu disposición a ayudar a los demás.*

*A Dora, Loving, Rayo y Kelly por enseñarme sobre fortaleza y determinación.*

## **Agradecimientos Institucionales**

Al Dr. Ernesto, gracias por ser un asesor dispuesto a escuchar y ayudar, aún con la pandemia siempre estuvo presente y atendió mis dudas. Admiro su inteligencia, gracias por los consejos académicos y de tipo personal.

Al Dr. Óscar Martínez Alvarado, miembro de mi comité tutor, agradezco el tiempo que dedicó a leer mis reportes semestrales y a realizar anotaciones puntuales en los documentos. Las sugerencias o preguntas realizadas ayudaron a mejorar la calidad de este trabajo.

A la Dra. Ana Luz Quintanilla Montoya, miembro del comité tutor, gracias por las recomendaciones generales sobre cómo estructurar el trabajo de investigación. También le agradezco la cordialidad y carisma para comunicarse conmigo.

A los sinodales, Dra. Rosmeri Porfirio Da Rocha, Dra. Michelle Simoes Reboita, Dr. Juan Cervantes Pérez y Dr. Juan Matías Méndez Pérez, por su cordialidad y el tiempo dedicado a la revisión de este documento. Las sugerencias indicadas mejoraron este trabajo.

Al Ing. Gustavo Vázquez Cruz por su apoyo en la resolución de problemas técnicos.

A la Dra. Christian Domínguez Sarmiento por la oportunidad de ser su ayudante en la asignatura de Simulación y Pronósticos Climáticos, lo que enriqueció mi formación profesional. Fuiste una excelente mentora para aprender a dar clases.

A la Universidad Nacional Autónoma de México (UNAM), por brindarme la oportunidad de una educación integral. Aquí aprendí sobre Ciencias Atmosféricas, danza, yoga, cultura, inglés y pedagogía.

Al Posgrado en Ciencias de la Tierra (PCT), por el apoyo económico para asistir a congresos. Particularmente a su coordinadora, Dra. Christina Siebe, por estar al pendiente de los estudiantes aún cuando la pandemia llegó.

Al personal administrativo del PCT (en especial a Araceli Chamán) por su paciencia, amabilidad y disposición para solucionar dudas o facilitar trámites.

Al Instituto de Geografía, por brindarme espacio en el cubículo de estudiantes de Geografía Física para desempeñar mi investigación.

Al Consejo Nacional de Ciencias y Tecnología (CONACyT) por otorgarme la beca número 473276 para realizar mis estudios de doctorado.

# ÍNDICE

DEDICATORIA.....	III
AGRADECIMIENTOS.....	IV
AGRADECIMIENTOS INSTITUCIONALES .....	V
RESUMEN .....	1
ABSTRACT.....	3
CAPÍTULO 1. INTRODUCCIÓN.....	5
ESTADO ACTUAL DE LAS ENERGÍAS RENOVABLES EN EL MUNDO .....	6
ESTADO ACTUAL DE LAS ENERGÍAS RENOVABLES EN MÉXICO .....	7
ANTECEDENTES .....	8
CAPÍTULO 2. DATOS Y MÉTODO .....	18
DATOS.....	18
MODELOS METEOROLÓGICOS.....	19
MÉTODO .....	21
CAPÍTULO 3. CARACTERIZACIÓN Y PRONÓSTICO DE RAMPAS DE POTENCIA EÓLICA EN LOS MODELOS OPERATIVOS NAM Y RAP .....	25
CAPÍTULO 4. SENSIBILIDAD DEL PRONÓSTICO DE VIENTO A LA PARAMETRIZACIÓN DE CAPA LÍMITE EN EL MODELO WEATHER RESEARCH AND FORECASTING (WRF).....	50
CAPÍTULO 5. CARACTERIZACIÓN DE RAMPAS DE VIENTO Y CORRECCIÓN ESTADÍSTICA DEL SESGO EN EL MODELO NAM .....	68
CAPÍTULO 6. CONCLUSIONES Y TRABAJO FUTURO .....	87
REFERENCIAS .....	93
ANEXO 1. MATERIAL SUPLEMENTARIO DEL CAPÍTULO 3.....	100
ANEXO 2. MATERIAL SUPLEMENTARIO DEL CAPÍTULO 4 .....	107
ANEXO 3. MATERIAL SUPLEMENTARIO DEL CAPÍTULO 5 .....	116

## Resumen

La decarbonización del sector eléctrico es un objetivo primordial para reducir las emisiones de dióxido de carbono y su efecto en el cambio climático. Sin embargo, el crecimiento de las instalaciones de energía renovable conduce a una mayor incertidumbre en la generación de electricidad derivada de la variabilidad de la circulación atmosférica. La caracterización y el pronóstico de las variaciones del recurso eólico pueden servir como herramientas para el manejo de los parques eólicos.

En este estudio se evaluó el efecto de la variabilidad del viento, rampas de potencia y eventos de generación de potencia eólica sobre el recurso eólico en el norte de México con 14 estaciones meteorológicas del Servicio Meteorológico Nacional (SMN). Se identificaron cuatro regiones impulsadas por la estacionalidad de los sistemas meteorológicos. En el área del Altiplano Mexicano, los vientos son modulados por sistemas frontales en invierno y circulaciones locales en verano, donde la topografía es el principal forzante. En el noreste de México, los sistemas frontales producen vientos intensos en invierno, mientras que el verano se caracteriza por vientos alisios moderados. En tanto, la compleja orografía de la Península de Baja California potencia la brisa marina en verano y una importante señal frontal durante el invierno. El área del Golfo de California experimenta vientos persistentes del norte durante el invierno, lo que provoca una canalización del flujo. En verano, la característica principal es la inversión de los vientos. Las regiones del Altiplano y Península de Baja California tienen mayor dispersión de viento y mayor frecuencia de eventos de rampa que las otras regiones. Cabe destacar que los frentes fríos producen rampas de potencia y eventos persistentes de alta generación de potencia eólica en invierno, mientras que los sistemas convectivos de mesoescala y las circulaciones locales las generan en el verano.

También se examinó el papel de los sistemas meteorológicos en el desempeño de los sistemas de pronóstico North American Mesoscale System (NAM) y Rapid Refresh (RAP) para 2013. Ambos modelos muestran buena habilidad. Sin embargo, presentan deficiencias sobre una topografía compleja, subestimando los vientos intensos y sobreestimando los vientos débiles. La variabilidad del viento pronosticada es más suave que la observada debido a las discretizaciones espaciales y temporales, lo que produce eventos de generación de potencia eólica de larga duración.

Ante la complejidad del terreno de la Península de Baja California se examinó la sensibilidad del pronóstico de viento al esquema de capa límite planetaria (PBL) para un mes de verano (junio 2013) e invierno (enero 2013) con 7 estaciones meteorológicas del SMN. La evaluación determinista de la velocidad del viento en superficie se realizó para simulaciones de 24 h con el modelo Weather Research and Forecasting (WRF). La configuración del modelo incluyó 31 niveles verticales (6 en los primeros 120 m) y 4 km de resolución horizontal. Las parametrizaciones de PBL evaluadas fueron: Yonsei University (YSU), Mellor-Yamada-Janjic (MYJ) y el Modelo Convectivo Asimétrico versión 2 (ACM2, por sus siglas en inglés). Los esquemas PBL se evaluaron utilizando el diagrama de Taylor, el Índice de Acierto del Error Absoluto Medio (MAESS, por sus siglas en inglés) y la anomalía estandarizada del Error Absoluto Medio. La predicción de rampas de viento se verificó en términos de magnitud, frecuencia y duración. El esquema YSU mejoró la precisión del pronóstico en invierno

para la mayoría de las estaciones meteorológicas. Mientras, la habilidad de los esquemas PBL varía según el entorno fisiográfico de la estación meteorológica en verano.

La última parte de este estudio consta de la caracterización de rampas extremas de viento y el post-procesamiento estadístico de NAM. Una rampa extrema es aquella que excede cuatro veces la desviación estandarizada de rampas de viento. Las rampas extremas de viento se atribuyeron a un sistema atmosférico, se contabilizó la duración de la rampa y la persistencia de vientos extremos. Los frentes fríos, suradas y Nortes contribuyen principalmente a la generación de rampas extremas de viento en el invierno. Los vientos intensos asociados a dichos sistemas persisten hasta 40 horas en promedio. En tanto que en el verano, las tormentas originan rampas extremas con duración de 1 a 3 horas, debido a las corrientes descendentes. Por otra parte, el efecto de la corrección de sesgo sobre las simulaciones del modelo NAM en 2016 fue probada para dos estaciones meteorológicas. Los métodos utilizados fueron: corrección de sesgo simple y el mapeo de cuantiles. El ajuste estadístico disminuyó el exceso de eventos de no-rampa pronosticado por el modelo NAM y mejoró la predicción de rampas según los índices derivados de las tablas de contingencia.

## Abstract

Decarbonization of the electricity sector is a primary objective to reduce carbon dioxide emissions and their effect on climate change. However, the growth of renewable energy installations leads to greater uncertainty related to the variability of the atmospheric circulation. Characterization and forecasting of wind resource variations can be tools for wind farm management. In this study, the effect of wind variability, wind ramps, and wind power generation events on the wind resource was assessed for northern Mexico, with 14 meteorological stations of the National Meteorological Service.

Four regions driven by weather systems seasonality were identified. The study reveals that in the Plateau area winds are modulated by frontal systems in winter and local circulations in summer, where the topography is the main forcing. In Northeastern Mexico, the frontal systems produce intense winds in winter, while moderate trade winds characterize the summer. Meanwhile, the complex terrain of the Baja California Peninsula enhances the sea breeze in summer and a significant frontal signal during winter. The Gulf of California area experiences persistent northerly wind during winter causing flow channeling. In summer, the main feature is the inversion of winds. Importantly, Plateau and Baja California Peninsula regions have greater wind dispersion than the other regions, which can be wind power ramps indicator. The analysis showed that cold fronts produce wind power ramps and persistent generating events in winter, while mesoscale convective systems and local circulations generate them in summer.

The role of weather systems in the performance of the North American Mesoscale System (NAM) and Rapid Refresh (RAP) forecast systems for 2013 was also examined. Both models show good skill. However, they have deficiencies over complex topography, underestimating strong winds and overestimating weak winds. In addition, the forecast wind variability is smoother than observations due to spatial and temporal averaging effects, producing long lasting wind power generation events.

Given the complexity of the terrain of the Baja California Peninsula, the sensitivity of the wind forecast to the planetary boundary layer (PBL) scheme was examined for a summer (June 2013) and a winter (January 2013) month with 7 SMN meteorological stations. The deterministic evaluation of the surface wind speed was done for 24 h simulations with the Weather Research and Forecasting (WRF) model. Model configuration had 31 vertical levels (6 levels below 120 m) and 4 km of horizontal resolution. PBL parameterizations evaluated were Yonsei University (YSU), Mellor-Yamada-Janjic (MYJ), and Asymmetric Convective Model version 2 (ACM2). PBL schemes were evaluated using the Taylor diagram, the Mean Absolute Error Skill Score (MAESS), and the standardized anomaly of Mean Absolute Error (z-score). Moreover, wind ramp prediction was verified in terms of magnitude, frequency, and duration. The results show that YSU scheme improved forecast accuracy in winter for most weather stations. Meanwhile, the ability of PBL schemes varied depending on the physiographic environment of the weather station in summer.

The last part of this study constitutes a characterization of extreme wind ramps and the statistical post-processing of NAM. An extreme ramp was defined as one exceeding four times the standard deviation of wind ramps. Extreme ramps were attributed to an atmospheric system. The analysis showed that cold fronts, Suradas and Nortes contribute mainly to the generation of extreme wind ramps in winter. Intense winds associated with these systems persist up to 40 hours on average in La Venta. Whilst in summer, storms cause extreme ramps lasting from 1 to 3 hours, due to downdrafts. Otherwise, bias correction effect on NAM model simulations on 2016 was tested for two weather stations. The methods used were simple bias correction and quantile mapping. The statistical adjustment decreased the excess of non-ramp events predicted by the NAM model and improved the prediction of ramps, according to the indices derived from the contingency tables.

## Capítulo 1. Introducción

Desde la Revolución Industrial, los procesos industriales se desarrollan utilizando combustibles fósiles. En un inicio el carbón alimentó la máquina de vapor, considerándose el principal combustible de la época. A mediados del siglo XX, el petróleo se convirtió en la materia prima para generación de electricidad debido a su bajo costo. Además, el petróleo y el gas se desempeñaron como fuentes energéticas para el motor de combustión interna. Actualmente, la demanda energética mundial continúa creciendo y se satisface esencialmente con combustibles fósiles como el petróleo, gas y carbón (BP, 2021; Ember, 2022). La emisión de gases de efecto invernadero derivado de actividades antropogénicas, incluida la generación de electricidad, ha producido un incremento de la concentración de dióxido de carbono respecto a períodos preindustriales que contribuyen al Cambio Climático Global (Allen *et al.*, 2019).

El actual modelo energético está basado principalmente en recursos finitos y carece de elementos básicos que garanticen la sostenibilidad del sector energético. Si un país importa combustibles para cubrir sus necesidades energéticas, será dependiente de los tratos comerciales y el suministro energético puede interrumpirse bajo situaciones políticas tensas. Una economía basada en este modelo conduce a la incertidumbre de la disponibilidad de energía y de sus precios a largo plazo. Otra desventaja de dicho modelo es el impacto considerable al entorno derivado de la producción y el consumo de energía (Aste *et al.*, 2019).

La preocupación por el Cambio Climático Global ocasionado por el incremento de los gases de efecto invernadero ha incentivado a varios países a realizar una transición energética hacia un modelo energético sostenible. La decarbonización del sector eléctrico, con predominio de fuentes de energía renovables, es uno de los pilares para un futuro energético sostenible (Aste *et al.*, 2019). El crecimiento de la energía solar y eólica puede originar que el porcentaje de generación de electricidad por fuentes renovables pase de 25% en 2017 al 85% en 2050 (IRENA, 2019). Esta transformación requiere nuevos enfoques en la planificación de la red eléctrica, las operaciones en sistemas y mercados y nuevas políticas públicas que prioricen la instalación de capacidades renovables (IRENA, 2019). Cabe destacar que este es uno de los objetivos prioritarios de desarrollo sostenible de la Organización de las Naciones Unidas (Aste *et al.*, 2019)

El crecimiento de instalaciones de energía renovable, particularmente eólica y solar, incrementa la exposición del sector energético al estado del tiempo y al clima (Deakin *et al.*, 2021). Por lo tanto, la cuantificación del riesgo meteorológico y climático en varias escalas temporales es relevante para garantizar una transición rápida y segura hacia un modelo energético con mayor participación de energías renovables.



### *Estado actual de las energías renovables en el mundo*

En 2020, la contribución de los combustibles fósiles a la generación de electricidad en el mundo fue de 61%, con una reducción del 4.7% respecto al año 2015 (Max y Ortíz-Ospina, 2022). El portafolio energético renovable generó el 16.85% de electricidad en centrales hidroeléctricas, el 5.47% en parques eólicos y el 2.72% en centrales solares. Las plantas nucleares contribuyeron al 10.12% de generación de electricidad (Max y Ortíz-Ospina, 2022).

Según cifras de la Agencia Internacional de Energías Renovables (IRENA, por sus siglas en inglés), a nivel mundial la capacidad instalada con energías renovables en 2020 fue de 2799.1 GW (IRENA, 2021). Las regiones con mayor participación de energías renovables son Asia (45.9% de la capacidad mundial) y Europa (21.7% de la capacidad mundial), mientras que la región con menor participación es Centroamérica y el Caribe (con 0.6% de la capacidad mundial) (IRENA, 2021). Por tipo de tecnología, la energía hidráulica concentró el 43.2% del total de capacidad mundial, seguido de la energía eólica con 26.2%, la energía solar con 25.5%, la bioenergía con 4.5 % y el restante 0.6% se atribuye a tecnologías con energía geotérmica y marina (IRENA, 2021).

En América Latina y el Caribe, gracias a la diversidad energética con la que cuenta, existe uno de los mercados de energía renovables más dinámicos del mundo (IRENA, 2020). Al cierre del 2020, la capacidad de generación por energías renovables fue 44.7 GW, de la cual la energía hidráulica representó la mayor participación del total regional con una capacidad instalada de 20.9 GW (IRENA, 2021) proveniente de grandes plantas mayores a 10 MW (Sawin *et al.*, 2016).

En esta región, algunos países han logrado generar altos porcentajes de electricidad desde fuentes renovables. Por ejemplo, Costa Rica generó el 98% de su electricidad con fuentes renovables en el primer trimestre de 2017. El agua, el viento y la geotermia son las fuentes principales de la matriz eléctrica nacional (EFE, 2017). Brasil ocupa el segundo lugar para nuevas plantas hidroeléctricas y el cuarto en capacidades eólicas, aunque su red eléctrica no ha permitido aprovechar el total de la energía eólica generada (Sawin *et al.*, 2016).

Los países con menor consumo per cápita de electricidad pueden diseñar una matriz energética con mayor participación de energías renovables. Sin embargo, cabe resaltar que si el consumo energético continúa aumentando, será difícil decarbonizar el sector eléctrico. Por ello los usuarios necesitan cambiar hábitos y hacer uso eficiente de la electricidad.

### *Estado actual de las energías renovables en México*

En México la energía eléctrica aún se genera en su mayoría a partir de combustibles fósiles (75.2%)(Max y Ortíz-Ospina, 2022). Las fuentes limpias aportan el 24.8% de la electricidad en el país, de las cuales, la energía hidroeléctrica constituye la principal fuente renovable (8.77%), seguida de la energía eólica (6.36%) y solar (3.42%)(IRENA, 2021). Las centrales nucleoelectricas aportaron el 7.26% de la electricidad generada en 2021.

En el país la generación eléctrica a partir de fuentes renovables, con excepción de las grandes centrales hidroeléctricas y geotérmicas, sigue limitada a pesar del potencial eólico disponible en el territorio. No obstante, la energía eólica fue añadida como una de las alternativas más factibles a corto y medio plazo (SENER, 2015). En el Programa de Desarrollo Eléctrico Nacional 2020-2034 (Centro Nacional de Control de Energía, 2021), se menciona la necesidad de cumplir con los compromisos internacionales en relación con el cambio climático y la reducción de emisiones mediante el incremento de la generación eléctrica con energías limpias. A partir del año 2012, la generación eólica mostró un crecimiento anual promedio de un 76.5%, con adiciones anuales en capacidad superiores a los 2,000 MW (SENER, 2015). De acuerdo con el PRODESEN, México ha establecido una meta del 35% de participación mínima de energías limpias para 2024 (SENER, 2015). Desafortunadamente, en los últimos años el crecimiento de capacidades renovables no ha sido el esperado.

La energía eólica exhibe una generación intermitente de electricidad dependiente de las condiciones atmosféricas. Los cambios grandes y abruptos en la rapidez del viento pueden derivar en cambios abruptos en la generación, lo que representa un riesgo para la estabilidad de la red eléctrica (Lacerda, Couto, y Estanqueiro, 2017). Los períodos de baja generación también pueden ocasionar problemas para la red eléctrica, particularmente cuando hay una limitada energía de reserva. Además, la diversificación de la matriz eléctrica con fuentes renovables implica un desafío en el balance de la oferta y demanda de electricidad. El mal manejo de las variaciones de viento y/o potencia puede incrementar el costo de producción de electricidad. En consecuencia, una adecuada caracterización del potencial eólico, requiere una caracterización de las fluctuaciones estacionales y diurnas que conduzca a un manejo eficiente de los parques eólicos.

Una variación grande en la generación eólica de una turbina en períodos cortos (hasta unas pocas horas) se denomina rampa de potencia. Los eventos de rampa pueden afectar el flujo de energía y el voltaje de la red eléctrica, propiciando daños en los equipos, inestabilidad y posibles apagones (Aguilar, 2019). Los operadores del sistema necesitan adquirir suficientes reservas operativas para contrarrestar la variabilidad e incertidumbre en el consumo de electricidad. La identificación de los fenómenos meteorológicos que

producen las rampas de potencia o las rampas de viento en una región aportan información sobre las principales características de las variaciones de la energía eólica. Por ejemplo, las rampas asociadas a tormentas son generalmente de corta duración comparadas con las ocasionadas por un frente frío (Pichault, Vincent, Skidmore, y Monty, 2021). Esta información es útil en la planificación del aprovechamiento del recurso eólico.

Una de las claves para gestionar con éxito la energía eólica es pronosticar con precisión la cantidad esperada de energía eólica suministrada a la red eléctrica. El conocimiento de los procesos atmosféricos relacionados a rampas permite identificar los refinamientos necesarios en la configuración de los modelos meteorológicos, con la finalidad de anticipar con mayor precisión dichos eventos. Un sistema de pronóstico regionalizado para los parques eólicos puede ayudar a mitigar los problemas de la inestabilidad de la red eléctrica y las pérdidas económicas asociadas.

#### *Antecedentes*

La electricidad a partir de la energía eólica se genera mediante turbinas eólicas que aprovechan la energía cinética del viento. La potencia eólica es proporcional al cubo de la velocidad del viento y al área de barrido de las palas del aerogenerador, por ello, la cantidad de energía que un aerogenerador puede transformar en electricidad es sensible a las variaciones en la rapidez del viento. La producción real de electricidad depende del diseño del aerogenerador, así que cada equipo cuenta con una curva de potencia. Un aerogenerador opera a su potencia nominal, cuando alcanza la máxima cantidad de potencia eléctrica para la que fue diseñado. En dicho momento, aunque se incremente la rapidez del viento, no se presenta un cambio en la generación eólica. Las fluctuaciones en la generación eólica suelen caracterizarse considerando la potencia nominal de la turbina eólica.

La red eléctrica actual es capaz de manejar pequeñas cantidades de incertidumbre y variabilidad, pero los eventos de rampa son una preocupación crítica para el sistema con alta penetración de energía eólica (Zhang *et al.*, 2017). La necesidad de integrar eficientemente la energía eólica al sistema eléctrico ha despertado el interés por la caracterización y pronóstico de los eventos de rampa.

Una rampa ocurre cuando hay un cambio en la potencia o en la magnitud del viento que excede un umbral dado en un rango de tiempo determinado. En la literatura se encuentra múltiples definiciones de rampa (Tabla 1) porque el umbral en el ésta es importante varía según el usuario (Bianco *et al.*, 2016), es decir, cada parque eólico puede definir la magnitud y duración del evento.

Tabla 1. Definiciones binarias de rampas (de potencia eólica y viento) encontradas en la literatura (Actualizada de Gallego-Castillo, Cuerva-Tejero, y Lopez-Garcia (2015)).  $P_R$  es la potencia nominal del caso de estudio

<b>Autor</b>	<b>Variación de potencia</b>	<b>Duración</b>	<b>Tamaño del caso de estudio</b>	<b>Comentarios</b>
Cutler <i>et al.</i> (2007)	75% $P_R$	3 h	65 MW	Resolución horaria
Cutler <i>et al.</i> (2007)	65% $P_R$	1 h	65 MW	Resolución cada 10 minutos
Freedman <i>et al.</i> (2008)	200 MW	30 min	~ 1GW	
Truewind (2008)	20% $P_R$	1 h	No especifica	Umbral para rampa ascendente
Truewind (2008)	15% $P_R$	1 h	No especifica	Umbral para rampa descendente
Potter <i>et al.</i> , (2009)	10% $P_R$	1 h	~ 1GW	
Bradford <i>et al.</i> (2010)	20% $P_R$	1 h	No especifica	Parque eólico
Kamath (2010)	10 - 12% $P_R$	30 min	~ 1GW	
Kamath (2010)	15 - 20% $P_R$	1 h	~ 1GW	
Cutler (2011)	200 MW	30 min	868 MW	
Cutler (2011)	150 MW	5 min	868 MW	
Cutler (2011)	150 MW	30 min	286 MW	
Cutler (2011)	75 MW	30 min	140 MW	
Bossavy <i>et al.</i> (2012)	30%	No aplica	8 MW	
Gan y Ke (2014)	40%	No aplica	No especifica	Rampa ascendente
Gan y Ke (2014)	30%	No aplica	No especifica	Rampa descendente
Sherry y Rival (2015)	20% $P_R$ , 15% $P_R$	1 h	1471 MW	Rampa ascendente y rampa descendente
(Sherry y Rival, 2015)	$\geq 50\%$ $P_R$	$\leq 4$ h	1471 MW	Rampa ascendente y rampa descendente
Deppe, Gallus, y Takle (2013)	$\geq 50\%$ $P_R$	$\leq 4$ h		
Deppe <i>et al.</i> (2013)	> 3 m/s	4 h o 2 h		La variación debe estar contenida en el rango de 6 a 12 m/s
Lacerda <i>et al.</i> (2017)	33%/6 and 67% $P_R$	6 h		Rampas ascendentes
Lacerda <i>et al.</i> (2017)	-35% and -56%	6 h		Rampas descendentes
Ohba, Kadokura, y Nohara (2016)	$\geq 30\%$ $P_R$	$\leq 6$ h		Rampas ascendentes y rampas descendentes
Aguilar (2019)	2000 MW	1 h		
Aguilar (2019)	$\pm 3 \sigma$	1 h		Frecuencia acumulada
Aguilar (2019)	$\pm 3 \sigma$	1 h		Años individuales

La aplicación de múltiples criterios a la identificación de rampas revela la sensibilidad de las mismas al umbral establecido. Por ello Zhang *et al.* (2017) sugiere la creación de múltiples estrategias para afrontar las diversas rampas de potencia eólica. Bianco *et al.* (2016) diseñaron una herramienta para evaluar la habilidad de los modelos de mesoescala en el pronóstico de rampas de potencia de amplitudes y duraciones variables. La flexibilidad del criterio de rampa permite que sea útil para diversos usuarios.

La comprensión de los fenómenos meteorológicos causantes de eventos de rampa es útil para el diseño de sistemas de pronósticos regionalizados. En algunos parques eólicos, los efectos locales derivados de la rugosidad del terreno, la topografía o las interacciones mar-tierra resultan relevantes en las fluctuaciones eólicas. Varios autores han estudiado el papel de los fenómenos atmosféricos en la generación de rampas de potencia y/o rampas de viento.

En verano, las rampas son ocasionadas por sistemas de mesoescala como: frentes de brisa, tormentas convectivas, ciclones tropicales, flujos catabáticos, entre otros. Deppe *et al.* (2013) encontraron que entre el 12% y el 17% de los eventos que analizaron fueron producidos por tormentas. Pichault *et al.* (2021) exploraron la precipitación no asociada con frentes fríos. Ellos mostraron que las variaciones en la rapidez del viento pueden estar asociados con procesos como corrientes descendentes, circulaciones de mesoescala o microrráfagas. Dicho trabajo ilustra dos casos de estudio de rampas relacionadas con actividad convectiva.

Por otra parte, Sherry y Rival (2015) hallaron que las rampas grandes de potencia eólica (50% de cambio en la potencia en 4 h) ocurrieron durante vientos Föhn en Alberta, Canada en el 50% de los eventos detectados. Los parámetros subjetivos para detectar los eventos Föhn fueron: vientos del suroeste o noroeste, rapidez del viento  $\geq 4.5$  m/s, un rápido incremento de la temperatura y una marcada disminución en la humedad relativa. Dichos cambios deben ocurrir de Octubre a Marzo, la época de los vientos Föhn o Chinook. En esa misma línea, Liu, Qian, y Berg (2022) analizaron un caso de estudio de rampa de viento debida a gradientes térmicos locales en un parque eólico de la cuenca de Columbia. La aceleración del viento por efectos térmicos ocurrió en la tarde, excediendo los 12 m/s en la noche, a la altura del rotor (Liu *et al.*, 2022).

Cutler, Kay, Jacka, y Nielsen (2007) analizaron los principales fenómenos que originan grandes rampas de potencia en la costa suroeste de Tasmania. En esta región los fenómenos de gran escala como las bajas presiones y los frentes produjeron cambios abruptos en la generación eólica. Cutler *et al.* (2007) analizaron las cartas de presión media al nivel del mar para seguir las trayectorias de frentes y vaguadas.

De forma similar, Freedman, Markus, y Penc (2008) examinaron la información meteorológica disponible y categorizaron los eventos de rampa según el fenómeno que lo originó. Freedman *et al.* (2008) encontraron para la región de Electric Reliability Council of Texas (ERCOT) que los frentes fríos provocaron la mayoría de las rampas de potencia ascendentes en la temporada invernal. Asimismo, Ohba *et al.* (2016) aplicaron mapas auto organizados en Japón para entender los impactos de sistemas de escala sinóptica en las rampas de potencia. Las rampas ascendentes se deben principalmente a ciclones extratropicales que se aproximan desde el este o el oeste hacia la región, mientras que las rampas descendentes se derivan de una reducción zonal o meridional de los gradientes de presión. Los efectos de sistemas de latitudes medias en la generación eléctrica para otras regiones del mundo han sido estudiados por Deppe *et al.* (2013) y Pichault *et al.* (2021).

Los sistemas sinópticos suelen dominar el estado del tiempo en invierno y son pronosticados con días de antelación con buena precisión. En verano, los efectos locales como el calentamiento diferencial de los valles y montañas o de la superficie oceánica y continental genera circulaciones térmicas que modulan el estado del tiempo. Además la humedad del suelo y la inestabilidad de la atmósfera contribuyen al desarrollo de lluvias dispersas y tormentas (Dolores, Caetano, López-Bravo, y Calheiros, 2019; López-Bravo, Caetano, y Magaña, 2018). Los fenómenos típicos de verano son más difíciles de predecir debido a su corta duración y su alta sensibilidad a las perturbaciones de ciertas variables como la mezcla turbulenta. Éstos presentan una interacción importante con la topografía, la humedad del suelo, la cobertura del suelo, entre otros.

La predicción de la generación eólica es un problema para el sector eléctrico. El modelo de mesoescala Weather Research and Forecasting (WRF, por sus siglas en inglés; Skamarock *et al.*, 2008) ha sido utilizado en diversos trabajos para simular el potencial eólico (Carvalho, Rocha, Gómez-Gesteira, y Silva Santos, 2014; Hu, Nielsen-Gammon, y Zhang, 2010; Mattar y Borvarán, 2016). En varios de ellos se han realizado pruebas de sensibilidad de las parametrizaciones de capa límite planetaria (PBL, por sus siglas en inglés) y capa superficial (SL, por sus siglas en inglés). El desempeño de estos esquemas de parametrización física depende en gran medida del área geográfica y el período bajo análisis (Tabla 2). Los resultados son diferentes para una simulación centrada en un período de verano/invierno o en un episodio meteorológico específico, debido a las diferentes condiciones atmosféricas y de estabilidad. La simulación del viento en la superficie sobre un terreno complejo es un desafío en el modelado regional. Por lo tanto, se han realizado estudios con el objetivo de identificar una configuración física del modelo WRF que minimice los errores sistemáticos de los vientos en superficie en las simulaciones.

Tabla 2. Experimentos de sensibilidad al esquema de capa límite planetaria (PBL) en el modelo WRF para fines de potencial eólico. CI: Condiciones Iniciales, \*con un factor de orografía no resuelta

Región	Configuración	Temporada	Parametrizaciones	Autor
Costas del mar mediterráneo (offshore)	CI: NCEP, ERA-INTERIM, ERA-40 40 niveles híbridos (7 niveles debajo de los 1000 m) Resolución: 15 km	Octubre a diciembre de 2001	12 configuraciones del modelo PBL probadas: ACM2, YSU, MYJ PBL con mejor desempeño: YSU	(Menendez <i>et al.</i> , 2014)
Sur del Mar del Norte	CI: ERA-INTERIM Niveles: 67 niveles verticales (niveles cada 20 m entre 0 y 200 m) Resolución: 27 km, 9 km y 3 km	Un año (2005)	PBL probadas: YSU, ACM2, MYJ, MYJNN, QNSE PBL con mejor desempeño: ACM2 (atmósfera muy inestable), MYJ (atmósfera estable), QNSE (atmósfera inestable)	(Krogsæter y Reuder, 2015)
Península Ibérica (onshore y offshore)	CI: ERA-INTERIM Niveles: 27 niveles Resolución: 25 km, 5 km (dominio anidado)	Un año (2008)	PBL probadas: YSU, MYJ, ACM2, QNSE, MYNN2.5 SL probadas: MM5, ETA, PX, QNSE, MYNN PBL con mejor desempeño: ACM2-PX (estación cálida) y YSU-MM5 (resto del año)	(D. Carvalho <i>et al.</i> , 2014; Jaramillo y Borja, 2004)
Andalucía (sur de España)	CI: ERA-INTERIM Resolución: 9 km, 3 km, 1 km 36 niveles verticales (niveles más bajos: 4,18,43,64,73 m)	Períodos seleccionados de 2005: 2-5 febrero 9-12 de abril 28-31 agosto 7-10 octubre	PBL probadas: MYJNN, YSU PBL con mejor desempeño: YSU	(Santos-Alamillos, Zquez, Ruiz-Arias, Lara-Fanego, y Tovar-Pescador, 2013)
Suiza	CI: ERA-INTERIM Resolución: 54 km, 18 km, 6 km, 2 km 40 niveles verticales (3 a 7 niveles en la PBL)	24 tormentas de viento históricas entre 1990 y 2010	PBL: YSU, MYJ, ACM2, YSU* PBL mejor desempeño: YSU*	(Gómez-Navarro, Raible, y Dierer, 2015)
Sur de Italia	CI: GFS Resolución: 1 km 41 niveles verticales (11 niveles por debajo de 1 km)	7-9 octubre de 2014	PBL: ACM2, MRF, YSU PBL: no se determinó mejor esquema de PBL	(Tyagi <i>et al.</i> , 2018)
Kaiga, India	CI: FNL Resolución: 9 km, 3 km, 1 km 36, 41, 49 y 53 niveles verticales	4-16 abril 2013, 30 noviembre-12 diciembre 2013, y 11-23 julio 2013	PBL: YSU, ACM2, MYJ, Boulac, MYNN3 PBL con mejor desempeño: YSU*	(Aravind <i>et al.</i> , 2022)

Los estudios mencionados anteriormente se enfocan en una evaluación determinista del pronóstico del viento. Sin embargo, el pronóstico probabilístico o por ensamble puede ser benéfico para el manejo de los parques eólicos. El uso de un conjunto de simulaciones con diferentes configuraciones de PBL, resolución de malla y condiciones iniciales puede capturar la incertidumbre del pronóstico del viento. Algunos autores exploraron la sensibilidad del pronóstico de viento con el modelo WRF a varios factores como: PBL, resolución de malla y condiciones iniciales.

El modelo WRF con 10 km de resolución horizontal fue utilizado para explorar la habilidad de predicción del viento a la altura típica del rotor de un aerogenerador (80 m) en Iowa, EUA (Deppe *et al.*, 2013). En este estudio se construyeron ensambles a partir de simulaciones con: diferentes esquemas de capa límite (PBL, por sus siglas en inglés), tres perturbaciones aleatorias a las condiciones iniciales de Global Forecast System (GFS, por sus siglas en inglés) y condiciones iniciales inicializadas en diferentes tiempos. El tercer ensamble mostró los mejores resultados con una mayor dispersión en los pronósticos de viento y un menor error absoluto medio (MAE). Los resultados mostraron que la frecuencia de eventos de rampa ascendentes y descendentes a 80 m fueron subestimados. La hora de máxima frecuencia de rampas simuladas coincidió con la hora observada (16 y 19 horas local). Los esquemas de mezcla local tuvieron un índice de probabilidad de detección (POD, por sus siglas en inglés) más alto, una razón de falsa alarma (FAR, por sus siglas en inglés) más bajo e Índice de Éxito Crítico (CSI, por sus siglas en inglés) más alto que los esquemas no locales para rampas ascendentes. Así los autores concluyen que los esquemas de mezcla locales exhibieron una mayor capacidad para simular estructuras internas como jets de bajos niveles.

Otro estudio evaluó la sensibilidad al esquema de capa límite planetaria, la resolución de la malla y la condiciones iniciales en el pronóstico de viento a la altura del rotor para una región en el oeste de Canadá (Siuta, West, y Stull, 2017). Se evaluaron ocho esquemas de capa límite para el modelo WRF con condiciones iniciales del modelo North American Mesoscale Forecast System (NAM) y el GFS para un pronóstico a corto plazo, así como el efecto de la corrección de sesgo. La evaluación se realizó usando: desviación estándar, correlación, Índice de Acierto del Error Absoluto Medio (MAESS, por sus siglas en inglés) y la anomalía estandarizada del Error Absoluto Medio (z score). En términos generales, el Modelo Convectivo Asimétrico versión 2 (ACM2; Pleim, 2007) produjo la mejor precisión sobre topografía compleja.

La caracterización de eventos de alta y baja generación de potencia eólica es otra herramienta útil en el manejo de los parques eólicos. Los operadores necesitan balancear la



oferta y la demanda en la red eléctrica. La mala gestión de estos eventos puede conducir a apagones, incremento del costo de producción e incumplimiento de los contratos de energía.

Un método para caracterizar los períodos de alta y baja generación de potencia eólica fue propuesto para Gran Bretaña con 33 años de viento de los reanálisis MERRA (Cannon, Brayshaw, Methven, Coker, y Lenaghan, 2015). Los reanálisis se utilizaron para construir una serie temporal horaria de generación eólica a nivel nacional, con la cual se exploró la variabilidad estacional e interanual de los eventos extremos de generación eólica. La serie se elaboró mediante la interpolación de la velocidad del viento de los reanálisis MERRA a las ubicaciones de los parques eólicos, luego se extrapoló verticalmente al nivel del rotor usando un perfil logarítmico. Posteriormente, la rapidez del viento se convirtió a potencia eólica con la curva de un aerogenerador. Finalmente se agregaron todos los parques eólicos. Los umbrales utilizados para definir períodos de alta y baja generación de potencia eólica se construyeron a partir del factor de planta (FP) horario acumulado en los 33 años. Los percentiles 1, 10 y 20 de FP corresponden a períodos de baja generación de potencia eólica, mientras los percentiles 99, 90 y 80 se utilizaron para caracterizar períodos de alta generación de potencia eólica.

Los estudios sobre potencial eólico en México se han enfocado en determinar el número de horas de viento útiles y la potencia eléctrica disponible (Cancino-Solórzano, Gutiérrez-Trashorras, y Xiberta-Bernat, 2011; Hernández-Escobedo, Manzano-Agugliaro, y Zapata-Sierra, 2010; Hernández-Escobedo, Saldaña-Flores, Rodríguez-García, y Manzano-Agugliaro, 2014; Jaramillo y Borja, 2004; Yáñez, Kunith, Chávez-Arroyo, Romo-Perea, y Probst, 2014). Sin embargo, los estudios sobre la variabilidad del recurso eólico son escasos, ya sea por ocurrencia de eventos de rampa o períodos de baja/alta generación. Recientemente, a la par en que se realizó esta investigación, algunos autores exploraron las fluctuaciones del viento y sus causas sobre México (Thomas, Martínez-Alvarado, Drew, y Bloomfield, 2021). Una correcta descripción del recurso eólico requiere la caracterización de rampas y/o eventos de baja generación de potencia eólica para que los operadores de parques eólicos cuenten con herramientas para la toma de decisiones. Este trabajo presenta una caracterización de eventos de rampa y la relación con fenómenos atmosféricos para varias regiones de México (Figura 1). Asimismo, un modelo de pronóstico regionalizado para los parques eólicos puede promover la correcta integración de la generación eólica en la red eléctrica nacional. En este estudio se exploró la sensibilidad del pronóstico de viento al esquema de PBL en el modelo WRF. También se evaluó el desempeño de los modelos NAM y Rapid Refresh (RAP; Benjamin *et al.*, 2016) en la reproducción del viento en superficie para México. Estos modelos se seleccionaron porque cubren parcialmente el país, son modelos operativos con salidas horarias y coinciden con el período de registro de

las estaciones meteorológicas usadas en este estudio. Ambos modelos operan en la escala gris, en este régimen numérico, los movimientos atmosféricos son resueltos parcialmente y la física de sub-cuadrícula se incorpora mediante parametrizaciones. La evaluación de estos modelos puede indicar los refinamientos necesarios y la relación costo-beneficio de aumentar la resolución horizontal. Finalmente, se aplicó una corrección estadística a las salidas del modelo NAM para reducir los errores sistemáticos y analizar su efecto sobre la predicción de rampas de viento.

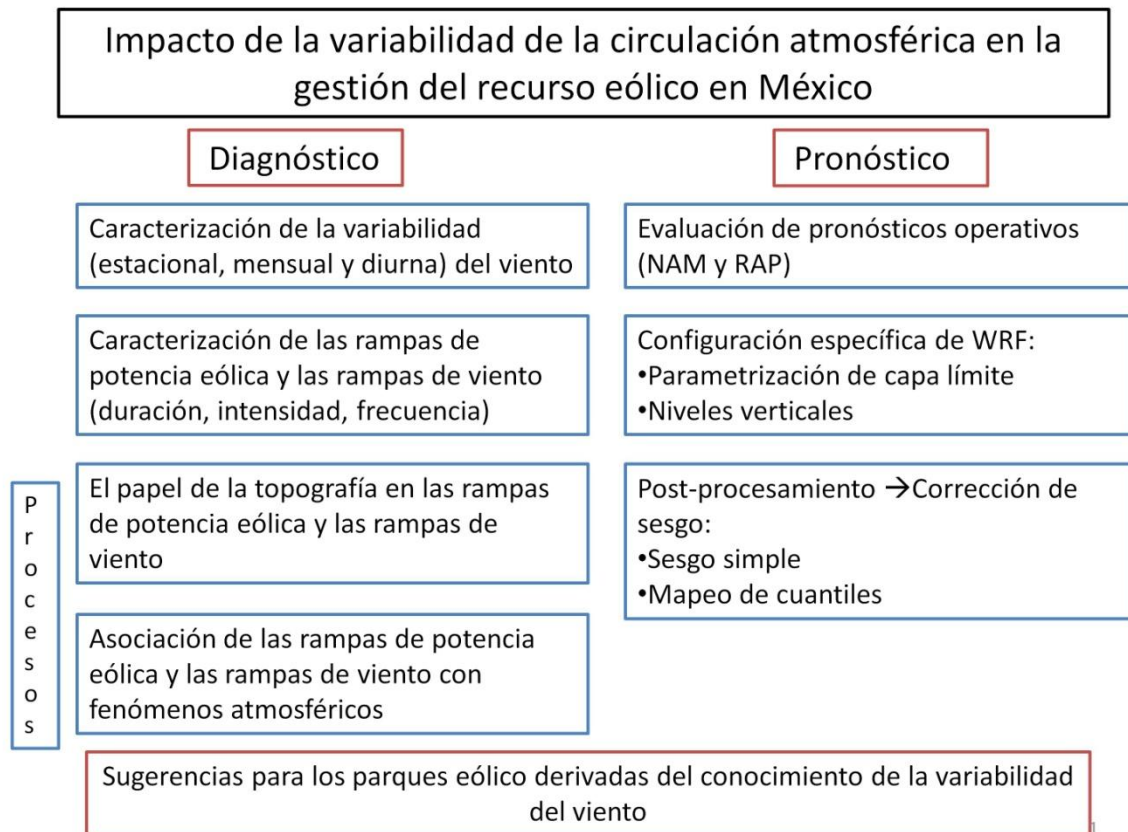


Figura 1. Esquema general de la tesis

**Hipótesis:** Las características y el pronóstico de las variaciones del recurso eólico (rampas de potencia, rampas de viento, períodos de alta y baja generación de potencia eólica) dependen de la estacionalidad de los sistemas atmosféricos, la topografía y la región.

**Objetivo general:** Caracterizar la variabilidad del recurso eólico y evaluar el pronóstico de las variaciones del recurso eólico (rampas de potencia, rampas de viento, períodos de alta y baja generación de potencia eólica) en los modelos de mesoescala.

**Objetivos específicos:**

- Caracterizar la variabilidad (estacional, mensual y diurna) del viento
- Caracterizar la duración, intensidad y frecuencia de rampas de viento y rampas de potencia
- Caracterizar la duración y frecuencia de los períodos de alta y baja generación de potencia eólica
- Explorar el papel de la topografía en las rampas de viento y rampas de potencia
- Asociar las rampas de potencia y las rampas de viento con eventos meteorológicos
- Evaluar el desempeño de los modelos de mesoescala en la predicción de rampas de viento y rampas de potencia
- Proponer refinamientos necesarios en los modelos de mesoescala para una mejor predicción de rampas de viento

La tesis consta de 6 capítulos (Figura 2):

Los resultados de esta tesis se constituyen por tres artículos publicados. En el primer capítulo de la tesis se aborda el panorama del sistema energético mundial y la participación de la energía eólica en México. También se plantea el problema de la generación eólica intermitente y el abordaje que se ha dado a este problema en el mundo. En el capítulo 2 se enlistan las definiciones de rampa y eventos de generación de potencia eólica, así como los métodos utilizados para la verificación del pronóstico de rampas en los modelos NAM, RAP y WRF. Además se indican las secciones de los artículos publicados donde se encuentran explicaciones más detalladas de los procedimientos empleados. Los capítulos 3, 4 y 5 corresponden a los artículos publicados:

- 3: Wind and Wind power ramp variability over Northern Mexico
- 4: WRF wind forecast over coastal complex terrain: Baja California Peninsula (Mexico) case study
- 5: Wind-ramp predictability

En el capítulo 6 se presentan las conclusiones sobre las características de las rampas y los eventos de generación eólica en México. Asimismo, se analiza el papel de la circulación atmosférica en los cambios abruptos de la potencia eólica. En esta sección se discuten algunas limitaciones de los modelos NAM y RAP en la predicción de rampas. Adicionalmente se sugieren algunos refinamientos necesarios en los modelos de mesoescala para una mejor predicción de las fluctuaciones eólicas.

R e s u l t a d o s	Capítulo 1	Introducción
	Capítulo 2	Datos y método
	Capítulo 3	Zona de estudio: Norte de México Contenidos: <ul style="list-style-type: none"> <li>•Caracterización estacional y diurna del viento</li> <li>•Caracterización estacional y diurna de rampas de potencia eólica</li> <li>•Atribución de rampas de potencia eólica a fenómenos meteorológicos</li> <li>•Verificación del pronóstico de rampas: POD, FAR, CSI</li> </ul>
	Capítulo 4	Zona de estudio: Península de Baja California Contenidos: <ul style="list-style-type: none"> <li>• Evaluación del esquema de capa límite con mejor desempeño para simular el viento en invierno/verano usando el modelo WRF</li> <li>• Evaluación del esquema de capa límite con mejor desempeño para simular rampas de viento usando el modelo WRF</li> </ul>
	Capítulo 5	Zona de estudio: 4 sitios de México Contenidos: <ul style="list-style-type: none"> <li>•Atribución de rampas extremas de viento a fenómenos meteorológicos</li> <li>•Evaluación del efecto del post-procesamiento en NAM para rampas de viento: corrección de sesgo simple y mapeo de cuantiles</li> </ul>
Capítulo 6	Conclusiones y trabajo futuro	
		Referencias
Anexo 1	Material Suplementario del Capítulo 3	
Anexo 2	Material Suplementario del Capítulo 4	
Anexo 3	Material Suplementario del Capítulo 5	

Figura 2. Estructura de la tesis

## Capítulo 2. Datos y método

En esta sección se enlistan los métodos o definiciones utilizadas para este estudio. Los detalles se encuentran en las publicaciones (Capítulos 3 a 5) y en el material suplementario (Anexos 1 a 3).

### *Datos*

La caracterización del viento en el norte de México se realizó con datos de 14 estaciones meteorológicas del Servicio Meteorológico Nacional (SMN) con períodos variables comprendidos entre 2010 y 2017 (más detalles en la sección 2.1 del capítulo 3). Éstas también se emplearon para la verificación del pronóstico de viento, pronóstico de eventos de generación de potencia eólica y rampas de potencia eólica en los modelos NAM y RAP para 2013. Este año se seleccionó por contar con el mayor número de registro de viento y disponibilidad de simulaciones en ambos modelos.

La evaluación de la sensibilidad del pronóstico de viento del modelo WRF al esquema de PBL para Baja California se realizó con 7 estaciones meteorológicas del SMN. La verificación se realizó para el viento en superficie (10 m) en un mes de invierno (enero 2013) y un mes de verano (junio 2013). Véase la sección Weather Stations del Capítulo 4 para más información.

En el análisis de rampas de viento y la corrección estadística se emplearon dos estaciones meteorológicas del SMN y dos estaciones anemométricas del Instituto Nacional de Electricidad y Energías Limpias (INEEL). Las estaciones meteorológicas midieron la rapidez y dirección del viento a 10 m cada 10 min. En tanto, los mástiles reportan vientos a 20 m en Francisco Villa (FCOV) y a 15 m en La Venta (LVEN) cada 10 min (véase la sección 2 Materials and Methods del Capítulo 5).

Tabla 3. Estaciones meteorológicas y torres anemométricas usadas en este estudio. En la sección Estudio se indica el artículo donde se emplearon: 3: Wind and Wind power ramp variability over Northern Mexico; 4: WRF wind forecast over coastal complex terrain: Baja California Peninsula (Mexico) case study; 5: Wind-ramp predictability

Nombre	ID	Estudio	Periodo de registro
Ciudad Cuauhtemoc	CDCU	3, 5	2010-2017
La Flor	LFLO	3	2010-2017
La Rumorosa	LARU	3,4	2010-2015
Villa Ahumada	VAHU	3	2010-2017
Ocampo	OCAM	3	2013-2017
Santa Cecilia	SNCE	3	2013-2015
Venustiano Carranza	VCAR	3	2010-2017
Cabo Pulmo	CPUL	3,4	2013-2017
Pinacate	PINA	3,4	2013-2017
Sierra la Laguna	SILA	3	2013-2017
Bahía de los Ángeles	BHAN	3, 4	2010-2017
Bahía de Loreto	BHLO	3,4	2013-2017
Cabo San Lucas	CSNL	3, 4 y 5	2010-2017
San Juanico	NICO	3 y 4	2010-2015
Francisco Villa	FCOV	5	2006-2007 y 2010-2012
La Venta	LVEN	5	2000-2007 y 2012

### *Modelos meteorológicos*

La evaluación del pronóstico de viento sobre México se realizó con dos modelos regionales: RAP y NAM de la NOAA. Ambos modelos cubren parcialmente México y utilizan el núcleo dinámico del modelo WRF. Los Centros Nacionales para la Predicción Ambiental (NCEP, por sus siglas en inglés) proporcionan gratuitamente las simulaciones horarias.

El sistema de pronóstico RAP produce pronósticos horarios sobre América del Norte con una resolución horizontal de 13 km hasta 18 horas. La asimilación de datos horarios utiliza observaciones recientes para ejecutar nuevos pronósticos cada hora. RAP usa coordenadas sigma con 51 capas verticales y una alta resolución vertical cerca de la superficie (Tabla 4). Entre sus aplicaciones se encuentran la gestión de sistemas de transporte, tiempo severo y energía.

Tabla 4. Configuración de los modelos NAM y RAP en 2013

<b>Configuración del modelo</b>	<b>RAP (Benjamin <i>et al.</i>, 2016b)</b>	<b>NAM</b>
Resolución horizontal	13 km	12 km
Niveles verticales	51	51
Condiciones de frontera	GFS	GFS
Asimilación	GSI 3D var	GSI híbrida con EnKF global
Parametrización PBL	MYJ (Janjić, 1994a)	MYJ 2.5 (Mesinger, 1993)
LSM	RUC (Benjamin, Grell, Brown, Smirnova, y Bleck, 2004)	Noah (Mukul Tewari <i>et al.</i> , 2004)
Cumulus	Grell (Grell y Dévényi, 2002)	Betts-Miller-Janijc (Betts, 1986; Betts y Miller, 1986)
Microfísica	Thompson (Thompson, Field, Rasmussen, y Hall, 2008)	Ferrier -Aligo
Radiación de onda corta	Goddard (Chou y Suarez, 1994)	RRTM (Mlawer, Taubman, Brown, Iacono, y Clough, 1997)
Radiación de onda larga	RRTM (Mlawer <i>et al.</i> , 1997)	RRTM (Mlawer <i>et al.</i> , 1997)

NAM se inicializa con un ciclo de asimilación de datos de 6 h utilizando el análisis de conjunto variacional híbrido NCEP para el dominio principal de 12 km. El pronóstico de NAM alcanza hasta 84 h con resolución horizontal de 12 km y 60 niveles verticales con coordenadas híbridas sigma-presión. Los pronósticos horarios de NAM son para 36 horas. La verificación del viento en los modelos NAM y RAP se realizó para 18 horas de pronóstico con la finalidad de realizar una comparación justa en términos del tiempo de pronóstico.

El modelo WRF versión 3.9.1 (Tabla 5) con resolución horizontal de 4 km se aplicó para producir un pronóstico de viento de 24 horas para enero y junio de 2013 utilizando las parametrizaciones de PBL: Mellor–Yamada–Janjic (MYJ; Janjić, 1994), el Modelo Convectivo Asimétrico, versión 2 (ACM2 por sus siglas en inglés; Pleim, 2007a; Pleim, 2007b) , y Yonsei University (YSU; Hong, Noh, y Dudhia, 2006). Los experimentos fueron inicializados con el modelo NAM de 12 km a las 0000 UTC y spin-up de 12 horas. Los niveles verticales se definieron para una resolución más fina en la PBL, 6 niveles se encuentran debajo de los 120 m y 31 niveles en total. Los niveles sigma más bajos de sigma están en 1.0, 0.998806, 0.9976, 0.99522, 0.99284, 0.99045 y 0.98807.

Tabla 5. Configuración del modelo WRF

Detalles del modelo	Configuraciones
Núcleo del WRF	ARW 3.9.1
Resolución horizontal	4 km
Niveles verticales	31 niveles
Superficie	Noah (Chen y Dudhia, 2001)
Microfísica	WRF single-moment 3-class (Hong, Dudhia, y Chen, 2004)
Cumulus	Kain-Fritsch (Kain, 2004)
Radiación de onda corta	Dudhia (Dudhia, 1989)
Radiación de onda larga	Rapid Radiative Transfer Model (Mlawer <i>et al.</i> , 1997)
Capa límite planetaria	YSU,MYJ, ACM2

## Método

### Clasificación de estaciones por topografía

Las estaciones meteorológicas se clasificaron según la pendiente máxima del terreno en un radio de 50 km para el análisis sobre el norte de México. Se consideró un radio de influencia porque los vientos en la capa límite son modificados por la topografía circundante. Se denomina topografía compleja cuando la pendiente del terreno excede los 10° dentro del radio de influencia. La topografía es moderadamente compleja cuando el valor máximo de la pendiente está entre 5° y 10°. Por último, una región plana muestra pendientes inferiores a 5°. Esta explicación se encuentra en la sección 2.1 del capítulo 3.

### Definición de rampa

En esta investigación se utilizaron las siguientes definiciones de rampa (Figura 3):

- Una rampa de potencia eólica se definió como un cambio del 20% o más en la potencia nominal en una hora, también se consideró un criterio relajando la ventana temporal a 3 horas. Esta definición se encuentra en la sección 2.2 del capítulo 3.
- Una rampa de viento es un cambio en la rapidez (cualquier magnitud) en un período que va de 1 a 16 horas. Esta definición más amplia se utilizó para evaluar la sensibilidad del pronóstico de viento al esquema de PBL. Se optó por esta definición para abarcar las variaciones del viento en diversas ventanas temporales. Esta información se encuentra en la sección Verification Metrics del capítulo 4.



- Una rampa extrema de viento es aquella que excede cuatro veces la desviación normalizada de las rampas de viento. Los detalles de esta definición se encuentra en la sección 2.3 del capítulo 5.

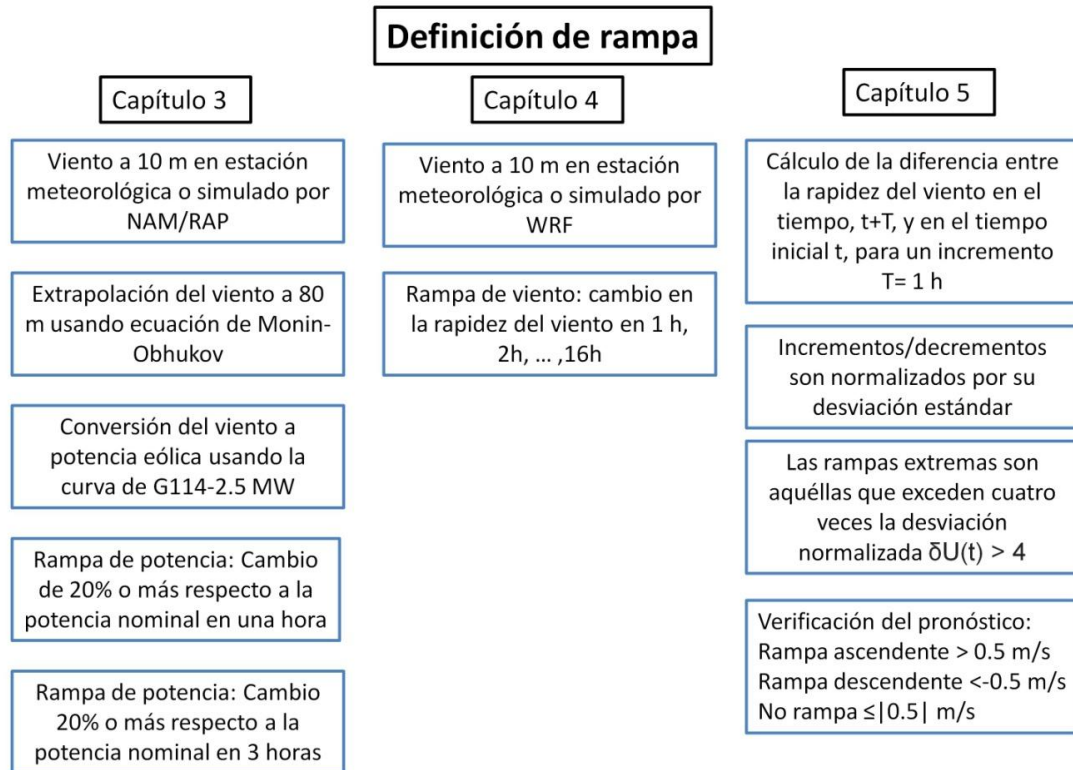


Figura 3. Definiciones de rampa

### Atribución de las rampas a un fenómeno atmosférico

Cada evento de rampa (ya sea de viento o de potencia) se asoció con un fenómeno atmosférico. En invierno las rampas se originan por el paso de sistemas frontales sobre la estación meteorológica. Mientras que en el verano, la circulación atmosférica tropical domina las variaciones abruptas en el viento. Los fenómenos típicos de esta temporada son: brisas valle-montaña, tormentas convectivas y ciclones tropicales. Las secciones 3.2.3 del capítulo 3 y 2.4 del capítulo 5 detallan los procedimientos utilizados para la clasificación de rampas por sistema atmosférico.

## **Eventos de generación de potencia eólica**

Los eventos de alta y baja generación de potencia eólica se calcularon considerando el factor horario de planta para cada estación meteorológica. A partir de la distribución acumulada de factores horarios de planta se calcularon eventos extremos de alta generación de potencia eólica (percentil 99), eventos extremos moderados de alta generación de potencia eólica (percentil 90) y eventos extremos de baja generación de potencia eólica (percentil 20). Esta explicación se halla en la sección 2.3.2 del capítulo 3.

## **Verificación del viento**

La evaluación determinista del pronóstico de corto plazo (18 horas) en los modelos NAM y RAP se abordó mediante las siguientes métricas: error absoluto medio (MAE, por sus siglas en inglés), sesgo y el coeficiente de correlación lineal descritas en la Tabla 2 del capítulo 3. Por su parte, la verificación de la sensibilidad al esquema de PBL en el modelo WRF se realizó mediante la anomalía estandarizada del MAE y el Índice de Acierto del MAE (definidos en la sección Verification Metrics del Capítulo 4). También se emplearon los Diagramas de Taylor para evaluar la correlación y la desviación estándar normalizada entre las observaciones y las simulaciones con distinto PBL (Sección Statistical scores en el capítulo 4).

## **Métricas de verificación de rampas en los modelos**

La verificación estadística de rampas simuladas en los modelos NAM, RAP y WRF se realizó mediante índices derivados de tablas de contingencia. Estos comparan los eventos de rampa observados contra los pronosticados. Los índices utilizados fueron: Probabilidad de Detección (POD, por sus siglas en inglés), Razón de Falsa Alarma (FAR, por sus siglas en inglés), Índice de Éxito Crítico (CSI, por sus siglas en inglés) y Sesgo de la Frecuencia (FBIAS, por sus siglas en inglés). Las definiciones se encuentran en la sección 2.3.2 del capítulo 3 y en la sección 2.7 del capítulo 5.

## **Rampas asociadas a tormentas**

La exploración de la contribución de las corrientes descendentes a las rampas de viento en verano se elaboró aplicando el esquema del MetOffice basado en Nakamura (Sheridan, 2011). Las corrientes descendentes de las tormentas poseen momento vertical, que al acercarse al suelo, se incorpora al campo horizontal. Éstas ráfagas pueden intensificar el viento medio, dando lugar a rampas de viento. La explicación detallada y la ecuación utilizada se presenta en la sección 2.5 del Capítulo 5.

### **Métodos de corrección de sesgo**

El post-procesamiento de las simulaciones con el modelo NAM se aplicó con la finalidad de reducir los errores sistemáticos encontrados en los capítulos 3 y 4. El principal objetivo de aplicar el método estadístico es ajustar la distribución de rampas simuladas a la distribución observada, reduciendo el exceso de rampas de viento débiles y no-rampas ( $<|0.5|$  m/s). Los métodos de corrección de sesgo empleados fueron: corrección simple de sesgo y mapeo de cuantiles. Los detalles sobre estos métodos se muestran en la sección 2.6 del Capítulo 5.

## Capítulo 3. Caracterización y pronóstico de rampas de potencia eólica en los modelos operativos NAM y RAP

### Artículo de investigación




#### "Wind and wind power ramp variability over Northern Mexico"

(Pereyra-Castro, Caetano, Martínez-Alvarado, y Quintanilla-Montoya, 2020)

**Resumen.** Se examina la variabilidad estacional y diurna del recurso eólico en el norte de México. Se agruparon catorce estaciones meteorológicas según la morfología del terreno y los sistemas meteorológicos que afectan a la región para evaluar el impacto sobre las rampas de potencia y los eventos persistentes de vientos fuertes. Se identifican cuatro áreas impulsadas por la estacionalidad de los sistemas meteorológicos. Las rampas de potencia eólica y los eventos de generación eólica persistente son producidos por frentes fríos en invierno, mientras que los sistemas convectivos de mesoescala y las circulaciones locales son dominantes en verano. Además, también se evaluó el pronóstico de viento de 2013 del Rapid Refresh Model (RAP) y los sistemas de pronóstico del North American Mesoscale Forecast System (NAM). En general, ambos sistemas tienen menos capacidad para predecir eventos de mesoescala y circulaciones locales sobre una topografía compleja, subestimando los vientos fuertes y sobreestimando los vientos débiles. Las variaciones del pronóstico del viento en el rango de mesoescala son más suaves que las observaciones debido a los efectos del promedio espacial y temporal, lo que produce menos rampas de energía eólica y eventos de generación de potencia eólica más duraderos. El estudio realizado muestra la importancia de evaluar modelos operativos en términos de variabilidad del viento, rampas de potencia eólica y eventos persistentes de generación eólica para mejorar el pronóstico eólico regional. Las características de los sistemas atmosféricos y la topografía de México requiere refinamientos del modelo para el manejo adecuado del recurso eólico.

Article

# Wind and Wind Power Ramp Variability over Northern Mexico

Karla Pereyra-Castro <sup>1</sup>, Ernesto Caetano <sup>2,\*</sup>, Oscar Martínez-Alvarado <sup>3</sup>  
and Ana L. Quintanilla-Montoya <sup>4</sup>

<sup>1</sup> Posgrado en Ciencias de la Tierra, Instituto de Geografía, Universidad Nacional Autónoma de México, Ciudad de México 04510, Mexico; karpereyra@comunidad.unam.mx

<sup>2</sup> Instituto de Geografía, Universidad Nacional Autónoma de México, Ciudad de México 04510, Mexico

<sup>3</sup> National Centre for Atmospheric Science, Department of Meteorology, University of Reading, Reading RG6 6ES, UK; o.martinezalvarado@reading.ac.uk

<sup>4</sup> Facultad de Ingeniería Civil, Universidad de Colima, Coquimatlán, Colima 28400, Mexico; analuzqm@uocol.mx

\* Correspondence: caetano@unam.mx; Tel.: +52-56230222 (ext. 45459)

Received: 24 September 2020; Accepted: 23 November 2020; Published: 27 November 2020



**Abstract:** The seasonal and diurnal variability of the wind resource in Northern Mexico is examined. Fourteen weather stations were grouped according to the terrain morphology and weather systems that affect the region to evaluate the impact on wind ramps and high wind persistent events. Four areas driven by weather systems seasonality are identified. Wind power ramps and persistent generation events are produced by cold fronts in winter, while mesoscale convective systems and local circulations are dominant in summer. Moreover, the 2013 wind forecast of the Rapid Refresh Model (RAP) and the North American Mesoscale Forecast System (NAM) forecast systems were also assessed. In general, both systems have less ability to predict mesoscale events and local circulations over complex topography, underestimating strong winds and overestimating weak winds. Wind forecast variations in the mesoscale range are smoother than observations due to the effects of spatial and temporal averaging, producing fewer wind power ramps and longer lasting generation events. The study carried out shows the importance of evaluating operational models in terms of wind variability, wind power ramps and persistence events to improve the regional wind forecast. The characteristics of weather systems and topography of Mexico requires model refinements for proper management of the wind resource.

**Keywords:** wind energy; wind variability; wind ramps; weather systems; Mexico

---

## 1. Introduction

Wind energy has undergone rapid growth in recent years, with record numbers of new worldwide wind power operative plants every year. The expansion of wind energy using existing technologies, power system improvements and creative policy making is leading the world towards a reduction on dependence of non-renewable energy sources. Mexico generates 71.2% of electricity from fossil fuels. The wind power installed capacity in Mexico is 4875 MW, approximately 20% of installed capacity of renewable energies [1].

The main drawback of wind power is the intermittent generation related to wind speed variability. Electricity generated by wind turbines can be highly variable at multi-time scales that range from sub-hourly to seasonal. Wind power needs to be scheduled to balance power generation and load demand in power systems. Large penetration of wind power could have a large impact on the operation and security of electric power grids [2].



Wind power ramps (sudden and large changes in wind energy generation) produce fluctuations of wind energy that can be challenging for system operators [3]. Mismanagement of ramps occurrence can reduce the power generation of a wind farm, causing differences between the real and estimated generation cost. An adequate assessment of potential wind power should include the characterization of wind power ramps.

Despite their importance for the operations of wind farms, there is no standard definition of wind power ramps. Instead, multiple wind ramp definitions exist. These definitions consider ramp characteristics such as their magnitude and duration [4]. The magnitude threshold of a ramp is usually expressed as a percentage of the rated power [4–8]. Usually, multiple ramp definitions may be required to be operational simultaneously as the appropriate threshold depends on the users. This leads to measuring the skill of numerical weather prediction models under different ramp definitions, from binary (ramp/non-ramp) [8], which can be very sensitive to threshold values [9], to more sophisticated ones [10,11]. Sensitivity studies of wind speed forecast during wind ramp events to parameters such as initial condition, model resolution and type of event has been done in order to explore forecast uncertainty [12].

The understanding of the weather systems' (WS) role and better anticipation of ramp events could help to achieve an efficient integration of wind energy in power systems. One of the keys to successfully managing wind energy is the ability to accurately forecast the expected amount of wind energy supplied to the power grid. Approaches to wind power forecasting have improved in recent years with an emphasis on short-term wind forecasting (18–24 h) [13–15]. The improvements have been achieved by new physics parameterization methods, and enhanced data assimilation techniques coupled to better-quality data available for assimilation [16].

Integration and management of wind power ramps have been topics of interest in places with significant wind power penetration [17–20], however, there are no studies about wind ramps variability associated with wind power generation in Mexico. The understanding of WS that causes ramp events is an important precursor to the development of a successful ramp forecast procedure [4].

Several studies have found that wind ramps occurrence at mid-latitudes is caused by extratropical cyclones in the winter season [5,19,21]. During summer, wind ramps are related to mesoscale systems: boundary layer processes, mountain-valley breezes, sea-land breezes and mesoscale convective systems (MCS) that produce changes of short duration in the wind speed [13,14].

Mexico is frequently affected by winter cold surges that propagate from the mid-latitudes, as a form of atmospheric mid-latitude-tropical interactions [22]. Meanwhile, during summer the mesoscale events are the main modulators of the tropical circulation. Furthermore, the Mexican topography is complex, with topographic gradients that can go from 5700 m to sea level in less than 100 km [23].

Some numerical weather prediction studies at multiple time horizons have shown that the ability of the Weather Research and Forecasting Model (WRF) to accurately forecast wind speed and ramp events mainly depends on the topography, the initial conditions, the spatial resolution and the parameterization scheme in the boundary layer [13,24–26]. The accuracy of the forecast is also related to domain sizes, the number and spacing of the vertical levels, and other parameterizations such as land surface. Carvalho et al. [24] showed that wind forecasts over the Iberian Peninsula with 90 km, 18 km and 3.6 km horizontal grid spacing are more accurate in regions with flat topography and the ability decreases in complex topography. In these sites, the thermal circulations and the flows induced by the terrain characteristics are crucial for the prediction of wind speed and direction.

This study examines the role of WS in wind power ramps and wind variability in Northern Mexico. Due to the variety of WS that affect the region, it is important to understand the factors that affect wind ramps, high and low generation events. To address this issue, seasonal and diurnal variations in wind energy are analyzed. Furthermore, proper management of wind farms involves also wind forecast. Therefore, a short-term wind forecast verification is carried out for two operational systems, namely the North American Mesoscale Forecast System (NAM) [27] and the Rapid Refresh Model (RAP) [15], which cover Northern Mexico. The purpose of this exercise is to examine the performance

of these models against observations at weather stations which experience the influence of different WS. Ramp forecasting skill is assessed by using ramp indices considering the timing and magnitude of wind power changes.

The rest of the paper is organized as follows. Section 2 describes the data and methodology used, including a brief description of the operational NAM [27] and RAP [15] models. Section 3 examines the wind variability for 14 weather stations and the wind forecast skill of NAM and RAP models for 2013. An evaluation of models to predict wind power ramp and extreme events is also discussed. Issues such as intermittency, variability and uncertainty in the forecasted wind power output are discussed. The conclusions are presented in Section 4.

## 2. Data and Method

### 2.1. Weather Stations

Wind variability in Northern Mexico is examined using 14 weather stations of the Mexico National Meteorological Service, the 10 m wind speed and direction are measured with a frequency of 10 min. The raw time series showed discontinuities and inconsistencies (e.g., persistent direction for several days, unrealistic winds, discrepancies on wind speed units). Therefore, a quality control process was performed on the raw data. During quality control, records with wind speed or wind direction beyond plausible values were filtered out as were periods with constant wind speed or wind direction or abrupt changes in the wind speed values. The former are typical of instrument fails and the latter correspond to changes in wind speed units, for example, m/s to kt. Wind speed and wind direction were also compared to wind gust speed and direction for internal consistency. This procedure resulted in some stations with nine years and others with only four years of consistent data (Table 1). The analysis was performed using the hourly average wind.

**Table 1.** Classification of the sites by topography and weather systems.

Region	Weather Station	ID Weather Station	Topography	Dry Season	Wet Season	Record Period
PLATEAU	Ciudad Cuauhtemoc	CDCU	MC	MLS	LC	2010–2017
	La Flor	LFLO	MC	MLS-LC	LC	2010–2017
	La Rumorosa	LARU	MC	MLS	LC	2010–2015
	Villa Ahumada	VAHU	MC	MLS	TC	2010–2017
NEMEX	Ocampo	OCAM	MC	MLS	TC	2013–2017
	Santa Cecilia	SNCE	MC	MLS	TC	2013–2015
	Venustiano Carranza	VCAR	MC	MLS	TC	2010–2017
GoC	Cabo Pulmo	CPUL	MC	MLS	MLS	2013–2017
	Pinacate	PINA	LC	MLS	MLS	2013–2017
	Sierra la Laguna	SILA	HC	LC	LC	2013–2017 *
BCP	Bahia de los Angeles	BHAN	C	LC	LC	2010–2017
	Bahia de Loreto	BHLO	MC	LC	LC	2013–2017 *
	Cabo San Lucas	CSNL	C	LC	LC	2010–2017
	San Juanico	NICO	MC	LC-MLS	LC-MLS	2010–2015

\* Missing 2015 data. C: complex topography; MC: moderately complex topography; HC: highly complex topography; MLS: mid-latitude systems; TC: Tropical circulation; LC: local circulation. Regions: (a) Plateau; (b) Northeastern Mexico (NEMEX); (c) Gulf of California (GoC); (d) Baja California Peninsula (BCP).

The fraction of hours that the surface winds exceeded 3 m/s, which corresponds to the cut-in wind speed in a typical power curve, was calculated. This metric is proportional to wind farm operation hours. However, it does not show the amount of power generated [28,29].

The exceedance frequency threshold of the 3 m/s for all stations has a terrain dependence on near-surface wind speed (Figure 1), and suggests different weather systems modulating the wind on the regions. Wind speed days means the number of hours >3 m/s divided by 24. Areas exceeding the wind threshold for 226 to 250 days per year are located in the Baja California Coast, where some wind farms are operating (Figure S1, in supplementary material). In contrast, in-land regions exceed this threshold just around 175 days at the Mexican Plateau. Low-frequency modes, such as El Niño–Southern



Oscillation (ENSO), Pacific Decadal Oscillation (PDO), and Atlantic Multidecadal Oscillation (AMO), might influence the occurrence of extreme winds [30]. However, this influence is not captured by the short-time data sample under analysis here.

Complex topography is a term commonly used in wind power assessment studies, but an objective definition is not given. In this study, the topography complexity classes are defined as in Bingöel [31], but with the incorporation of a 50 km radius of influence (Table 1). Complex topography is considered when terrain slope exceeds  $10^\circ$  within the radius of influence, moderately complex when the maximum slope value is between  $5^\circ$  and  $10^\circ$ , and flat for slopes of less than  $5^\circ$ . The reason for including a radius of influence is that boundary layer winds are modified by the surrounding topography of the site of interest. Storm downdrafts, local circulations such as sea-land breeze and mountain-valley breeze develop due to horizontal gradients of temperature, which are caused or reinforced by the terrain slopes.

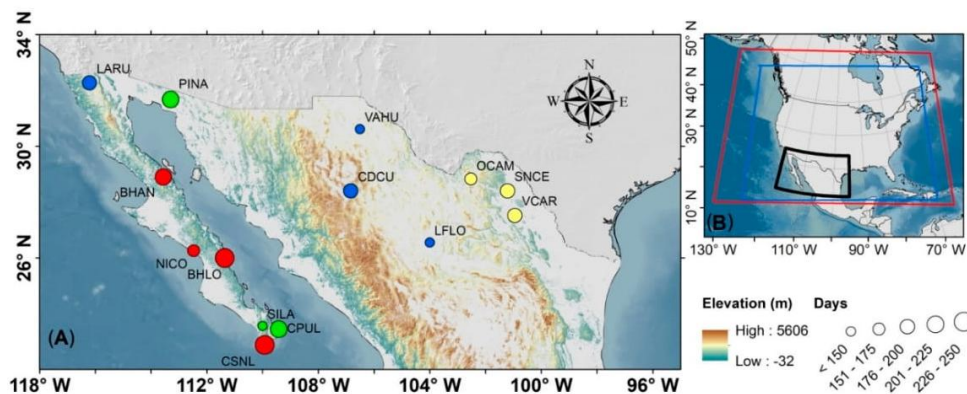


**Figure 1.** (A) Study area and (B) domain of the North American Mesoscale Forecast System (NAM) (red line) and the Rapid Refresh Model (RAP) (blue line) mesoscale models. Shaded areas represent terrain height (m) with slopes greater than  $5^\circ$ . The size of the circle indicates wind speed days  $>3$  m/s. The color in the circles indicate the regions: the Baja California Peninsula in red, Gulf of California in green, Plateau in blue and Northeastern Mexico in yellow. Topographic slopes were calculated as the magnitude of the gradient for the GTOPO30 [32] digital elevation model with a horizontal grid spacing of 30 arc seconds ( $\sim 1$  km).

## 2.2. Forecast Models

NOAA's Rapid Refresh (RAP) [7] and North American Mesoscale Forecast System (NAM) [27] models were selected as the basis for the wind forecast assessment over Northern Mexico. The reasons for choosing the regional models were that both models' domains cover Northern Mexico (see the model domain in Figure 1b), the output from both is freely provided by NCEP at hourly resolution, and both models utilize the underlying Advanced Research version of the WRF Model [33], which has been widely used by the scientific community for wind forecasting [13,14].

The RAP analysis and forecast system provides hourly forecasts over North America with a 13 km grid spacing for up to 18 h, with a new data assimilation forecast cycle using latest hourly observations to run new forecasts every hour [15]. The RAP uses sigma coordinates with 51 vertical layers with a high vertical resolution near surface. RAP uses a community supported data assimilation package, the Gridpoint Statistical Interpolation, to carry out 3-dimensional hybrid ensemble/variational data assimilation [34]. Among their applications are transportation system management, severe weather, and energy.

The NAM [27] run by the National Centers for Environmental Prediction (NCEP) is initialized hourly with a 12 h data assimilation cycle, producing 3 hourly analysis updates using the regional



Gridpoint Statistical Interpolation hybrid ensemble analysis. NAM forecast up to 84 h with 12 km horizontal resolution and 60 vertical levels with hybrid sigma-pressure coordinates.

### 2.3. Method

#### 2.3.1. Weather Station Groups

The 14 stations were grouped according to the terrain morphology and the WS affecting the area during the dry and wet seasons (Table 1). In Mexico, the winter rainfall pattern is dominated by mid-latitude WS [35,36] and in the summer by easterly tropical waves and tropical cyclones. These are important moisture carriers responsible for the seasonal precipitation (May–November) over the Mesoamerica [37].

Seasonal and daily wind roses were constructed to examine the WS that modulate the wind at each station. Prevailing intense winds from persistent direction during winter (e.g., CDCU) suggest passage of frontal systems. Examination of front position with the horizontal gradient of equivalent potential temperature at 700 and 500 mb and the horizontal surface wind (not shown) was calculated using ERA5 [38] reanalysis data. The analysis showed prefrontal and postfrontal wind intensification at weather stations. Cold front reports in newspapers and from the monthly climate review of CONAGUA (National Water Commission of Mexico) from 2014–2015 over Northern Mexico were also consulted to support the analysis. Furthermore, trade winds shifting during the boreal summer over Northeastern Mexico were explored using the 10 m wind monthly climatology of ERA5 from 1979–2018.

Local circulation patterns were assessed through the analysis of wind roses, considering that two dominant directions in a season indicate local circulation patterns. Furthermore, the existence of diurnal (9:00 to 19:00 local time) and nocturnal (20:00 to 8:00 local time) wind components along with a sharp topographic gradient or land cover differences found over the area surrounding the weather station, were used as a criterion for assigning a regional thermal circulation. As examples, the cases of Cabo Pulmo (CPUL) and Bahia de los Angeles (BHAN) are discussed. The coastline for both stations is oriented from northwest to southeast. The analysis of all day (daily), daytime and night-time wind roses for both stations is shown in Figure S2. CPUL does not show a clear reversal of wind direction from day to night hours, especially in winter. On the other hand, the wind in BHAN is from the southeast (from the land) at night and comes from the sea during the day in both seasons, June–July–August (JJA) and December–January–February (DJF), almost perpendicular to the coast. This situation is typical of the sea-land breeze, consistent with the diurnal reversal of wind direction from offshore to onshore. The wind is strongest ( $>7.5$  m/s) at night in JJA, suggesting katabatic winds. Certainly, other synoptic effects can be modulating the wind, especially in winter as in CPUL. However, the reversal of wind direction perpendicular to the coastline remains in the daily wind pattern (Figure S3, in supplementary material) even under synoptic winds predominance.

According to the previous criteria and the Northern Mexico topographic complexity, four regions were defined. Attribution of wind power variation to WS was made by exploring the cold front position in satellite images during winter and the related wind intensification (Figure S4, in supplementary material). The summer season is more complex given the tropical circulation in the region. Statements made about the effect on ramps by sea-land breezes and storms were explored in the wind data and reaffirmed with satellite or precipitation images. A wind power ramp is classified as related to storms when precipitation and intensification of wind are observed in the weather station, for instance during the 21 July 2012 event (Figures S5 and S6, in supplementary material).

#### 2.3.2. Model Verification

The evaluation of the models was carried out only for 2013 since this year had a larger number of wind records in all the selected stations and both model outputs were available for the diagnosis. The short-term deterministic forecast performance is addressed using the following metrics: mean absolute error (MAE), bias and the linear correlation coefficient ( $r$ ) (Table 2).

Since the model data represent spatial averages (in grid boxes of more than  $12 \text{ km} \times 12 \text{ km}$  for NAM and approximately  $13 \text{ km} \times 13 \text{ km}$  for RAP) and therefore are not expected to represent high-frequency variability, the weather station data were averaged hourly. In addition to making the data more comparable, the average wind speed allows the detection of ramps that persist for longer than 10 min.

For calculation of wind power ramps, observational and modeled power time series were derived to a representative turbine hub height ( $\sim 80 \text{ m}$ ). First, the observed wind profile was assumed to follow the Monin-Obukhov similarity theory [39,40]. Then wind speed was converted to wind power by applying a G114-2.5 MW wind power curve with the wind assumed to be parallel to the axis turbine (Figure 2). This power curve was chosen for illustrating the effect of wind ramps considering that winds over Northern Mexico are moderate ( $4 \text{ m/s}$  to  $8 \text{ m/s}$ ) to weak ( $<4 \text{ m/s}$ ). The turbine is designed for a wind class II turbine [41], which is commonly used in Mexico [42].

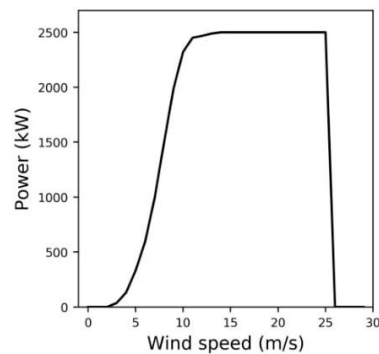


**Figure 2.** Power curve of the design performance of a G114-2.5MW wind turbine used in the wind power ramp detection. The turbine has a cut-in wind speed of 3 m/s, a rated wind speed of 13 m/s, and a cut-out wind speed of 25 m/s.

Wind power variations are assumed to be only associated with meteorological conditions. Technical effects on the power output as yaw misalignment, response lag, and wakes of other wind turbines are not considered in this analysis. A wind power ramp is considered as a change in power greater than or equal to 20% of rated power in 1 h [43,44]. The positive (negative) rapid change in the wind power generation qualifies as a ramp up (down). The idea is to assess large wind ramps over the region. It is worth mentioning that the characteristics of wind ramps must consider relevant aspects for the end users of wind farms. According to previous studies [4,9], the number of ramp events becomes very sensitive to the threshold chosen. For this reason, a 30% capacity factor change in 1 h, was also used in the assessment. However, daily and monthly wind ramp distribution behaves similarly for both cases, even though fewer ramp events were identified for the higher power change (Figure S7, in supplementary material).

To improve comparability between observed and forecast winds, the latter were bilinearly interpolated to the weather station location and the 10 m wind speed was extrapolated to 80 m assuming the Monin-Obukhov similarity theory [39,40]. Then, wind speed was converted to wind power using the G114-2.5 MW power curve.

The comparison of the forecast with the observations was made for the 18-h forecast length in both models to make a fair comparison in terms of leading time (NAM contains hourly forecasts up to 36 h, then it has outputs every 3 h up to 84 h, while RAP has a horizon of 18 h). The time series of model forecast were constructed by concatenating sets of forecast with lengths going out 18 h for NAM and RAP models, similar to the independent forecast run method used by Bianco et al. [11]. The disadvantage of this approach is that discontinuities between the start and the end of each forecast



run can create artificial ramps. However, a systematic creation of ramps was not detected. In addition, the errors of the series with the leading time did not show a clear increasing tendency.

**Table 2.** Wind and ramp-event forecast metrics.

Forecast Verification		
Metric	Definition	Formula
Mean Absolute Error (MAE)	Typical magnitude for the forecast error in a given verification data set. The MAE is the arithmetic average of the absolute values of the differences between the n pairs of forecasts ( $y_k$ ) and observations ( $o_k$ ).	$MAE = \frac{1}{n} \sum_{k=1}^n  y_k - o_k $
Correlation Coefficient (r)	It is a measure of the linear correlation between forecast ( $y_k$ ) and observations ( $o_k$ ). Ratio of observation and forecast covariance ( $cov(y, o)$ ) and the product of their standard deviations ( $s_y s_o$ ).	$r = \frac{cov(y, o)}{s_y s_o}$
Bias	The averaged difference between the forecast ( $y_k$ ) and observation ( $o_k$ ) pairs.	$Bias = \frac{1}{n} \sum_{k=1}^n (y_k - o_k)$
Contingency Table Derived Indices		
Probability of detection (POD)	The ratio between the number of true positives and the number of observed positives, which indicates the fraction of observed YES events that are actually forecast.	$POD = \frac{TP}{TP+FN}$
Critical Success Index (CSI)	The score is the number of correct YES events divided by the total number of occasions in which that event was forecast and/or observed.	$CSI = \frac{TP}{TP+FP+FN}$
Frequency bias score (FBIAS)	The index measures the ratio of the frequency of forecast YES events to the frequency of observed YES events. The ramp forecasting system tends to underforecast when FBIAS < 1.	$FBIAS = \frac{TP+FP}{TP+FN}$
False Alarm Rate (FAR)	This index measures the fraction of predicted YES events that did not occur.	$FAR = \frac{FP}{FP+TP}$

True positive (TP) represents the number of forecasted ramps that are observed in the actual power output; false positive (FP) is the number of forecasted ramps that are not observed in the actual wind power; false negative (FN) represents the number of observed ramps that are not predicted by the wind forecasting system; true negative (TN) is the number of non-occurring events for both observed and forecasting results [45].

Ramp metrics for events occurring in DJF and JJA in 2013 were calculated. Observed power changes that met the threshold but are not predicted are known as false negative (FN) (Figure S8a). A ramp produced by the model but not observed is defined as a false positive (FP) (Figure S8b). Finally, a ramp is considered as correctly forecasted (True positive: TP) if the threshold criterion is met in timing by the forecast and the observation (Figure S8c). The effect of relaxing the time threshold to 3 h was tested in the forecast.

The following forecast verification indices were calculated using a contingency table for observed and forecast ramp events: probability of detection (POD), frequency bias score (FBIAS) and False Alarm Rate (FAR) [45]. Their definitions are shown in Table 2.

Persistent high and low generation events were calculated for each weather station considering the instantaneous plant factor. Using the percentage of the hypothetical power obtained in one hour with respect to the nominal power of a wind turbine, the cumulative distribution of instantaneous

plant factors, extreme events of high generation (99th percentile), moderate extreme events of high generation (90th percentile) and extreme events of low generation (20th percentile) were obtained.

### 3. Results and Discussion

This section details the topographic and climate characteristics of the four regions defined in Section 2.3.1. The effects of WS on the monthly and daytime variability of ramps and persistent generation events are discussed. Finally, a verification of the NAM and RAP forecast for wind, wind power ramps and persistent generation events is examined.

#### 3.1. Study Regions

The stations were grouped for analysis considering the terrain morphology and WS in the region. The regions are: Plateau, Northeastern Mexico (NEMEX), Gulf of California (GoC) and Baja California Peninsula (BCP).

The Plateau is an arid-semiarid region (blue circles in Figure 1) extending from the United States border to the Trans-Mexican Volcanic Belt, and is bounded by the Sierra Madre Occidental and Sierra Madre Oriental to the west and east, respectively. The analysis described in Section 2.2 shows that local circulations develop in the region with a typical reversal of wind direction during the day in summer. However, winds are more intense in the winter associated with mid-latitude systems (Figure 3a,b). The weather stations included in this group are Ciudad Cuauhtemoc (CDCU), La Rumorosa (LARU), La Flor (LFLO) and Villa Ahumada (VAHU). The LARU station is not located over the Plateau region but is affected by WS similar to those affecting this group stations. Examination of wind power ramps and persistent events in Sections 3.2.1 and 3.2.2 confirms this statement. Therefore, for the analysis of the wind characteristics due to WS, this station was included in the group Plateau.

NEMEX is a flat terrain region with maritime influence reaching even the Ocampo (OCAM) weather station over a mountain–coast transition. Wind intensification is caused by trade winds northward shifting in summer (Figure 3d); these moist winds blowing from the Gulf of Mexico persist from June to August. Meanwhile, cold fronts moving into the Gulf of Mexico produce intense northerly winds in the winter [36,46]. The group's stations are OCAM, Santa Cecilia (SNCE) and Venustiano Carranza (VCAR), (yellow circles in Figure 1).

The Cabo Pulmo (CPUL) and El Pinacate (PINA) stations (green circles in Figure 1) were grouped together because the winds are associated with a predominantly synoptic circulation, northerly in winter and southerly during the summer (Figure 3e,f). The wind flowing between the mountainous systems Sierra La Laguna and the Sierra Madre Occidental, produces moderate channeled winds over the GoC. The Sierra La Laguna (SILA) station, located at the mountain (1949 m.a.s.l.), is also shown in this group.

BCP region is an area that combines coasts with mountain systems such as Sierra La Laguna, where the highest peak reaches 2080 m.a.s.l. In this region characterized by the inhomogeneity of the land (composition and morphology), there are thermal circulations such as the sea-land breeze and katabatic winds, which can combine to produce intense winds (Figure 3g,h). The weather stations of this region are Bahia de los Angeles (BHAN), Bahia de Loreto (BHLO), Cabo San Lucas (CSNL) and San Juanico (NICO) (red circles in Figure 1).

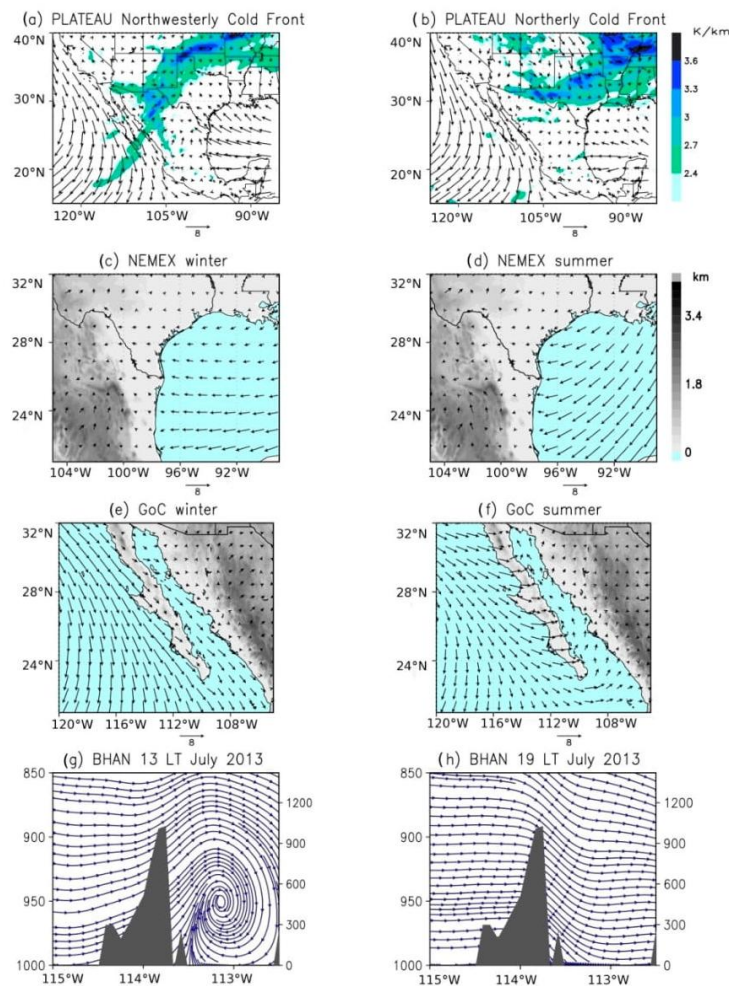


**Figure 3.** Typical weather systems modulating wind power ramp variability over four different regions in Mexico. Topography, in km (grey shaded). Composite pattern of gradient of equivalent potential temperature ( $\times 10^{-2}$  K/km) and ERA5 surface wind as front position indicator (Plateau) for 2014–2015 during (a) westerly cold front and (b) northerly cold front; NEMEX surface wind climatology from 1979–2018 during (c) winter, (d) summer; BCP surface wind climatology from 1979–2018 during (e) winter, (f) summer; mean circulation on the x–z plane calculated with the NAM analysis model at (g) 1300 local time (LT) for July 2013, (h) 1900 LT for July 2013 at BHAN latitude ( $28.89^\circ$  N).

### 3.2. Wind Power Variability

#### 3.2.1. Wind Power Ramp Characterization

The intraseasonal variability of wind ramps is mainly modulated by synoptic-scale systems during winter (Figure 4) as a consequence of the increment of cold front incursions over Mexico. Their effects last between 2 and 6 days, depending on the phase speed [47]. In this dry season (October–April), the northerly intense cold air associated to frontal systems increases the occurrence of wind ramps, more evident in the Plateau (Figure 4a), GoC (Figure 4c) and BCP (Figure 4b) regions.



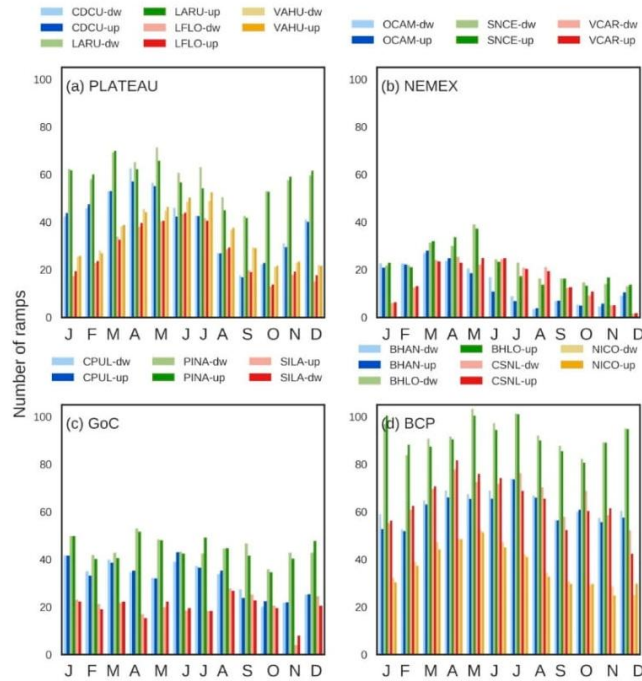


**Figure 4.** Monthly mean of wind power ramp-up (dark color) and ramp-down (light color) events for (a) Plateau, (b) NEMEX, (c) GoC, (d) BCP regions.

Wind ramps are also generated by diurnal variations in wind intensity, which can be related to the establishment of local circulations such as sea-land and valley-mountain breezes as well as MCS, similar behavior has been found over USA arid regions [14]. The coastal and Plateau regions experience these WS mainly from March to July (Figure 4a,d, further explanation is given in Section 3.2.3). A ramp produced by storms occurs when the increase in wind speed coincides with the precipitation in the station (Figure S5).

For the four regions, the increase in ramp events at the beginning of the wet season is associated with MCS. These events are more frequent from June to August over Mexico [48]. The spatial distribution of the systems reported by [49] shows MCS events over the PLATEAU and NEMEX regions, especially frequent from April to August. Sudden changes in wind power production are less frequent towards the end of the wet season (September to November), (Figure 4). Furthermore, there is a symmetrical behavior of the wind power ramp-up and ramp-down events (Figure 4).

Generally, ramps-up are more frequent between 10:00–16:00 local time (LT) (Figure 5a–c) in most of the weather stations, probably as a result of diurnal variation of ground heating and its interaction with the atmospheric boundary layer. In the afternoon, the decrease of solar radiation reaching the surface attenuates horizontal thermal gradients, resulting in weaker winds. This transition occurs between 19:00–22:00 LT (Figure S3), producing a maximum of ramp-down events (Figure 5a–c).

Different behavior is found in three stations over complex topography: CSNL, BHAN and SILA. In the first, a coastal area at the end of the Sierra La Laguna mountain range, the combination of local effects such as katabatic/land breeze circulation generates a second maximum on ramp-up frequency around 19:00 LT (Figure 5d). Otherwise, the frequency of wind power ramp-down is maximum from 7:00–10:00 LT due to the weakening of circulation driven by topography. Moreover, ramp-ups are more frequent at night in the hilly terrain of SILA station, when katabatic winds are set in.

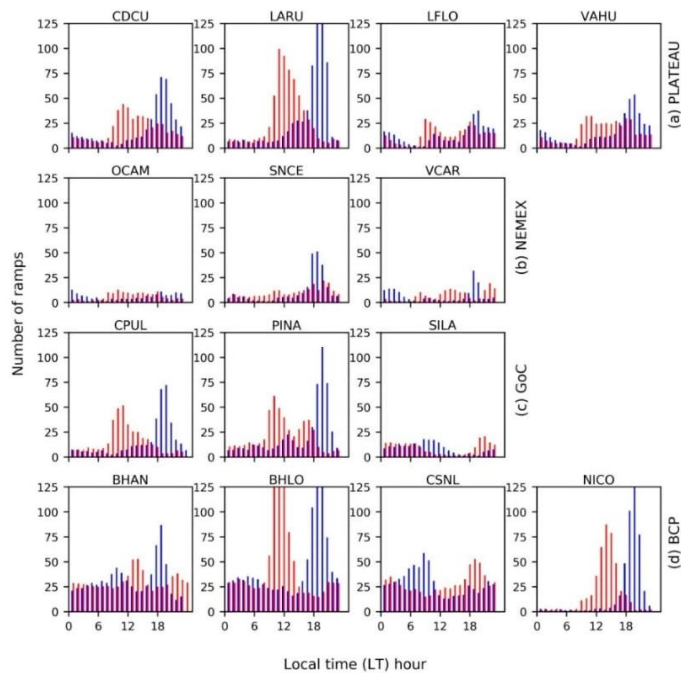


**Figure 5.** Hourly distribution of annual mean wind power ramp-up (red) and ramp-down (blue) events for (a) Plateau, (b) NEMEX, (c) GoC, (d) BCP regions.

### 3.2.2. Persistent High and Low Wind Power Generation Events

The maximum frequency of extreme high generation events in DJF and March–April–May (MAM) seasons is mainly caused by frontal systems passing over Northern Mexico. The satellite image (example in Figure S4) during the occurrence of an extreme event shows the frontal position over the deployed weather stations, as confirmed by a composite of gradient of equivalent potential temperature (Figure 3a,b). The annual distribution of extreme events varies spatially because frontal incursions come from the Pacific Ocean or from the north [35]. Some northerly winds affect just NEMEX and Plateau regions.

On the other hand, the maximum of extreme high generation events in JJA season is mainly associated to mesoscale systems, such as MCS. The northward shifting of trade winds during summer can favor the convection over NEMEX region [46]. Meanwhile, short generation events over Plateau and BCP are also related to thermal circulations.

Generally, extreme events of high generation are recurrent from March to August except for GoC stations. The intense winds in the latter are originated by frontal systems in DJF [50], leading to an increase in events of duration  $\geq 3$  h (Figure 6c). Moderate extreme events (not shown) are influenced by the same WS as extreme events.

Low generation events are more frequent from the end of the dry season to the beginning of the wet season, March to August months, for the four regions (details will be discussed in Section 3.3). For coastal regions, wind intensifies with the sea breeze establishment but the wind weakening during the transition to land breeze, gives place to periods of low generation. In addition, thunderstorm downdrafts can produce short high generation periods following by a low generation period when the storm ends (Figure S5), as observed in wind farms [51].

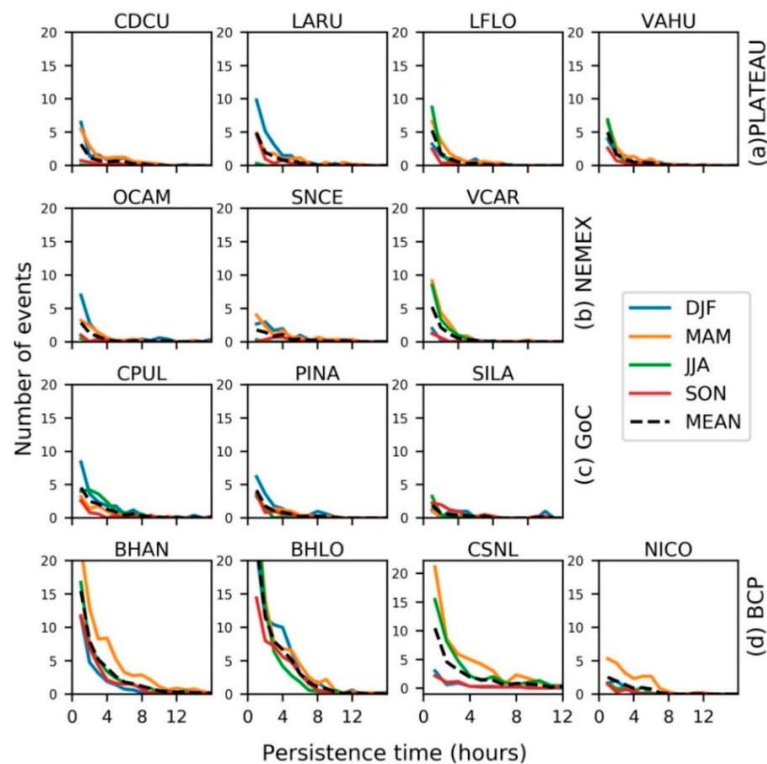


**Figure 6.** Seasonal mean number of extreme persistent high generation events (99 percentile of Capacity Factor) for (a) Plateau, (b) NEMEX, (c) GoC, (d) BCP regions. March–April–May (MAM), June–July–August (JJA), September–October–November (SON), December–January–February (DJF).

### 3.2.3. Weather Systems Underlying Wind Ramps

The average near-surface wind in Northern Mexico is weak ( $\sim 4$  m/s). The Plateau region experiences frontal systems to the end of the dry season, which leads to an increase in the average wind and the violin plot whiskers (Figure 7a). It is interesting to note that the moderate topographic gradients produce a bimodal wind behavior in LARU during summer (Figure 7) similar to that observed in coastal areas. Thermal circulations can be distinguished by two maxima in wind speed frequency, for example, in the sea-land breeze, there are a diurnal onshore wind and a nocturnal offshore wind.

The trade winds over NEMEX (Figure 3d) at the beginning of the wet season increases the average monthly wind speed and decreases the number of extreme events (reflected by a shortening of the violin tails in Figure 7b). In contrast, during winter, the influence of mid-latitude systems causes large changes in the wind speed (more elongated violin whiskers).

The predominant mean wind in the GoC is northerly in the winter and southerly in summer (Figure 3a,b). The morphology of the terrain combined with the passage of cold fronts generates wind channeling (Figure 3a,b), and great wind speed variability (elongation of violin plot in Figure 7c). Extreme winds in the central and southern BCP and GoC are due to tropical cyclones, particularly in August and September, as revealed by the Pacific Hurricane season [53].

A weak synoptic forcing, in the summer, allows the enhancement of land-sea breeze in BCP which is reflected in a wind speed bimodal behavior and greater data dispersion (more elongated violin) (Figure 7d). The nocturnal component wind (without katabatic flow) is usually weaker, around 3 m/s, with respect to the diurnal sea-breeze component ( $\sim 7$  m/s), resulting in an increase in wind power ramp-up/down events (Figure 4d).



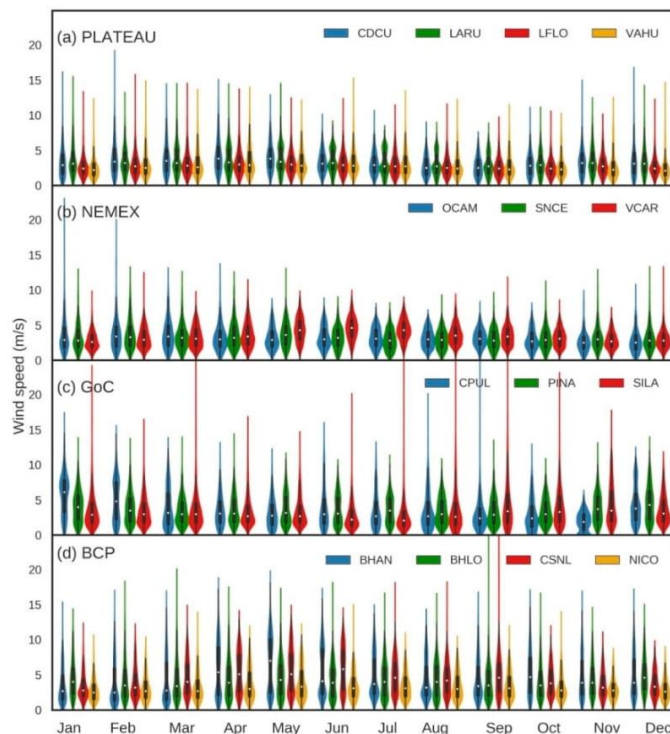


**Figure 7.** Violin plots of monthly 10 m wind speed for (a) Plateau, (b) NEMEX, (c) GoC, (d) BCP. Violin plot include a white point for the median of the data and a box indicating the interquartile range. Whiskers indicate variability outside the first and third quartile and below 1.5 times interquartile range. Outliers extend out the whiskers. Distribution of the data is shown by a kernel distribution [52].

Synoptic systems control wind power ramp events over Northern Mexico. Frontal systems and trade winds usually persist for days over the affected regions. This characteristic enables the occurrence of longer extreme events of high generation compared to sites dominated by local circulations. In the latter, the reversal of wind direction due to the thermally driven circulations increases the frequency of short-lived events of low power generation (Figure S10a,d).

The WS acting on the four regions are summarized in Table 1. The areas are classified in terms of the atmospheric system that drives wind fluctuations in the dry and wet seasons as well as topography complexity.

Local circulations play an important role over complex terrain at the end of the dry season. Wind veering and return flow are observed in the coastal complex terrain of BCP (Figure 3e,f). The circulation is strong during summer due to greater contrast between sea and land temperatures, weak large-scale flow and clear skies [54]. Over continental areas in steeper terrain, the diurnal cycle of surface heating induces baroclinicity relative to the background air causing upslope flow at the daytime and downslope flows at night, as observed over the Plateau region. This effect can also enhance sea breeze circulation over complex terrain. Therefore, the representativeness of thermal circulations in the models is essential to reproduce the variability of the wind near the surface, which depends on the proper description of the topography and land cover [13,14].

### 3.3. NAM and RAP Wind Forecasting

#### 3.3.1. Model Verification

The wind resource management requires not only the accurate prediction of wind but also that of sudden changes in wind power. The operational models, namely the NAM [27] and RAP [15] model systems, were used to assess the ability of wind forecast over the target region. A wind forecast evaluation is carried out in terms of ramp frequency and persistent high/low generation events. The 2013 forecast was selected for comparison purposes, due to the continuity and quality of the observed data during this year. Weather stations had around 98% of good quality records.

The Taylor diagram [55] summarizes the statistical parameters of correlation, standard deviation and centered root-mean-square (CRMS) difference for comparison. Wind forecasts that match the observations fall near the point on the  $x$ -axis called REF (Figure 8). The CRMS difference between forecast and observed winds is proportional to the distance to the point on the horizontal axis identified as REF. Semicircular contours indicate CRMS. At the REF point, the forecasts have a correlation of 1 and a standard deviation similar to that of the observations, which is interpreted as variations of the predicted variable of the same amplitude as observed.

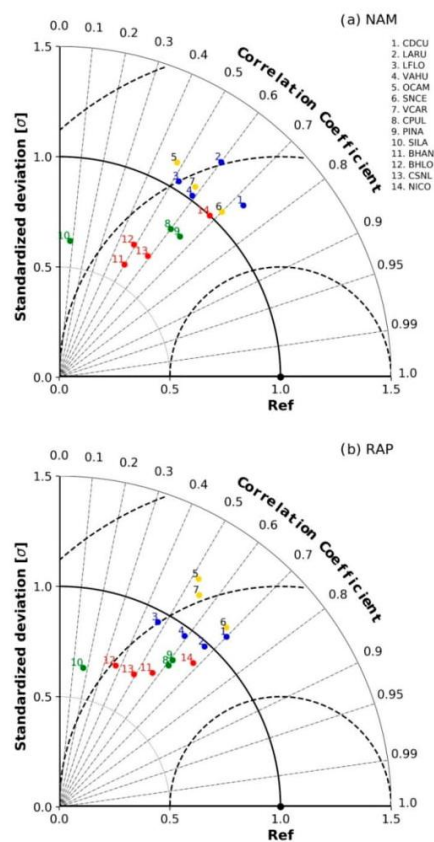


**Figure 8.** Taylor diagram for (a) NAM and (b) RAP of forecast 10 m wind speed and observations at 14 weather stations grouped in regions: Plateau (blue dots), NEMEX (yellow dots), GoC (green dots) and BCP (red dots). The radial coordinate is the magnitude of the standard deviation, which is normalized by the standard deviation from observation and denoted by black dot lines. The concentric black semi-circles denote centered root-mean-square (CRMS) difference values. The angular coordinate shows the correlation coefficient (denoted by grey dot lines).

NAM and RAP forecast metrics show a similar distribution in the Taylor diagram. A correlation pattern by regions is not found, but standard deviation pattern is observed (Figure 8). For instance, for stations located on Plateau and NEMEX, the standardized deviation ( $\sigma$ ) ranges from 0.9 to 1.1. The good forecast of wind variability in these regions is associated with the synoptic phenomena, cold fronts during the winter regime and set in of trade winds in NEMEX in summer. In the GoC region, the models show a decrease in this predictability ( $\sigma \sim 0.8$ ).

Low standardized deviation ( $<0.75$ ) is observed over complex terrain regions in the BCP (Figure 8), showing a low variability of the wind forecast by both models compared to the observed wind variability. The model accuracy can be affected by the slope of the terrain, which in the case of sites like BHAN, is smoothed out by both models (Figure 9). The representativeness of the topographic forcing is a fundamental element to reproduce the magnitude and variability of the wind [56]. The thermally driven winds are generated by horizontal temperature gradients, derived from the spatial changes in the characteristics of the terrain such as elevation, soil cover and soil moisture [57]. The inadequate description of the land surface produces differences between the observed and predicted energy budget and the respective thermal contrast.

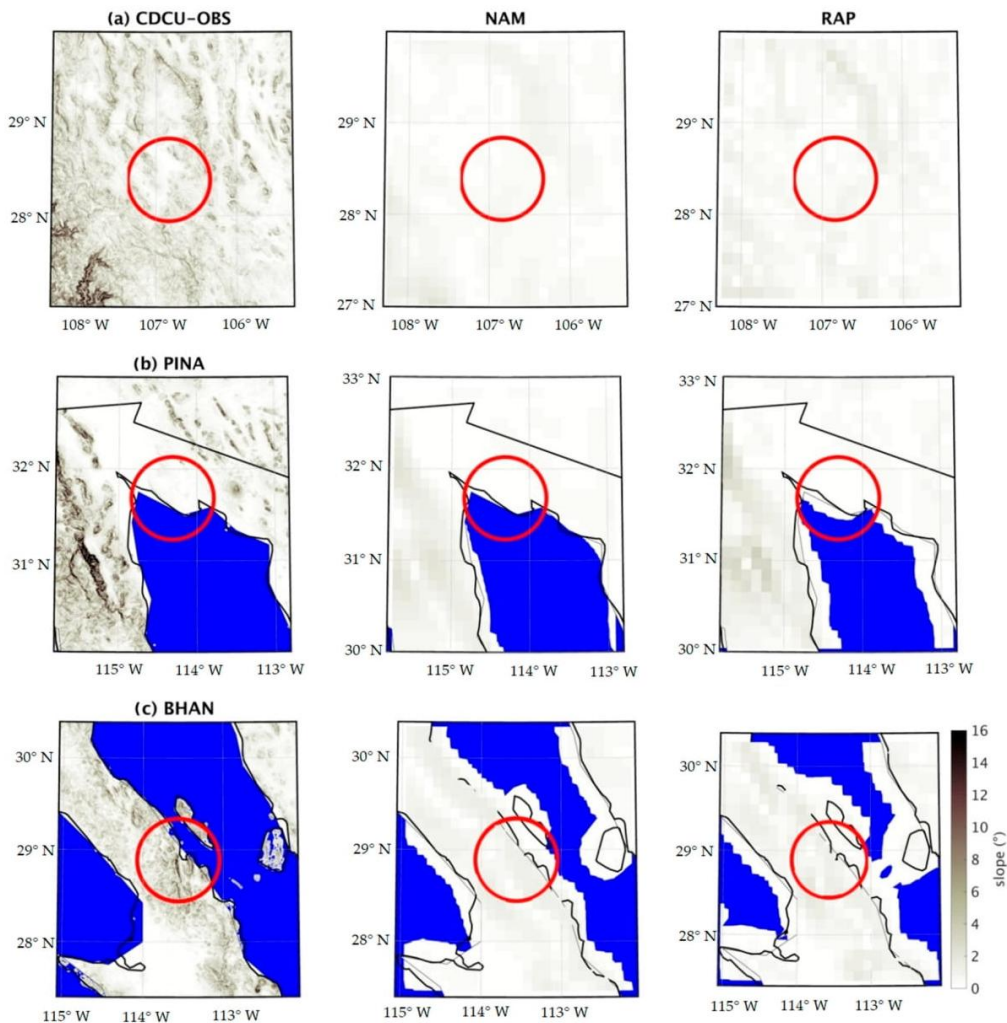


**Figure 9.** GTOPO30 [32] slope and represented slope terrain by NAM and RAP around weather stations. The red circles are 50 km in radius centered at (a) CDCU, (b) PINA and (c) BHAN weather station.



The comparison between the observed and predicted 10 m wind shows that both models tend to overestimate weak winds and to underestimate strong winds ( $>8$  m/s) (Figure 10b,c). The error is greater in weather stations with  $\sigma < 0.75$  as shown in Figure 10c for BHAN. The underestimation of winds in the planetary boundary layer may result from misrepresentation of topographic slope by the models. For instance, as the air rises over a ridge, compression of air layers accelerates the wind [58]. If the model considers the terrain smoothed out, the wind acceleration will be decreased or non-existent, forecasting weaker winds than those observed [58].

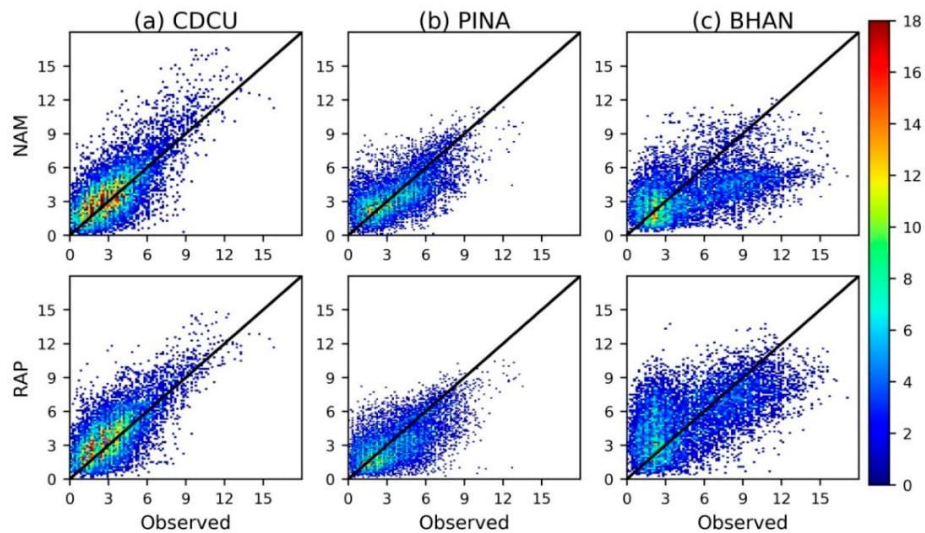


**Figure 10.** Comparisons between the 10 m wind speed between observations and NAM and RAP models in 2013 for (a) CDCU ( $1.1 < \sigma < 0.9$ ), (b) PINA ( $\sigma \sim 0.8$ ), (c) BHAN ( $\sigma \leq 0.75$ ). The number of occurrences are shown in shaded.

The annual mean absolute error (MAE) and bias vary with the characteristics of the terrain (Table 3). Over the four regions, wind speed bias in RAP is smaller than in NAM. Bias patterns by regions were not found. BCP stations located on complex topography have a MAE greater than regions with moderate and flat topography (NEMEX). A small error in wind speed can imply a large error in wind power, for that reason MAE and Bias of wind power are evaluated (Table S1 in supplementary material). MAE wind power errors range from 274 kW to 827 kW, the greatest MAE values correspond to BCP stations, with exception of NICO, in concordance with wind speed errors. NAM MAE of wind power tends to be smaller or equal than RAP MAE. There is no clear MAE tendency to increase with lead time for both models.

Jimenez and Dudhia [56] highlighted the deficiencies of the WRF model in wind forecast over regions of complex terrain, especially when there are significant differences between the actual and represented topography. An analysis of topography representativeness around the site of interest could give a deep insight into the role of topography than just considering the difference in altitude between the model and the weather station. Even if the site altitude is correct in the model, but the surrounding topography is not adequately represented (Figure 9), thermal forcing may not be captured by the models leading to an erroneous representation of local circulations and significant differences in the predicted wind (e.g., BHAN).

The valley-mountain and sea-land breeze are characterized by a diurnal inversion in the direction of flow. The accurate forecast wind direction can be a good indicator of the representation of local circulation by NAM and RAP. In general, the forecast wind direction by RAP is consistent with the observed, while NAM has deficiencies for some sites. For instance, NAM forecasts a land-sea breeze

weaker than observed in BHAN (Figure 11c). Furthermore, mountains and hills can block or channel the wind. For instance, the absence of mountains in the topographic representation of the NAM at the northeast of PINA did not block flow from this direction, as is observed (Figure 11b).

**Table 3.** Mean absolute error, bias and altitude difference for NAM and RAP in Plateau, NEMEX, GoC and BCP.

Region	Station	NAM			RAP		
		MAE (m/s)	BIAS (m/s)	$h_{obs}-h_{NAM}$ (m)	MAE (m/s)	BIAS (m/s)	$h_{obs}-h_{RAP}$ (m)
PLATEAU	CDCU	1.3	0.5	37.1	1.4	0.6	0.7
	LARU	1.5	0.5	-3.2	1.2	-0.1	6.2
	LFLO	1.3	-0.2	0.8	1.3	-0.3	7.2
	VAHU	1.3	0.2	-38.6	1.3	0.2	-55.9
NEMEX	OCAM	1.4	0.9	235.4	2.0	1.8	200.1
	SNCE	1.1	0.5	42.4	1.2	0.5	71.3
	VCAR	1.3	-0.2	683.4	1.4	0.1	695.5
GoC	CPUL	1.8	0.2	-28.8	1.8	0.1	-70.0
	PINA	1.3	-0.1	-93.41	1.4	-0.5	-72.0
	SLAG	1.7	-0.8	1224.9	1.6	-0.2	1104.4
BCP	BHAN	2.5	-1.2	-339.9	2.3	0.3	-315.3
	BHLO	2.0	-0.9	-156.1	2.2	-0.2	-84.4
	CSNL	2.0	-1.3	161.2	2.0	-0.3	41.3
	NICO	1.2	-0.2	-31.0	1.4	0.9	-2.3

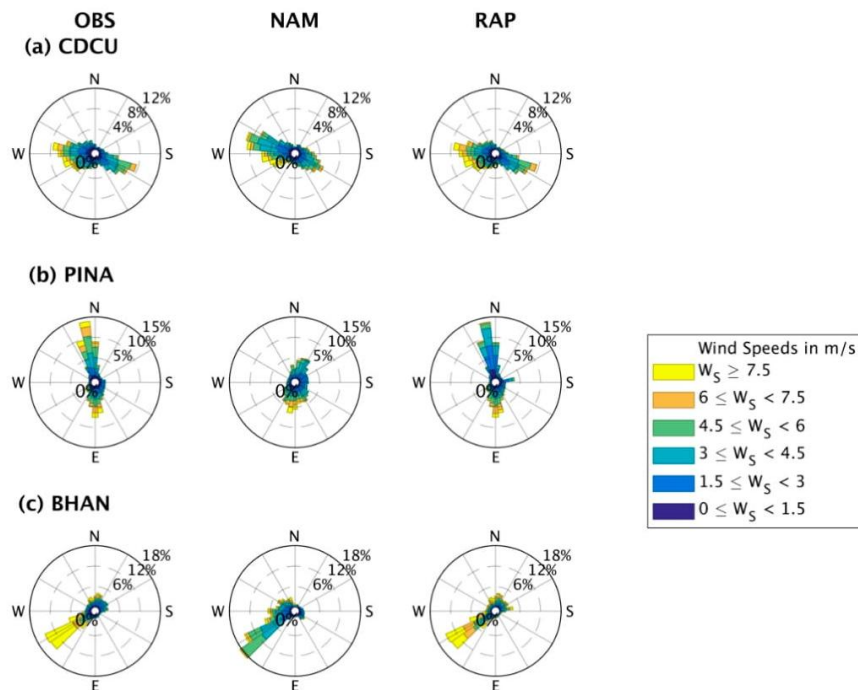


**Figure 11.** 2013 forecast and observed wind rose of hourly surface wind for (a) CDCU; (b) PINA; and (c) BHAN stations. For illustrative purposes only a good ( $1.1 < \sigma < 0.9$ ), regular ( $0.9 \leq \sigma < 0.75$ ) and low wind predictability ( $\sigma \leq 0.75$ ) station, according to the Taylor diagrams (Figure 8), is shown.

### 3.3.2. Ramp Indices

Predicting sudden wind changes can be challenging for forecast models. A model with good skill to predict wind ramps has a POD and FBIAS near 1, and a FAR near zero. NAM and RAP models show low skill to predict ramp events at the observed timing span (low POD) over the four regions. Both forecast systems tend to under forecast (FBIAS < 1) ramp events. According to ramp indices, RAP performs better than NAM in both seasons (Figure 12). There is no clear improvement in forecasting events from summer to winter.

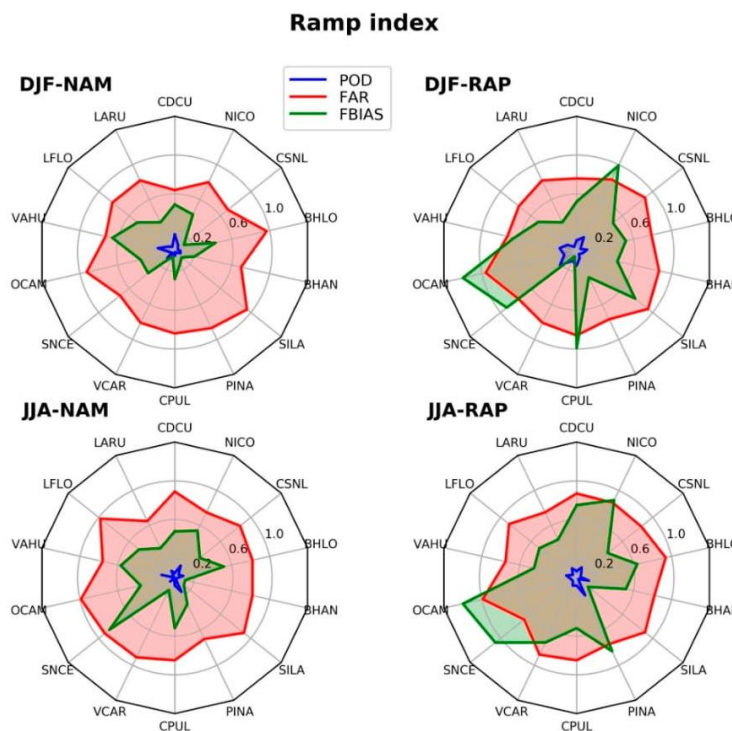


**Figure 12.** 2013 Seasonal Probability of detection (POD), False Alarm Rate (FAR) and Frequency Bias (FBIAS) metrics for forecast wind ramps by NAM and RAP models. Ramp event is defined as a variation of 20% in wind power in one hour.

The number of predicted and no-observed ramp-up events (FAR) by NAM is greater in summer than winter for NEMEX and some stations of the Plateau region (Figure 12). The establishment of trade winds on NEMEX increases the number of ramps predicted by both models, although there is no timing in the occurrence (low POD). No lag pattern was detected between observation and forecast.

Wind power ramps forecasting is improved by relaxing the time threshold for 3 h (Figure S9, in supplementary material), the number of corrected predictions increases (POD > 0.1) and the false predicted events are less frequent (FAR~0.7) in comparison to 1 h events.

The CSI is low (~0.1) for predicting power changes of 20% of rated power in 1 h over all the weather stations, which can be considered a strict threshold. Relaxing the time window, wind power ramps of the same magnitude occurring at 3 h are better predicted by NAM and RAP models. The RAP shows higher CSI than NAM, for most of the weather stations (Table 4).



**Table 4.** 2013 Critical Success Index (CSI) for wind power ramps in RAP and NAM models during December–January–February (DJF) and June–July–August (JJA) 2013. Ramps are power changes of 20% of rated power in 1 h or 3 h.

Region	Station	Critical Success Index (CSI) [RAP/NAM]			
		DJF (1 h)	JJA (1 h)	DEF (3 h)	JJA (3 h)
PLATEAU	CDCU	0.09/0.14	0.05/0.04	0.28/0.34	0.17/0.20
	LARU	0.05/0.08	0.08/0.06	0.17/0.20	0.43/0.32
	LFLO	0.09/0.06	0.04/0.01	0.21/0.21	0.12/0.11
NEMEX	VAHU	0.12/0.07	0.08/0.09	0.23/0.18	0.18/0.16
	OCAM	0.03/0.02	0.01/0.01	0.10/0.09	0.08/0.05
	SNCE	0.13/0.08	0.03/0.04	0.29/0.25	0.21/0.22
GoC	VCAR	0.06/0.01	0.05/0.01	0.21/0.06	0.11/0.05
	CPUL	0.07/0.04	0.08/0.05	0.21/0.13	0.21/0.24
	PINA	0.05/0.02	0.12/0.11	0.16/0.11	0.34/0.33
BCP	SILA	0.02/0.01	0.01/0.01	0.05/0.01	0.03/0.01
	BHAN	0.08/0.06	0.03/0.02	0.19/0.20	0.09/0.04
	BHLO	0.04/0.04	0.07/0.07	0.18/0.13	0.24/0.24
	CSNL	0.03/0.03	0.05/0.04	0.11/0.08	0.13/0.12
	NICO	0.09/0.06	0.07/0.10	0.29/0.24	0.28/0.24

### 3.3.3. Forecast of High Generation Events

Observed and forecast high generation events show similar behavior, most of the events tend to last 1 h. However, the frequency of short duration events is underestimated by both NAM and RAP (Figure 13) for the four regions. Moderate short high generation events are markedly underpredicted in Plateau and BCP, probably as a result of a misrepresentation of the thermal circulations modulating the winds around the year. The models reproduce long-lasting events (greater than 4 h) fairly well, especially over the coast along NEMEX during the trade wind establishment (Figure 13b).

As mentioned in Section 3.3.1, the comparison between the observed and predicted 10 m wind shows that both models tend to overestimate the magnitude of weak winds and to underestimate the magnitude of strong winds (>8 m/s). Therefore, low persistent events are less frequently forecasted (underestimated) by the models for all weather stations (Figure S10, in supplementary material). The prediction of high and low generation events for NEMEX is fairly good. Overall, RAP performance is better than NAM for predicting extreme generation events.

In some cases, both models overestimate events lasting 5 h, since they are unable to capture sudden short events (lasting  $\leq 1$  h). Abrupt changes in wind speed are usually missed out by the models, resulting in longer persistent events (Figure 13). Similar underestimation in the number of short-lasting events and overestimation of long-lasting events has been found using data from the MERRA global reanalysis [17]. This was deemed due to the underestimation of high-frequency variability in the modeled data [17], which might be also present in NAM and RAP.

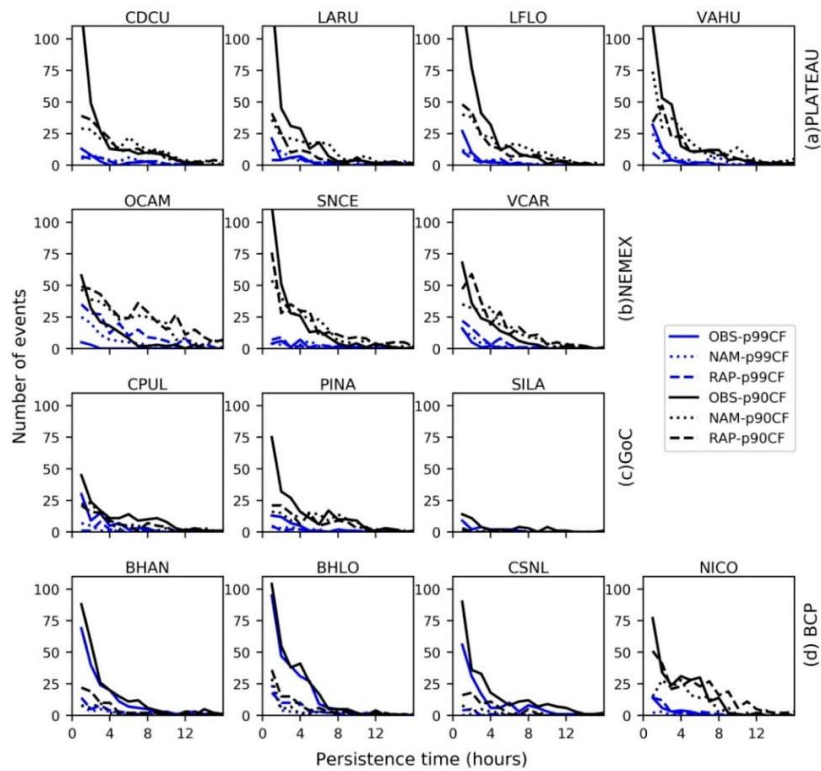


**Figure 13.** Extreme events of high generation observed (continuous line), NAM (dotted line) and RAP (dashed line) for 2013. Moderate extreme events correspond to the 90th percentile (black line) of instantaneous capacity factor (CF). Regions are (a) Plateau, (b) NEMEX, (c) GoC, (d) BCP.

#### 4. Conclusions

The efficient operation of a wind farm and its integration into the electricity grid depends on the proper evaluation of wind variability. Sharp and sudden changes in wind power (ramp events) are one of the biggest challenges the wind industry has to deal with. This paper examines daily and monthly distributions of ramp events in four regions of Northern Mexico, as well as seasonal low and high generation events. The regions are defined considering weather systems and terrain characteristics. Wind power ramp events are modulated by seasonal WS, which range from synoptic to local scale. Surface weather stations that experience thermal circulations, like those in the Plateau and BCP regions, have greater daily wind speed fluctuations and a greater occurrence of wind power ramps. Daily and monthly variations of wind ramps frequency in regions under the influence of trade winds are less pronounced. This characteristic implies less demanding management of wind power ramps. Moreover, the strength of trade winds on NEMEX in the summer leads to greater production of wind power during this part of the year. The GoC region seems to be suitable for wind farms deployment because there is persistence of 10 m wind speeds >3 m/s throughout the year (Figure 7c) and few monthly wind ramps.

Frontal and MCS are the main drivers of persistent events. Long-lasting high generation events are typical of trade winds and front passages. Meanwhile, short-lasting events of high generation are more frequent in regions experiencing thermal circulations (e.g., Plateau and BCP), and low generation events are numerous due to transitions between nocturnal and diurnal circulation.

The identification of meteorological phenomena causing wind power ramps and persistent generation events shows aspects that should be considered in the design and development of a



wind power ramp forecasting system. Microscale and mesoscale processes become relevant in sudden variations in wind power output of a single wind farm, especially over complex topography. Thermally driven circulations and storms are mesoscale events, with a horizontal extension ranging from 2 to 20 km, so they can affect a single wind farm with sudden variations in wind production. Otherwise, wind ramps of aggregate wind energy production in large areas (where groups of wind farms are distributed) are induced by synoptic phenomena such as cold fronts.

The forecasting models NAM and RAP show low ability to forecast wind variability over complex terrain ( $MAE > 2.0$  m/s;  $\sigma \leq 0.75$ ) and tend to underestimate intense winds and to overestimate weak winds, resulting in a general underestimation of high and low generation events. However, the models are able to capture long-lasting generation events with durations between 5 and 10 h. Therefore, a forecasting system for a specific wind farm must consider the atmospheric processes that originate wind ramps and high/low generation events. Northern Mexico is located in a subtropical–tropical transition region and over complex topography, so the interaction between atmospheric and topographic forcing implies further difficulties in examining variability and wind ramps in observations and models. The scale of atmospheric phenomena will define the horizontal and vertical resolution necessary for modeling as well as the configuration of physical processes settings. Evaluating whether the state-of-the-art numerical weather prediction models are able to capture ramp features accurately, as shown in this study, can be used for model validations and improvements.

**Supplementary Materials:** The following are available online at <http://www.mdpi.com/2073-4433/11/12/1281/s1>, Figure S1: Weather stations (red dot) used in the study and wind farms (black star) in operation over Mexico, Figure S2: All day (a,d,g,j), day (b,e,h,k) and night (c,f,i,l) surface windroses from CPUL and BHAN weather stations for June–July–August (JJA) and December–January–February (DJF), Figure S3: Diurnal variations of the horizontal surface vector for CPUL (a,b) and BHAN (c,d) weather station in June–July–August (JJA) and December–January–February (DJF), Figure S4: Cold front over Northern Mexico in 13 January 2013 during a ramp event in PLATEAU region. A cold front is seen as a curving line of clouds in the MODIS Corrected Reflectance imagery, Figure S5: Meteogram at CDCU for a storm of 21 July 2012, Figure S6: Example of summer ramp-up event at Ciudad Cuauhtémoc (red circle) in 21 July 2012. ERA5 surface wind speed and CMORPH daily precipitation in mm (shaded), Figure S7: Monthly mean of wind power ramp-up (dark color) and ramp-down (light color) events for (a) Plateau, (b) NEMEX, (c) GoC, (d) BCP regions. Ramp is a change of 30% or greater in rated power in 1 h, Figure S8: Example of wind power ramps ( $\geq 20\%$  of rated power) (a) observed, (b) predicted by RAP but not observed in one hour and (c) predicted by RAP and observed in 3 hours. Capacity factor is the ratio between the power generation and the rated power, Table S1: Wind power forecast Mean Absolute Error (MAE) and Bias error for 14 weather stations in 2013. Errors are in kW. Wind power was derived by extrapolating NAM, RAP and observation to 80 m and using the G114-2.5 wind power curve, Figure S9: POD, FAR and FBIAS metrics for a variation  $\geq 20\%$  of rated power in 3 hours for June–July–August (JJA) and December–January–February (DJF) 2013, Figure S10: Extreme events of low generation observed (continuous line), NAM (dotted line) and RAP (dashed line) for 2013. Extreme events correspond to the 20th percentile (black line) of instantaneous capacity factor (CF). Regions are (a) Plateau, (b) NEMEX, (c) GoC, (d) BCP.

**Author Contributions:** Conceptualization, K.P.-C. and E.C.; methodology, K.P.-C.; formal analysis, K.P.-C.; investigation, K.P.-C.; data curation, K.P.-C.; writing—original draft preparation, K.P.-C.; writing—review and editing, E.C., O.M.-A., A.L.Q.-M.; supervision, E.C. All authors have read and agreed to the published version of the manuscript.

**Funding:** This research was funded by The National Council of Science and Technology (CONACYT), grant number 473276 the first author’s PhD scholarship. OM-A’s contribution was funded by the UK National Centre for Atmospheric Science (NCAS) through the Atmospheric hazard in developing Countries: Risk assessment and Early Warning (ACREW) project (NE/R000034/1).

**Acknowledgments:** The authors are grateful to Edgar Dolores Tesillos for preparing the first figure.

**Conflicts of Interest:** The authors declare no conflict of interest. The funders had no role in the design of the study; in the collection, analyses, or interpretation of data; in the writing of the manuscript, or in the decision to publish the results.

## References

1. SENER. *Programa de Desarrollo del Sistema Eléctrico Nacional 2015–2029*; Secretaría de Energía: Ciudad de México, México, 2015; Available online: <https://www.gob.mx/sener/acciones-y-programas/programa-de-desarrollo-del-sistema-electrico-nacional-33462> (accessed on 24 September 2020).
2. DeCesaro, J.; Porter, K.; Milligan, M. Wind energy and power system operations: A review of wind integration studies to date. *Electr. J.* **2009**, *22*, 34–43. [[CrossRef](#)]
3. Greaves, B.; Collins, J.; Parkes, J.; Tindal, A. Temporal forecast uncertainty for ramp events. *Wind. Eng.* **2009**, *33*, 309–319. [[CrossRef](#)]
4. Gallego-Castillo, C.; Cuerva-Tejero, A.; Lopez-Garcia, O. A review on the recent history of wind power ramp forecasting. *Renew. Sustain. Energy Rev.* **2015**, *52*, 1148–1157. [[CrossRef](#)]
5. Cutler, N.; Kay, M.; Jacka, K.; Nielsen, T.S. Detecting, categorizing and forecasting large ramps in wind farm power output using meteorological observations and WPPT. *Wind. Energy* **2007**, *10*, 453–470. [[CrossRef](#)]
6. Bossavy, A.; Girard, R.; Kariniotakis, G. Forecasting Uncertainty Related to Ramps of Wind Power Production. In Proceedings of the European Wind Energy Conference and Exhibition 2010 (EWEC 2010), Warsaw, Poland, 20–23 April 2010; Curran Associates: Reed Hook, NY, USA, 2010; Volume 2, p. 9, ISBN 9781617823107. hal-00765885.
7. Kamath, C. Associating weather conditions with ramp events in wind power generation. In Proceedings of the 2011 IEEE/PES Power Systems Conference and Exposition, Phoenix, AZ, USA, 20–23 March 2011; pp. 1–8. [[CrossRef](#)]
8. Yang, Q.; Berg, L.K.; Pekour, M.; Fast, J.D.; Newsom, R.K.; Stoelinga, M.; Finley, C. Evaluation of WRF-predicted near-hub-height winds and ramp events over a Pacific Northwest site with complex terrain. *J. Appl. Meteorol. Clim.* **2013**, *52*, 1753–1763. [[CrossRef](#)]
9. Gallego, C.; Cuerva, A.; Costa, A. Detecting and characterising ramp events in wind power time series. *J. Physics: Conf. Ser.* **2014**, *555*, 012040. [[CrossRef](#)]
10. Cui, M.; Zhang, J.; Florita, A.R.; Hodge, B.-M.; Ke, D.; Sun, Y. An optimized swinging door algorithm for identifying wind ramping events. *IEEE Trans. Sustain. Energy* **2016**, *7*, 150–162. [[CrossRef](#)]
11. Bianco, L.; Djalalova, I.V.; Wilczak, J.M.; Cline, J.; Calvert, S.; Konopleva-Akish, E.; Finley, C.; Freedman, J. A wind energy ramp tool and metric for measuring the skill of numerical weather prediction models. *Weather. Forecast.* **2016**, *31*, 1137–1156. [[CrossRef](#)]
12. Smith, N.H.; Ancell, B.C. Variations in parametric sensitivity for wind ramp events in the Columbia river basin. *Mon. Weather. Rev.* **2019**, *147*, 4633–4651. [[CrossRef](#)]
13. Siuta, D.; West, G.; Stull, R. WRF Hub-height wind forecast sensitivity to PBL scheme, grid length, and initial condition choice in complex terrain. *Weather. Forecast.* **2017**, *32*, 493–509. [[CrossRef](#)]
14. Deppe, A.J.; Gallus, W.A.; Takle, E.S. A WRF Ensemble for improved wind speed forecasts at turbine height. *Weather. Forecast.* **2013**, *28*, 212–228. [[CrossRef](#)]
15. Benjamin, S.G.; Weygandt, S.S.; Brown, J.M.; Hu, M.; Alexander, C.R.; Smirnova, T.G.; Olson, J.B.; James, E.P.; Dowell, D.C.; Grell, G.A.; et al. A North American hourly assimilation and model forecast cycle: The rapid refresh. *Mon. Weather. Rev.* **2016**, *144*, 1669–1694. [[CrossRef](#)]
16. Archer, C.L.; Colle, B.A.; Monache, L.D.; Dvorak, M.J.; Lundquist, J.K.; Bailey, B.H.; Beaucage, P.; Churchfield, M.J.; Fitch, A.C.; Kosovic, B.; et al. Meteorology for coastal/offshore wind energy in the united states: Recommendations and research needs for the next 10 years. *Bull. Am. Meteorol. Soc.* **2014**, *95*, 515–519. [[CrossRef](#)]
17. Cannon, D.; Brayshaw, D.; Methven, J.; Coker, P.; Lenaghan, D. Using reanalysis data to quantify extreme wind power generation statistics: A 33 year case study in Great Britain. *Renew. Energy* **2015**, *75*, 767–778. [[CrossRef](#)]
18. Musilek, P.; Li, Y. Forecasting of wind ramp events-Analysis of cold front detection. In Proceedings of the 31st International Symposium on Forecasting, Prague, Czech Republic, 26–29 June 2011.
19. Ohba, M.; Kadokura, S.; Nohara, D. Impacts of synoptic circulation patterns on wind power ramp events in East Japan. *Renew. Energy* **2016**, *96*, 591–602. [[CrossRef](#)]
20. Sherry, M.; Rival, D.E. Meteorological phenomena associated with wind-power ramps downwind of mountainous terrain. *J. Renew. Sustain. Energy* **2015**, *7*, 033101. [[CrossRef](#)]



21. Walton, R.A.; Gallus, W.A.; Takle, E.S. Wind ramp events at turbine height-spatial consistency and causes at two Iowa wind farms. In Proceedings of the 4th Conference Weather, Climate, New Energy Economy, Austin, TX, USA, 5–10 January 2013; pp. 1–7.
22. Colle, B.A.; Mass, C.F. The structure and evolution of cold surges east of the Rocky Mountains. *Mon. Weather. Rev.* **1995**, *123*, 2577–2610. [[CrossRef](#)]
23. Fitzjarrald, D.R. Slope wind in Veracruz. *J. Clim. Appl. Meteorol.* **1986**, *25*, 133–144. [[CrossRef](#)]
24. Carvalho, D.; Rocha, A.; Gómez-Gesteira, M.; Santos, C.S. A sensitivity study of the WRF model in wind simulation for an area of high wind energy. *Environ. Model. Softw.* **2012**, *33*, 23–34. [[CrossRef](#)]
25. Carvalho, D.; Rocha, A.M.A.C.; Gómez-Gesteira, M.; Santos, C.S. Sensitivity of the WRF model wind simulation and wind energy production estimates to planetary boundary layer parameterizations for onshore and offshore areas in the Iberian Peninsula. *Appl. Energy* **2014**, *135*, 234–246. [[CrossRef](#)]
26. Draxl, C.; Hahmann, A.N.; Peña, A.; Giebel, G. Evaluating winds and vertical wind shear from Weather Research and Forecasting model forecasts using seven planetary boundary layer schemes. *Wind. Energy* **2014**, *17*, 39–55. [[CrossRef](#)]
27. Rogers, E.; DiMego, G.; Black, T.; Ek, M.; Ferrier, B.; Gayno, G.; Janjic, Z.; Lin, Y.; Pyle, M.; Wong, V. The NCEP North American mesoscale modeling system: Recent changes and future plans. In Proceedings of the 23rd Conference on Weather Analysis and Forecasting and 19th Conference on Numerical Weather Prediction, Omaha, NE, USA, 1–5 June 2009; p. 2A.4.
28. Hernandez-Escobedo, Q.; Manzano-Agugliaro, F.; Zapata-Sierra, A. The wind power of Mexico. *Renew. Sustain. Energy Rev.* **2010**, *14*, 2830–2840. [[CrossRef](#)]
29. James, E.P.; Benjamin, S.G.; Marquis, M. A unified high-resolution wind and solar dataset from a rapidly updating numerical weather prediction model. *Renew. Energy* **2017**, *102*, 390–405. [[CrossRef](#)]
30. Li, A.K.; Paek, H.; Yu, J.-Y. The changing influences of the AMO and PDO on the decadal variation of the Santa Ana winds. *Environ. Res. Lett.* **2016**, *11*, 64019. [[CrossRef](#)]
31. Bingoel, F. Complex Terrain and Wind Lidars. Ph.D. Thesis, Technical University of Denmark, Risoe National Laboratory for Sustainable Energy, Roskilde, DK, USA, 2019.
32. *USGS 30 ARC-second Global Elevation Data, GTOPO30 1997*; USGS: Reston, VA, USA, 1997. [[CrossRef](#)]
33. Skamarock, W.C.; Klemp, J.B.; Dudhia, J.; Gill, D.O.; Barker, D.M.; Duda, M.G.; Huang, X.Y.; Wang, W.; Powers, J.G. A description of the advanced research WRF Version 3, mesoscale and microscale meteorology division. *Natl. Cent. Atmos. Res. Boulder Color. USA* **2008**, *88*, 7–25.
34. Wu, W.-S.; Purser, R.J.; Parrish, D.F. Three-dimensional variational analysis with spatially inhomogeneous covariances. *Mon. Weather. Rev.* **2002**, *130*, 2905–2916. [[CrossRef](#)]
35. Henry, W.K. Some aspects of the fate of cold fronts in the gulf of Mexico. *Mon. Weather. Rev.* **1979**, *107*, 1078–1082. [[CrossRef](#)]
36. Perez, E.P.; Magana, A.V.; Caetano, E.; Kusunoki, S. Cold surge activity over the Gulf of Mexico in a warmer climate. *Front. Earth Sci.* **2014**, *2*. [[CrossRef](#)]
37. Dominguez, C.; Done, J.M.; Bruyère, C.L. Easterly wave contributions to seasonal rainfall over the tropical Americas in observations and a regional climate model. *Clim. Dyn.* **2019**, *54*, 191–209. [[CrossRef](#)]
38. Hersbach, H.; Bell, B.; Berrisford, P.; Hirahara, S.; Horányi, A.; Muñoz-Sabater, J.; Nicolas, J.; Peubey, C.; Radu, R.; Schepers, D.; et al. The ERA5 global reanalysis. *Q. J. R. Meteorol. Soc.* **2020**, *146*, 1999–2049. [[CrossRef](#)]
39. Monin, A.S.; Obukhov, A.M. Basic Laws of Turbulent Mixing in the Atmosphere near the Ground. *Tr. Akad. Nauk SSSR Geofiz. Inst.* **1954**, *24*, 163–187.
40. Stull, R. *An Introduction to Boundary Layer*, 1st ed.; Kluwer Academic Publishers: Dordrecht, The Netherlands, 2013; p. 666.
41. International Electrotechnical Commission. *Wind Turbines-Part. 1: Design Requirements, IEC 614001*, 3rd ed.; International Electrotechnical Commission: Geneva, Switzerland, 2005.
42. Hernández-Escobedo, Q.; Saldaña-Flores, R.; Rodríguez-García, E.; Manzano-Agugliaro, F. Wind energy resource in Northern Mexico. *Renew. Sustain. Energy Rev.* **2014**, *32*, 890–914. [[CrossRef](#)]
43. Kamath, C. Understanding wind ramp events through analysis of historical data. In Proceedings of the IEEE PES T&D 2010, Sao Paolo, Brazil, 8–10 November 2010; pp. 1–6.

44. Bradford, K.T.; Carpenter, R.L.; Shaw, B.L. Forecasting southern plains wind ramp events using the WRF Model At 3-Km. In Proceedings of the 9th Annual Student Conference of the American Meteorological Society, Atlanta, GA, USA, 16 January 2010; pp. 1–10.
45. Wilks, D.S. *Statistical Methods in the Atmospheric Science*, 2nd ed.; Elsevier: Burlington, MA, USA, 2006; ISBN 0-12-064490-8.
46. Magaña, V.; Amador, J.A.; Medina, S. The midsummer drought over Mexico and Central America. *J. Clim.* **1999**, *12*, 1577–1588. [[CrossRef](#)]
47. Schultz, D.M.; Bracken, W.E.; Bosart, L.F. Planetary-and synoptic-scale signatures associated with Central American cold surges. *Mon. Weather. Rev.* **1998**, *126*, 5–27. [[CrossRef](#)]
48. Manzanilla, A.V. Mesoscale convective systems in NW Mexico during the strong ENSO events of 1997–1999. *Atmósfera* **2015**, *28*, 143–148. [[CrossRef](#)]
49. Manzanilla, A.V.; Vázquez, M.C.; Francisco, J.J.P. Un estudio explorativo de los Sistemas Convectivos de Mesoescala de Mexico. *Investig. Geográficas* **2012**, *26*. [[CrossRef](#)]
50. Badan-Dangon, A.; Dorman, C.E.; Merrifield, M.A.; Winant, C.D. The lower atmosphere over the Gulf of California. *J. Geophys. Res. Space Phys.* **1991**, *96*, 16877–16896. [[CrossRef](#)]
51. Zhang, S.; Solari, G.; De Gaetano, P.; Burlando, M.; Repetto, M.P. A refined analysis of thunderstorm outflow characteristics relevant to the wind loading of structures. *Probabilistic Eng. Mech.* **2018**, *54*, 9–24. [[CrossRef](#)]
52. Parzen, E. On Estimation of a probability density function and mode. *Ann. Math. Stat.* **1962**, *33*, 1065–1076. [[CrossRef](#)]
53. Martínez-Sánchez, J.; Cavazos, T. Eastern Tropical Pacific hurricane variability and landfalls on Mexican coasts. *Clim. Res.* **2014**, *58*, 221–234. [[CrossRef](#)]
54. Morales-Acuña, E.; Torres, C.R.; Linero-Cueto, J.R. Surface wind characteristics over Baja California Peninsula during summer. *Reg. Stud. Mar. Sci.* **2019**, *29*, 100654. [[CrossRef](#)]
55. Taylor, K.E. Summarizing multiple aspects of model performance in a single diagram. *J. Geophys. Res. Space Phys.* **2001**, *106*, 7183–7192. [[CrossRef](#)]
56. Jiménez, P.A.; Dudhia, J. Improving the representation of resolved and unresolved topographic effects on surface wind in the WRF model. *J. Appl. Meteorol. Clim.* **2012**, *51*, 300–316. [[CrossRef](#)]
57. Parker, D.J. Mesoscale meteorology overview. *Encycl. Atmos. Sci.* **2015**, 316–322. [[CrossRef](#)]
58. Zardi, D.; Whiteman, C.D. Diurnal mountain wind systems. In *Mountain Weather Research and Forecasting*; Chow, F., De Wekker, S., Snyder, B., Eds.; Springer: Dordrecht, The Netherlands, 2013; pp. 35–119. ISBN 978-94-007-4098-3.

**Publisher's Note:** MDPI stays neutral with regard to jurisdictional claims in published maps and institutional affiliations.



© 2020 by the authors. Licensee MDPI, Basel, Switzerland. This article is an open access article distributed under the terms and conditions of the Creative Commons Attribution (CC BY) license (<http://creativecommons.org/licenses/by/4.0/>).

## Capítulo 4. Sensibilidad del pronóstico de viento a la parametrización de capa límite en el modelo Weather Research and Forecasting (WRF)

### Artículo de investigación

#### " WRF wind forecast over coastal complex terrain: Baja California Peninsula (Mexico) case study"

(Pereyra-Castro, Caetano, y Altamirano del Razo, 2021)

**Resumen.** Se examina la sensibilidad del pronóstico del viento en superficie al esquema de la capa límite planetaria (PBL) usando el modelo Weather Research and Forecasting (WRF) sobre un terreno complejo de la península de Baja California, México. Los esquemas de PBL de Yonsei University (YSU), Mellor-Yamada-Janjic (MYJ) y el Modelo convectivo asimétrico versión 2 (ACM2) se evalúan mediante el diagrama de Taylor, el Índice de Acierto del Error Absoluto Medio (MAESS) y la anomalía estandarizadas de error absoluto medio. Además, se analiza la distribución prevista de rampas de viento. El esquema YSU mejora la precisión del pronóstico en invierno para la mayoría de las estaciones meteorológicas. Mientras tanto, durante el verano, el rendimiento de los esquemas de PBL varía según el entorno fisiográfico de la estación meteorológica. El pronóstico WRF tiende a generar un mayor número de eventos de rampa de viento ascendentes/descendentes que los observados en el rango de 2 m/s. Todos los esquemas de PBL reproducen bien el comportamiento diurno de la velocidad del viento; sin embargo, la variabilidad de la velocidad del viento es más suave que la observada. La capacidad del esquema ACM2 para funcionar bien en invierno y verano puede estar relacionada con el factor crítico que determina la relación de contribución de la mezcla no local a la mezcla turbulenta total. El WRF es capaz de pronosticar con precisión el espectro de energía de escala sinóptica en invierno; sin embargo, en el rango de mesoescala, el espectro simulado subestima la energía para ambas estaciones.





# WRF wind forecast over coastal complex terrain: Baja California Peninsula (Mexico) case study

Karla Pereyra-Castro<sup>1</sup> · Ernesto Caetano<sup>2</sup> · Diego Altamirano del Razo<sup>3</sup>

Received: 31 March 2021 / Accepted: 23 August 2021 / Published online: 8 September 2021  
© Saudi Society for Geosciences 2021

## Abstract

Weather Research and Forecasting (WRF) near surface wind forecast sensitivity to planetary boundary layer (PBL) scheme over complex terrain of Baja California Peninsula, México, is examined. Yonsei University (YSU), Mellor-Yamada-Janjic (MYJ), and Asymmetric Convective Model version 2 (ACM2) PBL schemes are evaluated using the Taylor diagram, mean absolute error skill score (MAESS), and mean absolute error standardized anomaly metrics. Additionally, forecasted wind ramp distribution is analyzed. YSU scheme improves forecast accuracy in winter for most of the weather stations. Meanwhile, during summer, the performance of PBL schemes varies depending on physiographical environment of the weather station site. WRF forecast tends to generate a greater number of up/down wind ramp events than observed in the range of 2 m/s. The diurnal behavior of wind speed is well reproduced by all PBL schemes; however, the wind speed variability is smoother than the observed. The ability of the ACM2 scheme to perform well in winter and summer may be related to the critical factor that determines the contribution ratio of non-local mixing to total turbulent mixing. The WRF is capable of accurately forecasting the synoptic-scale energy power spectrum in winter; however, in the mesoscale range, the simulated spectrum underestimates the energy for both seasons.

**Keywords** PBL scheme · Power spectrum · Coastal complex terrain · WRF model

## Introduction

The necessity of reducing carbon dioxide emissions into the atmosphere has encouraged countries to move towards renewable energies. The use of clean energy sources is an advantage for local economies and promotes energy independence. The

need to import fossil fuels produces dependence on the economic and political circumstances of the supplier country that can compromise the energy supply national security.

Another reason to invest in renewable energies is that the costs of renewable energies evolve steadily downwards, while the general trend of costs for fossil fuels is the opposite (IRENA 2020). In relation to environment protection, the Energy Transition Law contemplates that the energy consumed coming from clean sources in Mexico will be about 35% by 2024 and covers up to 60% of the demand in 2050 (SENER 2018). One downside of renewable energies is the intermittent generation such as the wind power. This condition represents a challenge for its integration into the electrical system. In the case of Mexico, seasonal and diurnal wind variability is associated with meteorological systems ranging from the synoptic scale to the mesoscale (Pereyra-Castro et al. 2020). The knowledge of the variability of the wind resource and the adequate prediction of its fluctuations can contribute to reduce the uncertainty of electricity generation and maintain the balance of the electrical system.

Numerical prediction models are capable of producing high-resolution wind data; however, proper modeling of

---

This paper was selected from the 3rd Conference of the Arabian Journal of Geosciences (CAJG), Tunisia 2020

---

Responsible Editor: Zhihua Zhang

✉ Ernesto Caetano  
caetano@unam.mx

<sup>1</sup> Posgrado en Ciencias de la Tierra, Universidad Nacional Autónoma de México, Circuito de la Investigación Científica, 04510 Ciudad de México, México

<sup>2</sup> Instituto de Geografía, Universidad Nacional Autónoma de México, Circuito de la Investigación Científica, 04510 Ciudad de México, México

<sup>3</sup> Facultad de Ingeniería, Universidad Nacional Autónoma de México, Circuito de la Investigación Científica, 04510 Ciudad de México, México

atmospheric flows near the surface and their interaction with the topography is a challenge that is being worked on, particularly at sites of complex topography (Siuta et al. 2017; Olson et al. 2019). For instance, the Wind Forecast Improvement Project 2 (WFIP 2) (Draxl et al. 2014; Olson et al. 2019) aims to improve short-term weather forecast and understand physical processes such as stability, turbulence, and low-level jet that affect wind energy generation in complex terrain regions, such as coastlines, mountains, and canyons (Olson et al. 2019).

The adequate prediction of near surface winds is related to the representation of atmospheric processes in the planetary boundary layer (PBL). Several studies have studied the effects of WRF PBL physics parameterization on wind forecasts (Carvalho et al. 2012, 2014; Deppe et al. 2013; Menendez et al. 2014; Hahmann et al. 2015; Siuta et al. 2017). The PBL sensitivity depends on atmospheric stability, terrain type, and weather systems affecting the region (Carvalho et al. 2014; Draxl et al. 2014).

For this reason, the PBL schemes need to be evaluated over the region of interest. In this study, the wind sensitivity to PBL schemes for the Baja California Peninsula (BCP, Fig. 1) is examined. BCP is located in the semi-arid complex terrain region of northwestern Mexico, crossed

by a mountain range forming a nearly continuous barrier including Sierra Juarez and Sierra La Laguna. Along the west coast lies the southward cold California current and along the east coast the Gulf of California. The interaction of slope terrain and inhomogeneous land cover results in the enhancement of katabatic winds and sea-land breeze, under a weak synoptic forcing in summer (Turrent and Zaitsev 2014; Torres et al. 2016; Morales-Acuña et al. 2019; Pereyra-Castro et al. 2020). Therefore, for assessing wind power resources, it is important to determine which PBL scheme has the best performance to predict the wind speed and its variability for summer and winter months. To address this question, short-term deterministic evaluation of wind speed is done using 24-h WRF simulation in forecasting mode over the region. Additionally, mean absolute error skill score and standardized anomaly of MAE metrics are calculated. The ramp prediction is assessed in terms of magnitude, frequency, and duration.

The rest of this paper is organized as follows. The “Method” section describes the methodology used, including the WRF model setup and a brief description of the initial conditions. The “Results and discussion” section presents the results for the study period, and discussions about the weather systems affecting the

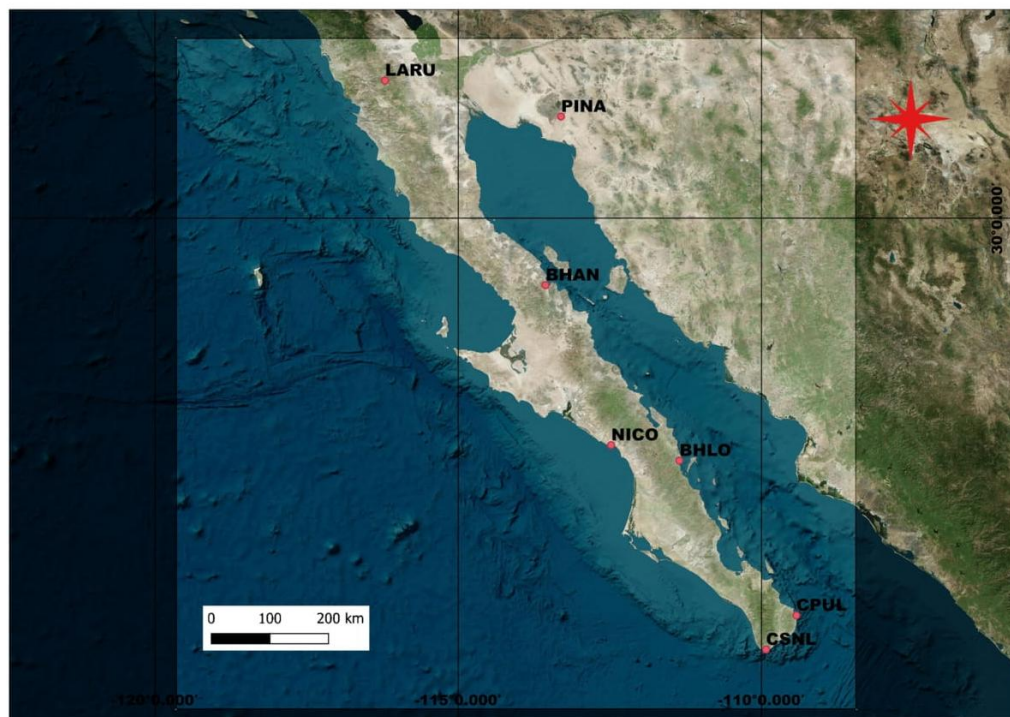


**Fig 1** Study region and WRF domain. Weather stations: Bahía de los Ángeles (BHAN), Bahía de Loreto (BHLO), Cabo Pulmo (CPUL), Cabo San Lucas (CSNL), La Rumorosa (LARU), San Juanico (NICO), El Pinacate (PINA)



wind variability. Conclusions are provided in the “Conclusion” section.

## Method

### Model configuration

The WRF model version 3.9.1 with 4-km horizontal grid was applied to produce 24-h wind forecast for January and June 2013 using the Mellor–Yamada–Janjic (MYJ) (Janjic 1994), the Asymmetric Convective Model, version 2 (ACM2) (Pleim 2007a, b), and the Yonsei University (YSU) (Hong et al. 2006) PBL parameterizations. The WRF domain and configuration used are shown in Fig. 1 and Table 1, respectively. Experiments were initialized with the 0000 UTC 12-km North American Mesoscale Forecast System (NAM), allowing a 12-h model spin-up. Spin-up times generally range from 6 to 12 h (Warner 2010). NAM model is run by National Centers for Environmental Prediction for 36 h weather forecasting with hourly output. Vertical levels have a finer resolution in the PBL, with 6 levels under 120 m and 31 levels in total. The lowest model sigma levels are at 1.0, 0.998806, 0.9976, 0.99522, 0.99284, 0.99045, and 0.98807. Forecast variable was extracted from the nearest neighboring grid point to the location of the weather stations.

The atmospheric circulation and weather conditions of BCP are driven by mid-latitude weather systems in winter and tropical weather systems in summer. The passage of the frontal systems from mid-latitudes in winter causes intense and persistent northwesterly wind events lasting 3 to 6 days (Badan-Dangon et al. 1991). The low-level circulation is influenced by the North Pacific High westward displacement during the winter. In the absence of cold fronts, the sea-breeze circulation is the meteorological system dominant in Baja California Peninsula. The intensity of the land breeze depends on the contrast between the continental temperature

and the surface temperature of adjacent seas (Badan-Dangon et al. 1991). The Baja California Peninsula is surrounded by two water bodies of different temperatures. During the night, the Pacific Ocean is relatively colder than the Gulf of California; the difference in temperature produces relatively higher pressure over the Pacific Ocean, generating a land breeze from the mainland towards the Gulf of California (Turrent and Zaitsev 2014). Meanwhile, in summer, the region is affected by the North American Monsoon and tropical systems. Diurnal near surface wind distribution over BCP is associated with the thermal contrasts of surrounding water bodies and the complex topography of the region (Morales-Acuña et al. 2019).

In order to assess the seasonal WRF model performance to reproduce the low-level winds, we ran two groups of simulations for boreal winter (January 2013) and boreal summer (June 2013). The months of January and June were chosen because they are representative of the respective seasons (see Fig. S1 for more details). In January, the mid-latitude weather regime is predominant meanwhile in summer prevails the tropical regime. Three PBL parametrization schemes were tested to evaluate the model accuracy to generate the meteorological conditions of each station. The WRF model is frequently used for wind and wind potential studies. Among the difficulties inherent in modeling the atmosphere is the representation of the sub-scale grid PBL processes. The most suitable physical configuration for a region depends on local atmospheric conditions and other characteristics such as topography, seasonal changes in land cover, and regional atmospheric circulation. Hence, a sensitivity study to the PBL scheme is essential in the configuration of the model for climatological studies.

### Weather stations

Ten-meter wind hourly averaged measurements from seven weather stations along the BCP (Table 2) were used to evaluate the WRF forecast. The complexity of the terrain may cause

**Table 1** WRF model settings used in the experiments

Model details	Settings
WRF core	ARW 3.9.1
Horizontal grid	4 km
Vertical grid	31 levels
Land Surface	Noah (Chen and Dudhia 2001)
Microphysics	WRF single-moment 3-class (Hong et al. 2004)
Cumulus	Kain-Fritsch (Kain 2004)
Shortwave radiation	Dudhia (Dudhia 1989)
Longwave radiation	Rapid Radiative Transfer Model (Mlawer et al. 1997)
Planetary boundary layer scheme	YSU,MYJ, ACM2



**Table 2.** List of weather stations used for forecast verification on Baja California Peninsula. The local altitude (m) and WRF altitude (m) at the nearest grid point to weather station are shown

Weather station	ID	Altitude (m)	Altitude (m) at the nearest point
Bahía de los Ángeles	BHAN	10	56.7
Bahía de Loreto	BHLO	25	9.1
Cabo Pulmo	CPUL	26	4.79
Cabo San Lucas	CSNL	224	24.2
La Rumorosa	LARU	1262	1288.9
El Pinacate	PINA	100	114.0
San Juanico	NICO	36	39.5

wind channeling and kata- or anabatic flows at some locations that may affect the PBL structure and its wind field substantially from one station to another.

### Verification metrics

Deterministic forecast performance was addressed through the following metrics: standardized deviation, correlation, and centered root-mean-square. The metrics are summarized in Taylor Diagram (Taylor 2001) for June and January 2013. The best forecast has standardized deviation near to 1, correlation near to 1, and CRMS near to 0. The Taylor diagram provides a visual framework to compare the PBL scheme ability to reproduce the evolution of surface winds over the seven sites for each month analysis. Further exploration of PBL sensitivity was made through calculation of mean absolute error (MAE) scores, the standardized anomaly or  $z$  score, and MAE skill score (MAESS). The first compares the MAE of each scheme ( $MAE_{scheme}$ ) to the mean MAE of all schemes ( $MAE_{all\ schemes}$ ) divided by the standard deviation of the scheme ( $S_{MAE\ scheme}$ ). Negative values indicate configurations performing better than the average MAE. MAESS measures the accuracy of a forecast ( $MAE_{scheme}$ ) with reference to the PBL scheme forecast with the lowest MAE ( $MAE_{reference}$ ).  $MAE_{perfect}$  is the value of forecast achieved by the perfect forecast (MAE = 0). A forecast is good when MAESS has large positive values.

$$MAE_{standardized\ anomaly} = \frac{MAE_{scheme} - \overline{MAE_{all\ schemes}}}{S_{MAE\ scheme}} \quad (1)$$

$$MAESS = \frac{MAE_{scheme} - MAE_{reference}}{MAE_{perfect} - MAE_{reference}} \quad (2)$$

The comparison of wind ramp distribution is made for every PBL scheme. There are many definitions of ramps (Bossavy et al. 2010) according to their magnitude, duration, and timing. Most definitions of ramps are established considering a change in the power produced by a hypothetical wind turbine. Here, a wind ramp is defined as a change in wind speed (of any magnitude) over a time span (increase/decrease

in wind speed over a period of 1 to 16 h, Bossavy et al. 2010). The change can be positive (ramp-up) or negative (ramp-down). The analysis shows the scheme that better reproduces wind speed fluctuations for January and June 2013.

### PBL schemes

The parameterization schemes describe the contributions made from unresolved atmospheric phenomena at the model grid points. The goal of a turbulence parameterization is to predict the trends of the forecast variables at all grid points of a numerical model due to unresolved turbulent motions. PBL schemes parameterize the turbulent layer that develops over the Earth's surface due to surface heating, wind shear, and friction. Vertical transports of heat, moisture, and momentum are driven by PBL processes (Stull 2012). They are classified as non-local and local closure schemes. Local closure schemes use variables and parameters defined at each model level or its neighboring (adjacent) levels, while non-local closure schemes use parameters that can depend on the whole vertical profile (García-Díez et al. 2013). A short description of the tested PBL schemes follows:

The YSU scheme expresses nonlocal mixing by adding a nonlocal adjustment term to the local gradient at the mean of each forecast variable (Hong et al. 2006). One of the main ingredients of the YSU algorithm is the explicit treatment of drag processes on top of the PBL. This top is determined by the level at which minimum turbulent flux exists (heat, momentum, moisture). The ACM2 scheme contains fluxes from the surface and flows of heat, moisture, and moment to/from the adjacent vertical layer. ACM2 is a combined nonlocal transient turbulence scheme (Stull 2012), with local eddy diffusivity during stable conditions and combined local and non-local transport in unstable conditions (Pleim 2007a). The scheme includes a critical factor that determines the contribution ratio of non-local mixing to total mixing. The MYJ (Janjić 1994) scheme is a local mixing, 1.5-order closure, that

prognostics turbulent kinetic energy (TKE). It is used operationally in the NAM (Siuta et al. 2017). Local closure schemes determine eddy diffusivity from prognostic TKE. Small turbulent eddies' contribution is accounted for TKE distribution.

## Results and discussion

### Statistical scores

The Taylor diagram shows a diagnosis of the performance of the boundary layer schemes for each of the meteorological stations (Fig. 2). The numbers indicate the weather stations and the colors the boundary layer schemes. For January 2013 (Fig. 2a), the YSU scheme provides the best forecast, that is, highest accuracy and correlation and similar standard deviation of observations at most weather stations. Exceptions are CPUL and CSNL, where the ACM2 scheme forecast is closest to the observed wind speed standard deviation. Forecast performance for CPUL, CSNL, and PINA stations are differentiated by their standardized deviation but theirs exhibit small differences among the three PBL schemes. According to the Taylor diagram, ACM2 and MYJ schemes show similar skill to forecast 10-m wind speed.

In June 2013 (Fig. 2b), the sensitivity of the surface wind to the election of the boundary layer scheme is higher according to the Taylor diagram (the data is less concentrated). There are subtle differences in the PBL schemes performance for stations BHLO and CPUL. However, the differences in correlation and accuracy (CRMS) are significant in stations CSNL and PINA. The schemes with the best performance in these stations were ACM2 and MYJ.

The potential for improvement in forecast accuracy under different PBL schemes can be examined by calculating MAESS (Fig. 3). Daily worst forecast is compared with the other two schemes and the average percentage of improvement for every scheme is calculated. Days with the lowest performance are included in the average to account for a general skill over the month. Averaging just days with good performance can conduct to overvaluation of PBL scheme. For January 2013 (Fig. 3a), the YSU scheme forecast shows the MAE maximum potential of improvement in BHLO and LARU stations (more than 35%). Meanwhile, for BHAN and NICO stations, forecast improvement is around 20% by choosing the MYJ scheme. Subtle sensitivity to PBL scheme is observed in CSNL. Finally, ACM2 and YSU schemes show similar performance for CPUL and PINA stations. MAESS is the greatest with more than 32% in those sites and the difference with the other scheme is significant. For June 2013 (Fig. 3b), the MYJ scheme presents better skill at most weather stations with exception of BHAN and BHLO. Significant differences (more than 10%) between MAESS due to the choice

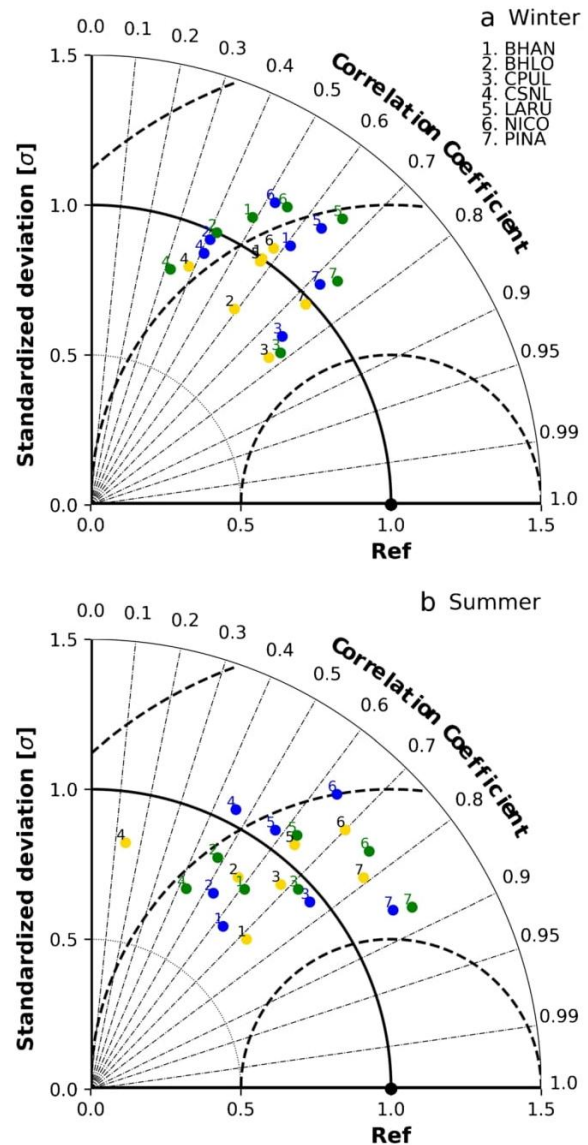


**Fig. 2** Taylor diagram for (a) January and (b) June 2013 forecast of 10 m wind speed and observations for seven weather stations at Baja California Peninsula (1 BHAN, 2 BHLO, 3 CPUL, 4 CSNL, 5 LARU, 6 NICO, 7 PINA). PBL schemes are ACM2 (blue dot), YSU scheme (yellow dot), and MYJ scheme (green dot). The radial coordinate is the model normalized standard deviation from observation (black dot lines). The concentric black semi-circles denote centered root-mean-square (CRMS) difference values. The angular coordinate shows the correlation coefficient (grey dot lines).

of the PBL scheme are observed in BHAN, BHLO, CPUL, CSNL, LARU, and NICO stations.

The standardized anomaly of MAE exhibits that the YSU scheme has better than average accuracy at most weather stations during January 2013 (Fig. 4a), except for the CSNL station. In the latter, the ACM2 scheme produces the best



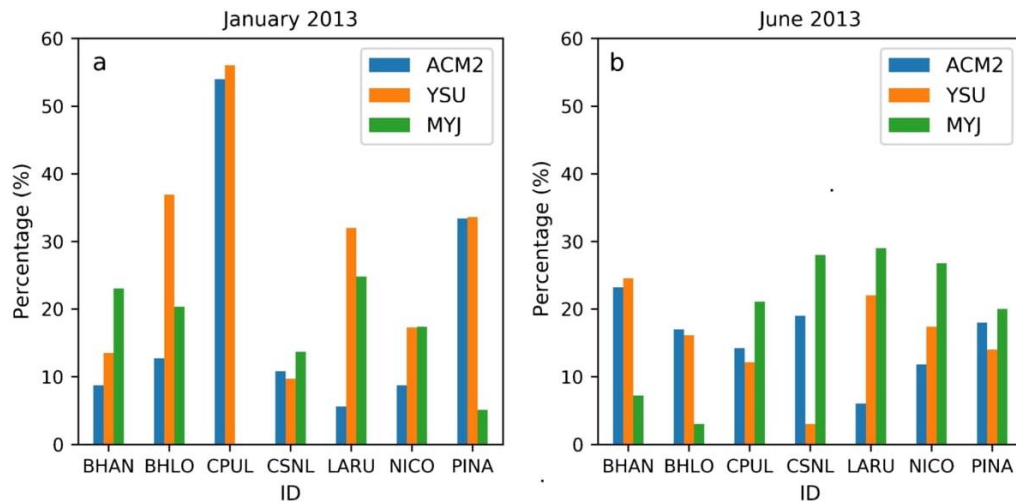


Fig. 3 MAE skill score (MAESS) in percentage for (a) January and (b) June 2013 for seven weather stations

forecast. Accuracy varies among weather stations in June 2013 (Fig. 4b); the MYJ scheme has better accuracy than average accuracy for CPUL, CSNL, LARU, NICO, and PINA stations. PBL schemes including non-local mixing (ACM2 and YSU) perform better for BHAN and BHLO stations. Both locations have a complex terrain, and during the summer season, local differential heating can lead to boundary layer circulation enhancing turbulent eddies that move from lower to higher layers and vice versa. This effect is incorporated in non-local schemes.

**Wind ramp distribution**

Ramp forecasting needs to be improved for the adequate management of sudden and large changes in wind power. Large

variability and uncertainty in wind power generation is a concern for energy planners. This section discusses the wind ramp distribution. During winter, MYJ and ACM2 schemes reproduce better the distribution of observed ramps (Fig. 5). Both schemes exhibit similar frequency and magnitude of forecasted ramps. All schemes tend to generate a greater number of wind ramp up and down events in the range of  $-2$  to  $2$  m/s than observed in BHLO, BHAN, LARU, and PINA stations. Milder wind ramps are forecasted by the three schemes in BHLO and CPUL stations, above (below) the range of  $8$  ( $-8$ ) m/s.

The distribution of wind ramps in summer is better simulated than in winter. The similarities in magnitude and frequency of the observed wind ramps are evident with the three schemes simulations (Fig. 6). Although wind ramp

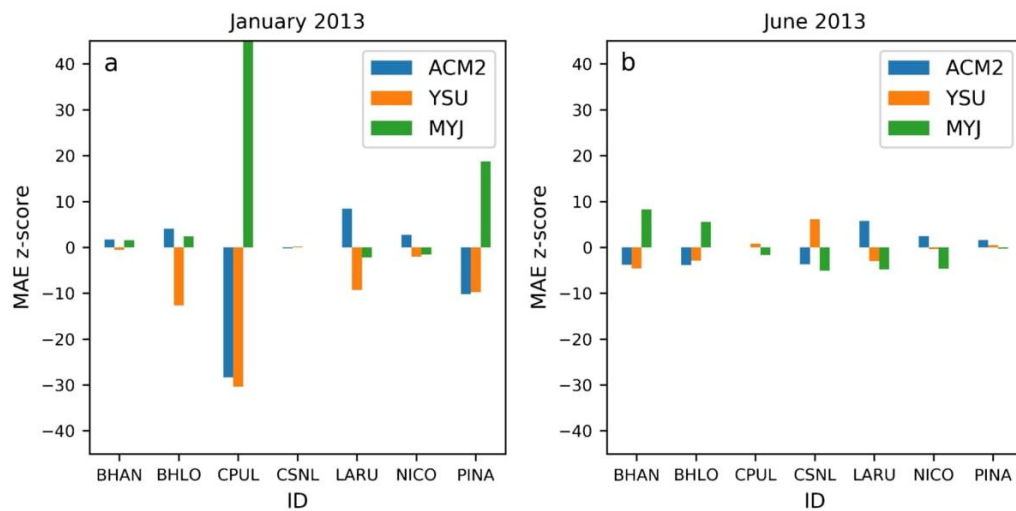
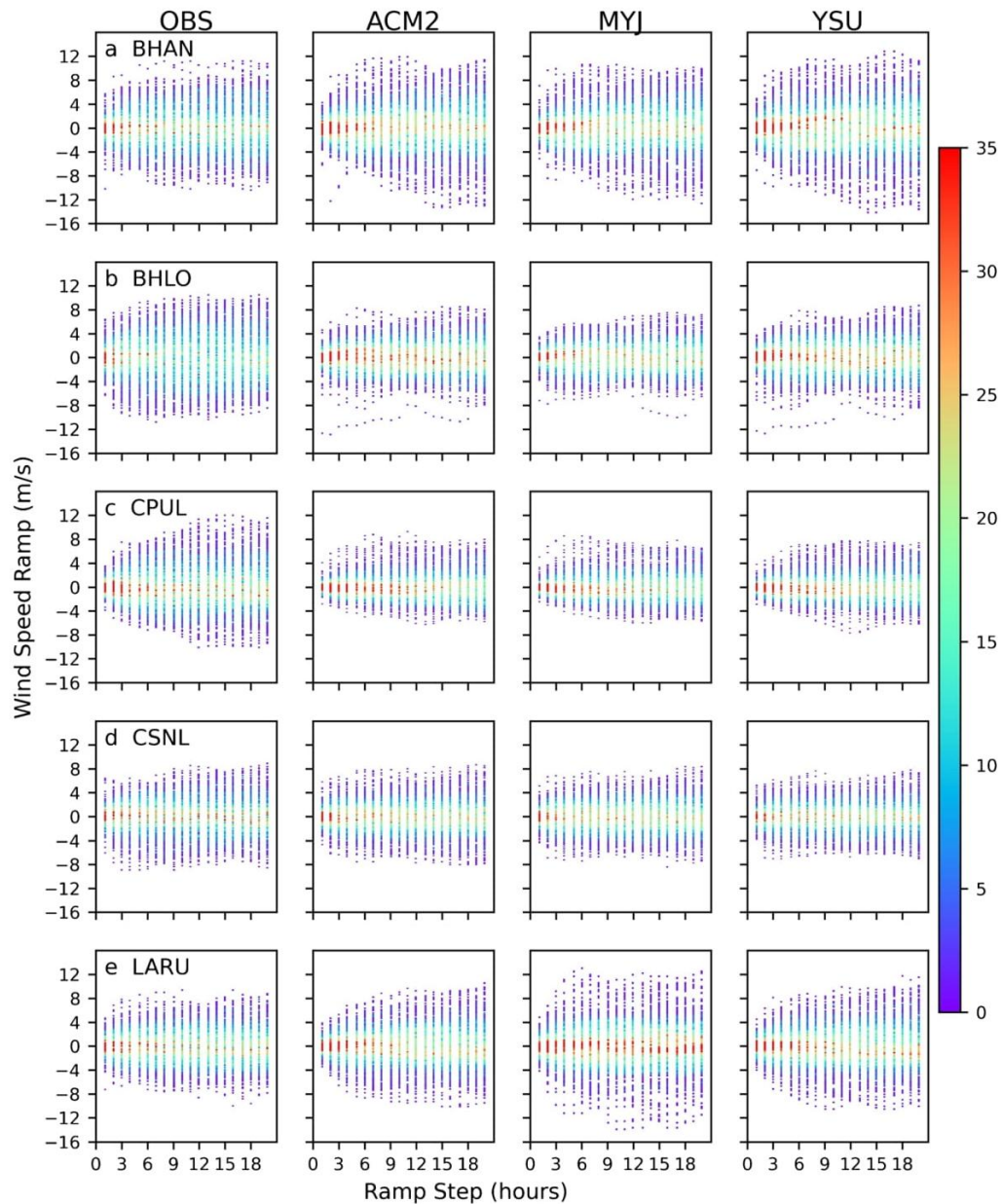


Fig. 4 Accumulated z score for 24-h wind forecast during (a) June and (b) January 2013 at seven weather stations



**Fig. 5** Observed and model wind ramp distribution for winter (January 2013). Wind ramps are in m/s and time window is indicated in hours

distribution using the YSU scheme is similar to that observed at CPUL and the best-simulated distribution of wind ramps is achieved by the MYJ scheme at NICO, ACM2 scheme captures slightly better the distribution and intensity of observed ramps in most of the sites. Wind ramp distribution is narrower than what were observed at BHLO, CPUL, and CSNL stations (Fig 6b, 6c, and 6d). Observed wind ramps are more intense than those simulated by the three PBL schemes. The tails of the observed wind ramp distributions reached 12 m/s, while

the simulated ones reached 8 m/s. This effect is most evident on ramps that last 1 to 6 h. The WRF model tends to smooth out changes of the wind due to the model’s dissipation mechanisms, related to the filtering and damping schemes of the model (Skamarock et al. 2005). Smoothing is enhanced during winter when intense wind ramps are expected due to the strong pressure gradients associated to frontal systems.

Tables 3 and 4 summarize the criteria, based on metrics, used to assess wind speed forecast under different PBL

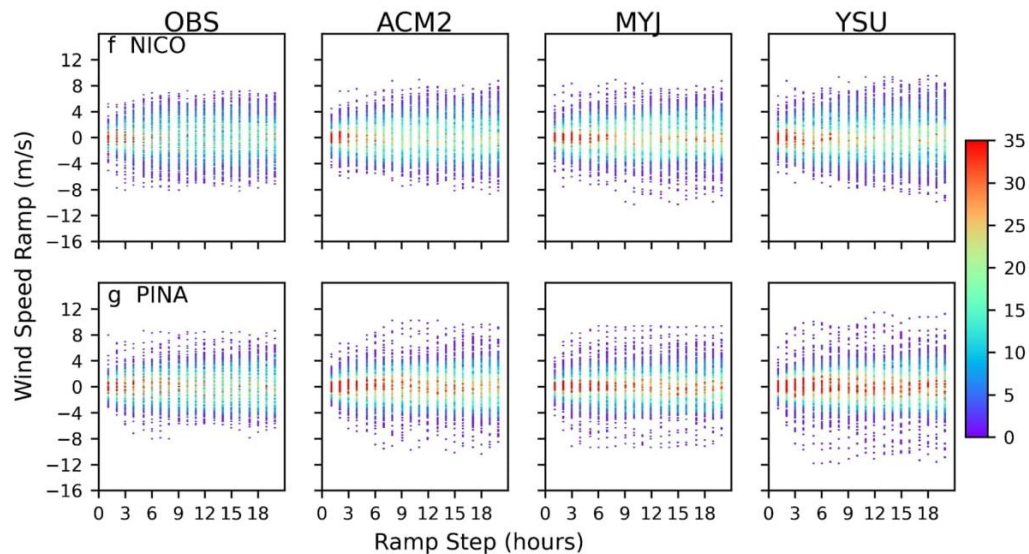


Fig. 5 continued.

schemes. Over all stations, the best forecast for the winter (January 2013) was with the YSU scheme, followed by ACM2 scheme. Meanwhile, MYJ and ACM2 schemes performed better during June 2013. The ability of ACM2 scheme to perform well in both seasons could be related to the fact that this scheme combines features of local and non-local schemes (Pleim 2007a). Updates in YSU scheme have improved wind speed estimations in stable regimes (Hu et al. 2013), which is more probable to occur in winter when surface temperatures tend to be colder.

### Wind analysis

A notable aspect in the wind speed time series is the presence of a diurnal frequency signal that is more evident in June. In the absence of synoptic systems during the warm season, local circulations are observed in coastal and mountainous regions due to horizontal temperature gradients that generate from differential terrain or slopes. Hourly wind vectors for seven weather stations give an idea of the impact of topography on the local wind field and the sea-breeze circulation experienced along Baja California Peninsula (Fig. S2 and Fig. S3). Wind reversal is observed at night in summer (~20:00 LT) (Fig. S3); however, the smooth sea-land temperature difference prevents a sharp diurnal shift in winter (~18:00 LT) (Fig. S2). At night, the onshore flow is stronger (> 7m/s) at BHAN and CSNL than the diurnal circulation. It is also noticed that the prevailing winds switch from northerly in January to southerly in June, a signal of the monsoon onset.

Diurnal wind local circulations remain during winter but cold fronts (Fig. 7) modulate them. For example, a cold front moving east-southeast reached northern Baja California on January 10, 2013 (Fig. S4). The prefrontal phase originated intense winds at 00Z (16:00 LT) January 11, 2013, at the north of Baja California (Fig. S4). Intense winds (>9 m/s) from the north and northeast extend along the Baja California Peninsula with the advance of the frontal system. The intense north wind extends in the PBL up to a height of 1200 m (Fig. S5). Wind channeling in CPUL station evidences this effect. The wind forecast is very similar in CPUL and CSNL stations based on Taylor diagram. However, the standardized deviation is lower in CPUL due to the smoothing of wind variability by the three schemes, producing milder wind ramps (Fig. 7). Otherwise, the wind ramps forecast in BHAN from 10 to 11 January 2013 using the MYJ scheme are considerably sharper than those observed (Fig. S6), which can lead to a wind farm mismanagement in the region of the BHAN station.

Accurate ramp prediction is relevant for the proper management of wind farms. A wind power producer can shut down turbines to avoid producing an excess of energy that cannot be compensated, or it can increase its generation in agreement with the system operator and utilities (Ferreira et al. 2011).

The diurnal behavior of wind speed is well reproduced by all PBL schemes (Fig. 8, see Fig. S7 for more details). At BHLO, CPUL, and CSNL, the WRF simulations tend to predict milder ramps (up to 8 m/s) than observed (up to 12 m/s); consequently, the form of the wind ramp distribution is narrow than the real (Fig. 6b, 6c, 6d). Hourly MAE shows that



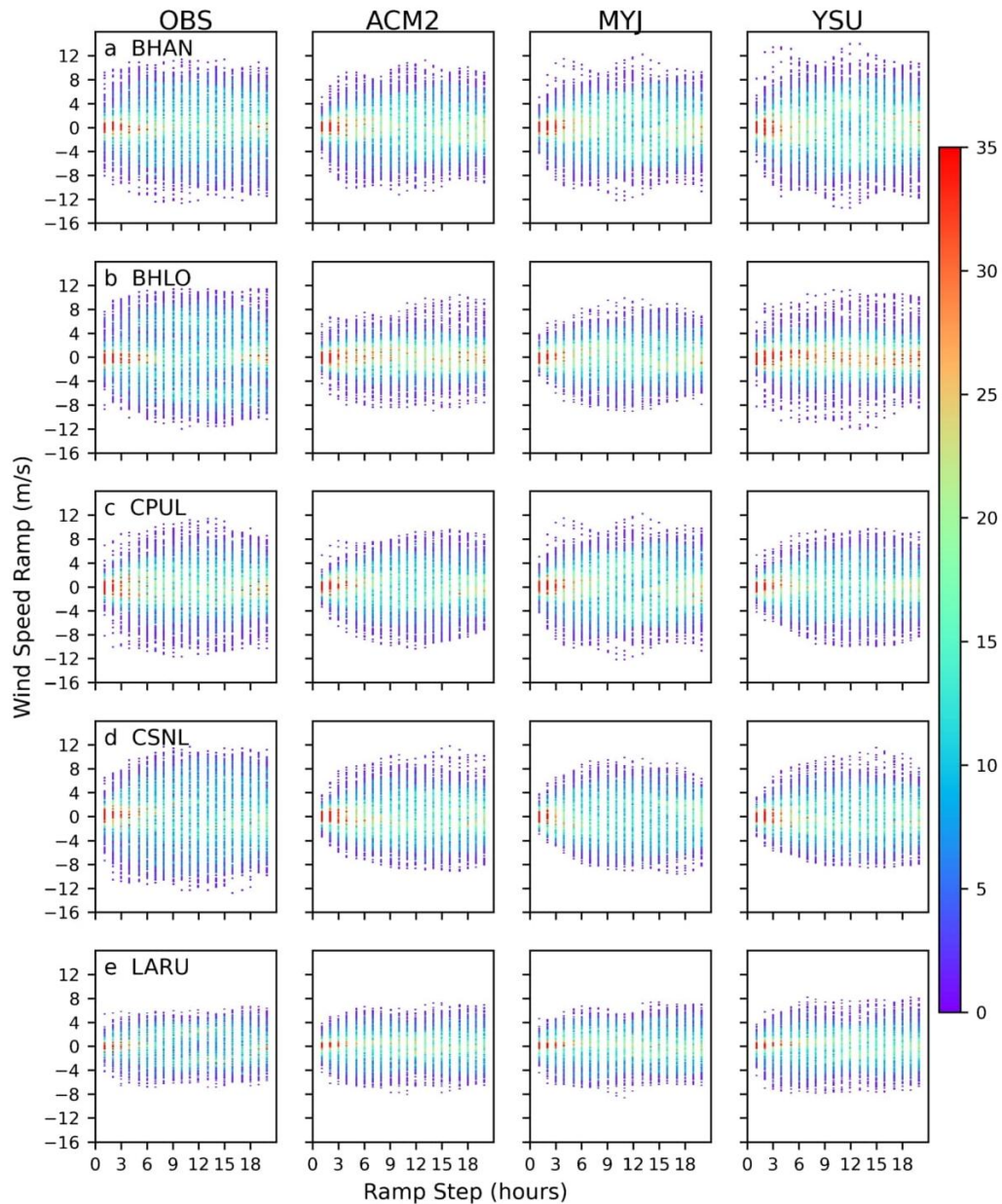


**Fig. 6** Observed and model wind ramps distribution for summer (June 2013). Wind ramps are in m/s and time window is indicated in hours

simulated wind speed is underestimated between 10Z and 16Z and overestimated between 20Z and 03Z. The forecast error did not increase with leading time but only at specific hours: 10Z and 16Z.

Simulated local circulations for a typical summer day (June 13) are analyzed. The presence of a valley-mountain breeze around 18Z in the WRF simulations is clear. A flow towards the mountain and convective activity can be seen on the slope at BHLO (Fig. 9). Moving away from the coast, over

the Gulf of California, the winds are strong and from the south. At night (03Z–10Z), downward flows from the mountain occur, the land breeze sets (~ 10 m/s), which in the case of BHAN station (not shown) is more intense than the sea breeze. These local winds are caused by the surface differential heating due to different land covers and/or slopes. The interaction of the land breeze with the mountain breeze results in wind intensification. Steep slopes create stronger breezes. This behavior of the wind produces the maximum speed (> 7

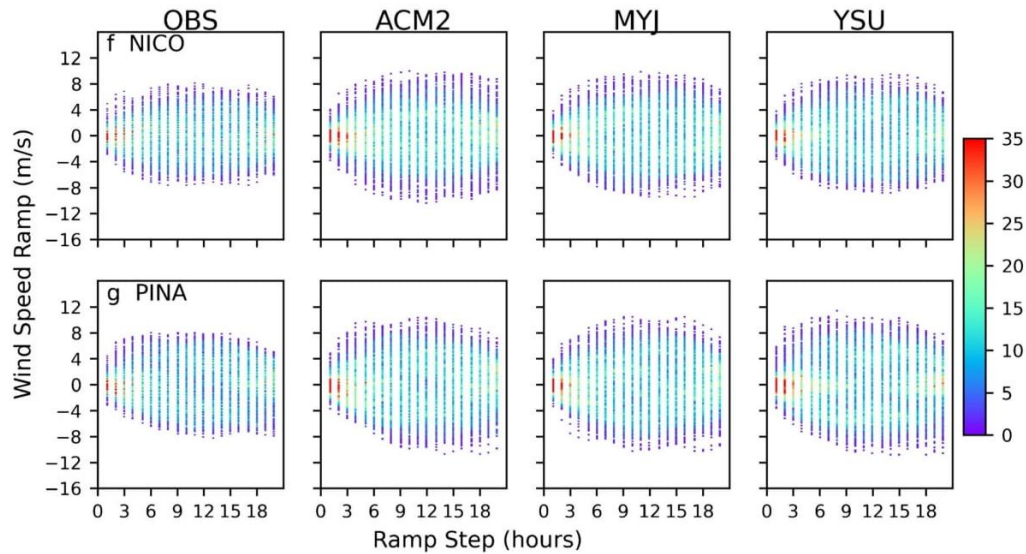


Fig. 6 continued.

m/s) of the wind during the night. A similar situation is observed with CPUL and CSNL stations. In the rest of the coastal stations, the maximum wind occurs in the afternoon due to the sea breeze. In the stations far from the coast (LARU and PINA stations), the intensification of the wind is due to local thermal contrasts originated by surrounding topography.

In general, differential surface warming modulates diurnal wind fluctuations during the summer, when tropical cyclones are not present. Sea breezes occur during the day due to unequal heating rates of land and sea. In January 2013, the ocean was warmer than the land from 18:00 to 8:00 LT (Fig. S8a). The temperature difference was between 3 and 10°C. Consequently, the cooler air over the land flowed over the ocean surface. On the other hand, the land tends to be warmer (2 to 3°C) than the ocean from 9:00 to 17:00 LT and a weak sea breeze can be observed. In June 2013, the sea-land thermal contrast is enhanced; the warm land reaches 1 to 10°C greater than the sea temperature (Fig. S8b), causing the diurnal wind

change, and the sea breeze is established. Nevertheless, at night, the land is at the same temperature or colder than the sea (1 to 5°C); the thermal contrast generates a land breeze with weak winds of ~ 3 m/s.

At the BHAN station (not shown), the mountain valley circulation (12Z) is established with downward flow over the mountain near the surface corroborating the effect of surface fluxes (energy balance) in the PBL. The circulation shown is characteristic of summer but may change in the presence of hurricanes in the region. The combination of flows due to orography and breeze circulation stands out. By 18Z, it shows a flow in the reverse direction of 12Z. Strong vertical upward movements determine valley-mountain breeze. These convective movements are caused by surface heating that determines the height of the PBL structure, favoring vertical transport.

In winter, strong winds are associated with cold fronts. The passage of these systems over the region generates northerly

**Table 3** Criteria used for assess forecast sensitivity to PBL in January 2013 at Baja California Peninsula. Similar behavior among the three PBL schemes is indicated with \*. The last column indicates the most appropriate parameterization for the region of the station under the metric criteria

Weather station	Taylor diagram	MAESS	Z score	Wind ramps	PBL scheme
BHAN	YSU	MYJ	YSU	YSU	YSU
BHLO	YSU	YSU	YSU	YSU*	YSU
CPUL	ACM2*	YSU	YSU	YSU*	YSU
CSNL	ACM2*	MYJ	ACM2	ACM2*	ACM2
LARU	YSU	YSU	YSU	ACM2-MYJ	YSU
NICO	YSU	YSU	YSU	ACM2*	YSU
PINA	YSU	ACM2-YSU	ACM2-YSU	ACM2	ACM2



**Table 4** Criteria used to assess forecast sensitivity to PBL in June 2013 at Baja California Peninsula. Similar behavior among the three PBL schemes is indicated with \*. The last column indicates the most appropriate parameterization for the region of the station under the metric criteria

Weather station	Taylor diagram	MAESS	Z score	Wind ramps	PBL scheme
BHAN	MYJ	YSU-ACM2	YSU-ACM2	MYJ	YSU-MYJ
BHLO	YSU	YSU-ACM2	ACM2-YSU	ACM2-YSU	YSU-ACM2
CPUL	ACM2-MYJ	MYJ	MYJ	ACM2-MYJ	ACM2-MYJ
CSNL	ACM2	MYJ	MYJ	ACM2*	ACM2-MYJ
LARU	YSU*	MYJ	MYJ	YSU*	YSU-MYJ
NICO	MYJ	MYJ	MYJ	MYJ	MYJ
PINA	ACM2	MYJ	MYJ	ACM2*	MYJ-ACM2

wind interacting with the topography causing flow acceleration in the coastal areas (Fig. 10). WRF-simulated wind field agrees quite well with ERA5 reanalysis wind. This northerly wind is channeled over the Gulf of California by the presence of mountainous systems, with moderate winds in the northern portion and intense winds in the southern portion. The cross-sections show that below 2000 m, the wind is from the north during January 11, 2013. As previously mentioned, the winds intensify towards the southern portion of the Baja California

Peninsula, where the BHLO and CPUL stations experience stronger wind than BHAN station.

**Wind power spectra**

Spectral studies of low-level horizontal wind speed have grown in importance, recently, for applications in wind energy (Vincent et al. 2011; Horvath et al. 2012; Larsén et al. 2016; Kang and Won 2016). They apply a spectral approach for a

**Fig. 7** Wind speed time series for January 2013 at seven weather stations. Observed wind (full black line), YSU PBL scheme (dashed yellow line), MYJ PBL scheme (dashed green line), ACM2 PBL scheme (dashed blue line), PBL simulations average (dashed red line)

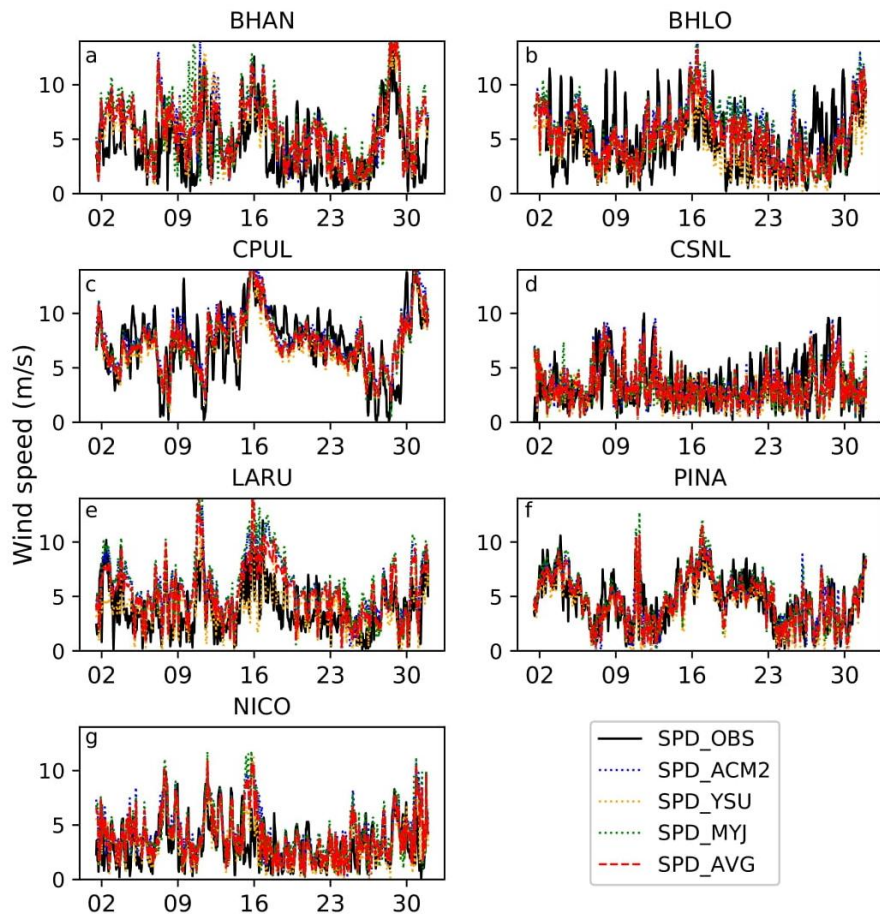
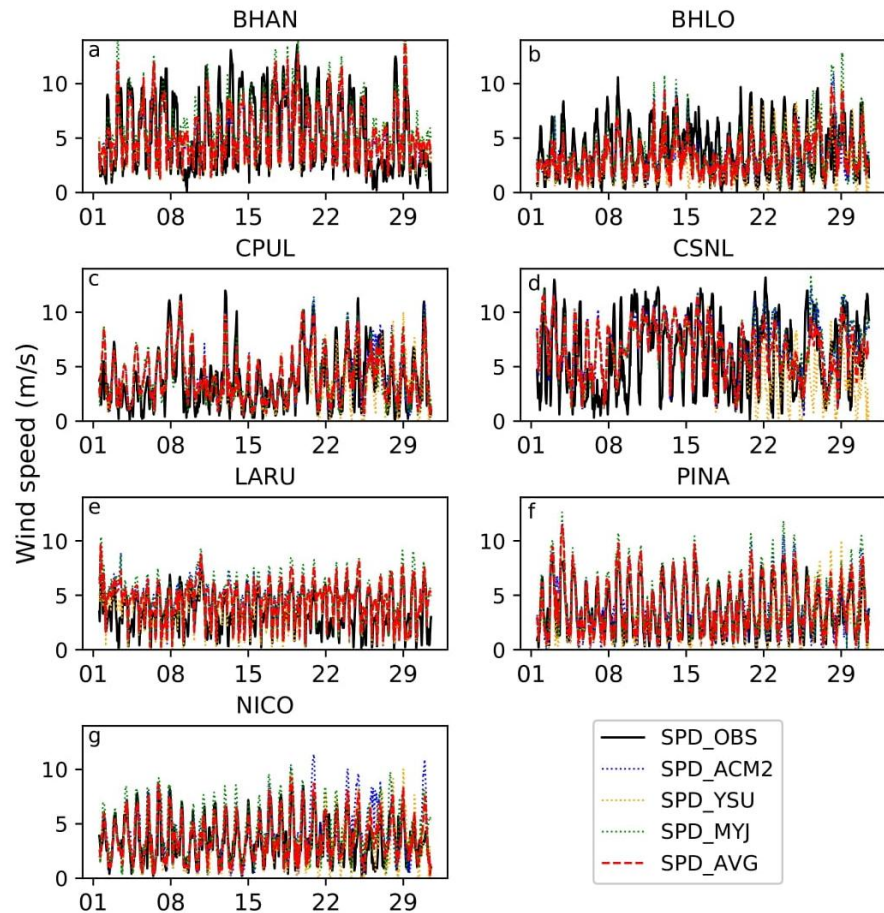




**Fig. 8** Wind speed time series for June 2013 at seven weather stations. Observed wind (full black line), YSU PBL scheme (dashed yellow line), MYJ PBL scheme (dashed green line), ACM2 PBL scheme (dashed blue line), PBL simulations average (dashed red line)



quantitative assessment of their mesoscale model experiments with observations. Spectral approach can provide scale-dependent performance of models (Horvath et al. 2012). The regions of the spectra that are poorly represented suggest that they need improvements in model precision and the occurrence of the corresponding meteorological systems at those frequencies is required. The analysis of observed and forecasted wind power spectra for June 2013 (Fig. 11) shows spectral peaks in  $9 \times 10^{-6}$  Hz ( $\sim 30$  h) and  $2 \times 10^{-5}$  ( $\sim 13$  h) Hz frequencies. At frequencies higher than  $8 \times 10^{-5}$  Hz, the spectrum falls off for all the sites. Forecast wind power spectrums for all PBL schemes are similar between  $6 \times 10^{-5}$  and  $1 \times 10^{-4}$  Hz. The simulated spectral curves show a steeper slope than observations, similar to finding by Larsén XG et al. (2016) at an offshore site in Denmark. The differences in the high-frequency side of the spectrum are more evident for BHAN, BHLO, CSNL, and CPUL stations. Numerical models underestimate wind ramp tails due to the spatial and temporal smoothing and, consequently, there is a misrepresentation of

the energy at mesoscale range for atmospheric systems for less than 5-h time span. For events lasting more than 2 days, the model and observations power spectrums show discrepancies. The ACM2 PBL scheme simulates higher energy in the lower frequency side of the spectrum from June (Fig. 11) except at BHAN, CPUL, and CSNL stations, while the YSU PBL scheme simulates lower energy for spectrums lower frequencies at BHLO and CSNL stations.

Wind power spectra for January (Fig. 12) show marked differences with June spectra. Low-frequency events ( $\sim 6$  days) are more common in winter, as a consequence of frontal systems over Northern Mexico. Energy peaks associated with local circulations are less evident. The simulated energy spectrum for the three PBL schemes is similar; the spectrum lines overlap. The simulated energy in the range of  $10^{-6}$  to  $4 \times 10^{-5}$  Hz is close to the energy observed in most weather stations. The deviations from the observations are found at the CPUL and BHLO stations, where the simulated energy is less than that observed. The improved simulation of the winter

**Fig. 9** Vertical cross-section of simulated horizontal wind calculated with the WRF model at (a) 1800Z (12 LT) and (b) 03Z (21 LT) for June 13, 2013, at BHLO latitude (26° N). A green asterisk indicates weather station location

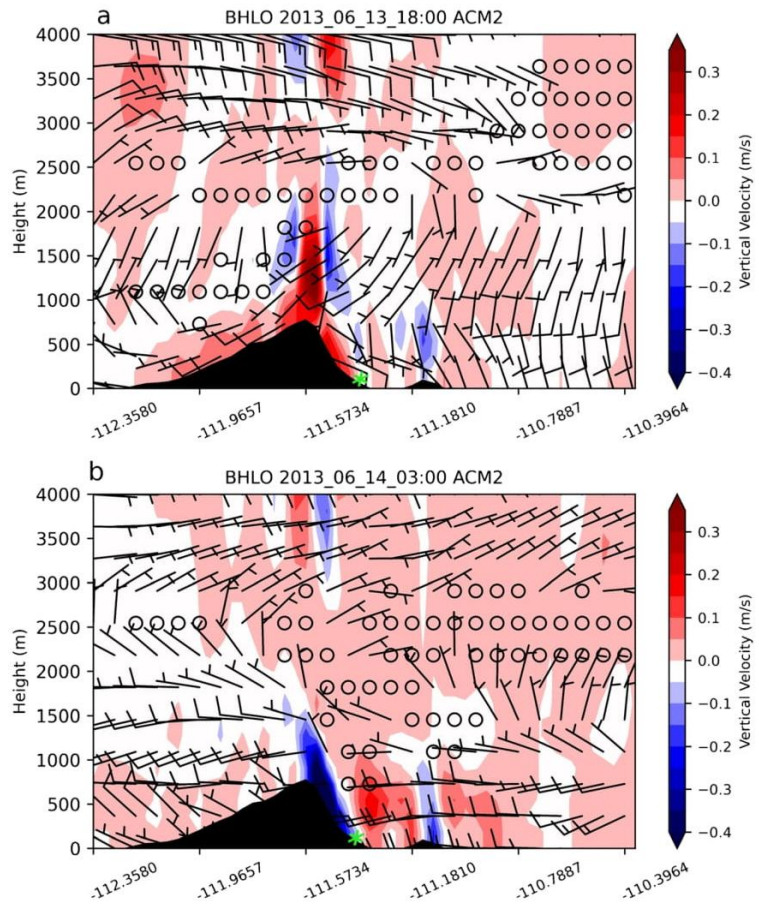


**Fig. 10** Vertical cross-section of simulated horizontal wind calculated with the WRF model (green barb) and ERA5 wind (blue barb) at 1800Z (11 LT) for January 11, 2013, at (a) BHAN, (b) BHLO, and (c) CPUL latitude stations during a cold front event. A green asterisk indicates weather station location

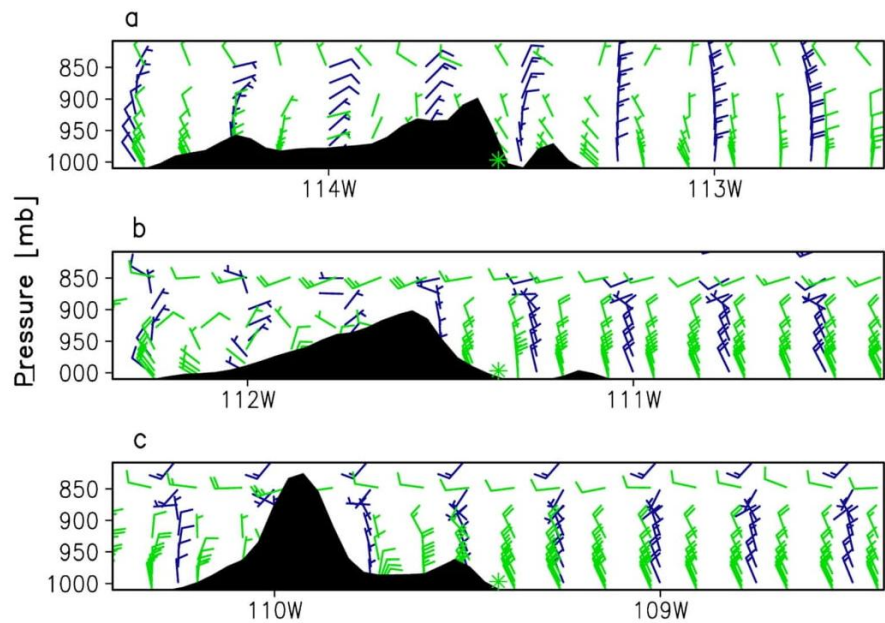
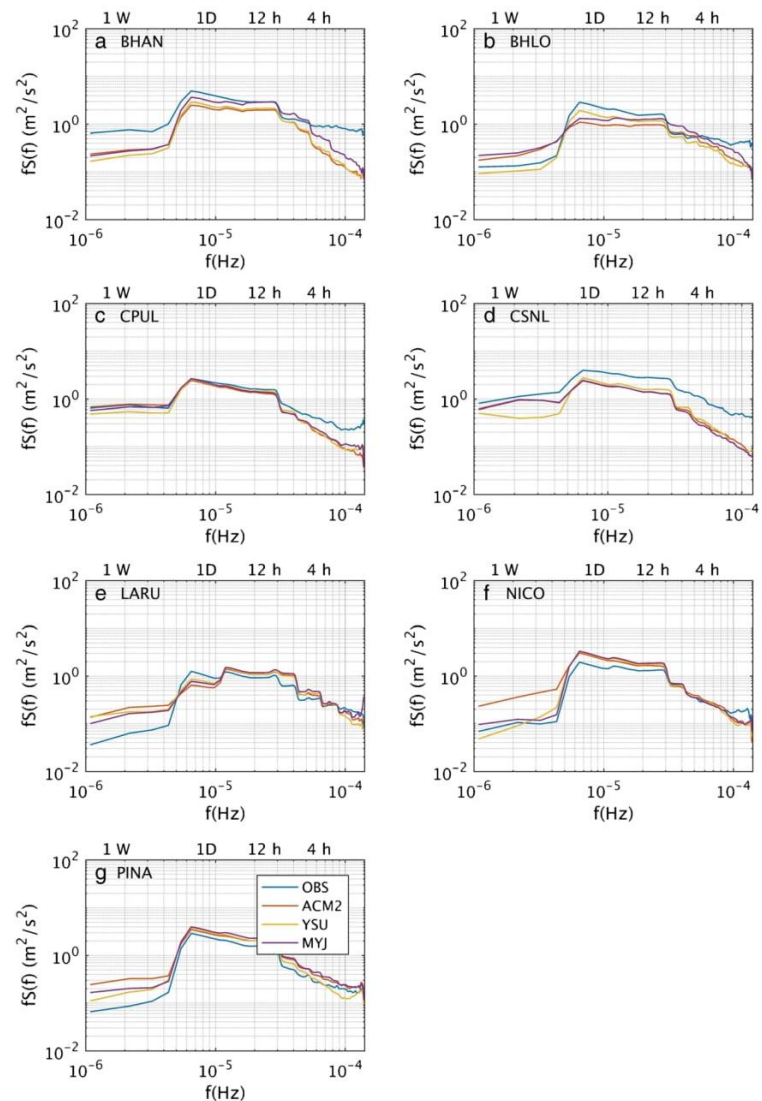




**Fig. 11** June 2013 smoothed frequency-weighted spectra  $fS(f)$  as a function of frequency ( $f$ ) of horizontal wind speed for (a) BHAN, (b) BHLO, (c) CPUL, (d) CSNL, (e) LARU, (f) NICO, and (g) PINA stations. Observed spectrum (blue line), YSU PBL scheme (yellow line), MYJ PBL scheme (purple line), ACM2 PBL scheme (orange line)

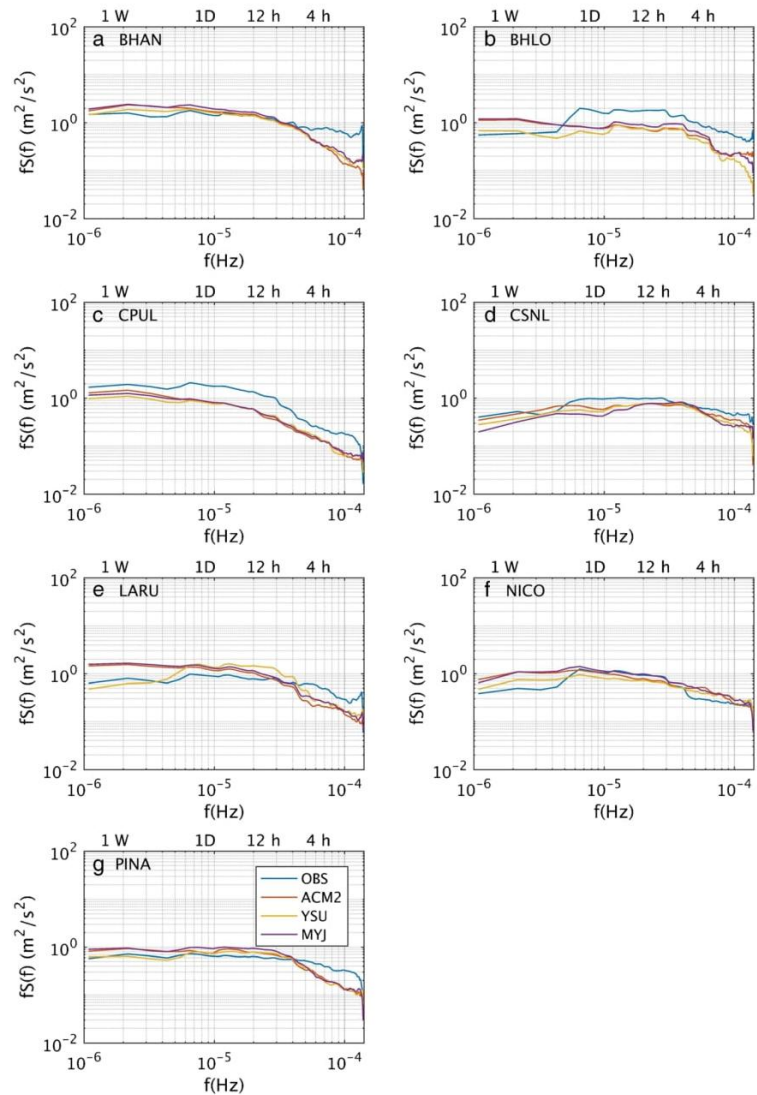


spectrum is due to synoptic organized mid-latitude systems. In the high-frequency side of the spectra, the simulated wind power spectrum shows a steeper slope than observations, more evident at BHAN, BHLO, CPUL, and LARU stations. Comparisons between the WRF forecasts and the observed power spectrum show that it is important to choose the most suitable PBL scheme for the summer season due to the significant differences in their performances. However, all PBL schemes tend to underpredict energy on the high-frequency side of the spectrum leading to large forecast errors.

The smoothing effect in the mesoscale range reflects the misrepresentation of wind variability for phenomena lasting 12 h or less. The smoothing effect is a common

issue in the mesoscale modeled winds (Skamarock et al. 2005, 2011; Frehlich and Sharman 2008; Larsén et al. 2012). The unappropriated simulation of thunderstorms, sea-breeze, and katabatic flows impacts the quality of wind ramp forecast, especially in the summer season. The intermittent nature of wind source can make it difficult to manage. Ramp events generate sudden increases or decreases in answer to changes in wind speed, because the wind power is proportional to the wind speed to the power of three. A small error in wind speed can translate to a large error in wind power, leading to challenges for balancing generation and load at all times. The improvement of wind ramp forecasting should include a correction

**Fig. 12** January 2013 smoothed frequency-weighted spectra  $fS(f)$  as a function of frequency  $f$  of horizontal wind speed for (a) BHAN, (b) BHLO, (c) CPUL, (d) CSNL, (e) LARU, (f) NICO, and (g) PINA. Observed spectrum (blue line), YSU PBL scheme (yellow line), MYJ PBL scheme (purple line), ACM2 PBL scheme (orange line)



of the power spectrum in the mesoscale range using the approach, as instance, proposed by Larsén et al. (2012).

**Conclusion**

Wind energy is an intermittent source of energy and this is the main challenge the renewable energy industry has to deal with for integration in the electrical system. The WRF model is commonly used for wind potential and wind forecast evaluations. In this study, we focused on the ability of WRF to simulate near surface wind on Baja California Peninsula. The results suggest that the PBL schemes tested tend in

general, to simulate smoother wind variability than observations, especially when mesoscale systems affect the region. This shortcoming in the forecast of changes in wind speed can cause a deficit or surplus in the production of wind energy that conditions the reliability of energy planning. Therefore, the accurate prediction of wind speed fluctuations under different PBL schemes is an important issue to be examined.

This work was conducted with the main goal of analyzing the WRF model wind simulations sensitivity to PBL schemes for June (summer) and January (winter) 2013 for Baja California Peninsula, Mexico. The YSU scheme shows the best statistical scores for winter in most of the weather stations. Energy planners will likely benefit the most by using the



YSU scheme during winter. However, the most suitable PBL scheme selection for summer varies by location. The MYJ and ACM2 schemes present good results for summer.

Choosing an adequate PBL scheme can reduce MAE up to 60%. The sensitivity to PBL scheme varies from one weather station to another due to the typical atmospheric conditions and physiographical characteristics of the region. Wind power production is highly sensitive to wind speed fluctuations. Therefore, even subtle improvements due to the correct choice of PBL scheme can lead to better management of wind energy.

The wind ramp distribution is reasonably well simulated by WRF for all schemes. However, at particular weather stations, wind ramp magnitude differs from observations due to overestimation of wind speed at night. In addition, the WRF tends to predict more weak wind speed ramps events (magnitude between 0 and 2 m/s). Energy planners and utilities that use wind energy forecasts should be careful of these findings for proper management of wind farms. The three boundary layer schemes show similar ramp distributions and frequencies. The ACM2 scheme captures slightly better the distribution and intensity of observed ramps in most of the sites.

The WRF simulates energy in the range of  $10^{-6}$  to  $4 \times 10^{-5}$  Hz more accurately during January 2013 than in June 2013, due to the better skill to predict mid-latitude systems. Tropical systems provide also energy in the same region of the spectrum; however, the WRF has less ability to forecast these convective systems during the summer, and therefore, there are greater differences between observation and forecast. PBL schemes show a subtle difference in performance among themselves. However, significant differences between the observed and forecasted power spectrum are observed in the high-frequency side of the spectrum ( $< 4$  h) for January and June. Model spectrum shows steeper slope conducting to underestimation of energy in the mesoscale range. In June, the energy on the low-frequency side of the spectrum is overestimated or underestimated depending on the chosen PBL scheme. This factor needs to be considered when applying the WRF model for wind energy assessment or forecasting.

The results suggest that error minimization in the wind forecast could be expected by choosing the suitable PBL scheme, especially in the summer season. Also, it shows that wind forecast needs to be managed carefully by energy planners in order to correctly manage wind farms. Future improvements to wind forecast can be derived from bias correction or from the use of ensemble wind forecast, particularly during the summer season when differences among PBL schemes are more relevant.

**Supplementary Information** The online version contains supplementary material available at <https://doi.org/10.1007/s12517-021-08317-3>.

**Acknowledgments** The authors thankfully acknowledge computer resources, technical advice and support provided by Laboratorio Nacional

de Supercomputo del Sureste de México (LNS), a member of the CONACYT national laboratories, with project No. 201801023n. The authors acknowledge the comments made by the anonymous reviewers that helped to improve the quality of the manuscript.

**Author contribution** Conceptualization, Karla Pereyra-Castro and Ernesto Caetano; methodology, Karla Pereyra-Castro; formal analysis, Karla Pereyra-Castro; investigation, Karla Pereyra-Castro, Ernesto Caetano, and Diego Altamirano-del Razo; data curation, Karla Pereyra-Castro and Diego Altamirano-del Razo; writing—original draft preparation, Karla Pereyra-Castro and Ernesto Caetano; writing—review and editing, Ernesto Caetano; supervision, Ernesto Caetano. All authors have read and agreed to the published version of the manuscript.

**Funding** This research was funded by The National Council of Science and Technology (CONACYT), grant number 473276, the first author's PhD scholarship.

**Availability of data and material** Data and material are available to any reader directly from the corresponding author upon reasonable request.

**Code availability** Code/algorithm/software is available to any reader directly from the corresponding author upon reasonable request.

## Declarations

**Conflict of interest** The authors declare no competing interests.

## References

- Badan-Dangon A, Dorman CE, Merrifield MA, Winant CD (1991) The lower atmosphere over the Gulf of California. *J Geophys Res Ocean* 96:16877–16896. <https://doi.org/10.1029/91JC01433>
- Bossavy A, Girard R, Kariniotakis G (2010) Forecasting uncertainty related to ramps of wind power production. In: European Wind Energy Conference and Exhibition 2010, EWEC 2010. European Wind Energy Association, Warsaw, Poland, pp 9 pages-ISBN 9781617823107
- Carvalho D, Rocha A, Gómez-Gesteira M, Santos C (2012) A sensitivity study of the WRF model in wind simulation for an area of high wind energy. *Environ Model Softw* 33:23–34. <https://doi.org/10.1016/j.envsoft.2012.01.019>
- Carvalho D, Rocha A, Gómez-Gesteira M, Silva Santos C (2014) Sensitivity of the WRF model wind simulation and wind energy production estimates to planetary boundary layer parameterizations for onshore and offshore areas in the Iberian Peninsula. *Appl Energy* 135:234–246. <https://doi.org/10.1016/j.apenergy.2014.08.082>
- Chen F, Dudhia J (2001) Coupling an advanced land surface–hydrology model with the Penn State–NCAR MM5 modeling system. Part I: model implementation and sensitivity. *Mon Weather Rev* 129:569–585. [https://doi.org/10.1175/1520-0493\(2001\)129<0569:CAALSH>2.0.CO;2](https://doi.org/10.1175/1520-0493(2001)129<0569:CAALSH>2.0.CO;2)
- Deppe AJ, Gallus WA, Takle ES (2013) A WRF ensemble for improved wind speed forecasts at turbine height. *Weather Forecast* 28:212–228. <https://doi.org/10.1175/WAF-D-11-00112.1>
- Draxl C, Hahmann AN, Peña A, Giebel G (2014) Evaluating winds and vertical wind shear from Weather Research and Forecasting model forecasts using seven planetary boundary layer schemes. *Wind Energy* 17:39–55. <https://doi.org/10.1002/we.1555>
- Dudhia J (1989) Numerical study of convection observed during the winter monsoon experiment using a mesoscale two-dimensional

- model. *J Atmos Sci* 46:3077–3107. [https://doi.org/10.1175/1520-0469\(1989\)046<3077:NSOCOD>2.0.CO;2](https://doi.org/10.1175/1520-0469(1989)046<3077:NSOCOD>2.0.CO;2)
- Ferreira C, Gama J, Matias L, et al (2011) A survey on wind power ramp forecasting. Argonne National Lab.(ANL), Argonne, IL (United States)
- Frehlich R, Sharman R (2008) The use of structure functions and spectra from numerical model output to determine effective model resolution. *Mon Weather Rev* 136:1537–1553. <https://doi.org/10.1175/2007MWR2250.1>
- García-Díez M, Fernández J, Fita L, Yagüe C (2013) Seasonal dependence of WRF model biases and sensitivity to PBL schemes over Europe. *Q J R Meteorol Soc* 139:501–514. <https://doi.org/10.1002/qj.1976>
- Hahmann AN, Vincent CL, Peña A, Lange J, Hasager CB (2015) Wind climate estimation using WRF model output: method and model sensitivities over the sea. *Int J Climatol* 35:3422–3439. <https://doi.org/10.1002/joc.4217>
- Hong S-Y, Dudhia J, Chen S-H (2004) A revised approach to ice microphysical processes for the bulk parameterization of clouds and precipitation. *Mon Weather Rev* 132:103–120. [https://doi.org/10.1175/1520-0493\(2004\)132<0103:ARATIM>2.0.CO;2](https://doi.org/10.1175/1520-0493(2004)132<0103:ARATIM>2.0.CO;2)
- Hong S-Y, Noh Y, Dudhia J (2006) A new vertical diffusion package with an explicit treatment of entrainment processes. *Mon Weather Rev* 134:2318–2341. <https://doi.org/10.1175/MWR3199.1>
- Horvath K, Koracin D, Vellore R, Jiang J, Belu R (2012) Sub-kilometer dynamical downscaling of near-surface winds in complex terrain using WRF and MM5 mesoscale models. *J Geophys Res Atmos* 117:1–19. <https://doi.org/10.1029/2012JD017432>
- Hu XM, Klein PM, Xue M (2013) Evaluation of the updated YSU planetary boundary layer scheme within WRF for wind resource and air quality assessments. *J Geophys Res Atmos* 118:10490–10505. <https://doi.org/10.1002/jgrd.50823>
- IRENA (2020) Renewable power generation costs in 2019. Abu Dhabi
- Janjić ZI (1994) The step-mountain eta coordinate model: further developments of the convection, viscous sublayer, and turbulence closure schemes. *Mon Weather Rev* 122:927–945. [https://doi.org/10.1175/1520-0493\(1994\)122<0927:TSMECM>2.0.CO;2](https://doi.org/10.1175/1520-0493(1994)122<0927:TSMECM>2.0.CO;2)
- Kain JS (2004) The Kain–Fritsch convective parameterization: an update. *J Appl Meteorol* 43:170–181. [https://doi.org/10.1175/1520-0450\(2004\)043<0170:TKCPAU>2.0.CO;2](https://doi.org/10.1175/1520-0450(2004)043<0170:TKCPAU>2.0.CO;2)
- Kang S-L, Won H (2016) Spectral structure of 5 year time series of horizontal wind speed at the Boulder Atmospheric Observatory. *J Geophys Res Atmos* 121:11946–11967. <https://doi.org/10.1002/2016JD025289>
- Larsén XG, Ott S, Badger J, Hahmann AN, Mann J (2012) Recipes for correcting the impact of effective mesoscale resolution on the estimation of extreme winds. *J Appl Meteorol Climatol* 51:521–533. <https://doi.org/10.1175/JAMC-D-11-090.1>
- Larsén XG, Larsen SE, Petersen EL (2016) Full-scale spectrum of boundary-layer winds. *Boundary-Layer Meteorol* 159:349–371. <https://doi.org/10.1007/s10546-016-0129-x>
- Menendez M, García-Díez M, Fita L, Fernández J, Méndez FJ, Gutiérrez JM (2014) High-resolution sea wind hindcasts over the Mediterranean area. *Clim Dyn* 42:1857–1872. <https://doi.org/10.1007/s00382-013-1912-8>
- Mlawer EJ, Taubman SJ, Brown PD, Iacono MJ, Clough SA (1997) Radiative transfer for inhomogeneous atmospheres: RRTM, a validated correlated-k model for the longwave. *J Geophys Res Atmos* 102:16663–16682. <https://doi.org/10.1029/97JD00237>
- Morales-Acuña E, Torres CR, Linero-Cueto JR (2019) Surface wind characteristics over Baja California Peninsula during summer. *Reg Stud Mar Sci* 29:1–6. <https://doi.org/10.1016/j.rsma.2019.100654>
- Olson JB, Kenyon JS, Djalalova I, Bianco L, Turner DD, Pichugina Y, Choukulkar A, Toy MD, Brown JM, Angevine WM, Akish E, Bao JW, Jimenez P, Kosovic B, Lundquist KA, Draxl C, Lundquist JK, McCaa J, McCaffrey K et al (2019) Improving wind energy forecasting through numerical weather prediction model development. *Bull Am Meteorol Soc* 100:2201–2220. <https://doi.org/10.1175/BAMS-D-18-0040.1>
- Pereyra-Castro K, Caetano E, Martínez-Alvarado O, Quintanilla-Montoya AL (2020) Wind and wind power ramp variability over Northern Mexico. *Atmosphere (Basel)* 11:1281. <https://doi.org/10.3390/atmos11121281>
- Pleim JE (2007a) A combined local and nonlocal closure model for the atmospheric boundary layer. Part I: model description and testing. *J Appl Meteorol Climatol* 46:1383–1395. <https://doi.org/10.1175/JAM2539.1>
- Pleim JE (2007b) A combined local and nonlocal closure model for the atmospheric boundary layer. Part II: application and evaluation in a mesoscale meteorological model. *J Appl Meteorol Climatol* 46:1396–1409. <https://doi.org/10.1175/JAM2534.1>
- SENER (2018) *Prospectiva de Energías Renovables 2018-2032*. México
- Siuta D, West G, Stull R (2017) WRF hub-height wind forecast sensitivity to PBL scheme, grid length, and initial condition choice in complex terrain. *Weather Forecast* 32:493–509. <https://doi.org/10.1175/WAF-D-16-0120.1>
- Skamarock WC, Klemp JB, Dudhia J, et al (2005) A description of the advanced research WRF version 2. NCAR Technical Note NCAR/TN-468+STR, Boulder, CO
- Stull R (2012) *An introduction to boundary layer*, First edn. Kluwer Academic Publishers
- Taylor KE (2001) Summarizing multiple aspects of model performance in a single diagram. *J Geophys Res Atmos* 106:7183–7192. <https://doi.org/10.1029/2000JD900719>
- Torres CR, Lanz EE, Larios SI (2016) Effect of wind direction and orography on flow structures at Baja California Coast: a numerical approach. *J Comput Appl Math* 295:48–61. <https://doi.org/10.1016/j.cam.2015.02.039>
- Turrent C, Zaitsev O (2014) Seasonal cycle of the near-surface diurnal wind field over the bay of La Paz, Mexico. *Boundary-Layer Meteorol* 151:353–371. <https://doi.org/10.1007/s10546-014-9908-4>
- Vincent CL, Pinson P, Giebela G (2011) Wind fluctuations over the North Sea. *Int J Climatol* 31:1584–1595. <https://doi.org/10.1002/joc.2175>
- Warner TT (2010) *Numerical weather and climate prediction*. Cambridge University Press



## Capítulo 5. Caracterización de rampas de viento y corrección estadística del sesgo en el modelo NAM

Artículo de investigación

"Wind-Ramp Predictability"

(Pereyra-Castro y Caetano, 2022)

La naturaleza intermitente de los recursos eólicos es un desafío para su integración en el sistema eléctrico. La identificación de los sistemas meteorológicos y el pronóstico preciso de las rampas de viento pueden mejorar la gestión de la energía eólica. En este estudio, las rampas extremas de viento se caracterizaron en términos de duración, persistencia y sistema atmosférico para cuatro sitios geográficos diferentes. Los sistemas de latitudes medias son la principal causa de rampas de viento en México durante el invierno. Las rampas asociadas duran alrededor de 3 h, pero los vientos intensos se mantienen hasta por 40 h. Las tormentas provocan rampas extremas de viento en verano debido a la contribución de la corriente descendente a la ráfaga de viento. Esos eventos duran alrededor de 1 a 3 h. La reducción de escala dinámica es costosa desde el punto de vista computacional y las técnicas estadísticas pueden mejorar la previsión del viento. Por ello, se realizó una evaluación del modelo operativo North American Forecast System (NAM) y el efecto de dos métodos de corrección de sesgo (sesgo simple y mapeo de cuantiles) para simular rampas de viento en dos sitios seleccionados. El ajuste estadístico reduce el exceso de no-rampas ( $\leq |0.5|$  m/s) previsto por NAM en comparación con las rampas de viento observadas. De acuerdo con los índices derivados de la tabla de contingencia, la corrección de la distribución de la rampa de viento con el método de sesgo simple o el método de mapeo de cuantiles mejora la predicción de rampas positivas y negativas.



Article

# Wind-Ramp Predictability

Karla Pereyra-Castro <sup>1</sup>  and Ernesto Caetano <sup>2,\*</sup> 

<sup>1</sup> Posgrado en Ciencias de la Tierra, Universidad Nacional Autónoma de México, Ciudad de México 04510, Mexico; karpereyra@comunidad.unam.mx

<sup>2</sup> Instituto de Geografía, Universidad Nacional Autónoma de México, Ciudad de México 04510, Mexico

\* Correspondence: caetano@unam.mx; Tel.: +52-55-5623-0222 (ext. 45459)

**Abstract:** The intermittent nature of wind resources is challenging for their integration into the electrical system. The identification of weather systems and the accurate forecast of wind ramps can improve wind-energy management. In this study, extreme wind ramps were characterized at four different geographical sites in terms of duration, persistence, and weather system. Mid-latitude systems are the main cause of wind ramps in Mexico during winter. The associated ramps last around 3 h, but intense winds are sustained for up to 40 h. Storms cause extreme wind ramps in summer due to the downdraft contribution to the wind gust. Those events last about 1 to 3 h. Dynamic downscaling is computationally costly, and statistical techniques can improve wind forecasting. Evaluation of the North American Mesoscale Forecast System (NAM) operational model to simulate wind ramps and two bias-correction methods (simple bias and quantile mapping) was done for two selected sites. The statistical adjustment reduces the excess of no-ramps ( $\leq |0.5|$  m/s) predicted by NAM compared to observed wind ramps. According to the contingency table-derived indices, the wind-ramp distribution correction with simple bias method or quantile mapping method improves the prediction of positive and negative ramps.

**Keywords:** wind ramp; weather forecasting; wind energy



**Citation:** Pereyra-Castro, K.; Caetano, E. Wind-Ramp Predictability.

*Atmosphere* **2022**, *13*, 453. <https://doi.org/10.3390/atmos13030453>

Academic Editors: Massimiliano Burlando and Jimy Dudhia

Received: 29 December 2021

Accepted: 8 March 2022

Published: 11 March 2022

**Publisher's Note:** MDPI stays neutral with regard to jurisdictional claims in published maps and institutional affiliations.



**Copyright:** © 2022 by the authors. Licensee MDPI, Basel, Switzerland. This article is an open access article distributed under the terms and conditions of the Creative Commons Attribution (CC BY) license (<https://creativecommons.org/licenses/by/4.0/>).

## 1. Introduction

Wind energy is an alternative electricity generation prospect, and can reduce carbon dioxide emissions into the atmosphere, unlike fossil fuels. The intermittent nature of this power source has prompted the development/refinement of wind forecasting systems. One aspect to consider when evaluating models is their ability to reproduce the high-frequency variations of the wind. These changes in the magnitude of the wind in periods ranging from minutes to hours are defined as ramps. Ramp events can represent a critical situation for energy systems, due to an energy imbalance and associated costs. There are several definitions of wind-power ramp [1,2], such as, for instance, a percentage of change of the rated power or as a specific value of power related to the size of the wind farm. Wind-power ramps obtained from wind farm records can originate from the management of the wind farm and are not necessarily associated with an atmospheric phenomenon [2]. Wind ramps reveal the presence of atmospheric phenomena such as cold fronts, hurricanes, storms, sea-land breezes, valley-mountain breezes, etc.

Wind-power ramps are challenging for power-system operators, as they must manage grid operations to optimize costs and avoid damage to the power grid or wind turbines. The prediction of wind ramps is useful for reducing the uncertainty of electricity generation. Wind-power operators need to anticipate the amplitude and timing of wind ramps for better integration into the power grid. With the planned growth of the wind-power share of the global electricity portfolio, wind ramps may become a critical issue. Intermittent and abrupt changes in wind speed pose a risk to grid stability, especially during periods of low generation when there is limited availability of reserve power [3]. Curtailment of wind ramps represents a loss of potential profits and a possible increase in energy prices [4].

Mismanagement of wind ramps can result in power outages. Recently, assessment of wind-ramp forecasting using NWP models has grown [2,3,5–7], in order to implement adequate management of wind farms and mitigate issues as grid instability and economic losses. Regions with wind-energy potential are usually located over complex terrain where the near-surface flow is difficult to simulate. As result, model improvements are necessary for better wind-speed and wind-ramp prediction. Forecast errors can be associated with initial conditions or with the description of physical processes in the models [7].

Improving numerical weather prediction (NWP) (see Table S1 in Supplementary Material for a list of abbreviations) models require relevant observational data for the assessment of NWP performance for wind energy. Observations of meteorological towers and LiDAR permit the evaluation of the horizontal and vertical distribution of the wind; the latter is particularly important to determine the wind speed at the height of the rotor layer, to avoid vertical wind interpolation. Projects such as the Wind Forecast Improvement Project (WFIP) [4] have been designed to improve the accuracy of short-term (0–6 h) wind-power forecasting. The WFIP used wind profile radars, sodars, several LiDARs, and surface flux stations, instrumented tall towers, and nacelle anemometers. A reduction (12–5% for forecast hours 1–12) in power root-mean-square error was achieved from the combination of improved numerical weather prediction models and the assimilation of new observations [8]. A reduction of errors can also be obtained through statistical correction or post-processing data. Post-processing is used to adjust the model bias to historical observational data [9]. Ensemble predictions of NWP are constructed under several initial conditions or several physical parameterizations, and the runs capture the inherent uncertainty in model outputs. An ensemble prediction of planetary boundary layer (PBL) parameterizations can be useful in wind forecast [10].

A short-range weather forecast is a key component for the improvement of decision-making under weather situational awareness. NWP forecasts especially for rapidly changing weather conditions require frequent updates. In response to that problem, the Rapid Update Cycle was created [11]. This was replaced by the Rapid Refresh Model (RAP) in 2012. RAP is used for various applications including aviation, severe weather, and energy [11]. The ability of the model for capturing severe weather conditions can help predict wind ramps related to storms.

Understanding the weather systems that generate wind ramps at specific locations can be helpful for designing a model configuration that reproduces adequately weather event characteristics. Middle-latitude systems are the main weather systems that produce large wind-speed changes in winter in Mexico [12]. However, a common issue in the prediction of wind ramps is their magnitude and timing.

On the other hand, predictability in summer is low because the systems that originate the ramps are mesoscale systems such as valley–mountain and sea–land breezes or Mesoscale Convective Systems [12]. Synoptic systems dominate the weather in winter and they can be forecasted days in advance with good accuracy. In summer, local effects such as the differential warming of hills and valleys or land and sea surfaces produce thermally driven circulations that dominate the weather. Soil moisture and atmospheric instability help the development of scattered showers and thunderstorms [13]. The triggers for a thunderstorm development can be difficult to determine some hours before its formation. The atmospheric processes involved in summer weather are complex, with an important interaction of topography. In mesoscale models, surface inhomogeneities resulting from a rough description of terrain and/or surface features generates an inadequate representation of the above-mentioned processes [13]. Mesoscale models can reproduce horizontal and vertical temperature and humidity with high accuracy, but they have problems modeling adequately shallow and deep convection, leading to misallocation of centers of convection activation [13].

The identification of the meteorological phenomena that produce wind ramps in a region provides information on the characteristics of the ramps and the necessary refinements in the physical configuration of the model. The focus of the study is to present



some tools to improve wind-ramp forecast. Wind generation cannot be fully controlled, unlike to conventional power plants (thermal or hydropower plants). The assessment of extreme wind events and the underlying role of weather regimes in triggering these events is crucial. Characterization can permit an increase in the predictability of wind ramps in terms of the seasonality of weather systems generating these ramps and the persistence of intense winds. Additionally, the examination of post-processing statistical tools for adjusting NWP outputs to local conditions can improve wind-ramp prediction. Cold fronts account for most of the ramps in winter. As a typical synoptic event, they are predictable several days in advance. However, ramps associated with storm events can be difficult to accurately predict more than a couple of hours in advance. Better storm prediction (time, intensity, and location) can lead to improved wind-ramp prediction in summer. In this study, extreme wind ramps were characterized at four different geographical sites in terms of duration, persistence, and weather system. Additionally, the skill in predicting ramps of an operational forecast model available for Mexico, the North American Mesoscale Forecast System (NAM), is evaluated. The outputs are freely accessible and contain information since 2006; however, its use for wind energy purposes has been little explored.

Section 2 introduces the horizontal wind observational data from weather stations and masts used in this study and a brief description of the NAM model. Additionally, in this section the definition of wind ramps, indices for the verification of ramp events, and bias-correction methods applied to NAM outputs are presented. The weather systems generating wind ramps at four different geographical sites in Mexico are discussed in Section 3. Ramp verification is included in Section 3. Lastly, conclusions are presented in Section 4.

## 2. Materials and Methods

The observational wind data used in this study are from two weather stations of the National Meteorological Service and two masts from the National Institute of Electricity and Clean Energies (Figure 1). Location and record periods are indicated in Table 1. Weather stations measure 10-m wind speed and direction every 10 min. Meanwhile, wind masts report winds at 20 m in Francisco Villa (FCOV) and at 15 m in La Venta (LVEN) every 10 min.

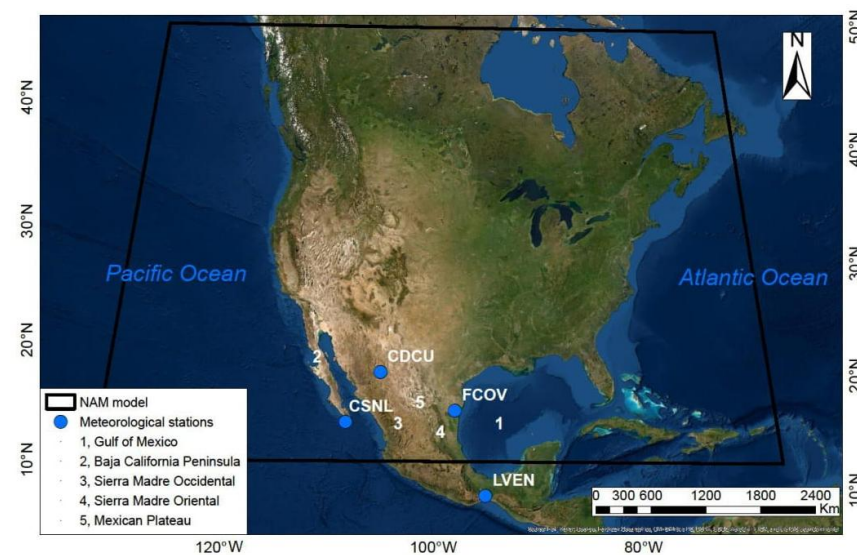


**Figure 1.** Weather stations and masts (blue dots) used in the study and North American Forecast System (NAM) domain (black line). Cabo San Lucas (CSNL), Ciudad Cuauhtemoc (CDCU), Francisco Villa (FCOV), and La Venta (LVEN).

**Table 1.** Description of measurement sites.

Station	ID	Latitude	Longitude	Period
Cabo San Lucas	CSNL	22.881	−109.926	2010–2016
Ciudad Cuauhtemoc	CDCU	28.396	−106.839	2010–2016
Francisco Villa	FCOV	25.020	−98.0875	2006–2007 and 2010–2012
La Venta	LVEN	16.579	−94.816	2000–2007 and 2012

The mast installed in FCOV and LVEN measured the wind speed and the wind direction with NRG Maximum 40 cup anemometers and NRG 200P wind vane, respectively. The station monitored the variables every 2 s. It calculated and recorded speed average wind speed, wind gust, and wind direction every 10 min. The data-logger was a Campbell CR100. There are no specifications available of the equipment in Ciudad Cuauhtemoc (CDCU) and Cabo San Lucas (CSNL) weather stations. The observed hourly wind gust is the maximum 10 min wind gust observed for one hour.

### 2.1. NAM Model

NAM outputs were used to assess the ability of an operational model to predict wind ramps in Mexico. Bias-correction methods were applied to the model data for adjusting to the observed wind-ramp distribution. After this correction, NAM non-corrected and NAM-corrected data performance were assessed. CDCU and CSNL weather stations were used for wind-ramp evaluation because both have the longest and recent record periods (2010–2016). Additionally, both areas have wind-power potential, but wind farms have not been installed yet.

The NAM is one of the National Centers for Environmental Prediction’s (NCEP) major models for producing regional weather forecasts. NAM model forecasts were obtained from the National Oceanic and Atmospheric Administration’s (NOAA) National Centers for Environmental Information [14]. The NAM model has been running with a non-hydrostatic version of the Weather Research and Forecasting (WRF) model at its core since June 2006. The NAM is initialized with a 6-h data assimilation cycle with hourly analysis updates using the NCEP hybrid variational ensemble analysis for the 12 km parent domain (Figure 1). Wind-ramp verification was done using the 24-h NAM forecast initialized at 0000 UTC at 10 m height (the wind measurement height of weather station). The model uses hybrid sigma-pressure vertical coordinates, with 2 mb model top pressure and 60 vertical layers. Presently, NAM includes a full set of parameterizations for physical processes, including the Janjic-modified Betts–Miller convection and Mellor–Yamada–Janjic 2.5 scheme for turbulent exchange [15].

The NAM model runs multiple domains of weather forecasts over the North American continent at various horizontal resolutions [14]. High-resolution forecast windows are generated over fixed regions and are occasionally run to follow significant weather events, such as hurricanes. The NAM system is constantly tested and its configurations are modified to improve the quality of forecasts [16,17]. This system has been evaluated in terms of the process associated with convection initiation [18], which can influence the ability to predict wind ramps associated with storms. The NOAA Environmental Modeling Center looked extensively into the cause of noisy profiles of temperature and moisture in the presence of strong updrafts in NAMv3 [19], and ultimately developed a routine to stabilize all vertical layers above the boundary layer [20]. These changes were implemented in NAM version 4, which became operational in early 2017 [18]. The recent model improvements resulted in best simulation of storms tracks and outflows.

### 2.2. Wind-Power Spectra

The power spectra of wind-speed data were computed using the Fourier transform. For a clear representation of spectral peaks and valleys, the frequency-weighted form of the spectrum  $fS(f)$  is used [21–23]. We investigate the spectral structure for the four geo-



graphical sites. The construction of the wind-energy spectra was used to detect the relevant atmospheric phenomena in the production of wind ramps for each region. Atmospheric phenomena that significantly affect the region generate energy peaks in the spectrum, which are associated with a periodicity.

### 2.3. Wind Ramps

Probability density function (PDF) of the hourly wind-speed increments/decrements normalized by their standard deviation is constructed to analyze the differences among the four geographic locations, a similar procedure applied by DeMarco et al. [24].

For a time increment ( $\tau = 1$  h), the wind-speed ramp is defined as the difference between the wind speed at time  $t + \tau$  and the wind speed at the starting time ( $t$ ). The wind increment/decrement values are normalized by the standard deviation ( $\sigma_{\delta U}$ ) [24].

$$\delta U(t) = \frac{U(t + \tau) - U(t)}{\sigma_{\delta U}} \quad (1)$$

The periods used for the calculation of observed PDFs are shown in Table 1. Observed PDFs of wind ramps show similar shape and heavier tails than Gaussian PDFs for different meteorological and topographical conditions (Figure S1 in Supplementary Material). Based on similar distributions for all four sites, we define extreme ramps as those exceeding four times the normalized deviation of the wind ramps ( $\delta U(t) > 4$ ).

The verification of the ramp simulation with the NAM model was carried out by constructing indices derived from contingency tables. The ramp is considered positive (ramp-up) or negative (ramp-down) whether the wind speed increases or decreases over time. On verification, a ramp-up (down) event occurs when the wind-speed change is greater (less) than 0.5 m/s (−0.5 m/s) for one hour. A wind magnitude changing  $\leq |0.5|$  m/s is considered a no-ramp event.

### 2.4. Ramp Categorization

The weather circulation types are identified for every wind-ramp event. Winter wind ramps are mainly related to frontal system passages that cause prevailing intense wind from a persistent direction. Examining surface winds and the horizontal gradient of equivalent potential temperature at 700 mb using ERA5 shows the displacement of a cold front over the region. The verification of cold front position near the weather station was done using the MODIS-corrected reflectance images [25] for the day of the wind-ramp event. Cold front reports in newspapers were also consulted. Prefrontal and postfrontal wind intensification is usually experienced at weather station. In locations near the Gulf of Mexico, such as FCOV and LVEN masts, the interaction between topography and the high pressure systems associated with the cold front originates wind intensification events known as a “Norte” [26] or “Surada” [27].

Tropical cyclones and easterly tropical waves were associated with wind-ramp events examining trajectories of these systems in the NOAA Tropical Cyclone Reports [28].

A wind ramp is classified as related to storms when intensification of wind is observed in the weather station and precipitation occurs on the weather station or nearby. Additionally, cloud top height (AIRS2RET\_NRT, [29]) and MODIS cloud top temperature [30] were analyzed to identify Mesoscale Convective Systems [31].

### 2.5. Downdrafts

Gustiness in horizontal winds near the surface is often associated with convection. Downdrafts possess vertical momentum which, on approaching the ground, is deflected to the horizontal [32,33]. Different convective gust models have been proposed [33]. Nakamura [32] considers that downdrafts are driven by three terms: the momentum of the parcel at the top of the downdraft, the latent heat-induced negative buoyancy of the air, and



the precipitation loading effect. For quantifying the possible contribution of downdrafts in the wind ramps, we employed Nakamura-based scheme used by the Met Office [33].

$$U_g = 0.67 \sqrt{U^2_{T_w=0} + \frac{gH_{T_w=0}T_{deficit}}{T_{mean}} + \frac{2gH_{T_w=0}P_{max}}{(5)(60)(60)}} \quad (2)$$

where  $T_{mean}$  is the absolute temperature of the environment in K over depth  $H_{T_w=0}$  in m, calculated under the assumption that for summer thunderstorms, the downdraught originates near the melting level for precipitation, given by the wet bulb temperature freezing level ( $H_{T_w=0}$ ).  $T_{deficit}$  is the difference between the  $T_{mean}$  and  $T_{surface}$  in K.  $U_{T_w=0}$  is the initial wind speed in m/s,  $P_{max}$  is the maximum precipitation rate in mm/h and  $g$  is the acceleration due to gravity in  $m/s^2$ .

## 2.6. Bias-Correction Methods

Bias adjustment is usually applied to model wind time series for reproducing similar statistical properties of observations [34], reducing systematic errors. They result from the inability of the NWP to reproduce all the relevant atmospheric processes and orographic interactions of flows. Additionally, bias originates from the initialization of data and model resolution [35]. In this study, two bias-adjustment methods have been applied to the 24-h NAM forecast of wind ramps: simple bias adjustment and quantile mapping adjustment.

The simple bias-correction scheme is summarized as:

$$y'_i = (y_i - \bar{y}) \frac{\sigma_x}{\sigma_y} + \bar{x} \quad (3)$$

Wind-ramp anomalies are calculated by subtracting the forecast mean ( $\bar{y}$ ) to each forecast at a particular time ( $y_i$ ). A new wind-ramp forecast ( $y'_i$ ) is calculated by multiplying the NAM non-corrected forecast anomaly by the ratio of the standard deviation of the reference dataset (observations) ( $\sigma_x$ ) to the standard deviation of the NAM non-corrected wind-ramp forecast ( $\sigma_y$ ). Finally, the mean of the reference data set ( $\bar{x}$ ) is added to the anomaly.

Quantile mapping (QM) correction involves transforming the distribution functions of the modeled wind ramp into the observed ramp distribution using a mathematical function [34,36]. The method employs the PDFs of the reference dataset and the PDFs of the NAM forecasts in the reference period and then the empirical cumulative distribution function (CDF) is defined. A transfer function for correcting an independent forecast  $y_f(t)$  is defined as:

$$y'_i = F_x^{-1}(F_y(y_f(t))) \quad (4)$$

with  $y'_i$  a NAM-corrected forecast in a particular time,  $F_y$  is the cumulative distribution function of NAM data and  $F_x^{-1}$  is the inverse cumulative distribution function of observation during the reference period. The QM method uses the quantile–quantile relationship to converge the simulated variables' distribution function to the observed one. In cases where the data had missing values, the corresponding simulated values were omitted to obtain time series of equal length [37]. The years 2010–2015 were used as the reference period.

## 2.7. Contingency Table

Addressing the ability of NAM-corrected and NAM non-corrected is done through a contingency table [38]. The table summarizes the relationship between observed and forecasted wind ramps. A Hit or True Positive (TP) is the number of times a wind ramp is reproduced by the model, meanwhile the number of times a wind ramp is not forecasted is called a Miss or False Negative (FN). The events that are forecasted but not observed are called False Alarm or False Positive (FP). False Negative (FN) is the absence of wind ramps events correctly forecasted by the models. Indices for evaluating model performance in the

detection of wind ramps are constructed with the elements of the contingency table. The following indices were used [38]:

Probability of detection (*POD*) measures the percentage of observed wind ramps (*TP*) that are correctly predicted by the model (*TP + FN*).

$$POD = \frac{TP}{TP + FN} \quad (5)$$

False Alarm Rate (*FAR*) is the percentage of forecasted events that were not observed.

$$FAR = \frac{FP}{FP + TP} \quad (6)$$

Frequency bias (*FBIAS*) measures the ratio of forecasted ramp events to observed ramp events.

$$FBIAS = \frac{TP + FP}{TP \times FN} \quad (7)$$

Critical success ratio (*CSI*) is the number of True Positive events between the forecasted events and the missed events (*TP + FP + FN*).

$$CSI = \frac{TP}{TP + FP + FN} \quad (8)$$

### 3. Results

#### 3.1. Wind-Power Spectra

In this section, the analysis of long-term mean wind and turbulence data is discussed. Spectral peaks are evident in  $3 \times 10^{-8}$  Hz (1 year, see Figure S2), between  $2 \times 10^{-6}$  Hz and  $3 \times 10^{-6}$  Hz (3.9 to 5.7 days) and  $1 \times 10^{-5}$  Hz (1 day). Near-surface diurnal and sub-diurnal wind maxima decrease slightly with height. At frequencies higher than  $8 \times 10^{-5}$  Hz, the spectrum falls off  $-2/3$  slope for the four sites (Figure 2). On the low-frequency side of the frequency-weighted spectrum, the yearly spectrum rises at  $f^{+1}$  from  $10^{-7}$  to  $10^{-6}$  Hz except for LVEN mast.

Low-frequency events (~6 days) are more common in winter (yellow and orange lines in Figure 2) due to frontal systems over Mexico. Although these do not simultaneously affect the analyzed sites, they are the main middle latitudes synoptic modulators of winter weather. The effect of those systems is clearly observed at CDCU station (Figure 2b), during December–January–February (DJF) and March–April–May (MAM) as an increase in energy at the low-frequency side of the spectrum. Low-frequency maximum is associated with easterly waves during summer on southern Mexico. LVEN is the mast with the largest energy in the low-frequency side of the spectrum (Figure 2d), showing these synoptic phenomena are relevant for wind energy in the region. At CSNL station, the seasonal maximum of the spectrum in low-frequency events occurs in September–October–November (SON) (Figure 2a), due to tropical cyclone activity in the Pacific Ocean [39] and cold fronts passage over the region.

In summer, June–July–August (JJA) and starting in spring, local circulations intensify, as synoptic systems weaken, there is a decrease in energy associated with low-frequency events (Figure 2). The thermal differences caused by the heterogeneity of the surfaces produce local circulations with duration between 8 and 12 h, manifesting as daytime and hourly maxima in the spectrum that are more evident in the summer period. The spectral peak in  $1 \times 10^{-5}$  Hz of sea-breeze circulation is higher than the observed in middle latitudes. The appropriated prediction of these weather systems is important in spring and summer for a better representation of wind and wind ramps as mentioned by Pereyra-Castro et al. [12]. Near-surface diurnal and sub-diurnal wind maxima decrease slightly with height, they become less relevant as the wind rotor is far from the surface.

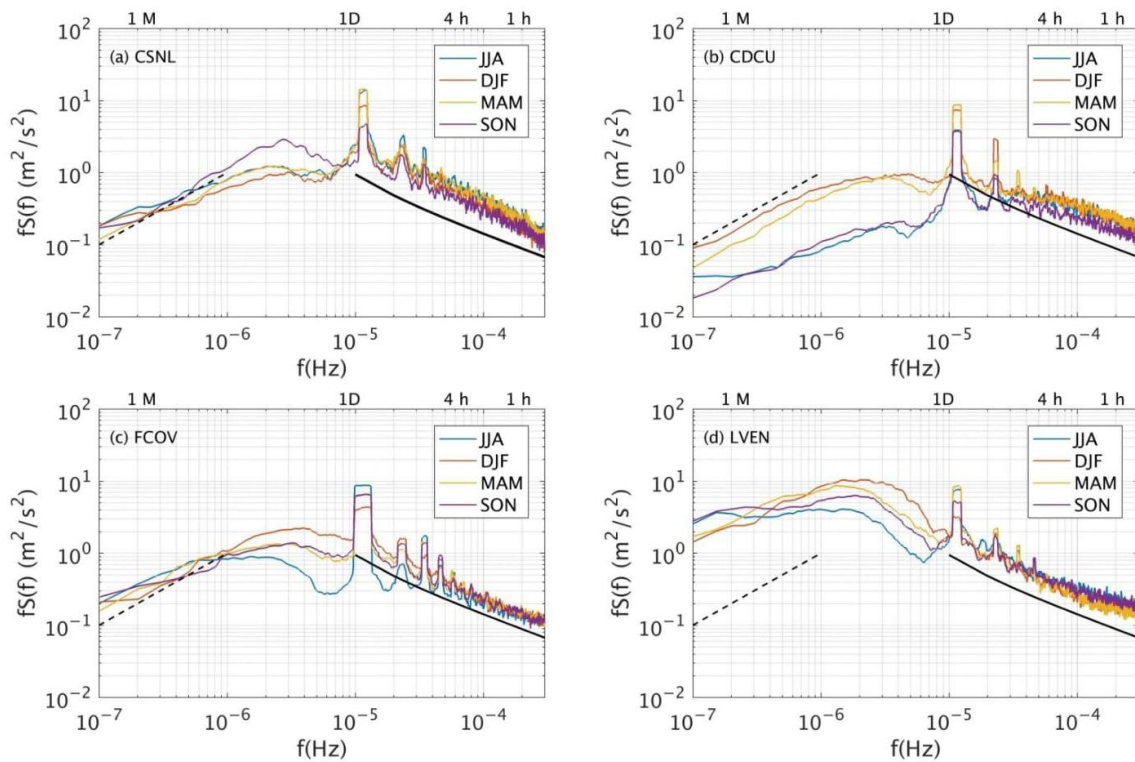


**Figure 2.** Seasonal smoothed frequency-weighted spectra  $fS(f)$  of horizontal wind speed for (a) Cabo San Lucas (CSNL), (b) Ciudad Cuauhtemoc (CDCU), (c) Francisco Villa (FCOV), (d) La Venta (LVEN). The solid black line corresponds to the slope  $f^{-2/3}$ . The dotted black line represents the  $f^{+1}$  slope. JJA: June–July–August (blue line); DJF: December–January–February (orange line); MAM: March–April–May (yellow line); SON: September–October–November (purple line).

### 3.2. Characteristics of the Persistence of Wind Ramps

Extreme ramp events are caused by frontal systems during winter (Figures 3 and S3–S5). Figure 3 shows the wind-ramp duration for extreme events. Every event started with a wind change exceeding four times the normalized deviation of wind ramps in one hour. After the initial increase in wind speed, it can continue going up, lasting from 2 to 4 h (ramp-up). After a wind-ramp event, the wind speed can be sustained within a given interval of intense wind-speed values, the duration is defined as persistence [40] (Figure S6). The regional orographic characteristics modify the persistence and intensity of the wind ramps. In LVEN mast, the low-level atmospheric flow is channeled into the Isthmus of Tehuantepec, where the winds associated with cold fronts generate ramps with an average duration of 6 h and intense winds lasting on average 40 h (Figure 3d). In FCOV mast, the ramps associated with cold fronts last 2.5 h and persist for 7 h on average. In the sites located in the northwest of Mexico, CDCU and CSNL, the intense events persist for 4 h (Figure 3a,b). One characteristic of cold fronts that needs to be highlighted is that a front that moves over the region of FCOV mast tends to generate intense winds in the Mexican Plateau (CFT), the effect of which can be seen in CDCU station. Similarly, a cold front over the Mexican Plateau will affect the intensity of the winds in the region of FCOV mast (CFP) and Baja California Peninsula.



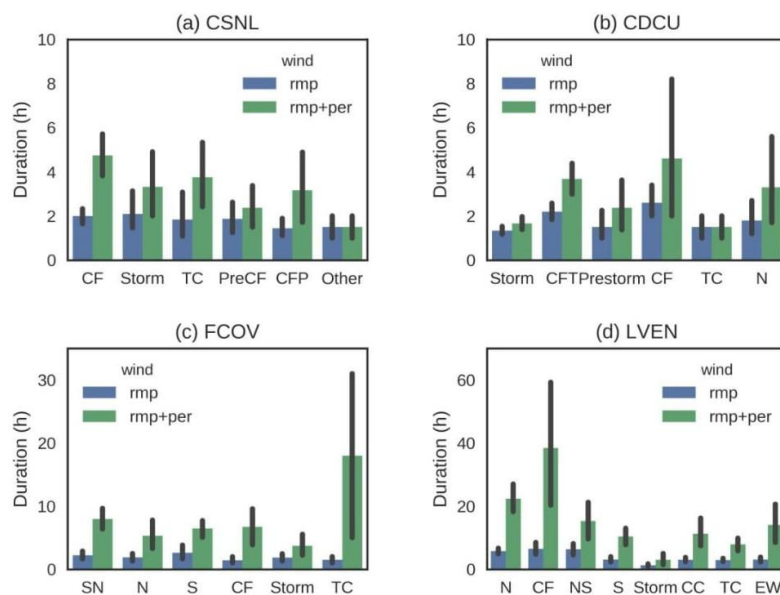


**Figure 3.** Wind-ramp duration and associated intense winds at (a) CSNL, (b) CDCU, (c) FCOV, (d) LVEN. Weather systems: Cold front (CF), Tropical Cyclone (TC), Pre-Cold Front (PreCF), Nortés (N), Surada (S), Transition Surada to Norte (SN), Easterly wave (EW), Cyclonic Circulation (CC). Cold front over Plateau (CFP) and cold front over FCOV (CFT). Rmp means wind ramp and (Rmp + per) refers to the wind ramp and persistence of intense winds.

The anticyclonic circulations associated with the mid-latitude wave can cause northerly winds in the Gulf of Mexico  $> 30$  m/s. These intense winds over the Gulf of Mexico are called Nortés. The average duration of the intense winds is 22 h in LVEN station and 6 h in FCOV mast with ramps of 4 to 5 h. Before a Norte, warm and intense southerly winds known as Suradas can be generated. These winds persist for up to 10 h in LVEN mast and 8 h in FCOV mast. Some extreme ramps originate from Nortés to Surada or Surada to Nortés event transitions, which occur in 2 to 3 h periods, but strong winds persist for 10 to 14 h (Figure 3c).

In summer, the formation of Mesoscale Convective Systems (MCS) in some regions of Mexico generates extreme wind ramps of short duration; the winds intensify for 1 or 2 h and are sustained for another hour. Its duration does not vary with regional topographic characteristics. Strong winds associated with tropical cyclones and/or hurricanes can last for days, as seen in FCOV mast (Figure 3c). The persistence of ramp events depends on the proximity of the tropical cyclones to the study site, generating intense winds in periods of 1 to 8 h. At some stations during these events, the sensors do not register the wind, showing ramp events shorter than those observed.

### 3.3. Weather Conditions Generating Extreme Wind Ramps

Wind-ramp events observed during winter months are caused by the passage of cold fronts over Mexico; examples are shown in Figure 4. Surface winds are front position indicators at CDCU, CSNL, FCOV and LVEN. Westerly cold fronts tend to pass over CDCU station intensifying wind speed (Figure 4b). As they move eastward, they can also generate wind ramps at FCOV mast (Figure 4c) and LVEN mast. Cold fronts accelerate wind in the station, even if the cold front is not directly over the study point (Figure 4b). Wind-power variability can be dominated by synoptic phenomena for days changing the power production. The energy increase in the lower frequency side of the power spectrum during DEF and MAM (Figure 2). When passing over the Mexican Plateau, there is an intense

westerly wind at CDCU station, generating ramps. At the same time, strong wind from the east or southeast is observed over the Gulf of Mexico (Figure 4b). These events generate wind ramps in the region of the FCOV station, when the wind is from the southeast. These events are similar to the weather patterns reported by Thomas et al. (2020) [41], they are common from January to May and they contribute significantly to extreme winds. The winter wind ramps in CDCU station and FCOV mast are related, the passage of a frontal system over CDCU station tends to generate ramps in FCOV mast and vice versa.

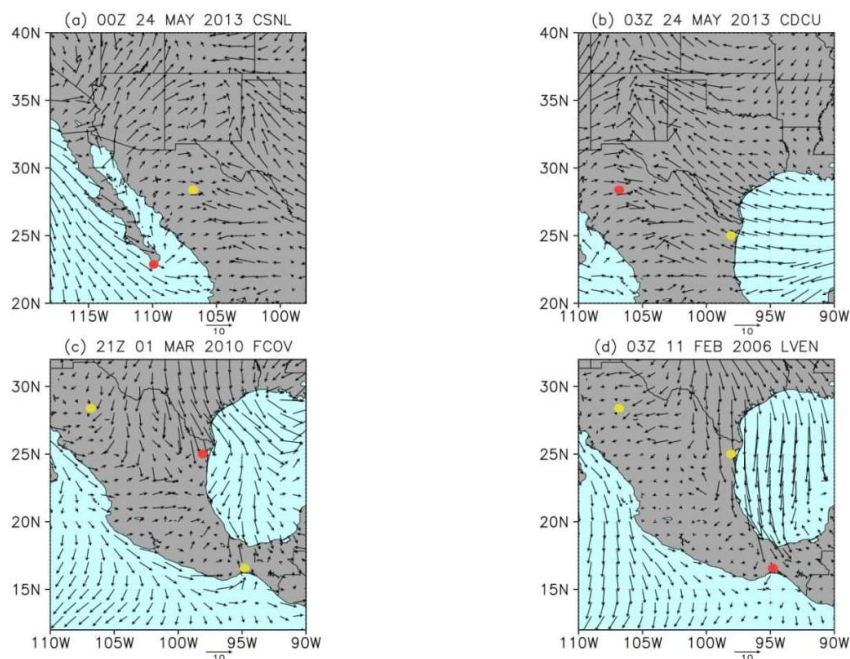


**Figure 4.** Cold fronts affecting (a) CSNL, (b) CDCU, (c) FCOV and (d) LVEN. From ERA5 [42] surface wind for typical cold fronts causing wind ramp. Dots show weather stations location. Red dot indicates weather station or mast experiencing the wind ramp.

Wind-ramp events at CDCU and CSNL stations in summer are mainly caused by downdrafts of convective systems forming in Sierra Madre Occidental (Figure 5c) or around the region (Figure 5a). These events are usually short duration. Most intense precipitation occurs around the wind-ramp timing (lasting around 2 h). Trade winds intensification from the Gulf of Mexico also contributes to wind ramps over CDCU station and FCOV mast (Figure 5b). Trade winds carry moisture inland and can favor storm formation. Convective systems can also contribute to wind-ramp generation in LVEN mast.

The meteogram illustrates the ramp event that occurred at CSNL station on 1 August 2013 (Figure 6). The storm formed over the Sierra Madre Occidental, then it moved eastward and reached the eastern coast of Baja California at 07:00 Z, where maximum precipitation presented according to CMORPH [43] data at 09:00 Z when the ramp occurs. According to the Nakamura storm gust formula [33] (Equation (2)), the gust in the core of the storm intensifies at 07:00 Z and it stands for 3 h and as the storm approaches the station, the ramp occurs. At 10:00 Z, the storm weakens considerably and a new core of maximum precipitation forms towards the north of Baja California Sur (Figure S7). At this new location, the precipitation is still intense but the distance between the station and the core of the storm is ~70 km (Figure S7). The wind ramp lasts around one hour due to the rapid dissipation of the storm. The storm trajectory forecasted by NAM model differs according to the initialization forecast hour (Figure S7), the displacement of the storm is



more accurately predicted by the 06:00 Z NAM forecast initialization, near the ramp set up. On the other hand, the 00:00 Z NAM initialization predicts the movement of the storm parallel to the Sierra Madre Occidental.

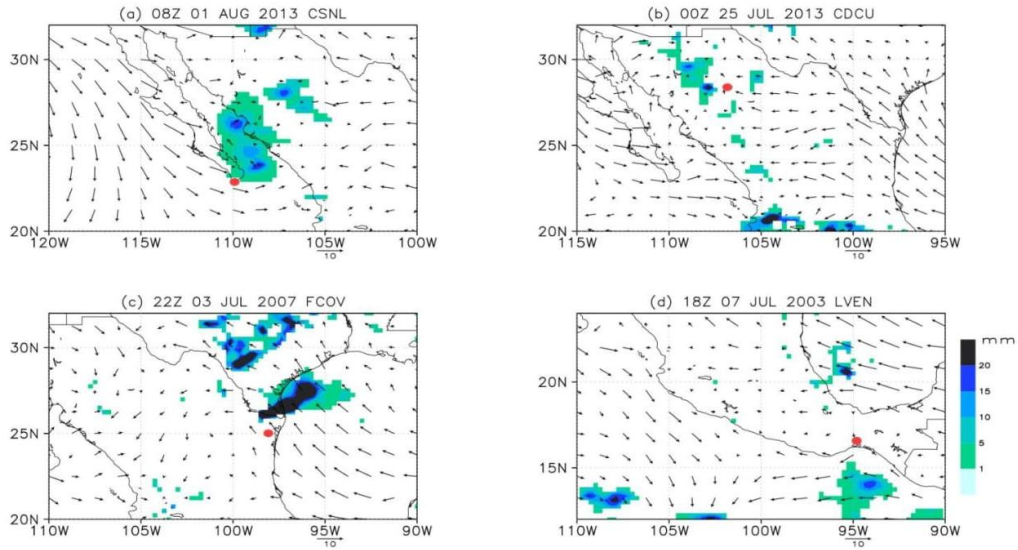


**Figure 5.** Summer ramp-up events at (a) CSNL, (b) CDCU, (c) FCOV and (d) LVEN. Weather station location is indicated with a red circle. 3 h average ERA5 [42] surface wind speed and CMORPH [43] accumulated precipitation in mm (shaded) centered around the wind-ramp occurrence (weather station).

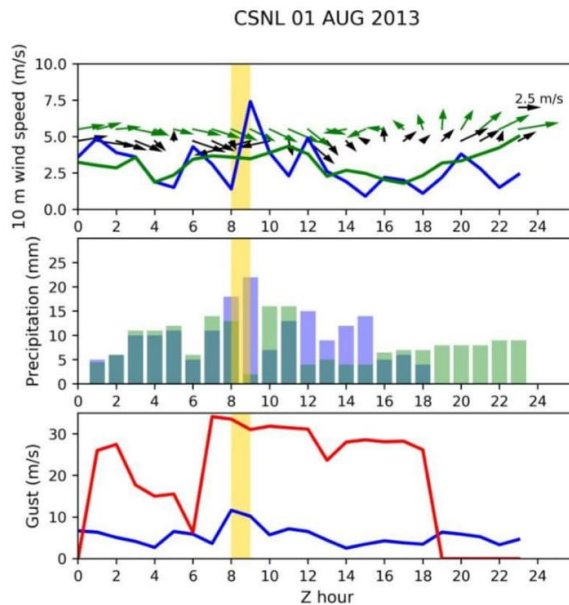


**Figure 6.** Meteogram at CSNL station for a storm at 09:00 Z 01 August 2013. Wind-ramp timing is shaded in yellow. CMORPH [43] maximum precipitation in the center of the storm is in blue bars. Estimated wind gust in the storm is in red line and observed wind gust at CSNL is in blue. Forecasted wind speed, wind vector and precipitation are in green.

In the rest of the ramps shown in Figure 5, the time of occurrence of the ramp coincides with the moment when the storm is closest to the station, even when the precipitation is not the most intense observed during the day (Figures S8–S10). The calculated wind gusts (Equation (2)) due to convection are more intense than the ramps observed at the weather stations because the winds decrease due to the surface friction and the distance between the weather stations and the location where the storms are generated. The displacement of the storm can generate in some cases changes in the mean wind direction before the occurrence of the ramp.

### 3.4. Ramp Distribution Correction

Reanalysis data shows underestimation of high-frequency variability of wind [40]. Winds derived from simulations using mesoscale models also tend to be underestimated due to the spatial and temporal resolutions [44]. The smoothing effect conducts to the overestimation of weak ramp events in comparison to the observed ramps [45]. For this reason, it is necessary to adjust the simulated wind-ramp distribution to the observed distribution. The adjustment is done through simple bias and quantile mapping methods. The statistical corrections fit the predicted ramp distribution fairly well with respect to the observed distribution (Figure 7). Furthermore, to assess the correction effects on ramp forecasting, we use indices derived from contingency tables to compare the onset time of observed and forecast wind ramps. Both methods, as will be seen later, enhance POD index, improving wind-ramp forecasting.

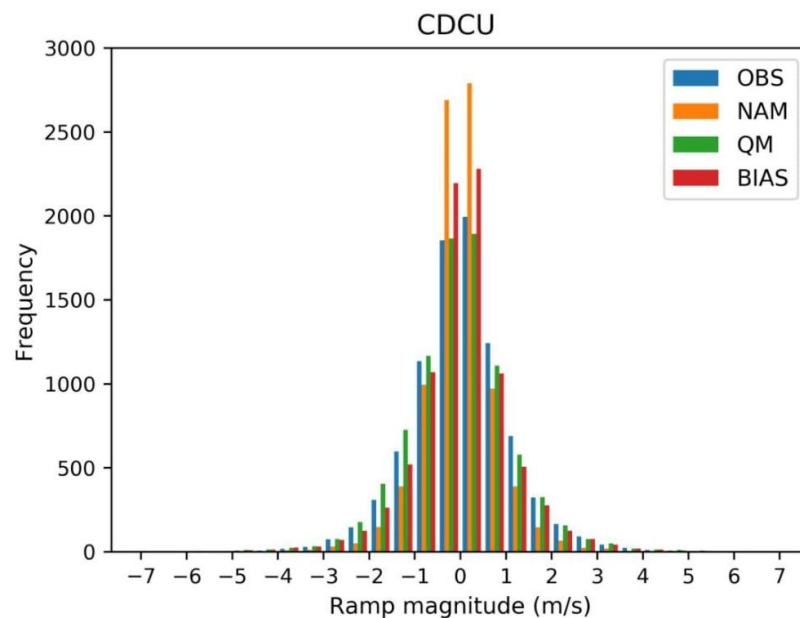


**Figure 7.** Wind-ramp distribution for CDCU observations (blue bar), NAM (orange bar), Quantile mapping correction (QM) (green bar) and Simple bias correction (red bar).

A positive (negative) ramp is an increase (decrease) in wind speed for one hour. The ramp is correctly forecasted when an increment (decrement) in wind-speed change in 1 h is presented in the model wind speed for the same local hour of observation, this event is known as TP (Figure S11). A positive (negative) ramp produced by the model but not observed is a FP (Figure S11). Observed wind-speed changes that show an increment (decrement), but are not predicted are known FN (Figure S11). The effect of relaxing the time threshold was not tested in this study, in those cases a more sophisticated metric that incorporates phase, duration, and amplitude errors is discussed in Bianco et al. [5].

The ramps were grouped into no-ramps  $\leq |0.5|$  m/s, positive ramps ( $>0.5$  m/s) and negative ramps ( $<-0.5$  m/s). In CDCU, the probability of predicting a no-ramp event at the observed timing is 67.3% with NAM non-corrected forecast and decreases with simple bias correction and QM correction to 54.7% and 46.1% respectively (Table 2). The QM statistical adjustment redistributes the excess of predicted no-ramps in the other ramp magnitudes [34]. Therefore, there is an improvement in POD for positive ramps, 36.5% is correctly predicted using simple bias correction and 38.8% using QM correction. An increase in the predictability of negative ramps of 7.1% and 12.5% occur by simple bias and QM correction, respectively. The probability of false detection is slightly lower without applying statistical correction, FAR increases 2% with simple bias correction and  $\sim 3.6\%$  with QM for negative ramps. In the case of positive ramps, FAR increases by  $\sim 2\%$  with simple bias correction and 3.1% with QM adjustment (Table 2). The application of the statistical correction does not significantly affect the FAR of no-ramp events.

**Table 2.** Derived contingency table indexes wind NAM forecast (non-corrected), bias-corrected, and quantile mapping (QM)-corrected for CDCU.

	<b> Ramp  <math>\leq 0.5</math> m/s</b>	<b>Ramp <math>&gt; 0.5</math> m/s</b>	<b>Ramp <math>&lt; -0.5</math> m/s</b>
	<i>POD</i>		
NAM forecast	0.673	0.288	0.272
Simple bias-corrected	0.547	0.365	0.343
QM-corrected	0.461	0.388	0.397
	<i>FAR</i>		
NAM forecast	0.490	0.596	0.615
Simple bias-corrected	0.485	0.614	0.635
QM-corrected	0.489	0.627	0.651
	<i>FBIAS</i>		
NAM forecast	1.320	0.712	0.708
Simple bias-corrected	1.063	0.947	0.938
QM-corrected	0.902	1.040	1.138
	<i>CSI</i>		
NAM forecast	0.409	0.202	0.190
Simple bias-corrected	0.361	0.230	0.215
QM-corrected	0.319	0.234	0.228

Regarding the relationship between predicted ramps and observed ramps (FBIAS), the NAM non-corrected forecast overestimates the frequency of no-ramps and underestimates the positive and negative ramps by  $\sim 30\%$ . However, the forecast with QM adjustment underestimates the weak ramps and overestimates the frequency of negative and positive events around 10% (Table 2). The simple bias correction adjusts the number of predicted positive events with the number of observed positive events (FBIAS  $\sim 1$ ). The frequency of negative ramps predicted with simple bias is slightly underestimated  $\sim 6\%$ .

Finally, the CSI index shows QM correction is the best method for improving the prediction of positive ramps and negative ramps in CDCU station (Table 2) (See Table S2 for more details of adjustment effect on wind ramp magnitudes).

The statistical adjustment of the ramp distribution at CSNL improves the POD of positive (negative) ramps by 13.6% (16.8%) and 10.2% (9.8%) using simple bias method and QM method, respectively. However, statistical adjustment reduces the detection of no-ramps by 30% and 19.1%, respectively (Table 3). False alarms are not substantially altered by both bias-correction methods on negative and no-ramp events. FAR increases by  $\sim 2\%$  when applying the simple bias adjustment.

In CSNL, NAM non-corrected forecast overestimates no-ramp events by  $>50\%$ . QM correction adjusts the number of negative predicted events to the number of observed events (FBIAS  $\sim 1$ ). There is also an improvement in the positive predicted events (FBIAS = 0.884) (Table 3). However, the best fit for this type of event occurs with a simple bias approach (FBIAS = 0.99). The adjustment in the frequency of the events with simple bias method is



reduced for no-ramp and negative events. It is worth mentioning that although the number of events is similar to the number of observed events, they do not coincide in timing, so the POD is ~30%.

**Table 3.** Derived contingency table indexes wind NAM forecast (non-corrected), bias-corrected, and quantile mapping (QM)-corrected for CSNL.

	$ \text{Ramp}  \leq 0.5 \text{ m/s}$	$\text{Ramp} > 0.5 \text{ m/s}$	$\text{Ramp} < -0.5 \text{ m/s}$
	<i>POD</i>		
NAM forecast	0.669	0.189	0.183
Simple bias-corrected	0.369	0.325	0.351
QM-corrected	0.478	0.291	0.281
	<i>FAR</i>		
NAM forecast	0.563	0.655	0.720
Simple bias-corrected	0.559	0.672	0.725
QM-corrected	0.557	0.671	0.719
	<i>FBIAS</i>		
NAM forecast	1.529	0.548	0.654
Simple bias-corrected	0.837	0.990	1.274
QM-corrected	1.079	0.884	1.001
	<i>CSI</i>		
NAM forecast	0.359	0.139	0.125
Simple bias-corrected	0.251	0.195	0.182
QM-corrected	0.298	0.182	0.163

Finally, positive and negative ramps are well reproduced with both statistical adjustments in CSNL station, with a slight advantage of simple bias (3 to 7%) (Table 3) (See Table S3 for more details of adjustment effect on wind ramp magnitudes).

#### 4. Discussion and Conclusions

The management of sudden changes in wind-power generation due to wind-speed variations is challenging for wind-power operators. The identification of meteorological phenomena causing wind ramps needs to be considered in the development of forecasting systems for wind farms to improve the predictability of wind ramps. In this study, we analyzed wind data from four different geographical sites in Mexico. The analysis of the long-term wind-speed spectrum was useful for detecting the energy peaks associated with weather systems. Synoptic phenomena are important throughout the year for sites such as LVEN; however, the contribution of cold fronts to the energy spectrum is relevant during the dry season in sites such as CDCU. Semidiurnal peaks are more pronounced during the spring and summer seasons when thermally driven circulations and storms become more frequent.

Cold fronts are the most common weather systems that originate extreme ramps. LVEN and FCOV masts can also experience wind ramps due to Nortes and Suradas. A winter wind ramp lasts 1 to 4 h, but the persistence of intense winds varies from 5 h in CSNL station to 40 h in LVEN station. These differences are caused by topographic interaction with near-surface flow. In LVEN masts, the channeling of wind flow originates long-lasting intense winds. Meanwhile, in summer, tropical cyclone activity contributes to the production of extreme wind ramps. Summer extreme ramps are also caused by surface gusts from thunderstorm downdrafts moving near observation sites. These events last 1 to 3 h. A case study at CSNL station shows that the onset of a wind ramp is more influenced by the distance between the storm and the weather station than by the precipitation rate at the core of the storm.

Wind-ramp prediction could help manage wind farms more efficiently. Presently, most of the operational regional mesoscale models run in the so-called gray-zone, such as NAM, where the representations of turbulence, convective processes, and the representation of topography are not fully resolved [46]. Statistical correction of model outputs to local condi-



tions was assessed through simple bias correction and QM correction methods. Forecasted NAM no-ramps are more frequent than observed ones, and can produce long-lasting low-generation events in the region as discovered in [12]. Both statistical correction methods reduce the difference between the frequencies of the predicted ramps and the observed ramps in the range of  $-1$  to  $1$  m/s, which leads to an improvement in the simulation of wind ramps and low-generation events.

Statistical correction enhances the *POD* of positive and negative wind ramps. The best performance was obtained using QM correction in the CDCU station and simple bias correction in the CSNL station, which is also suggested by *CSI* index. False alarm events are not substantially modified after statistical correction.

The integration of wind generation in the electricity grid is a challenge for energy operators; therefore, the characterization of wind ramps and the underlying role of meteorological systems is a relevant tool. Additionally, exploring statistical tools to adjust NWP results for local conditions can improve the predictability of wind ramps.

The main drawback of statistical downscaling is the simplification assumptions that can lead to divergences from the physical system under representation [47]. However, other more sophisticated methodologies, such as the Complete Stochastic Modeling Solution (CoSMos), could be applied for ramp forecasting [48]. Deep-learning technologies can also be applied to the post-processing of NWP results for wind-power applications [47,49]. Regarding atmospheric processes, to improve the prediction of wind ramps associated with storms, high-resolution numerical simulations are being carried out to evaluate the sensitivity of the parameterizations of physical processes (e.g., PBL, convection, etc.) during the passage of storms near/over wind farms over complex terrain.

## 5. Simple Summary

A large variation in wind energy production observed in a wind farm in short periods (up to a few hours) is denominated a wind-ramp. Ramp events are a significant source of uncertainty in wind-power generation. The identification of meteorological phenomena causing wind ramps needs to be considered in forecasting systems design to improve wind farm management. This study examines the characteristics of wind ramps for four sites with wind-power potential in Mexico. Cold fronts are the most common weather systems originating extreme ramps, lasting 1 to 4 hours, but the persistence of intense winds varies from 5 hours to 40 hours. In summer, tropical cyclone activity and surface gusts from thunderstorm downdrafts contribute to produce extreme wind ramps. These events last 1 to 3 hours. Nowadays, most of the operational regional forecasting systems run in the so-called gray-zone, where the representation of turbulence, convective processes, and topography is not fully resolved. Model outputs show more frequent no-ramps events than observed ones that can produce long-lasting low generation events in the region. Statistical correction methods reduce the difference between the frequencies of the predicted ramps and the observed ramps leading to an improvement in wind-ramp simulations and low-generation events.

**Supplementary Materials:** The following supporting information can be downloaded at: <https://www.mdpi.com/article/10.3390/atmos13030453/s1>, Figure S1. Probability density functions (PDF) of wind ramps ( $\delta u$ ) from (a)CSNL, (b) CDCU, (c) FCOV and (d) LVEN. The wind increment and decrements values are normalized by the corresponding standard deviations; Figure S2. Annual smoothed frequency-weighted spectra  $fS(f)$  of horizontal wind speed for Ciudad Cuauhtemoc (CDCU); Figure S3. Cold fronts affecting Mexico in 24 May 2013. A cold front is seen as a curving line of clouds in the MODIS Corrected Reflectance imagery; Figure S4. Cold fronts affecting Mexico in 1 March 2010. A cold front is seen as a comma clouds in the MODIS Corrected Reflectance imagery; Figure S5. Cold fronts affecting Mexico in 11 February 2006. A cold front is seen as a comma clouds in the MODIS Corrected Reflectance imagery; Figure S6. Example of extreme wind ramp event and the consecutive persistent winds; Figure S7. Storm trajectory at 01 August 2013 calculated with the maximum precipitation in core of the storm using a) CMORPH data (magenta line), b) 00:00 Z NAM initialization forecast (blue line) and c) 06:00 Z NAM initialization forecast (green line). The end of

the track is indicated with a cross; Figure S8. Meteogram at CDCU for a storm at 00:00 Z 25 July 2013. Wind ramp timing is shaded in yellow. CMORPH maximum precipitation in the center of the storm is in blue bars. Estimated wind gust in the storm is in red line and observed wind gust at CDCU is in blue. Forecasted wind speed, wind vector and precipitation are in green; Figure S9. Meteogram at FCOV for a storm at 22:00 Z 03 July 2007. Wind ramp timing is shaded in yellow. CMORPH maximum precipitation in the center of the storm is in blue bars. Estimated wind gust in the storm is in red line and observed wind gust at FCOV is in blue. Forecasted wind speed, wind vector and precipitation are in green; Figure S10. Meteogram at LVEN for a storm at 18:00 Z 07 July 2003. Wind ramp timing is shaded in yellow. CMORPH maximum precipitation in the center of the storm is in blue bars. Observed wind gust at LVEN is in blue; Figure S11. Example of wind ramps. Wind ramp observed and predicted (TP), wind ramp predicted by NAM but not observed (FP), and wind ramp observed but not predicted by NAM (FN). Events occurred in different days; Table S1. List of abbreviations; Table S2. Derived contingency table indexes wind NAM forecast (non-corrected), bias corrected and quantile mapping (QM) corrected for CDCU; Table S3. Derived contingency table indexes wind NAM forecast (non-corrected), bias corrected and quantile mapping (QM) corrected for CSNL.

**Author Contributions:** Conceptualization, K.P.-C. and E.C.; methodology, K.P.-C. and E.C.; formal analysis, K.P.-C.; investigation, K.P.-C. and E.C.; data curation, K.P.-C.; writing—original draft preparation, K.P.-C. and E.C.; writing—review and editing, K.P.-C. and E.C.; supervision, E.C. All authors have read and agreed to the published version of the manuscript.

**Funding:** This research was funded by The National Council of Science and Technology (CONACYT), grant number 473276 the first author's PhD scholarship.

**Institutional Review Board Statement:** Not applicable.

**Informed Consent Statement:** Not applicable.

**Data Availability Statement:** Data and material are available to any reader directly from the corresponding author upon reasonable request. Code/algorithm/software is available to any reader directly from the corresponding author upon reasonable request.

**Acknowledgments:** The authors are grateful to Tania Isabel Rodríguez Mosqueda for preparing the Figure 1. The authors thank to thank to Ricardo Saldaña Flores, Instituto Nacional de Electricidad y Energías Limpias (INEEL) Coordinator of the Mexican Wind Atlas Project (AEM) for providing the wind data.

**Conflicts of Interest:** The authors declare no conflict of interest. The funders had no role in the design of the study; in the collection, analyses, or interpretation of data; in the writing of the manuscript, or in the decision to publish the results.

## References

1. Bossavy, A.; Girard, R.; Kariniotakis, G. Forecasting Uncertainty Related to Ramps of Wind Power Production. In Proceedings of the European Wind Energy Conference and Exhibition 2010, Warsaw, Poland, 20–23 April 2010; European Wind Energy Association: Warsaw, Poland, 2010; Volume 2, pp. 1–9, ISBN 9781617823107.
2. Gallego-Castillo, C.; Cuerva-Tejero, A.; Lopez-Garcia, O. A review on the recent history of wind power ramp forecasting. *Renew. Sustain. Energy Rev.* **2015**, *52*, 1148–1157. [[CrossRef](#)]
3. Zhang, J.; Cui, M.; Hodge, B.M.; Florita, A.; Freedman, J. Ramp forecasting performance from improved short-term wind power forecasting over multiple spatial and temporal scales. *Energy* **2017**, *122*, 528–541. [[CrossRef](#)]
4. Pichault, M.; Vincent, C.; Skidmore, G.; Monty, J. Characterisation of intra-hourly wind power ramps at the wind farm scale and associated processes. *Wind Energy Sci.* **2021**, *6*, 131–147. [[CrossRef](#)]
5. Bianco, L.; Djalalova, I.V.; Wilczak, J.M.; Cline, J.; Calvert, S.; Konopleva-Akish, E.; Finley, C.; Freedman, J. A Wind Energy Ramp Tool and Metric for Measuring the Skill of Numerical Weather Prediction Models. *Weather Forecast.* **2016**, *31*, 1137–1156. [[CrossRef](#)]
6. Storm, B.; Dudhia, J.; Basu, S.; Swift, A.; Giammanco, I. Evaluation of the weather research and forecasting model on forecasting low-level jets: Implications for wind energy. *Wind Energy* **2009**, *12*, 81–90. [[CrossRef](#)]
7. Olson, J.B.; Kenyon, J.S.; Djalalova, I.; Bianco, L.; Turner, D.D.; Pichugina, Y.; Choukulkar, A.; Toy, M.D.; Brown, J.M.; Angevine, W.M.; et al. Improving Wind Energy Forecasting through Numerical Weather Prediction Model Development. *Bull. Am. Meteorol. Soc.* **2019**, *100*, 2201–2220. [[CrossRef](#)]



8. Wilczak, J.; Finley, C.; Freedman, J.; Cline, J.; Bianco, L.; Olson, J.; Djalalova, I.; Sheridan, L.; Ahlstrom, M.; Manobianco, J.; et al. The Wind Forecast Improvement Project (WFIP): A Public–Private Partnership Addressing Wind Energy Forecast Needs. *Bull. Am. Meteorol. Soc.* **2015**, *96*, 1699–1718. [CrossRef]
9. Vannitsem, S.; Bremnes, J.B.; Demaeyer, J.; Evans, G.R.; Flowerdew, J.; Hemri, S.; Lerch, S.; Roberts, N.; Theis, S.; Atencia, A.; et al. Statistical Postprocessing for Weather Forecasts: Review, Challenges, and Avenues in a Big Data World. *Bull. Am. Meteorol. Soc.* **2021**, *102*, E681–E699. [CrossRef]
10. Siuta, D.; West, G.; Stull, R. WRF hub-height wind forecast sensitivity to PBL scheme, grid length, and initial condition choice in complex terrain. *Weather Forecast.* **2017**, *32*, 493–509. [CrossRef]
11. Benjamin, S.G.; Weygandt, S.S.; Brown, J.M.; Hu, M.; Alexander, C.R.; Smirnova, T.G.; Olson, J.B.; James, E.P.; Dowell, D.C.; Grell, G.A.; et al. A North American Hourly Assimilation and Model Forecast Cycle: The Rapid Refresh. *Mon. Weather Rev.* **2016**, *144*, 1669–1694. [CrossRef]
12. Pereyra-Castro, K.; Caetano, E.; Martínez-Alvarado, O.; Quintanilla-Montoya, A.L. Wind and Wind Power Ramp Variability over Northern Mexico. *Atmosphere* **2020**, *11*, 1281. [CrossRef]
13. López-Bravo, C.; Caetano, E.; Magaña, V. Forecasting Summertime Surface Temperature and Precipitation in the Mexico City Metropolitan Area: Sensitivity of the WRF Model to Land Cover Changes. *Front. Earth Sci.* **2018**, *6*, 6. [CrossRef]
14. NCEI. North American Mesoscale Forecast System. Available online: <https://www.ncei.noaa.gov/products/weather-climate-models/north-american-mesoscale> (accessed on 1 October 2021).
15. NCEP. North American Mesoscale Forecast System. Available online: [https://www.emc.ncep.noaa.gov/emc/pages/numerical\\_forecast\\_systems/nam.php](https://www.emc.ncep.noaa.gov/emc/pages/numerical_forecast_systems/nam.php) (accessed on 1 October 2021).
16. Rogers, E.; DiMego, G.; Black, T.; Ek, M.; Ferrier, B.; Gayno, G.; Janjic, Z.; Lin, Y.; Pyle, M.; Wong, V. The NCEP North American mesoscale modeling system: Recent changes and future plans. In Proceedings of the 23rd Conference on Weather Analysis and Forecasting/19th Conference on Numerical Weather Prediction, Omaha, NE, USA, 1 June 2009; pp. 1–21.
17. Rogers, E.; Lin, Y.; Mitchell, K.; Wu, W.; Ferrier, B.; Gayno, G.; Pondeca, M.; Pyle, M.; Wong, V.; Ek, M. The NCEP North American Mesoscale Modeling System: Final Eta model/analysis changes and preliminary experiments using the WRF-NMM. In Proceedings of the 21st Conference on Weather Analysis and Forecasting/17th Conference on Numerical Weather, Prediction, Washington, DC, USA, 1 August 2005; pp. 1–21.
18. Colbert, M.; Stensrud, D.J.; Markowski, P.M.; Richardson, Y.P. Processes Associated with Convection Initiation in the North American Mesoscale Forecast System, Version 3 (NAMv3). *Weather Forecast.* **2019**, *34*, 683–700. [CrossRef]
19. Janjić, Z.; Black, T.L.; Pyle, H.-Y.; Chuang, E.R.; DiMego, G.J. The NCEP WRF-NMM Core. Available online: <https://www2.mmm.ucar.edu/wrf/users/workshops/WS2005/presentations/session2/9-Janjic.pdf> (accessed on 15 October 2021).
20. Ferrier, B.S.; Janjić, Z.; Aligo, E.; Jovic, D.; Roger, E.; Carley, J.R.; Pyle, M.; DiMego, G.J. NMMB Model Changes as Part of the NAMv4 Upgrade. Available online: <https://ams.confex.com/ams/97Annual/webprogram/Paper312628.html> (accessed on 15 October 2021).
21. Stull, R. *An Introduction to Boundary Layer*, 1st ed.; Kluwer Academic Publishers: Dordrecht, The Netherlands, 2012.
22. Finnigan, J.J.; Einaudi, F.; Fua, D. The Interaction between an Internal Gravity Wave and Turbulence in the Stably-Stratified Nocturnal Boundary Layer. *J. Atmos. Sci.* **1984**, *41*, 2409–2436. [CrossRef]
23. Kang, S.-L.; Won, H. Spectral structure of 5 year time series of horizontal wind speed at the Boulder Atmospheric Observatory. *J. Geophys. Res. Atmos.* **2016**, *121*, 11946–11967. [CrossRef]
24. Demarco, A.; Basu, S. On the tails of the wind ramp distributions. *Wind Energy* **2018**, *21*, 892–905. [CrossRef]
25. MODIS Characterization Support Team MODIS 250m Calibrated Radiances Product. Available online: <https://doi.org/10.5067/MODIS/MYD02QKM.061> (accessed on 1 July 2021).
26. Vázquez-Aguirre, J.L. Caracterización Objetiva de Los Nortes del Golfo de México y su Variabilidad Interanual. Bachelor’s Thesis, Universidad Veracruzana, Veracruz, México, 1999.
27. Méndez-Pérez, I.R.; Rodríguez-Damián, J.J.; Tejeda-Martínez, A. Caracterización y Tipología de eventos de “Suradas” del Golfo de Tehuantepec al Centro del estado de Veracruz, México. In Proceedings of the El Clima: Aire, Agua, Tierra y Fuego, Cartagena, Colombia, 17–19 October 2018; Montávez Gómez, J.P., Ed.; Asociación Española de Climatología; Agencia Estatal de Meteorología: Madrid, Spain, 2018; pp. 529–538.
28. Atlantic Hurricane Season. Available online: <https://www.nhc.noaa.gov/data/tcr/index.php?season=2013&basin=atl> (accessed on 1 October 2021).
29. AIRS Project Aqua/AIRS L2 Near Real Time (NRT) Standard Physical Retrieval (AIRS-only) V7.0. Available online: [https://disc.gsfc.nasa.gov/datasets/AIRS2RET\\_NRT\\_7.0/summary](https://disc.gsfc.nasa.gov/datasets/AIRS2RET_NRT_7.0/summary) (accessed on 1 October 2021).
30. NASA MODIS Adaptive Processing System MODIS Atmosphere L2 Cloud Product (06\_L2). Available online: [http://doi.org/10.5067/MODIS/MYD06\\_L2.061](http://doi.org/10.5067/MODIS/MYD06_L2.061) (accessed on 1 October 2021).
31. Valdés Manzanilla, A.; Cortéz Vázquez, M.; Francisco, P.; José, J. Un estudio explorativo de los Sistemas Convectivos de Mesoescala de México. *Investig. Geográficas* **2005**, *56*, 26–42. [CrossRef]
32. Nakamura, K.; Kershaw, R.; Gait, N. Prediction of near-surface gusts generated by deep convection. *Meteorol. Appl.* **1996**, *3*, 157–167. [CrossRef]
33. Sheridan, P. Review of Techniques and Research for Gust Forecasting and Parameterisation. 2011. Available online: <https://digital.nmla.metoffice.gov.uk> (accessed on 15 October 2021).

34. Li, D.; Feng, J.; Xu, Z.; Yin, B.; Shi, H.; Qi, J. Statistical Bias Correction for Simulated Wind Speeds Over CORDEX-East Asia. *Earth Space Sci.* **2019**, *6*, 200–211. [[CrossRef](#)]
35. Torralba, V.; Doblas-Reyes, F.J.; MacLeod, D.; Christel, I.; Davis, M. Seasonal Climate Prediction: A New Source of Information for the Management of Wind Energy Resources. *J. Appl. Meteorol. Climatol.* **2017**, *56*, 1231–1247. [[CrossRef](#)]
36. Enayati, M.; Bozorg-Haddad, O.; Bazrafshan, J.; Hejabi, S.; Chu, X. Bias correction capabilities of quantile mapping methods for rainfall and temperature variables. *J. Water Clim. Chang.* **2020**, *12*, 401–419. [[CrossRef](#)]
37. Jakob Themeßl, M.; Gobiet, A.; Leuprecht, A. Empirical-statistical downscaling and error correction of daily precipitation from regional climate models. *Int. J. Climatol.* **2011**, *31*, 1530–1544. [[CrossRef](#)]
38. Wilks, D.S. *Statistical Methods in the Atmospheric Science*, 2nd ed.; Academic Press: San Diego, CA, USA, 2006; ISBN 0-12-064490-8.
39. Zhao, H.; Raga, G.B. On the distinct interannual variability of tropical cyclone activity over the eastern North Pacific. *Atmósfera* **2015**, *28*, 161–178. [[CrossRef](#)]
40. Cannon, D.J.; Brayshaw, D.J.; Methven, J.; Coker, P.J.; Lenaghan, D. Using reanalysis data to quantify extreme wind power generation statistics: A 33 year case study in Great Britain. *Renew. Energy* **2015**, *75*, 767–778. [[CrossRef](#)]
41. Thomas, S.R.; Martínez-Alvarado, O.; Drew, D.; Bloomfield, H. Drivers of extreme wind events in Mexico for windpower applications. *Int. J. Climatol.* **2021**, *41*, E2321–E2340. [[CrossRef](#)]
42. Hersbach, H.; Bell, B.; Berrisford, P.; Hirahara, S.; Horányi, A.; Muñoz-Sabater, J.; Nicolas, J.; Peubey, C.; Radu, R.; Schepers, D.; et al. The ERA5 global reanalysis. *Q. J. R. Meteorol. Soc.* **2020**, *146*, 1999–2049. [[CrossRef](#)]
43. Joyce, R.J.; Janowiak, J.E.; Arkin, P.A.; Xie, P. CMORPH: A Method that Produces Global Precipitation Estimates from Passive Microwave and Infrared Data at High Spatial and Temporal Resolution. *J. Hydrometeorol.* **2004**, *5*, 487–503. [[CrossRef](#)]
44. Larsén, X.G.; Ott, S.; Badger, J.; Hahmann, A.N.; Mann, J. Recipes for Correcting the Impact of Effective Mesoscale Resolution on the Estimation of Extreme Winds. *J. Appl. Meteorol. Climatol.* **2012**, *51*, 521–533. [[CrossRef](#)]
45. Pereyra-Castro, K.; Caetano, E.; Altamirano del Razo, D. WRF wind forecast over coastal complex terrain: Baja California Peninsula (Mexico) case study. *Arab. J. Geosci.* **2021**, *14*, 1972. [[CrossRef](#)]
46. Chow, F.K.; Schär, C.; Ban, N.; Lundquist, K.A.; Schlemmer, L.; Shi, X. Crossing Multiple Gray Zones in the Transition from Mesoscale to Microscale Simulation over Complex Terrain. *Atmosphere* **2019**, *10*, 274. [[CrossRef](#)]
47. Schultz, M.G.; Betancourt, C.; Gong, B.; Kleinert, F.; Langguth, M.; Leufen, L.H.; Mozaffari, A.; Stadler, S. Can deep learning beat numerical weather prediction? *Philos. Trans. R. Soc. A Math. Phys. Eng. Sci.* **2021**, *379*, 20200097. [[CrossRef](#)]
48. Papalexiou, S.M.; Serinaldi, F.; Porcu, E. Advancing Space-Time Simulation of Random Fields: From Storms to Cyclones and Beyond. *Water Resour. Res.* **2021**, *57*, e2020WR029466. [[CrossRef](#)]
49. Mora, E.; Cifuentes, J.; Marulanda, G. Short-term forecasting of wind energy: A comparison of deep learning frameworks. *Energies* **2021**, *14*, 7943. [[CrossRef](#)]



## Capítulo 6. Conclusiones y trabajo futuro

El funcionamiento eficiente de un parque eólico y su integración en la red eléctrica depende de la adecuada evaluación de la variabilidad del viento. Los cambios bruscos y repentinos en la energía eólica (eventos de rampa) son uno de los mayores desafíos a los que se enfrenta la industria eólica. Asimismo, los períodos de baja generación eólica pueden desencadenar apagones. Este estudio presenta la caracterización de eventos de rampa en términos de su magnitud, estacionalidad y duración para varias regiones de México, así como la atribución de estos eventos a un fenómeno atmosférico (Figura 4). Respecto a la predicción de las variaciones de la potencia eólica, se exploró la habilidad de los modelos operativos de mesoescala NAM y RAP para pronosticar rampas de potencia y eventos de alta/baja generación de potencia eólica. Adicionalmente, el efecto de la corrección de sesgo en el pronóstico de rampas de viento por el modelo NAM fue examinada para dos sitios de México. Éstas últimas estaciones meteorológicas cuentan con registros de 2010-2016, mismo período disponible en el modelo NAM.

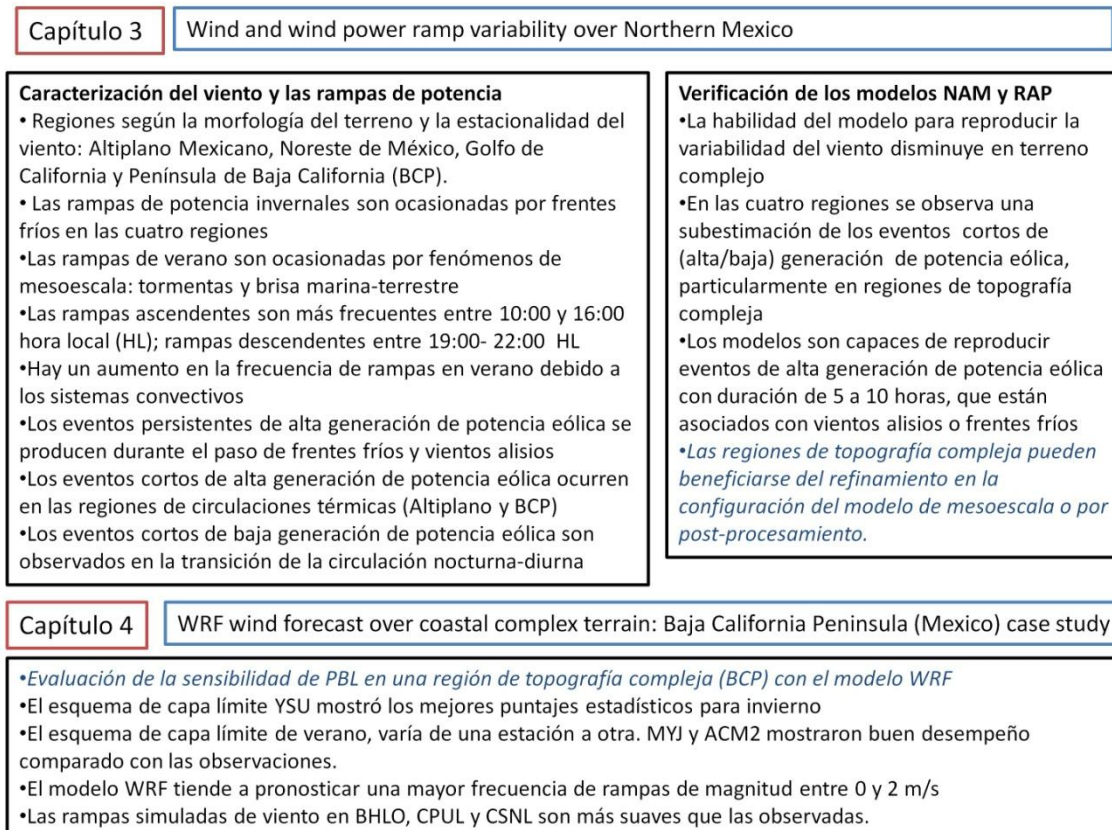


Figura 4. Principales resultados obtenidos de la investigación

En este trabajo se mostró la distribución mensual y diaria de eventos de rampa en cuatro regiones del norte de México: Península de Baja California, Altiplano Mexicano, Noroeste de México y Golfo de California. Dichas regiones se definieron considerando las condiciones climáticas y topográficas. Las regiones donde se producen circulaciones locales experimentan más variaciones diarias de la rapidez del viento, en consecuencia, las rampas de potencia ascendentes/descendentes y los eventos de baja/alta generación de potencia eólica son más frecuentes. Las regiones con vientos persistentes, como el Noroeste de México con los vientos alisios, producen menos rampas de potencia y un período más productivo durante el verano. El Golfo de California se caracteriza por viento intenso predominante del norte en invierno y una inversión del flujo en el verano. La integración de la electricidad producida en estas últimas regiones es menos desafiante que en las regiones con circulaciones térmicas.

Las características de las variaciones del recurso eólico dependen de los fenómenos atmosféricos que las origina. El paso de un frente frío sobre las estaciones analizadas producen una rampa intensa seguida de un evento de alta generación de potencia eólica, que puede sostenerse más de 10 horas. Por su parte, las circulaciones térmicas producen eventos cortos de alta generación de potencia eólica cuando se establecen (~ 12 hora local) y eventos cortos de baja generación de potencia eólica durante la inversión del flujo (~ 20 hora local). Las tormentas típicas del verano también ocasionan una repentina intensificación de los vientos (rampa ascendente) seguida de una abrupta relajación (rampa descendente) cuando la tormenta se aleja del sitio o se disipa. Por ello, los fenómenos de mesoescala requieren un manejo estratégico por parte de los operadores de parques eólicos ya que desencadenan fluctuaciones abruptas y cortas de la generación eólica.

El análisis del espectro de energía es una herramienta útil en el diagnóstico de los fenómenos que modulan las fluctuaciones del viento. Esto se presentó en la caracterización de rampas del capítulo 5. En estaciones como La Venta, Oaxaca, los fenómenos de escala sinóptica contribuyen durante todo el año a la generación eólica, mientras que en otras regiones sus efectos son más marcados de diciembre a mayo, como es el caso de Ciudad Cuauhtémoc. Las Suradas y Nortes son fenómenos típicos del Golfo de México, los cuales se asociaron con vientos intensos de septiembre a abril en estaciones como La Venta, Oaxaca y Francisco Villa, Tamaulipas. Aunque ambas estaciones son afectadas por el mismo fenómeno, la duración de los vientos intensos depende de la interacción del flujo con la topografía regional. Por ejemplo, los vientos intensos causados por un Norte persisten durante 20 horas en promedio en La Venta, Oaxaca; mientras que en Francisco Villa, los vientos se mantienen intensos por 7 horas.

En verano, las rampas de viento ocurrieron ante la presencia de un ciclón tropical o una tormenta. Los ciclones tropicales pueden producir vientos intensos durante más de 10 horas, sin embargo, dada la magnitud de vientos que pueden alcanzar, es necesario apagar los aerogeneradores para prevenir daños en el equipo. El análisis de casos de estudio de rampas asociadas a tormentas mostró que las corrientes descendentes de éstas originan una intensificación significativa de los vientos. La rampa de viento se origina por la cercanía de la tormenta a la estación, aún cuando no precipite en el sitio de análisis. En este sentido, el monitoreo de tormentas cercanas a los parques eólicos ayuda a prevenir los cambios abruptos de generación eólica.

Las tasas de producción de energía eólica fluctúan más que las de combustibles fósiles. Para optimizar la eficiencia de energía eólica se necesitan pronósticos precisos. En este estudio se realizó una evaluación de la habilidad de los modelos de mesoescala NAM y RAP para predecir rampas de potencia y eventos de alta y baja generación de potencia eólica. Los dominios de estos modelos cubren parcialmente el territorio mexicano y sus pronósticos operativos son de libre acceso, por lo que los operadores de parques eólicos pueden utilizarlos como fuente de pronóstico de viento con algunas reservas.

La evaluación del pronóstico de viento y rampas de potencia por los modelos RAP y NAM para el noroeste de México en 2013 mostró que a mayor complejidad de la topografía, hay una reducción en la habilidad de los modelos para reproducir las fluctuaciones del viento. En las regiones de topografía compleja, las circulaciones térmicas juegan un papel importante en las variaciones horarias del viento. La magnitud y dirección del viento pronosticado por RAP es semejante a la observada, incluso en las regiones con circulaciones térmicamente inducidas como Bahía de los Ángeles o Bahía de Loreto.

Actualmente, la mayoría de los modelos operativos regionales de mesoescala se ejecutan en la llamada zona gris. NAM y RAP tienen una resolución espacial de 12 km y 13 km, respectivamente. En la zona gris, la representación de turbulencia, procesos convectivos y topografía no están completamente resueltos, lo que afecta la predicción de rampas de viento, especialmente aquellas de corta duración. Este suavizado de las fluctuaciones horarias del viento conduce a una subestimación de rampas, eventos cortos de alta generación de potencia eólica y eventos cortos de baja generación de potencia eólica por ambos modelos. Específicamente, las rampas de potencia eólica fueron definidas como un cambio del 20% del factor de planta en 1 hora. NAM y RAP sólo acertaron en ~ 10% de las rampas observadas en la estación meteorológica. Probablemente este criterio fue muy estricto para evaluar modelos con resolución espacial ~ 12 km, así que al relajar el umbral de tiempo a 3 horas, los modelos presentaron una mayor probabilidad de detección (~ 20%). Los modelos NAM y RAP mostraron un desempeño aceptable en las regiones de

vientos persistentes como el Golfo de California y el Noreste de México. NAM y RAP fueron capaces de representar los eventos de alta generación de potencia eólica con duración mayor de 5 horas. Por último, RAP mostró un mejor desempeño en la reproducción de variaciones eólicas respecto a NAM.

La caracterización realizada previamente sobre los fenómenos causantes de rampas de potencia sugiere refinamientos necesarios en la configuración de los modelos meteorológicos para mejorar el pronóstico de viento, particularmente en regiones de topografía compleja. La adecuada representación de los vientos en superficie está sujeta a la representación de los procesos en la capa límite planetaria. El esquema de capa límite con el mejor rendimiento para simular la variabilidad del viento en los meses de verano e invierno depende de la estabilidad atmosférica y los sistemas atmosféricos que modulan cada estación. La evaluación estadística de la sensibilidad del pronóstico de viento al esquema de PBL con el modelo WRF para la Península de Baja California muestra que el esquema YSU se desempeñó mejor para enero de 2013 y para un evento de frente frío (10-13 enero). En junio 2013 (verano), la elección del mejor esquema de PBL varía entre las 7 estaciones meteorológicas analizadas. En general, la simulación del viento en superficie con los esquemas MYJ y ACM2 se aproxima más a las observaciones en verano. La distribución de rampas de viento simulado con el esquema ACM2 se asemeja a la distribución observada tanto en verano como en invierno. La habilidad de este esquema para representar adecuadamente los vientos en verano e invierno puede deberse a un factor de mezclado no local que le permite ajustarse a atmósferas estables e inestables.

Hay algunos errores en las simulaciones que los operadores de parques eólicos deben considerar en la toma de decisiones. Los experimentos usando los 3 esquemas de PBL simulan una mayor frecuencia de rampas en el rango de -2 m/s a 2 m/s, este efecto es más marcado en las estaciones meteorológicas de Bahía de Loreto, Bahía de los Ángeles, La Rumorosa y Pinacate. Además, las observaciones muestran rampas intensas ( $> |8|$  m/s) que no fueron predichas por ninguno de los esquemas de PBL en Bahía de Loreto y Cabo Pulmo para verano e invierno.

De forma general, la correcta selección del esquema de PBL puede reducir los errores de predicción del viento y de rampas de viento. En invierno, los sistemas de pronóstico para Baja California pueden beneficiarse de la elección del esquema YSU en la configuración física del modelo WRF. En tanto que, la parametrización de PBL más apropiada para el verano varía según la estación meteorológica, pero ACM2 muestra un buen desempeño para las condiciones atmosféricas de la región.



El error sistemático de los modelos de mesoescala NAM, RAP y WRF para predecir mayor frecuencia de rampas suaves (-2 m/s a 2 m/s) o vientos débiles (< 2 m/s) comparados con las observaciones, conduce a la subestimación de rampas intensas y eventos cortos de alta generación. La mejora de la predicción de rampas de viento se puede realizar a través de simulaciones atmosféricas a resoluciones más altas para representar con mayor precisión los procesos atmosféricos, en particular, la convección y la turbulencia que están fuertemente relacionadas con las fluctuaciones de alta frecuencia de los vientos. Sin embargo, los costos computacionales de mayor resolución a veces no son compensados por las mejoras en los resultados. Ante una limitada capacidad computacional, se puede optar por una corrección estadística de los resultados del modelo a las condiciones locales. La técnica consiste en determinar una relación estadística entre las variables observadas y pronosticadas. La calidad de la corrección depende de la calidad y duración de las mediciones. El último enfoque fue examinado en este estudio con dos métodos de ajuste de sesgo: corrección de sesgo simple y mapeo de cuantiles.

El ajuste estadístico de sesgo utilizando ambos métodos redujo las diferencias entre la distribución de rampas de viento observadas y simuladas. Una disminución del exceso de fluctuaciones del viento débiles se observó claramente. La corrección de sesgo también mejoró los índices de desempeño de los modelos, se incrementó la POD y aumentó el CSI.

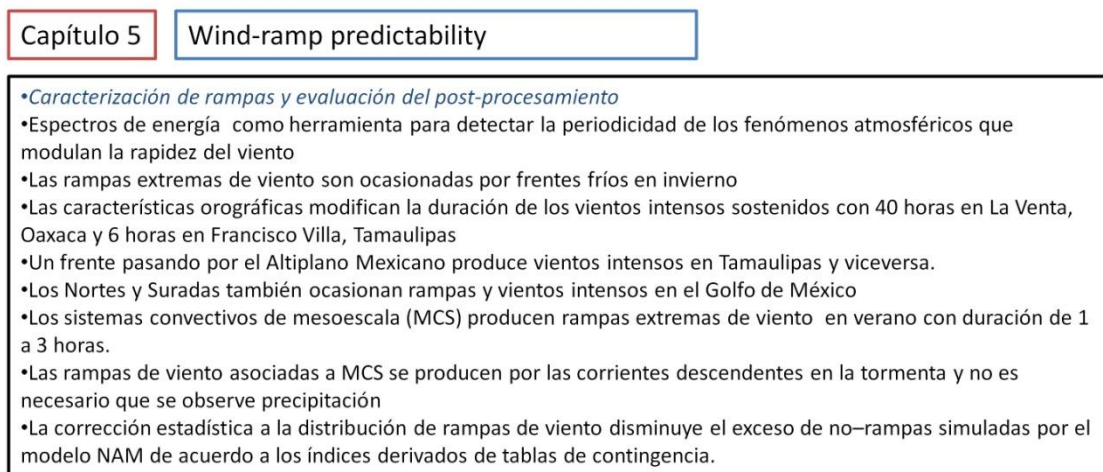


Figura 4. Principales resultados obtenidos de la investigación (continuación)

En resumen, el diseño de un sistema de pronóstico para un parque eólico necesita una exploración inicial de los fenómenos atmosféricos que modulan las fluctuaciones del viento. Esta caracterización brinda información sobre el tipo de rampas de verano e invierno. La elección del esquema de capa límite es uno de los parámetros más investigados con fines eólicos. Como se ha mostrado anteriormente, las corrientes

descendentes contribuyen a la generación de rampas eólicas intensas y repentinas durante el verano en México. Por ello, un esquema de capa límite que combina turbulencia local y no local, como es ACM2, es útil para el verano, cuando suelen ocurrir procesos convectivos.

Una capacidad limitada de recursos computacionales puede restringir la refinación del sistema de pronóstico, de ser así, los modelos operativos NAM y RAP pueden fungir como herramientas para operadores de parques eólicos con las limitaciones mencionadas anteriormente. Éstos se desempeñan mejor en regiones de vientos persistentes estacionalmente. La reducción de los errores sistemáticos del pronóstico mediante la corrección de sesgo es una alternativa menos costosa de optimizar el pronóstico. Su aplicación sobre la distribución de rampas ha mostrado mejorar la probabilidad de detección de dichos eventos.

La predicción de rampas es un desafío vigente para el sistema energético mundial, ya que la generación intermitente requiere estrategias de manejo para una óptima integración en el portafolio energético. La atribución de rampas a sistemas atmosféricas mostró que las tormentas de verano ocasionan cambios abruptos en la generación eólica. Por ello, el refinamiento de la predicción de tormentas, en términos de sus trayectorias y tiempos de ocurrencia, conducirá a mayor predictibilidad de los eventos de rampa. Un pronóstico por ensambles para diferentes tiempos de inicialización de las condiciones iniciales también podría ser útil para el manejo de tormentas. Los espectros estacionales de energía señalan la necesidad de trabajar en la correcta simulación los procesos de mesoescala, ya que tienden a modelar menor energía en esa región del espectro.

Por otra parte, la reducción de los errores sistemáticos de los modelos es un paso necesario para refinar los pronósticos. El post-procesamiento de las salidas de los modelos de mesoescala con métodos más sofisticados como Complete Stochastic Modelling Solution (CoSMos)(Papalexiou, Serinaldi, y Porcu, 2021) es una opción para mejorar la predicción de rampas con un menor costo computacional. En este mismo sentido, las redes neuronales pueden establecer relaciones no lineales que ayuden a describir la variabilidad del viento.

## Referencias

- Aguilar, T. A. (2019). *Detecting the Long-Term Frequency of Large-Scale Wind Power Ramp Events Observed in ERCOT's Aggregated Wind Power Time-Series Data*. Texas Tech University. Retrieved from <https://ttu-ir.tdl.org/bitstream/handle/2346/85506/AGUILAR-DISSERTATION-2019.pdf?sequence=1&isAllowed=y>
- Allen, M. R., Dube, O. P., Solecki, W., Aragón-Durand, F., W., C., Humphreys, S., ... Y. Mulugetta, R. Perez, M. Wairiu, and K. Z. (2019). Framing and Context. In P. R. S. Masson-Delmotte, V., P. Zhai, H.-O. Pörtner, D. Roberts, J. Skea, E. L. A. Pirani, W. Moufouma-Okia, C. Péan, R. Pidcock, S. Connors, J.B.R. Matthews, Y. Chen, X. Zhou, M.I. Gomis, & and T. W. T. Maycock, M. Tignor (Eds.), *Global Warming of 1.5°C. An IPCC Special Report on the impacts of global warming of 1.5°C above pre-industrial levels and related global greenhouse gas emission pathways, in the context of strengthening the global response to the threat of climate change*. In Press.
- Aravind, A., Srinivas, C. V., Shrivastava, R., Hegde, M. N., Seshadri, H., & Mohapatra, D. K. (2022). Simulation of atmospheric flow field over the complex terrain of Kaiga using WRF: sensitivity to model resolution and PBL physics. *Meteorology and Atmospheric Physics*, 134(1), 1–25. <https://doi.org/10.1007/s00703-021-00848-4>
- Aste, N., Bocciolone, M. F., Dmitrii, B., Brost, E., Christian, B., Victoria, B., ... Thomas, E. (2019). *Roadmap to 2050 A Manual for Nations to Decarbonize by Mid-Century*. Sustainable Development Solutions Network and Fondazione Eni Enrico Mattei. Retrieved from <https://roadmap2050.report/static/files/roadmap-to-2050.pdf>
- Benjamin, S. G., Grell, G. A., Brown, J. M., Smirnova, T. G., & Bleck, R. (2004). Mesoscale Weather Prediction with the RUC Hybrid Isentropic–Terrain-Following Coordinate Model. *Monthly Weather Review*, 132(2), 473–494. [https://doi.org/10.1175/1520-0493\(2004\)132<0473:MWPWTR>2.0.CO;2](https://doi.org/10.1175/1520-0493(2004)132<0473:MWPWTR>2.0.CO;2)
- Benjamin, S. G., Weygandt, S. S., Brown, J. M., Hu, M., Alexander, C. R., Smirnova, T. G., ... Manikin, G. S. (2016a). A North American Hourly Assimilation and Model Forecast Cycle: The Rapid Refresh. *Monthly Weather Review*, 144(4), 1669–1694. <https://doi.org/10.1175/MWR-D-15-0242.1>
- Benjamin, S. G., Weygandt, S. S., Brown, J. M., Hu, M., Alexander, C. R., Smirnova, T. G., ... Manikin, G. S. (2016b). A North American Hourly Assimilation and Model Forecast Cycle: The Rapid Refresh. *Monthly Weather Review*, 144(4), 1669–1694. <https://doi.org/10.1175/MWR-D-15-0242.1>
- Betts, A. K. (1986). A new convective adjustment scheme. Part I: Observational and theoretical basis. *Quarterly Journal of the Royal Meteorological Society*, 112(473), 677–691. <https://doi.org/https://doi.org/10.1002/qj.49711247307>

- Betts, A. K., & Miller, M. J. (1986). A new convective adjustment scheme. Part II: Single column tests using GATE wave, BOMEX, ATEX and arctic air-mass data sets. *Quarterly Journal of the Royal Meteorological Society*, 112(473), 693–709. <https://doi.org/https://doi.org/10.1002/qj.49711247308>
- Bianco, L., Djalalova, I. V, Wilczak, J. M., Cline, J., Calvert, S., Konopleva-Akish, E., ... Freedman, J. (2016). A Wind Energy Ramp Tool and Metric for Measuring the Skill of Numerical Weather Prediction Models. *Weather and Forecasting*, 31(4), 1137–1156. <https://doi.org/10.1175/WAF-D-15-0144.1>
- Bossavy, A., Girard, R., Kariniotakis, G., Bossavy, A., Girard, R., Kariniotakis, G., ... Antipolis, S. (2012). Forecasting Uncertainty Related to Ramps of Wind Power Production.
- BP. (2021). *Statistical Review of World Energy*. London, UK. Retrieved from <https://www.bp.com/content/dam/bp/business-sites/en/global/corporate/pdfs/energy-economics/statistical-review/bp-stats-review-2021-full-report.pdf>
- Cancino-Solórzano, Y., Gutiérrez-Trashorras, A. J., & Xiberta-Bernat, J. (2011). Current state of wind energy in Mexico, achievements and perspectives. *Renewable and Sustainable Energy Reviews*, 15(8), 3552–3557. <https://doi.org/10.1016/j.rser.2011.05.009>
- Cannon, D. J., Brayshaw, D. J., Methven, J., Coker, P. J., & Lenaghan, D. (2015). Using reanalysis data to quantify extreme wind power generation statistics: A 33 year case study in Great Britain. *Renewable Energy*, 75, 767–778. <https://doi.org/10.1016/j.renene.2014.10.024>
- Carvalho, D., Rocha, A., Gómez-Gesteira, M., & Silva Santos, C. (2014). Sensitivity of the WRF model wind simulation and wind energy production estimates to planetary boundary layer parameterizations for onshore and offshore areas in the Iberian Peninsula. *Applied Energy*, 135, 234–246. <https://doi.org/10.1016/j.apenergy.2014.08.082>
- Centro Nacional de Control de Energía. (2021). *Programa Nacional del Sistema Eléctrico Nacional 2020-2034*. Ciudad de México. Retrieved from <https://www.gob.mx/cenace/documentos/programa-de-desarrollo-del-sistema-electrico-nacional-2020-2034>
- Chen, F., & Dudhia, J. (2001). Coupling an Advanced Land Surface–Hydrology Model with the Penn State–NCAR MM5 Modeling System. Part I: Model Implementation and Sensitivity. *Monthly Weather Review*, 129(4), 569–585. [https://doi.org/10.1175/1520-0493\(2001\)129<0569:CAALSH>2.0.CO;2](https://doi.org/10.1175/1520-0493(2001)129<0569:CAALSH>2.0.CO;2)
- Chou, M.-D., & Suarez, M. J. (1994). An efficient thermal infrared radiation parameterization for use in general circulation models.
- Cutler, N. (2011). *Final report on UNSW Project for AEMO to develop a prototype wind power forecasting tool for potential large rapid changes in wind power*.



- Cutler, N., Kay, M., Jacka, K., & Nielsen, T. S. (2007). Detecting, categorizing and forecasting large ramps in wind farm power output using meteorological observations and WPPT. *Wind Energy*, 10(5), 453–470. <https://doi.org/10.1002/we.235>
- Deakin, M., Bloomfield, H., Greenwood, D., Sheehy, S., Walker, S., & Taylor, P. C. (2021). Impacts of heat decarbonization on system adequacy considering increased meteorological sensitivity. *Applied Energy*, 298, 117261. <https://doi.org/https://doi.org/10.1016/j.apenergy.2021.117261>
- Deppe, A. J., Gallus, W. A., & Takle, E. S. (2013). A WRF Ensemble for Improved Wind Speed Forecasts at Turbine Height. *Weather and Forecasting*, 28(1), 212–228. <https://doi.org/10.1175/WAF-D-11-00112.1>
- Dolores, E., Caetano, E., López-Bravo, L. C., & Calheiros, A. (2019). Influence of soil moisture on mesoscale convective initiation in central Mexico. *European Journal of Remote Sensing*, 52(1), 640–652. <https://doi.org/10.1080/22797254.2019.1700397>
- Dudhia, J. (1989). Numerical Study of Convection Observed during the Winter Monsoon Experiment Using a Mesoscale Two-Dimensional Model. *Journal of the Atmospheric Sciences*, 46(20), 3077–3107. [https://doi.org/10.1175/1520-0469\(1989\)046<3077:NSOCOD>2.0.CO;2](https://doi.org/10.1175/1520-0469(1989)046<3077:NSOCOD>2.0.CO;2)
- EFE. (2017, April 4). Costa Rica generó el 99% de su electricidad con fuentes de energía limpias en el primer trimestre. *ElEconomista.Es*, p. 1. Retrieved from <https://www.economista.es/economia-eAm-mexico/noticias/8270895/04/17/Costa-Rica-genero-el-99-de-su-electricidad-con-fuentes-de-energia-limpias-en-el-primer-trimestre.html>
- Ember. (2022). World electricity generation by source. Retrieved March 28, 2021, from <https://ember-climate.org/>
- Freedman, J., Markus, M., & Penc, R. (2008). Analysis of West Texas Wind Plant Ramp-up and Ramp-down Events. *AWS Truewind, LLC*, 251–278. Retrieved from [https://scholar.google.com/scholar?q=freedman+Markus+pen+analysis+of+west+texas&btnG=&hl=en&as\\_sdt=0,37#0](https://scholar.google.com/scholar?q=freedman+Markus+pen+analysis+of+west+texas&btnG=&hl=en&as_sdt=0,37#0)
- Gallego-Castillo, C., Cuerva-Tejero, A., & Lopez-Garcia, O. (2015). A review on the recent history of wind power ramp forecasting. *Renewable and Sustainable Energy Reviews*, 52, 1148–1157. <https://doi.org/10.1016/j.rser.2015.07.154>
- Gan, K., & Ke, D. P. (2014). Wind power ramp forecasting based on least-square support vector machine. *Applied Mechanics and Materials*, 535, 162–166.
- Gómez-Navarro, J. J., Raible, C. C., & Dierer, S. (2015). Sensitivity of the WRF model to PBL parametrisations and nesting techniques: Evaluation of wind storms over complex terrain. *Geoscientific Model Development*, 8(10), 3349–3363. <https://doi.org/10.5194/gmd-8-3349-2015>

- Grell, G. A., & Dévényi, D. (2002). A generalized approach to parameterizing convection combining ensemble and data assimilation techniques. *Geophysical Research Letters*, 29(14), 34–38. <https://doi.org/10.1029/2002GL015311>
- Hernández-Escobedo, Q., Manzano-Agugliaro, F., & Zapata-Sierra, A. (2010). The wind power of Mexico. *Renewable and Sustainable Energy Reviews*, 14(9), 2830–2840. <https://doi.org/10.1016/j.rser.2010.07.019>
- Hernández-Escobedo, Q., Saldaña-Flores, R., Rodríguez-García, E. R., & Manzano-Agugliaro, F. (2014). Wind energy resource in Northern Mexico. *Renewable and Sustainable Energy Reviews*, 32, 890–914. <https://doi.org/10.1016/j.rser.2014.01.043>
- Hong, S.-Y., Dudhia, J., & Chen, S.-H. (2004). A Revised Approach to Ice Microphysical Processes for the Bulk Parameterization of Clouds and Precipitation. *Monthly Weather Review*, 132(1), 103–120. [https://doi.org/10.1175/1520-0493\(2004\)132<0103:ARATIM>2.0.CO;2](https://doi.org/10.1175/1520-0493(2004)132<0103:ARATIM>2.0.CO;2)
- Hong, S.-Y., Noh, Y., & Dudhia, J. (2006). A New Vertical Diffusion Package with an Explicit Treatment of Entrainment Processes. *Monthly Weather Review*, 134(9), 2318–2341. <https://doi.org/10.1175/MWR3199.1>
- Hu, X. M., Nielsen-Gammon, J. W., & Zhang, F. (2010). Evaluation of three planetary boundary layer schemes in the WRF model. *Journal of Applied Meteorology and Climatology*, 49(9), 1831–1844. <https://doi.org/10.1175/2010JAMC2432.1>
- IRENA. (2019). *Transformación energética mundial: Resumen ejecutivo*. Abu Dhabi. Retrieved from [https://www.irena.org/-/media/Files/IRENA/Agency/Publication/2018/Apr/IRENA\\_Global\\_Energy\\_Transformation\\_2018\\_summary\\_ES.pdf?la=en&hash=A5492C2AAC7D8E7A7CBF71A460649A8DEDB48A82](https://www.irena.org/-/media/Files/IRENA/Agency/Publication/2018/Apr/IRENA_Global_Energy_Transformation_2018_summary_ES.pdf?la=en&hash=A5492C2AAC7D8E7A7CBF71A460649A8DEDB48A82)
- IRENA. (2020). *Plan de Acción Regional: Acelerando el despliegue de energía renovable en Latinoamérica*. Abu Dhabi.
- IRENA. (2021). *Estadísticas de capacidad renovable 2021*. Abu Dhabi. Retrieved from <https://www.irena.org/publications/2021/March/Renewable-Capacity-Statistics-2021-ES>
- Janjić, Z. I. (1994a). The Step-Mountain Eta Coordinate Model: Further Developments of the Convection, Viscous Sublayer, and Turbulence Closure Schemes. *Monthly Weather Review*, 122(5), 927–945. [https://doi.org/10.1175/1520-0493\(1994\)122<0927:TSMECM>2.0.CO;2](https://doi.org/10.1175/1520-0493(1994)122<0927:TSMECM>2.0.CO;2)
- Janjić, Z. I. (1994b). The Step-Mountain Eta Coordinate Model: Further Developments of the Convection, Viscous Sublayer, and Turbulence Closure Schemes. *Monthly Weather Review*, 122(5), 927–945. [https://doi.org/10.1175/1520-0493\(1994\)122<0927:TSMECM>2.0.CO;2](https://doi.org/10.1175/1520-0493(1994)122<0927:TSMECM>2.0.CO;2)

0493(1994)122<0927:TSMEECM>2.0.CO;2

- Jaramillo, O. A., & Borja, M. A. (2004). Wind speed analysis in La Ventosa, Mexico: A bimodal probability distribution case. *Renewable Energy*, 29(10), 1613–1630. <https://doi.org/10.1016/j.renene.2004.02.001>
- Kain, J. S. (2004). The Kain–Fritsch Convective Parameterization: An Update. *Journal of Applied Meteorology*, 43(1), 170–181. [https://doi.org/10.1175/1520-0450\(2004\)043<0170:TKCPAU>2.0.CO;2](https://doi.org/10.1175/1520-0450(2004)043<0170:TKCPAU>2.0.CO;2)
- Krogsæter, O., & Reuder, J. (2015). Validation of boundary layer parameterization schemes in the weather research and forecasting model under the aspect of offshore wind energy applications— Part I: Average wind speed and wind shear. *Wind Energy*, 18, 769–782. <https://doi.org/DOI: 10.1002/we.1727>
- Lacerda, M., Couto, A., & Estanqueiro, A. (2017). Wind Power Ramps Driven by Windstorms and Cyclones. *Energies*, 10(10). <https://doi.org/10.3390/en10101475>
- Liu, Y., Qian, Y., & Berg, L. K. (2022). Local-thermal-gradient and large-scale-circulation impacts on turbine-height wind speed forecasting over the Columbia River Basin. *Wind Energy Science*, 7(1), 37–51. <https://doi.org/10.5194/wes-7-37-2022>
- López-Bravo, C., Caetano, E., & Magaña, V. (2018). Forecasting Summertime Surface Temperature and Precipitation in the Mexico City Metropolitan Area: Sensitivity of the WRF Model to Land Cover Changes. *Frontiers in Earth Science*, 6, 6. <https://doi.org/10.3389/feart.2018.00006>
- Mattar, C., & Borvarán, D. (2016). Offshore wind power simulation by using WRF in the central coast of Chile. *Renewable Energy*, 94, 22–31. <https://doi.org/10.1016/j.renene.2016.03.005>
- Max, R., & Ortíz-Ospina, E. (2022). Share of electricity production by source. Retrieved April 1, 2022, from <https://ourworldindata.org/grapher/share-electricity-source-facet?country=~GBR>
- Menendez, M., García-Díez, M., Fita, L., Fernández, J., Méndez, F. J., & Gutiérrez, J. M. (2014). High-resolution sea wind hindcasts over the Mediterranean area. *Climate Dynamics*, 42(7–8), 1857–1872. <https://doi.org/10.1007/s00382-013-1912-8>
- Mesinger, F. (1993). Forecasting upper tropospheric turbulence within the framework of the Mellor-Yamada 2.5 closure. *Res. Activ. Atmos. Oceanic Mod.*
- Mlawer, E. J., Taubman, S. J., Brown, P. D., Iacono, M. J., & Clough, S. A. (1997). Radiative transfer for inhomogeneous atmospheres: RRTM, a validated correlated-k model for the longwave. *Journal of Geophysical Research: Atmospheres*, 102(D14), 16663–16682. <https://doi.org/10.1029/97JD00237>

- Mukul Tewari, N., Tewari, M., Chen, F., Wang, W., Dudhia, J., LeMone, M., ... Wegiel, J. (2004). Implementation and verification of the unified NOAA land surface model in the WRF model (Formerly Paper Number 17.5). In *Proceedings of the 20th Conference on Weather Analysis and Forecasting/16th Conference on Numerical Weather Prediction, Seattle, WA, USA* (Vol. 14).
- Ohba, M., Kadokura, S., & Nohara, D. (2016). Impacts of synoptic circulation patterns on wind power ramp events in East Japan. *Renewable Energy*, 96(2016), 591–602. <https://doi.org/10.1016/j.renene.2016.05.032>
- Papalexiou, S. M., Serinaldi, F., & Porcu, E. (2021). Advancing Space-Time Simulation of Random Fields: From Storms to Cyclones and Beyond. *Water Resources Research*, 57(8), 1–26. <https://doi.org/10.1029/2020WR029466>
- Pereyra-Castro, K., & Caetano, E. (2022). Wind-Ramp Predictability. *Atmosphere*, 13(3). <https://doi.org/10.3390/atmos13030453>
- Pereyra-Castro, K., Caetano, E., & Altamirano del Razo, D. (2021). WRF wind forecast over coastal complex terrain: Baja California Peninsula (Mexico) case study. *Arabian Journal of Geosciences*, 14(19), 1972. <https://doi.org/10.1007/s12517-021-08317-3>
- Pereyra-Castro, K., Caetano, E., Martínez-Alvarado, O., & Quintanilla-Montoya, A. L. (2020). Wind and Wind Power Ramp Variability over Northern Mexico. *Atmosphere*, 11(12), 1281. <https://doi.org/10.3390/atmos11121281>
- Pichault, M., Vincent, C., Skidmore, G., & Monty, J. (2021). Characterisation of intra-hourly wind power ramps at the wind farm scale and associated processes. *Wind Energy Science*, 6(1), 131–147. <https://doi.org/10.5194/wes-6-131-2021>
- Pleim, J. E. (2007a). A Combined Local and Nonlocal Closure Model for the Atmospheric Boundary Layer. Part I: Model Description and Testing. *Journal of Applied Meteorology and Climatology*, 46(9), 1383–1395. <https://doi.org/10.1175/JAM2539.1>
- Pleim, J. E. (2007b). A Combined Local and Nonlocal Closure Model for the Atmospheric Boundary Layer. Part II: Application and Evaluation in a Mesoscale Meteorological Model. *Journal of Applied Meteorology and Climatology*, 46(9), 1396–1409. <https://doi.org/10.1175/JAM2534.1>
- Pleim, J. E., & Chang, J. S. (1992). A non-local closure model for vertical mixing in the convective boundary layer. *Atmospheric Environment Part A, General Topics*, 26(6), 965–981. [https://doi.org/10.1016/0960-1686\(92\)90028-J](https://doi.org/10.1016/0960-1686(92)90028-J)
- Santos-Alamillos, F. J., Zquez, D. P. V., Ruiz-Arias, J. A., Lara-Fanego, V., & Tovar-Pescador, J. (2013). Analysis of WRF model wind estimate sensitivity to physics parameterization choice and terrain representation in Andalusia (Southern Spain). *Journal of Applied Meteorology and Climatology*, 52(7), 1592–1609. <https://doi.org/10.1175/JAMC-D-12-0204.1>



- Sawin, J. L., Sverrisson, F., Seyboth, K., Adib, R., Murdock, H. E., Lins, C., ... Martinot, E. (2016). *Renewables 2016 Global Status Report* (Rapport sur le statut mondial des énergies renouvelables 2016 Faits essentiels Année record pour les énergies renouvelables: nouvelles installations, nouveaux objectifs politiques, nouveaux investissements et nouveaux emplois). France. Retrieved from [http://inis.iaea.org/search/search.aspx?orig\\_q=RN:47082519](http://inis.iaea.org/search/search.aspx?orig_q=RN:47082519)
- SENER. (2015). *Programa de Desarrollo del Sistema Eléctrico Nacional 2015-2029*. Ciudad de México.
- Sheridan, P. (2011). *Review of techniques and research for gust forecasting and parameterisation. UK MetOffice Forecasting Research Technical Report 570*.
- Sherry, M., & Rival, D. (2015). Meteorological phenomena associated with wind-power ramps downwind of mountainous terrain. *Journal of Renewable and Sustainable Energy*, 7(3), 1–13. <https://doi.org/10.1063/1.4919021>
- Siuta, D., West, G., & Stull, R. (2017). WRF hub-height wind forecast sensitivity to PBL scheme, grid length, and initial condition choice in complex terrain. *Weather and Forecasting*, 32(2), 493–509. <https://doi.org/10.1175/WAF-D-16-0120.1>
- Skamarock, W. C., Klemp, J. B., Dudhia, J., Gill, D. O., Barker, D. M., Duda, M. G., ... Powers, J. G. (2008). A description of the advanced research WRF Version 3, Mesoscale and Microscale Meteorology Division. *National Center for Atmospheric Research, Boulder, Colorado, USA*, 88, 7–25.
- Thomas, S. R., Martínez-Alvarado, O., Drew, D., & Bloomfield, H. (2021). Drivers of extreme wind events in Mexico for windpower applications. *International Journal of Climatology*, 41(S1), E2321–E2340. <https://doi.org/10.1002/joc.6848>
- Thompson, G., Field, P. R., Rasmussen, R. M., & Hall, W. D. (2008). Explicit Forecasts of Winter Precipitation Using an Improved Bulk Microphysics Scheme. Part II: Implementation of a New Snow Parameterization. *Monthly Weather Review*, 136(12), 5095–5115. <https://doi.org/10.1175/2008MWR2387.1>
- Tyagi, B., Magliulo, V., Finardi, S., Gasbarra, D., Carlucci, P., Toscano, P., ... Gioli, B. (2018). Performance Analysis of Planetary Boundary Layer Parameterization Schemes in WRF Modeling Set Up over Southern Italy. *Atmosphere*, 9(7). <https://doi.org/10.3390/atmos9070272>
- Yáñez, J. P., Kunith, A., Chávez-Arroyo, R., Romo-Perea, A., & Probst, O. (2014). Assessment of the capacity credit of wind power in Mexico. *Renewable Energy*, 72, 62–78. <https://doi.org/10.1016/j.renene.2014.06.038>
- Zhang, J., Cui, M., Hodge, B. M., Florita, A., & Freedman, J. (2017). Ramp forecasting performance from improved short-term wind power forecasting over multiple spatial and temporal scales. *Energy*, 122, 528–541. <https://doi.org/10.1016/j.energy.2017.01.104>

## Anexo 1. Material Suplementario del Capítulo 3

*Supplementary material*

# Wind and Wind Power Ramp Variability over Northern Mexico

Karla Pereyra-Castro <sup>1</sup>, Ernesto Caetano <sup>2,\*</sup>, Oscar Martínez-Alvarado <sup>3</sup> and Ana L. Quintanilla-Montoya <sup>4</sup>

<sup>1</sup> Posgrado en Ciencias de la Tierra, Instituto de Geografía, Universidad Nacional Autónoma de México, Ciudad de México 04510, México; karpereyra@comunidad.unam.mx

<sup>2</sup> Instituto de Geografía, Universidad Nacional Autónoma de México, Ciudad de México 04510, México

<sup>3</sup> National Centre for Atmospheric Science, Department of Meteorology, University of Reading, Reading RG6 6ES, United Kingdom; o.martinezalvarado@reading.ac.uk

<sup>4</sup> Facultad de Ingeniería Civil, Universidad de Colima, Coquimatlán, Colima 28400, México; analuzqm@ucol.mx

\* Correspondence: caetano@unam.mx; Tel.: +52-56230222 (ext. 45459)

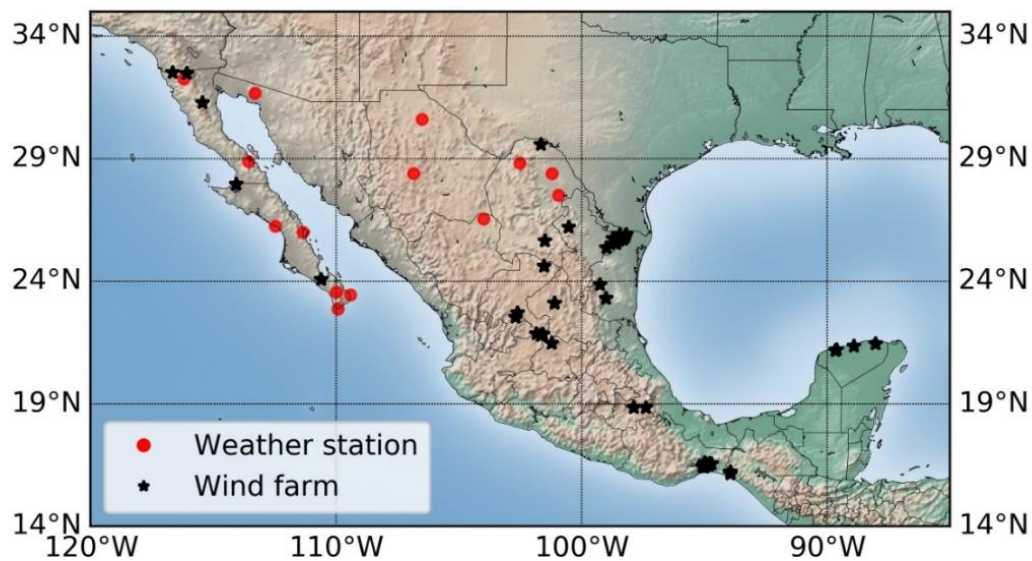


**Figure S1.** Weather stations (red dot) used in the study and wind farms (black star) in operation over Mexico.

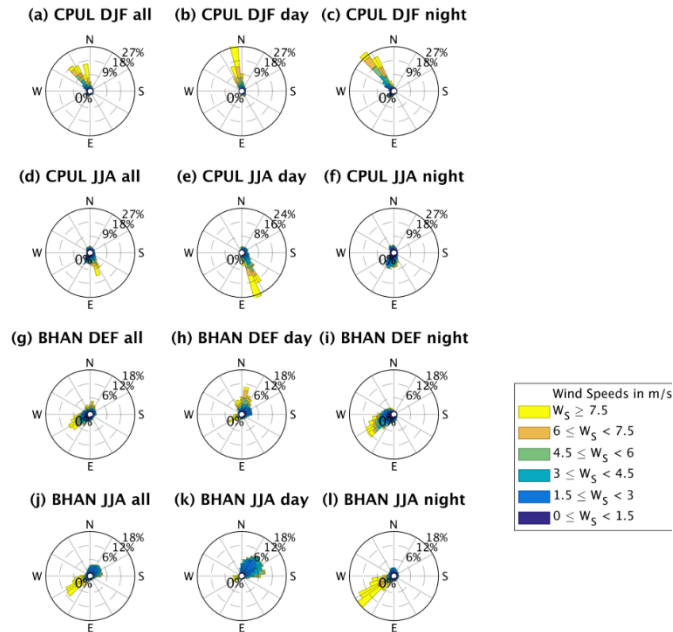
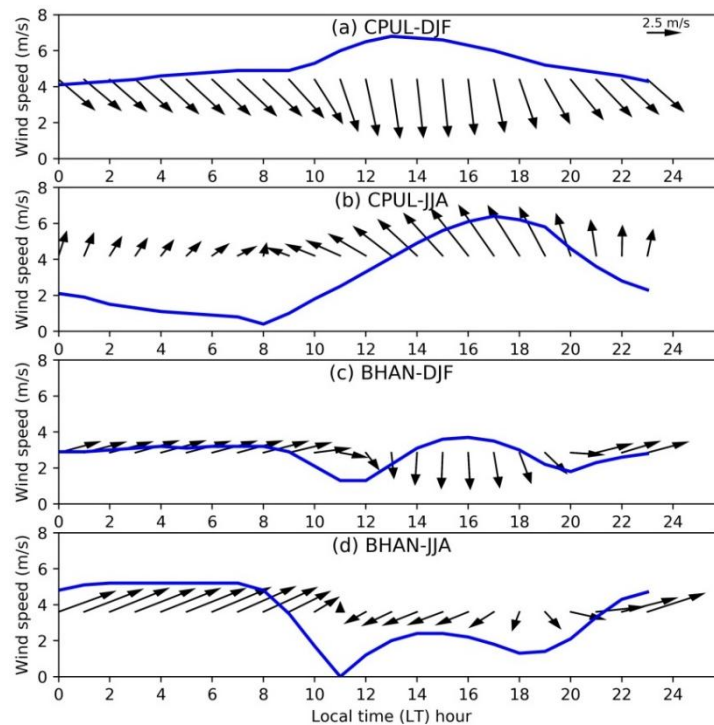


**Figure S2.** All day (a,d,g,j), day (b,e,h,k) and night (c,f,i,l) surface windroses from CPUL and BHAN weather stations for June-July-August (JJA) and December-January-February (DJF).



Periods are 2013-2017 for CPUL and 2010-2017 for BHAN. Blue line indicates wind speed in m/s.

**Figure S3.** Diurnal variations of the horizontal surface vector for CPUL (a,b) and BHAN (c,d) weather station in June-July-August (JJA) and December-January-February (DJF).



**Figure S4.** Cold front over Northern Mexico in 13 January 2013 during a ramp event in PLATEAU region. A cold front is seen as a curving line of clouds in the MODIS Corrected Reflectance imagery.

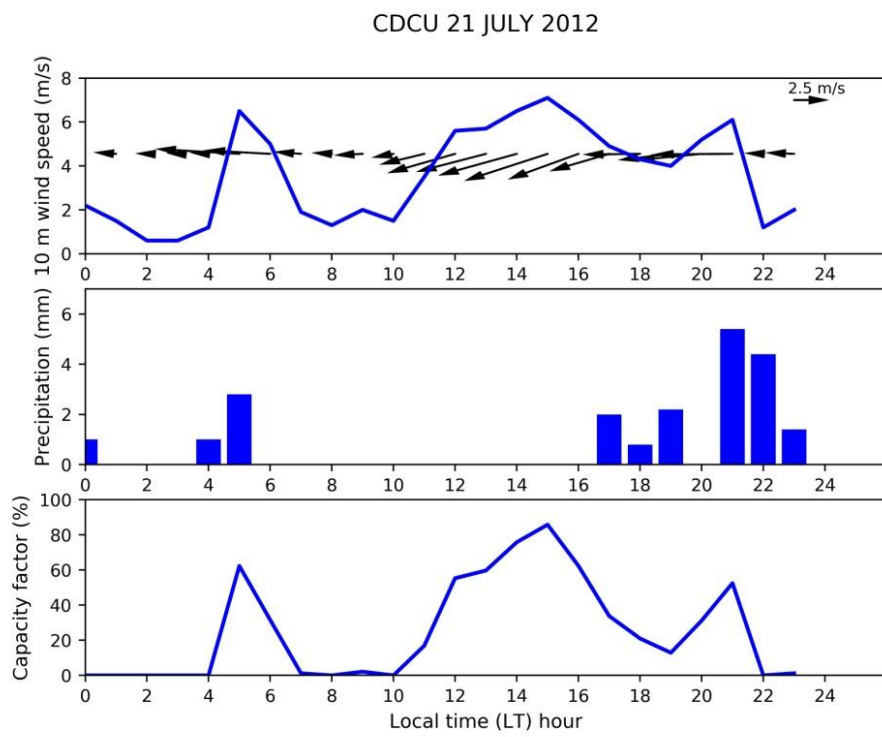


**Figure S5.** Meteogram at CDCU for a storm of 21 July 2012.



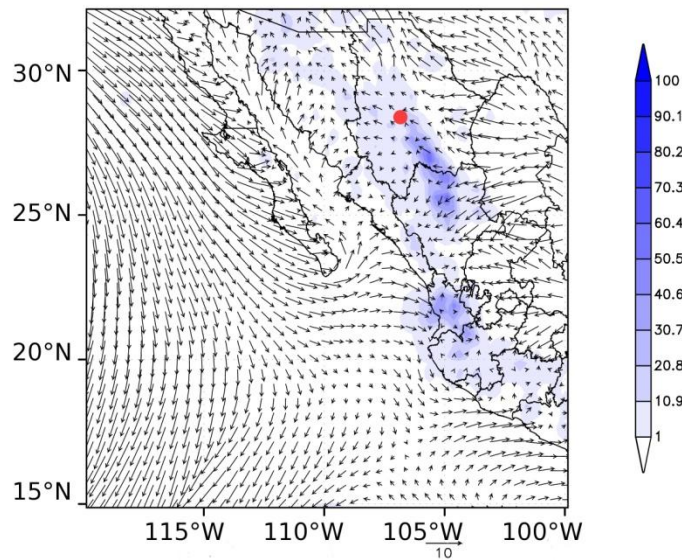


**Figure S6.** Example of summer ramp -up event at Ciudad Cuauhtémoc (red circle) in 21 July 2012. ERA5 surface wind speed and CMORPH daily precipitation in mm (shaded).

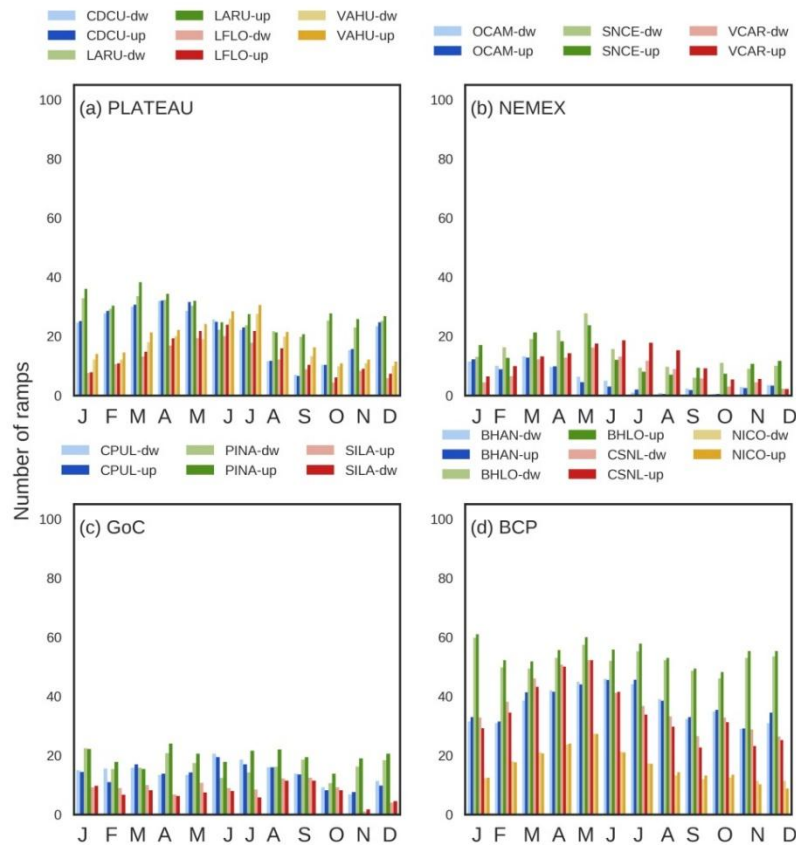


**Figure S7.** Monthly mean of wind power ramp-up (dark color) and ramp-down (light color) events for (a) Plateau, (b) NEMEX, (c) GoC, (d) BCP regions. Ramp is a change of 30% or greater in rated power in 1 hour.

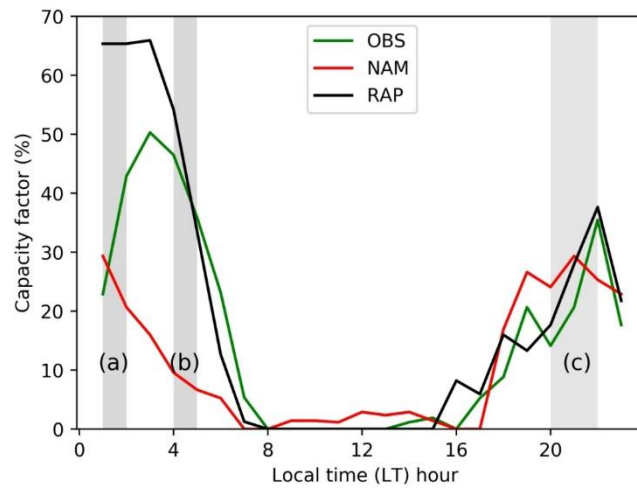


**Figure S8.** Example of wind power ramps ( $\geq 20\%$  of rated power) a) observed but not predicted, b) predicted by RAP but not observed in one hour and c) predicted by RAP and observed in 3 hours. Capacity factor is the ratio between the power generation and the rated power.

**Table S1.** Wind power forecast Mean Absolute Error (MAE) and Bias error for 14 weather stations in 2013. Errors are in kW. Wind power was derived by extrapolating NAM, RAP and observation to 80 m and using the G114-2.5 wind power curve.

Station	Model	Annual Bias	Annual MAE	Lead time								
				2	4	6	8	10	12	14	16	18
CDCU	RAP	178.3	363.9	329.3	337.0	373.8	332.1	364.4	369.3	375.5	369.9	372.8
	NAM	119.0	323.1	304.4	318.0	316.5	291.6	318.9	324.7	334.4	337.3	336.1
LARU	RAP	-53.4	390.4	445.7	358.0	433.1	420.3	365.2	401.3	393.6	346.7	369.3
	NAM	113.9	490.0	500.8	474.3	520.3	498.9	468.7	485.9	489.1	475.2	457.3
LFLO	RAP	-75.5	274.0	253.3	251.9	269.9	254.4	268.9	291.8	282.2	274.5	286.7
	NAM	-22.1	275.2	252.9	282.7	290.9	235.8	285.0	271.1	247.8	276.6	301.2
VAHU	RAP	17.1	285.2	259.5	267.7	266.9	256.6	278.4	272.8	272.4	298.9	300.6
	NAM	195.7	399.8	369.0	409.1	388.7	392.8	407.3	422.9	379.0	395.4	418.3
OCAM	RAP	730.2	756.2	603.1	666.2	704.2	754.2	805.9	810.7	832.4	857.0	868.9
	NAM	299.0	391.7	337.0	383.9	403.0	374.7	423.2	435.2	389.8	438.0	285.7
SNCE	RAP	144.0	341.3	276.9	328.2	381.6	318.0	327.9	372.3	341.5	368.3	414.2
	NAM	102.6	303.3	267.6	282.7	340.0	299.9	297.4	356.3	292.9	312.6	294.2
VCAR	RAP	64.4	449.0	446.6	426.7	460.5	423.6	453.2	426.7	452.7	436.2	467.5
	NAM	-42.6	398.7	373.6	389.4	407.7	365.7	411.2	371.6	385.0	414.1	422.9
CPUL	RAP	-13.6	489.5	466.0	491.4	496.8	478.7	496.8	491.3	460.5	513.4	521.6
	NAM	30.4	497.6	496.8	503.0	518.8	478.0	485.4	507.3	479.2	507.8	507.9
PINA	RAP	-173.4	397.3	383.2	375.4	403.1	397.9	415.4	384.3	380.4	406.0	405.1
	NAM	-90.1	370.1	343.0	338.9	370.4	364.6	385.2	381.1	378.3	402.4	349.1
SILA	RAP	-69.8	329.7	334.2	340.2	303.5	347.3	343.2	299.1	323.8	347.6	313.4
	NAM	-147.1	309.9	317.9	315.4	294.0	321.0	325.8	296.6	305.1	325.7	272.5
BHAN	RAP	153.3	650.6	660.1	657.3	719.5	659.8	609.4	609.7	645.4	627.9	598.3
	NAM	-459.8	740.1	694.5	725.8	742.3	723.7	776.4	758.1	720.0	753.0	726.4
BHLO	RAP	-19.9	827.3	778.2	848.8	899.3	789.0	803.1	870.3	759.0	827.7	898.5
	NAM	-318.0	739.6	702.0	722.0	776.7	686.4	731.8	800.9	717.7	754.4	818.9
CSNL	RAP	-66.3	680.7	702.3	668.3	670.5	683.7	696.2	665.8	664.3	672.7	692.5
	NAM	-426.6	665.8	677.9	681.6	651.4	662.3	686.5	645.6	645.4	654.4	631.6
NICO	RAP	288.6	418.5	402.2	398.4	375.4	429.7	411.6	381.4	454.0	456.0	422.0
	NAM	-23.7	299.6	312.9	295.4	279.2	327.4	296.3	282.3	321.6	297.9	286.9

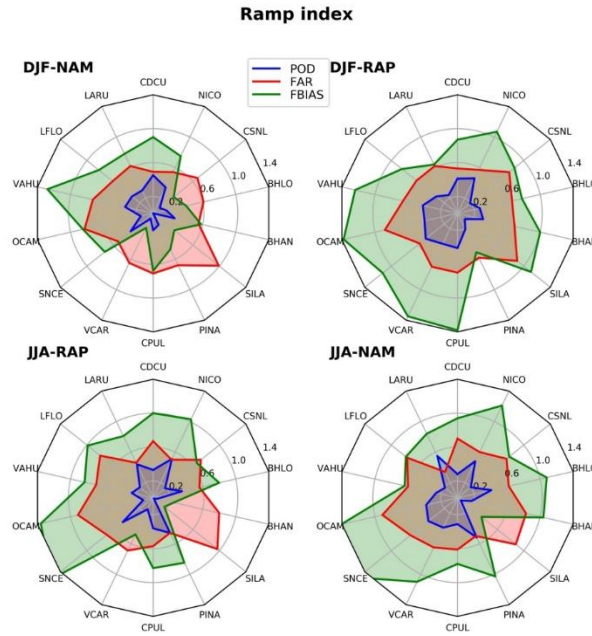


**Figure S9.** POD, FAR and FBIAS metrics for a variation  $\geq 20\%$  of rated power in 3 hours for June-July-August (JJA) and December-January-February (DJF) 2013.

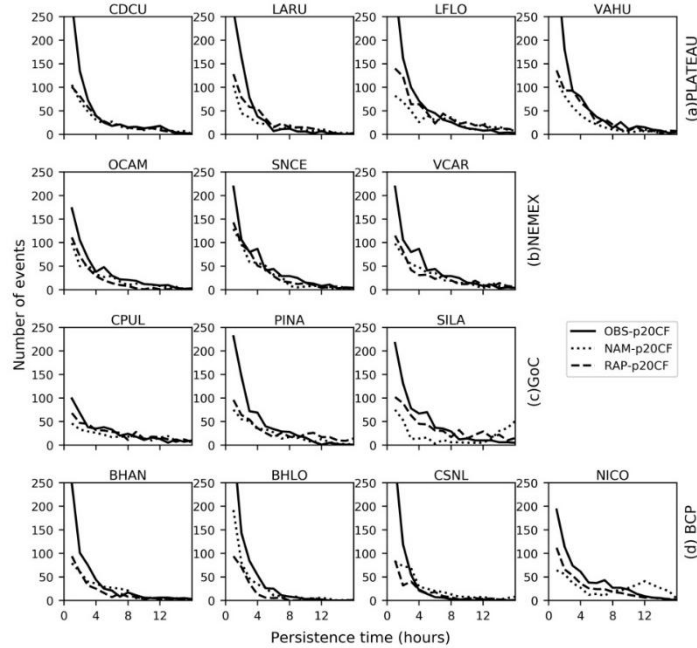


**Figure S10.** Extreme events of low generation observed (continuous line), NAM (dotted line) and RAP (dashed line) for 2013. Extreme events correspond to the 20th percentile (black line) of instantaneous capacity factor (CF). Regions are (a) Plateau, (b) NEMEX, (c) GoC, (d) BCP.

**Publisher’s Note:** MDPI stays neutral with regard to jurisdictional claims in published maps and institutional affiliations.



© 2020 by the authors. Submitted for possible open access publication under the terms and conditions of the Creative Commons Attribution (CC BY) license (<http://creativecommons.org/licenses/by/4.0/>).



---

## **Anexo 2. Material Suplementario del Capítulo 4**

### **WRF WIND FORECAST OVER COASTAL COMPLEX TERRAIN: BAJA CALIFORNIA PENINSULA (MEXICO) CASE STUDY**

Karla Pereyra-Castro<sup>a</sup>, Ernesto Caetano<sup>b\*</sup>, Diego Altamirano-del Razo<sup>c</sup>

<sup>a</sup> Posgrado en Ciencias de la Tierra, Universidad Nacional Autónoma de México, Circuito de la Investigación Científica, 04510, Ciudad de México, México. <https://orcid.org/0000-0001-8246-4447>

<sup>b</sup> Instituto de Geografía, Universidad Nacional Autónoma de México, Circuito de la Investigación Científica, 04510, Ciudad de México, México, [caetano@unam.mx](mailto:caetano@unam.mx). <https://orcid.org/0000-0002-9142-5340>

<sup>c</sup> Facultad de Ingeniería, Universidad Nacional Autónoma de México, Circuito de la Investigación Científica, 04510, Ciudad de México, México

\*Corresponding author: Ernesto Caetano

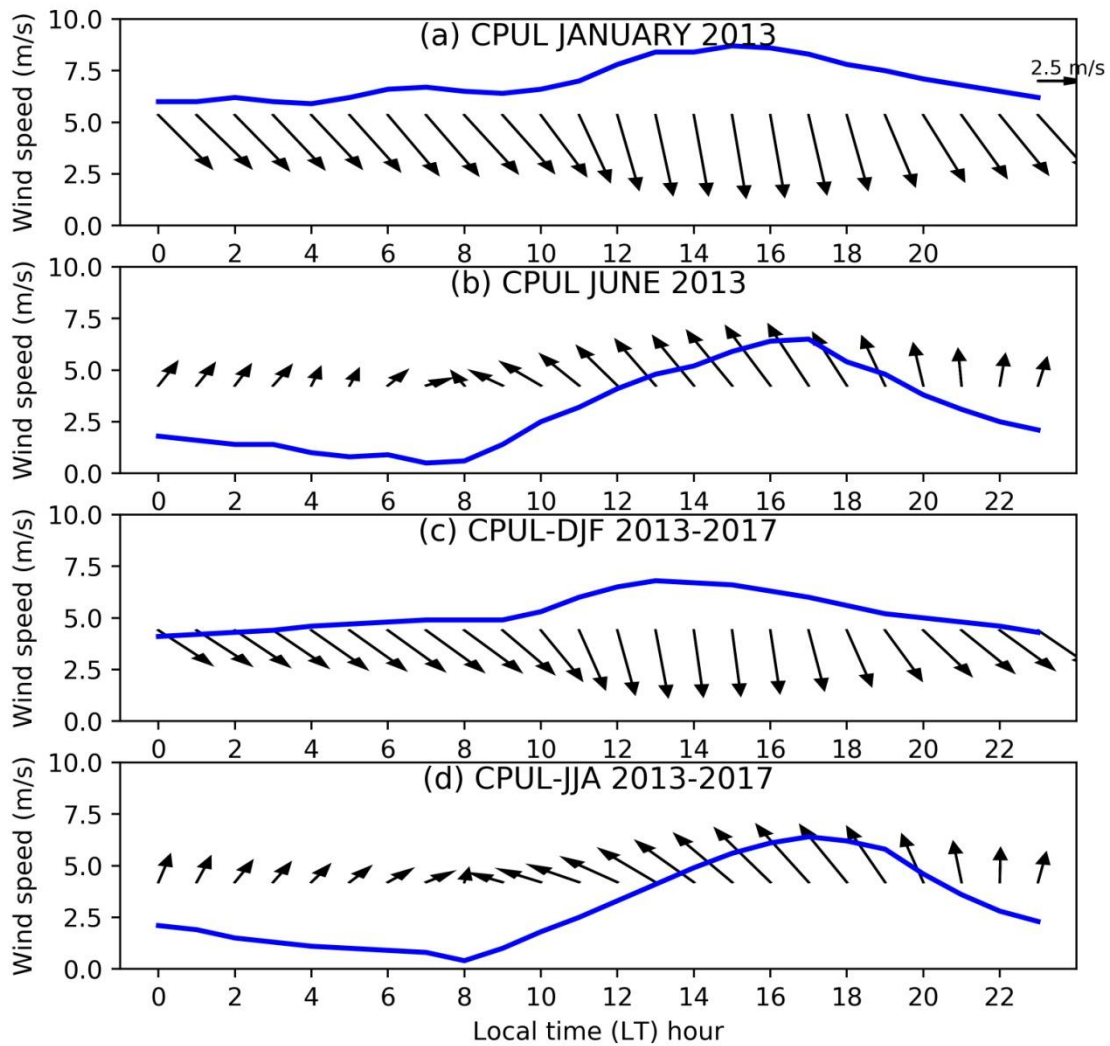


**Fig. S1** Diurnal variations of the horizontal surface wind for CPUL weather station in a) January 2013, b) June 2013, c) June-July-August (JJA) from 2010 to 2017 and December-January-February (DJF) from 2010 to 2017. Blue line indicates wind speed in m/s. A similar behavior was found for the rest of the stations.

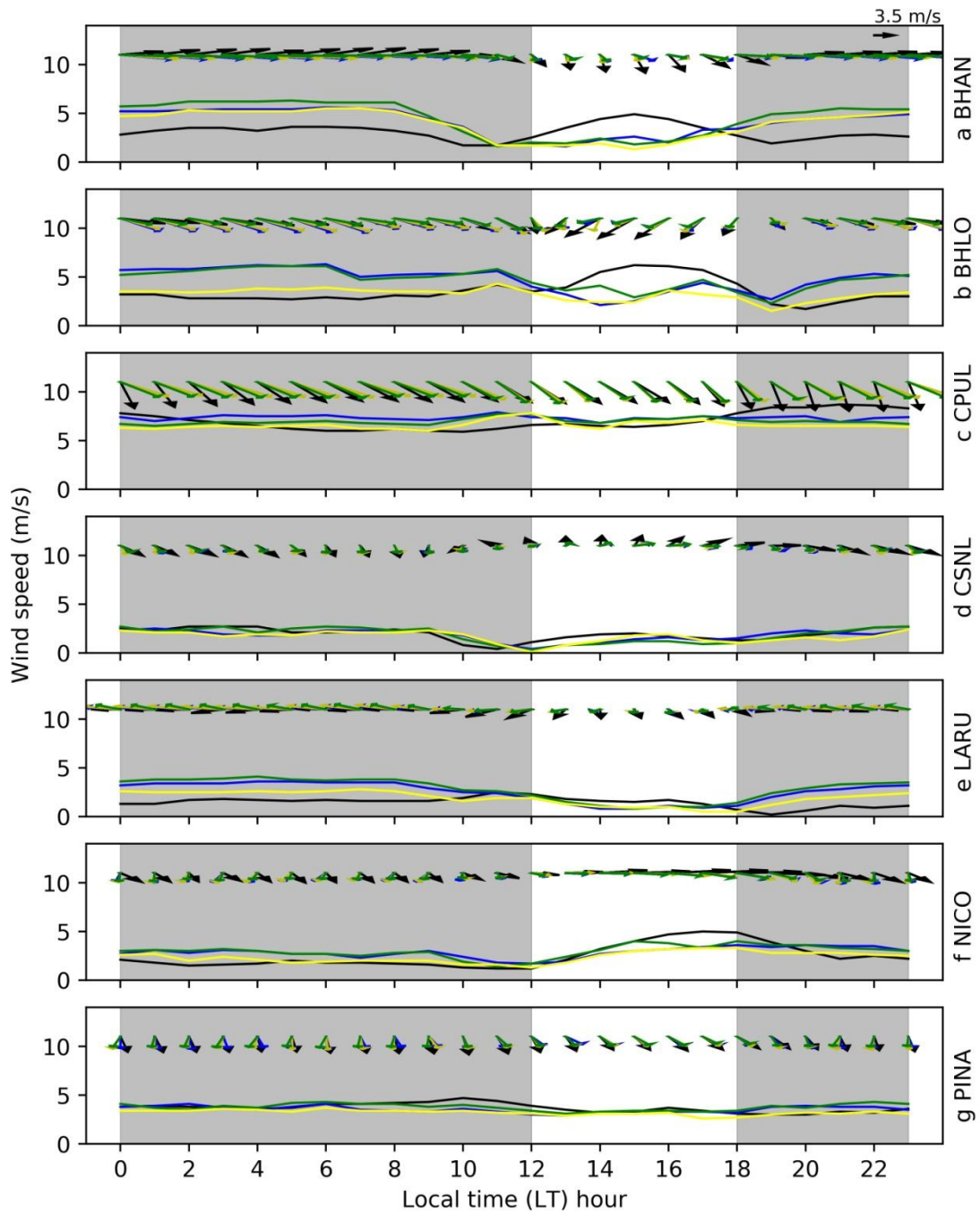


**Fig. S2** Observed and WRF simulated diurnal variations of the horizontal surface wind for seven weather stations in January 2013. Line indicates wind speed in m/s. Observed wind (black line), YSU PBL scheme (yellow line), MYJ PBL scheme (green line), ACM2 PBL scheme (blue line)

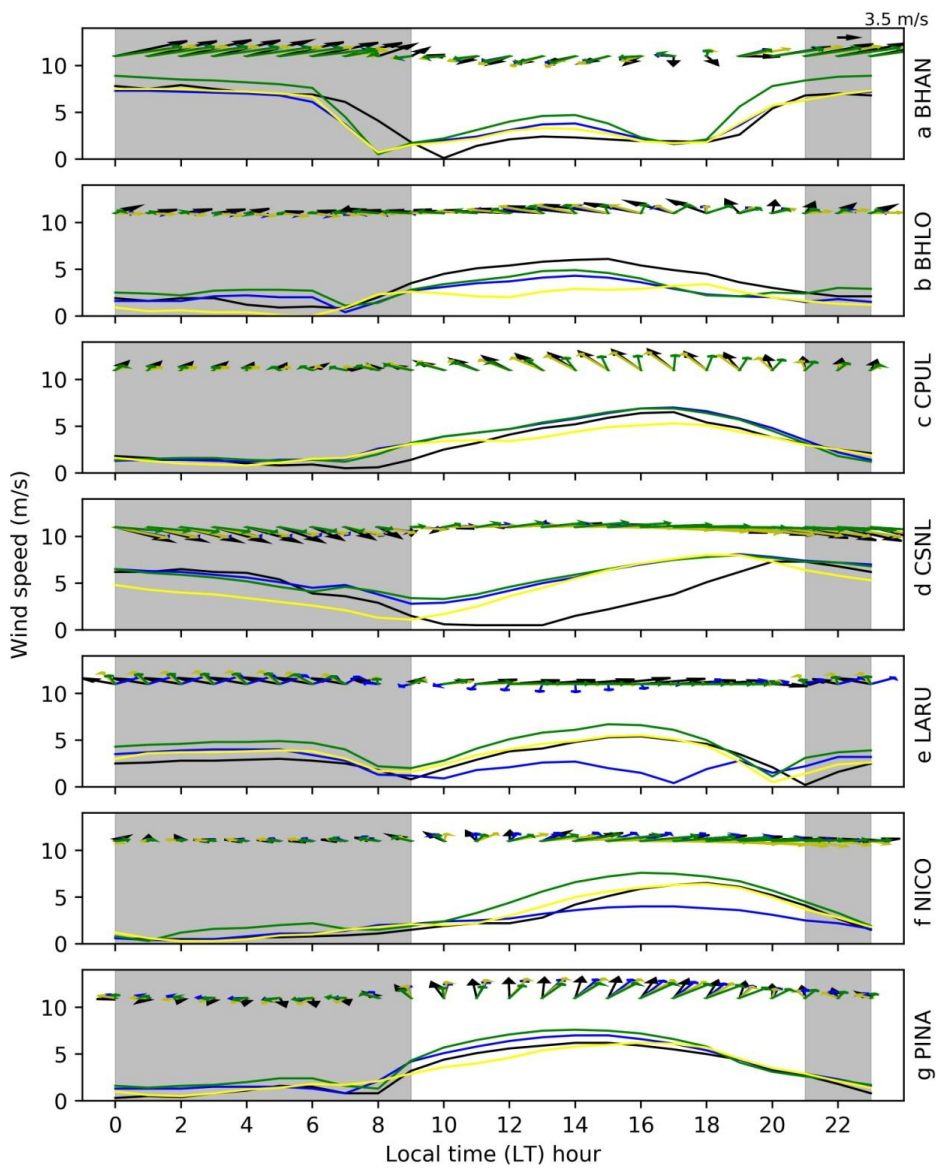


**Fig. S3** Observed and WRF simulated diurnal variations of the horizontal surface wind for seven weather stations in January 2013. Line indicates wind speed in m/s. Observed wind (black line), YSU PBL scheme (yellow line), MYJ PBL scheme (green line), ACM2 PBL scheme (blue line)



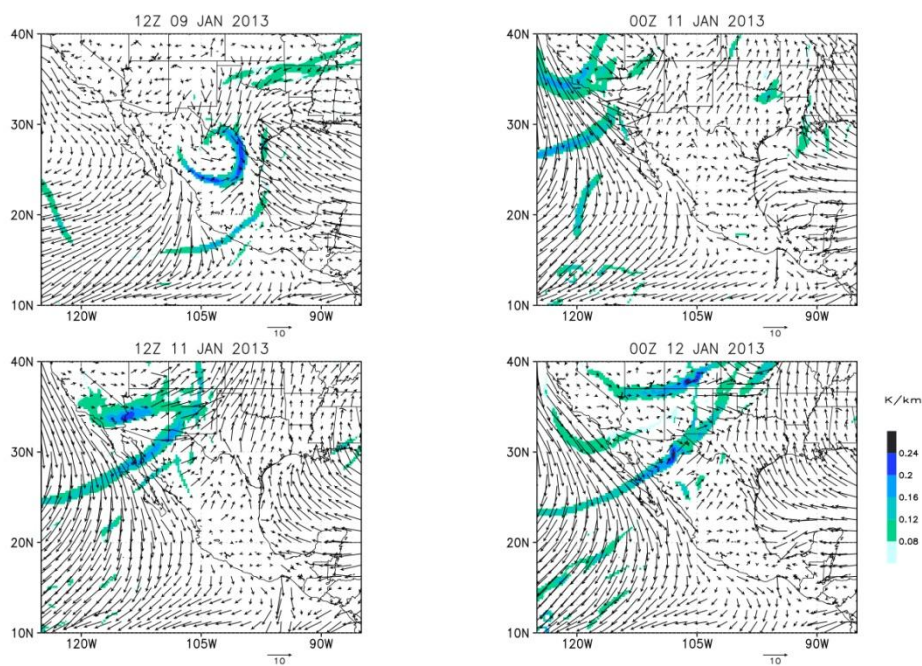


**Fig. S4** Composite pattern of gradient of equivalent potential temperature (K/km) and ERA5 surface wind as front position indicator for a) 12Z 09 January 2013, b) 00Z 11 January 2013, c) 12Z 11 January 2013 and d) 00Z 12 January 2013

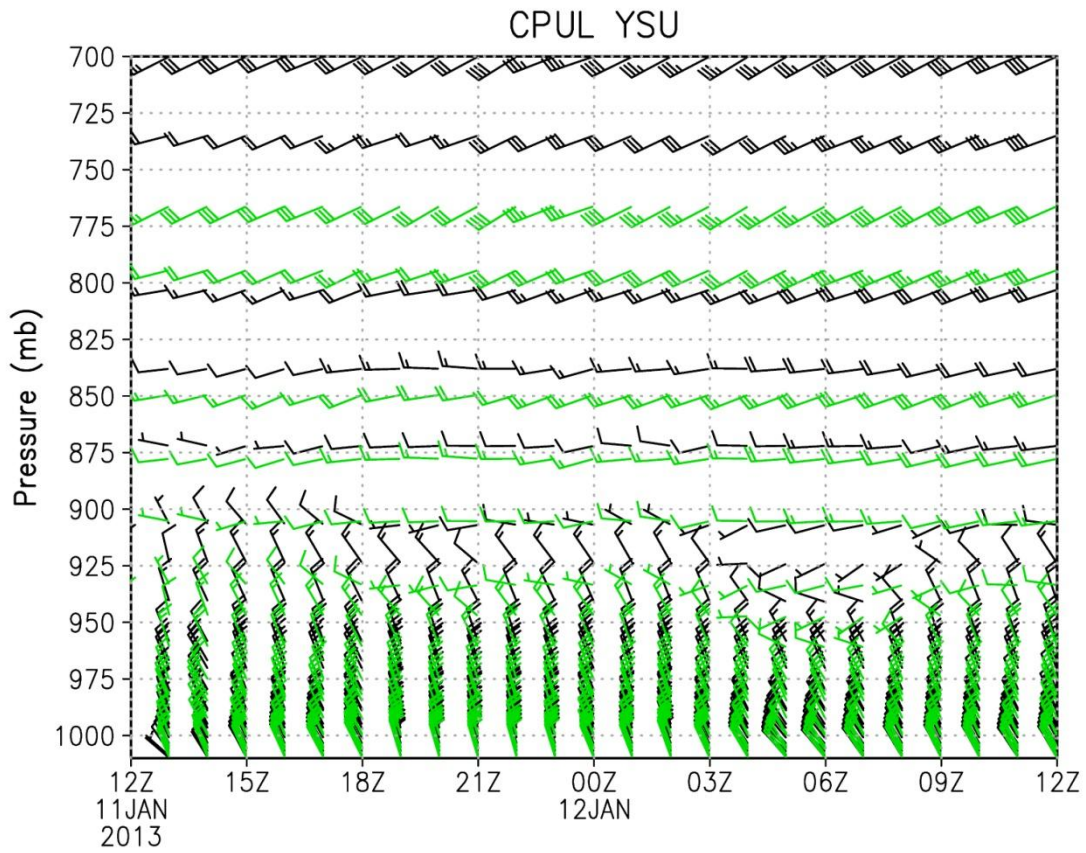


**Fig. S5** Meteogram of horizontal wind speed during a cold front passage over Baja California Peninsula at CPUL (23.45° N, 109.92°W). WRF wind (green barbs) and ERA5 wind vector (black barbs) in kt

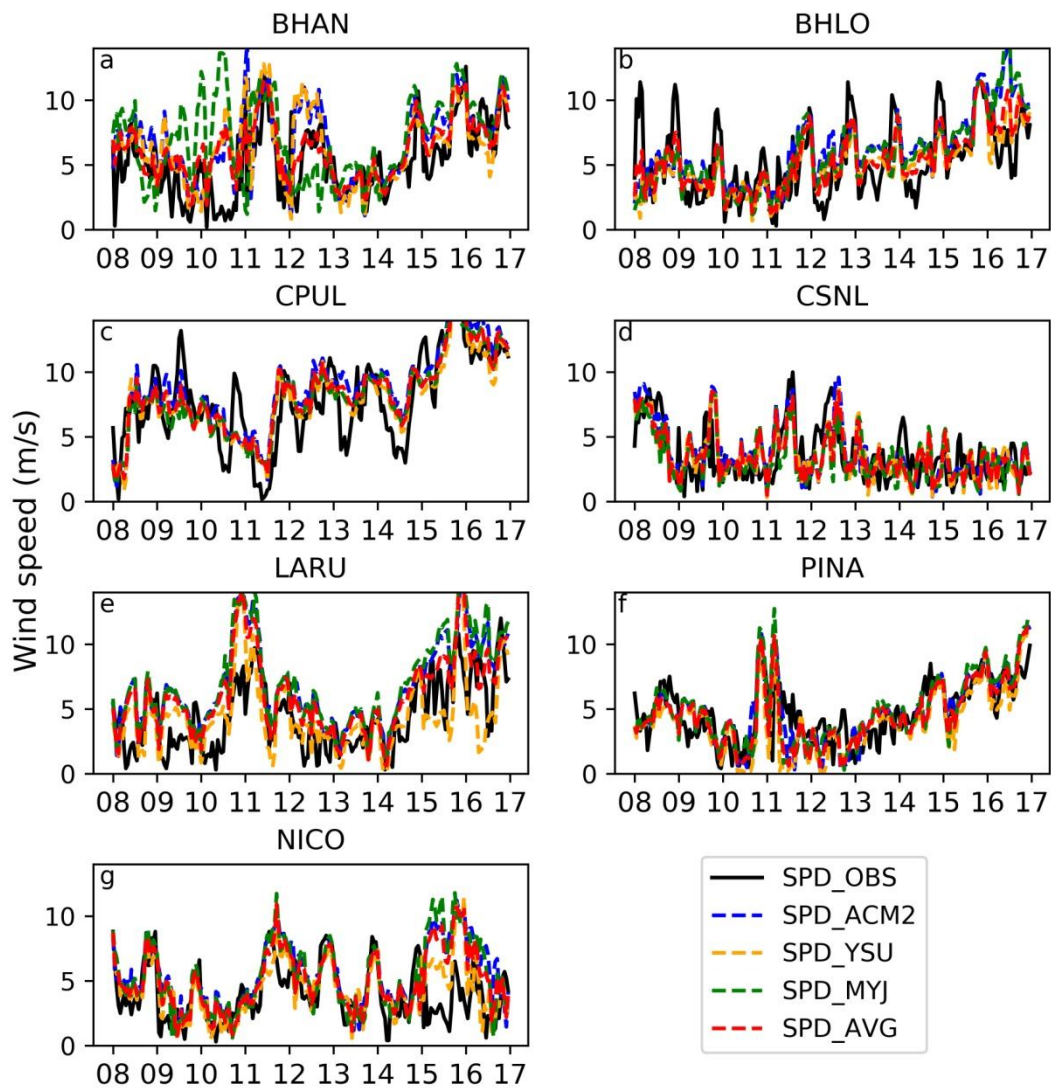


**Fig. S6** Observed and WRF simulated wind speed time series for 8-17 January 2013 at seven weather stations. Observed wind (full black line), YSU PBL scheme (dashed yellow line), MYJ PBL scheme (dashed green line), ACM2 PBL scheme (dashed blue line), PBL simulations average (dashed red line)

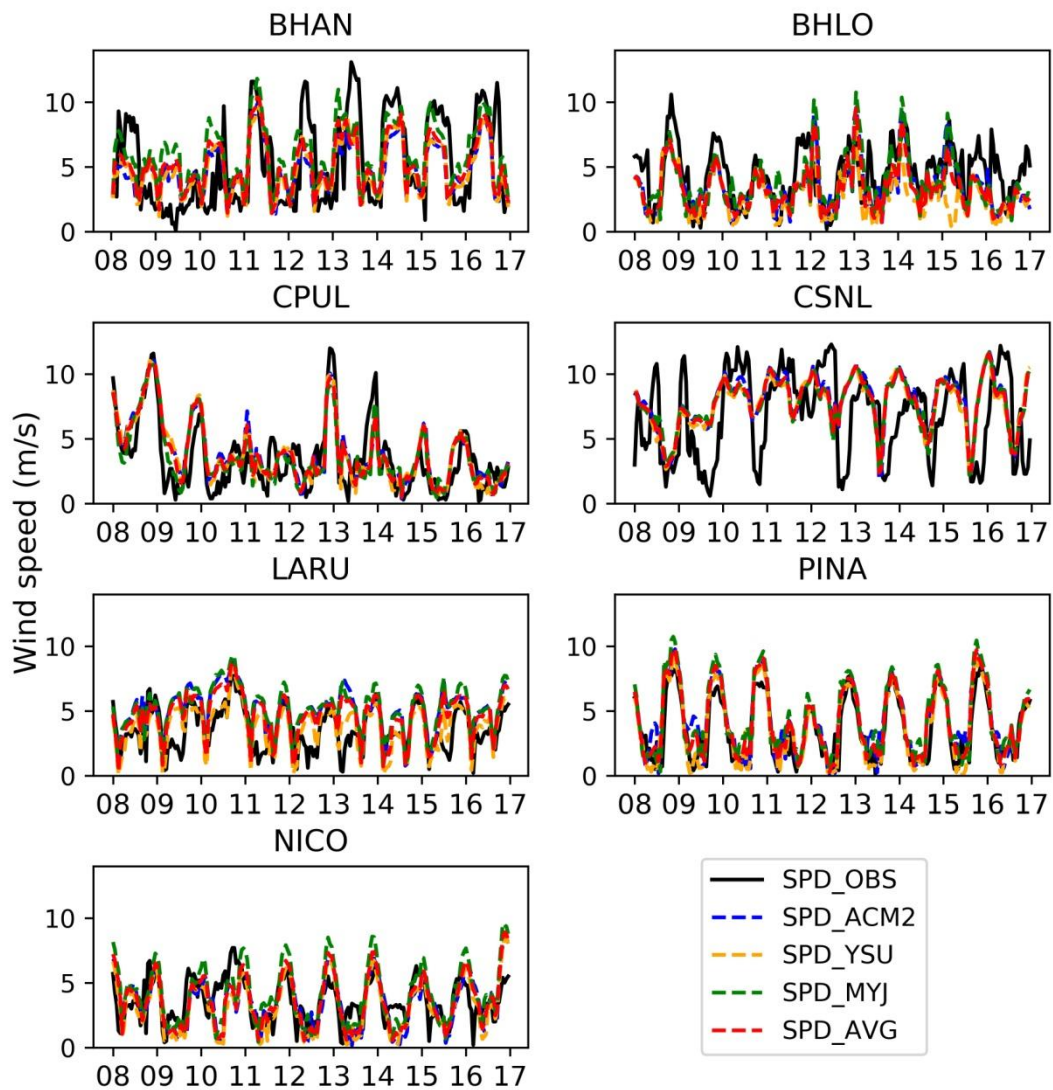


**Fig. S7** Observed and WRF simulated wind speed time series for 8-17 June 2013 at seven weather stations. Observed wind (full black line), YSU PBL scheme (dashed yellow line), MYJ PBL scheme (dashed green line), ACM2 PBL scheme (dashed blue line), PBL average (dash red line)



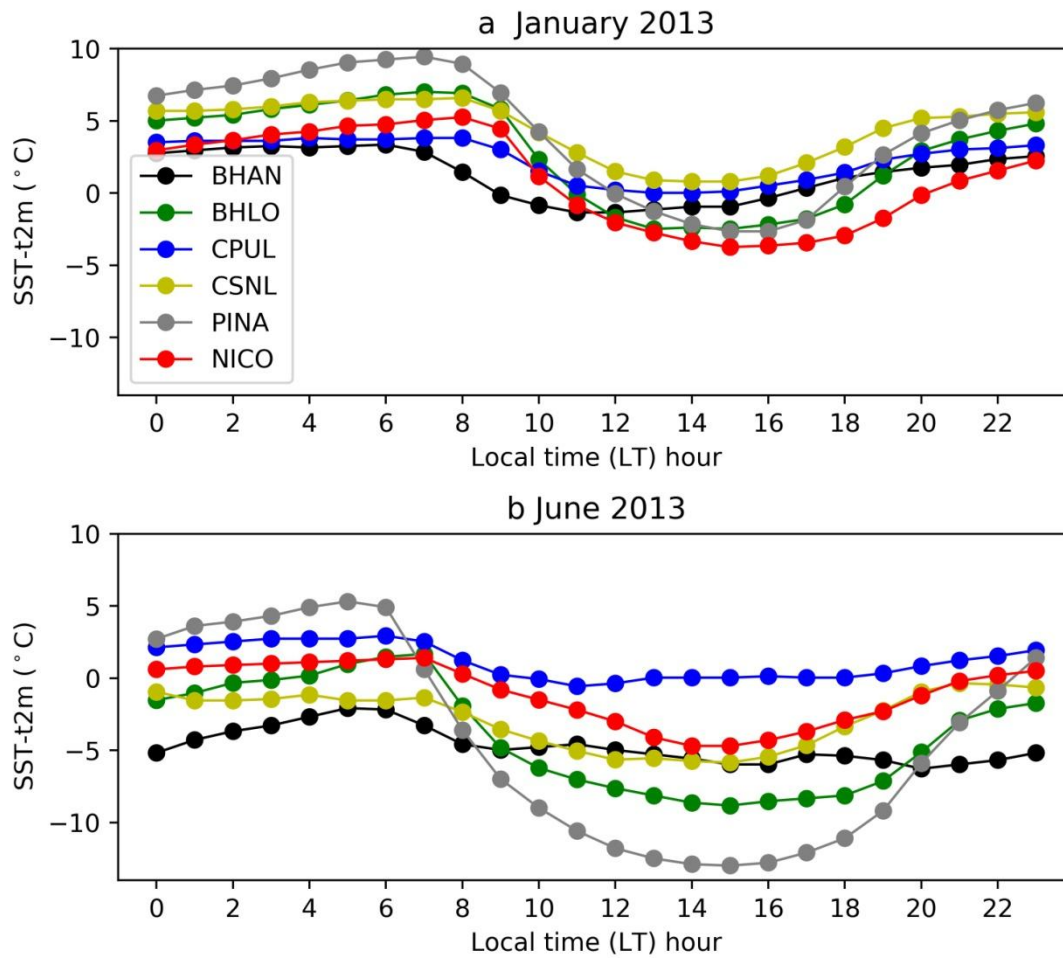


**Fig. S8** Diurnal variation of land-sea temperature difference for a) January 2013 and b) June 2013 for six weather stations in Baja California Peninsula. Multi-scale ultra-high resolution (MUR) SST of data point located ~40 km from the weather station location. The MUR SST dataset is provided by NASA and is freely available online at <http://mur.jpl.nasa.gov>

---

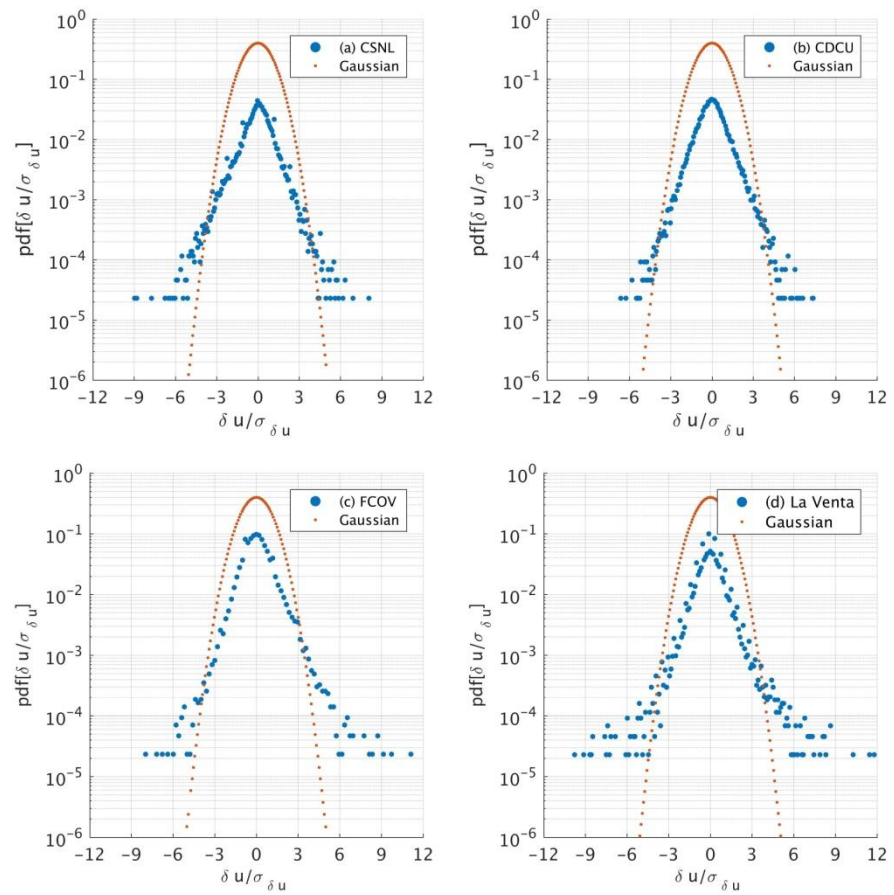
## Anexo 3. Material Suplementario del Capítulo 5

# Supplementary Materials: Wind-Ramp Predictability

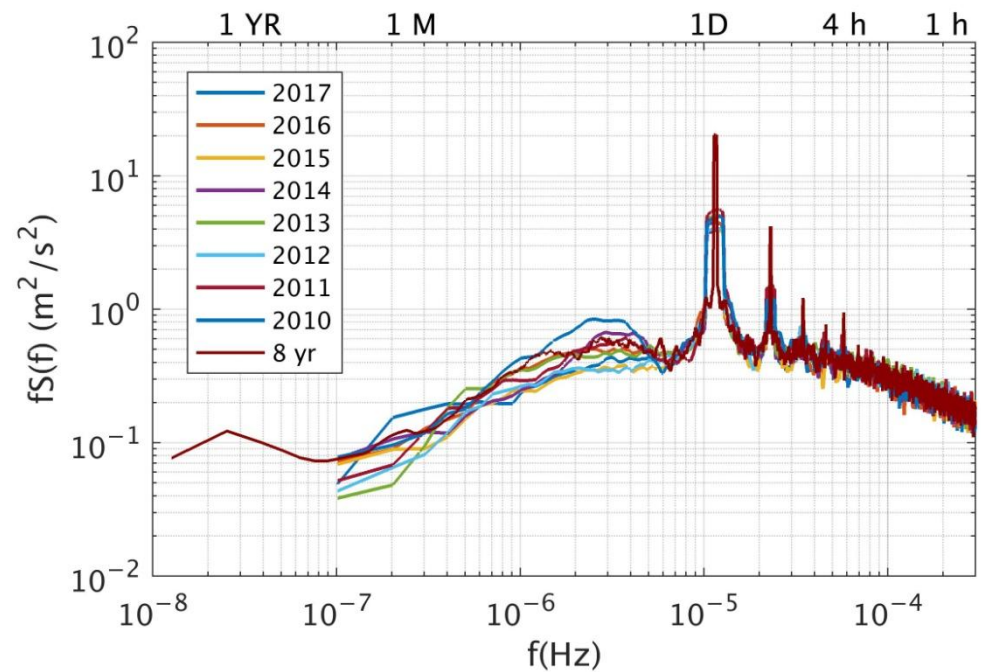
Karla Pereyra-Castro <sup>1</sup> and Ernesto Caetano <sup>2,\*</sup>

Table S1. List of abbreviations.

Abbreviation	Definition
NWP	Numerical Weather Prediction
WFIP	Wind Forecast Improvement Project
PBL	Planetary Boundary Layer
RAP	Rapid Refresh Model
NAM	North American Mesoscale Forecast System
FCOV	Francisco Villa
LVEN	La Venta
CSNL	Cabo San Lucas
CDCU	Ciudad Cuauhtémoc
NCEP	National Centers For Environmental Prediction
NOAA	National Oceanic and Atmospheric Administration
WRF	Weather Research and Forecasting
PDF	Probability density function
TP	True Positive
FN	False Negative
FP	False Positive
POD	Probability of Detection
FAR	False Alarm Rate
FBIAS	Frequency bias
CSI	Critical success ratio
QM	Quantile mapping
CDF	Cumulative distribution function
DJF	December-January-February
MAM	March-April-May
JJA	June-July-August
SON	September-October-November
MCS	Mesoscale Convective Systems
CFP	Cold front over Plateau
CFT	Cold front over Tamaulipas



**Figure S1.** Probability density functions (PDF) of wind ramps ( $\delta u$ ) from (a)CSNL, (b) CDCU, (c) FCOV and (d) LVEN. The wind increment and decrements values are normalized by the corresponding standard deviations.



**Figure S2.** Annual smoothed frequency-weighted spectra  $fS(f)$  of horizontal wind speed for Ciudad Cuauhtemoc (CDCU).



**Figure S3.** Cold fronts affecting Mexico in 24 May 2013. A cold front is seen as a curving line of clouds in the MODIS Corrected Reflectance imagery.



**Figure S4.** Cold fronts affecting Mexico in 1 March 2010. A cold front is seen as a comma clouds in the MODIS Corrected Reflectance imagery.

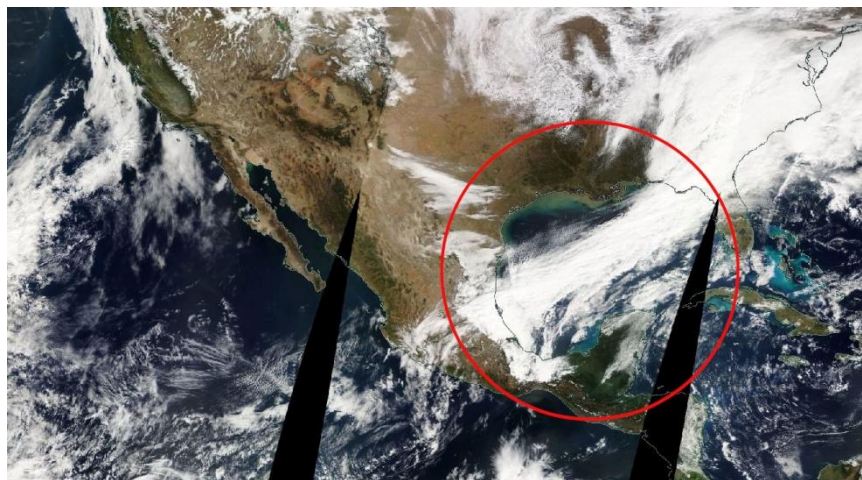


**Figure S5.** Cold fronts affecting Mexico in 11 February 2006. A cold front is seen as a comma clouds in the MODIS Corrected Reflectance imagery.



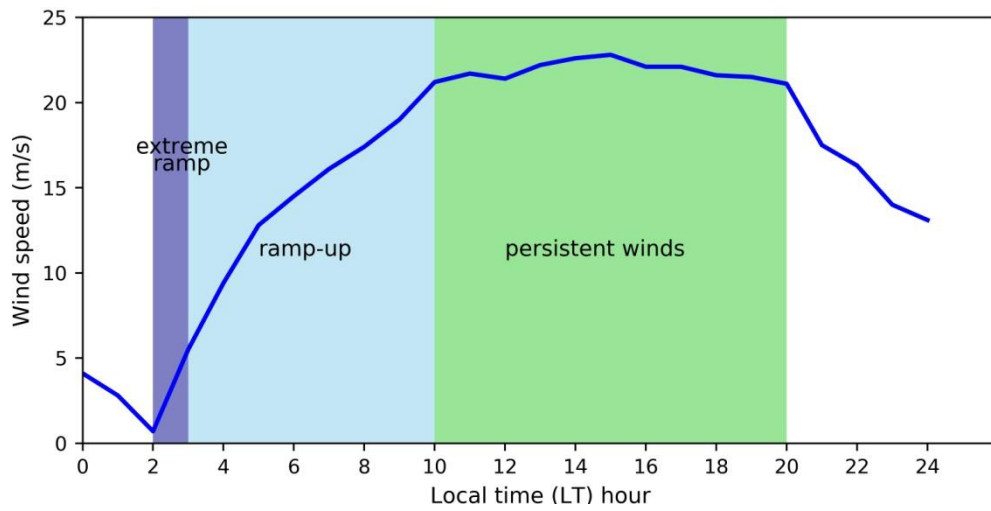


**Figure S6.** Example of extreme wind ramp event and the consecutive persistent winds.

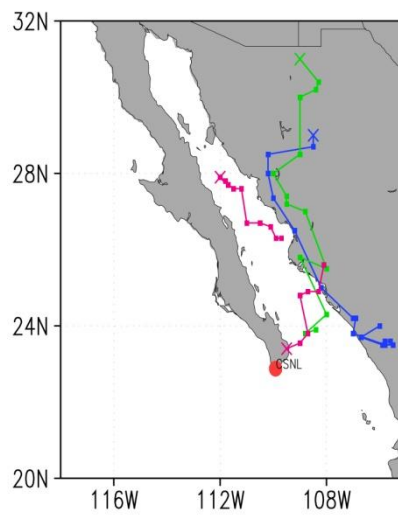


**Figure S7.** Storm trajectory at 01 August 2013 calculated with the maximum precipitation in core of the storm using a) CMORPH data (magenta line), b) 00:00 Z NAM initialization forecast (blue line) and c) 06:00 Z NAM initialization forecast (green line). The end of the track is indicated with a cross.

CDCU 24 JUL 2013

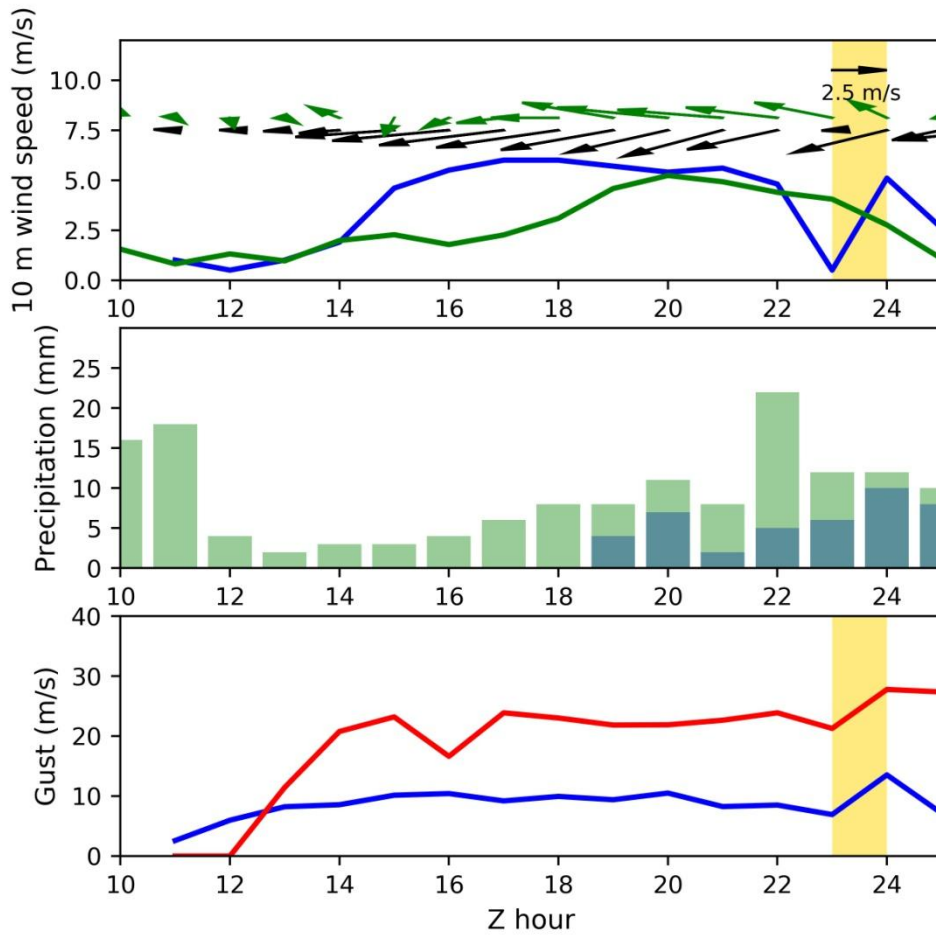


**Figure S8.** Meteogram at CDCU for a storm at 00:00 Z 25 July 2013. Wind ramp timing is shaded in yellow. CMORPH maximum precipitation in the center of the storm is in blue bars. Estimated wind gust in the storm is in red line and observed wind gust at CDCU is in blue. Forecasted wind speed, wind vector and precipitation are in green.

FCOV 03 JUL 2007

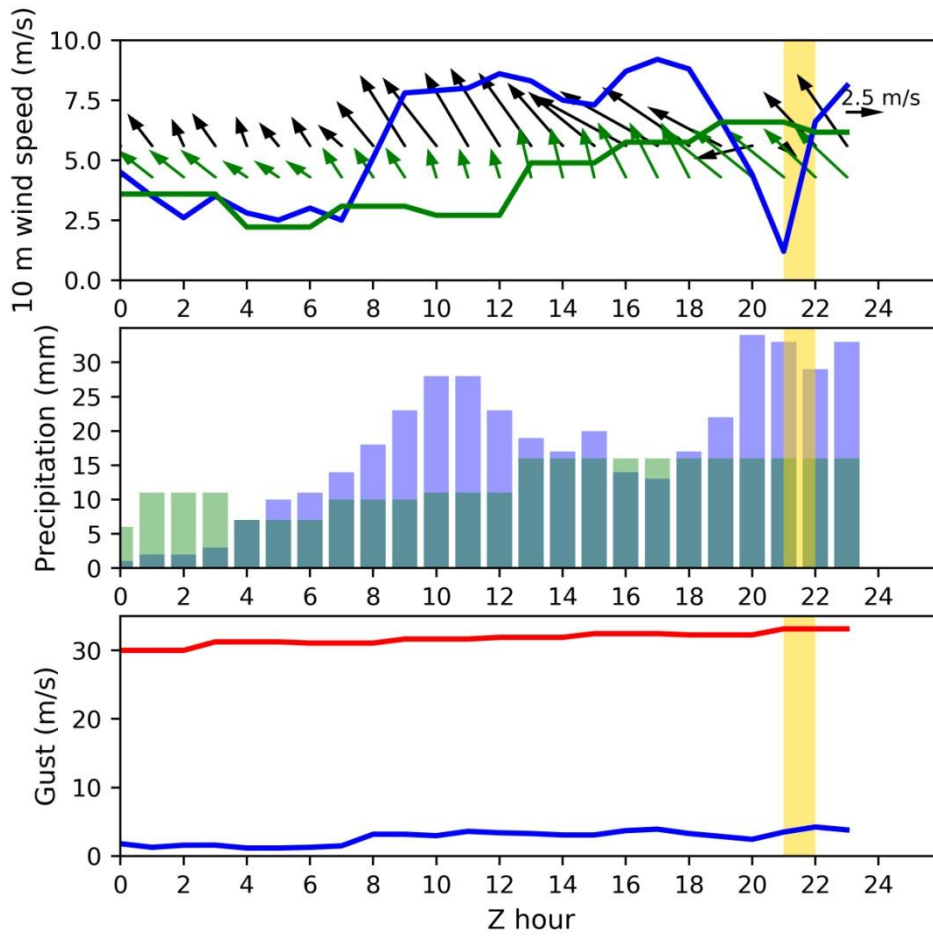


**Figure S9.** Meteogram at FCOV for a storm at 22:00 Z 03 July 2007. Wind ramp timing is shaded in yellow. CMORPH maximum precipitation in the center of the storm is in blue bars. Estimated wind gust in the storm is in red line and observed wind gust at FCOV is in blue. Forecasted wind speed, wind vector and precipitation are in green.

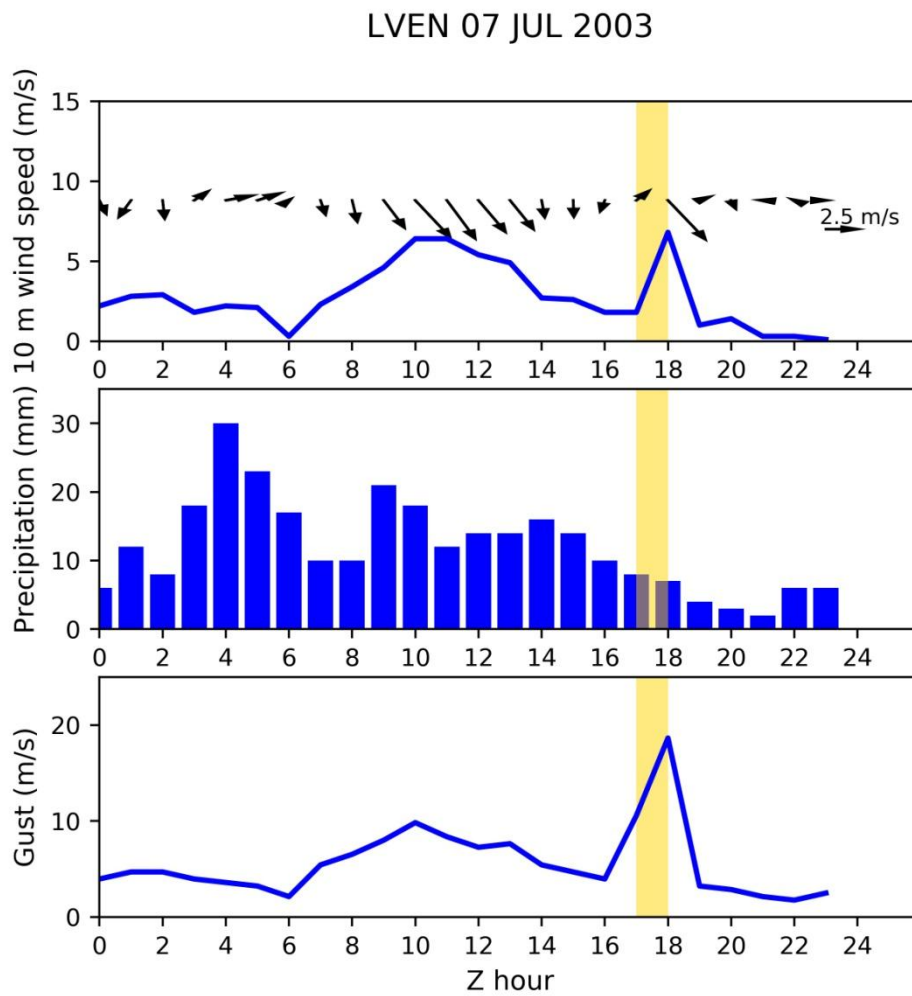


**Figure S10.** Meteoграм at LVEN for a storm at 18:00 Z 07 July 2003. Wind ramp timing is shaded in yellow. CMORPH maximum precipitation in the center of the storm is in blue bars. Observed wind gust at LVEN is in blue.

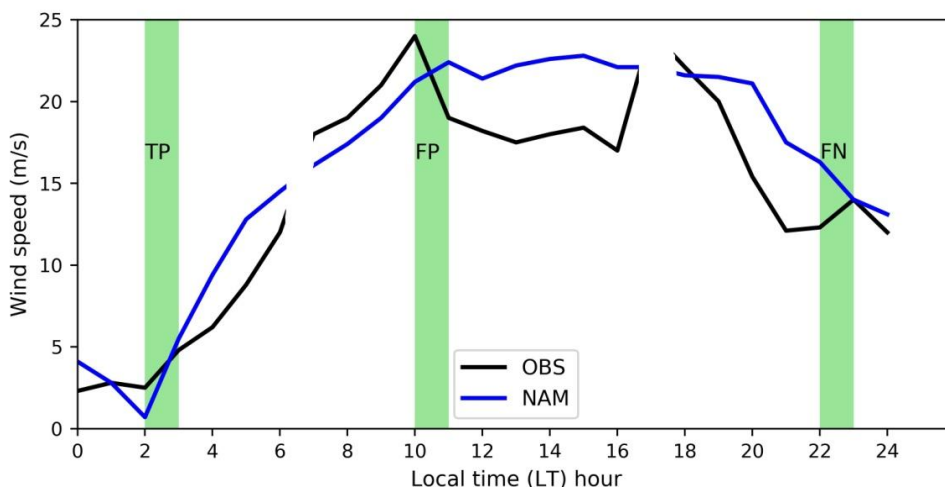


**Figure S11.** Example of wind ramps. Wind ramp observed and predicted (TP), wind ramp predicted by NAM but not observed (FP), and wind ramp observed but not predicted by NAM (FN). Events occurred in different days.



**Table S2.** Derived contingency table indexes wind NAM forecast (non-corrected), bias corrected and quantile mapping (QM) corrected for CDCU.

<b>Interval</b>		<b>POD</b>	<b>FAR</b>	<b>FBIAS</b>
(-1.5 to -0.5) m/s	NAM forecast	0.200	0.749	0.800
	Simple bias corrected	0.229	0.757	0.941
	QM corrected	0.258	0.764	1.090
(-2.5 to -1.5) m/s	NAM forecast	0.079	0.899	0.438
	Simple bias corrected	0.137	0.881	0.852
	QM corrected	0.101	0.894	1.280
(0.5 to 1.5) m/s	NAM forecast	0.205	0.756	0.840
	Simple bias corrected	0.239	0.758	0.985
	QM corrected	0.251	0.760	1.06
(1.5 to 2.5) m/s	NAM forecast	0.050	0.873	0.435
	Simple bias corrected	0.098	0.880	0.819
	QM corrected	0.117	0.881	0.990

**Table S3.** Derived contingency table indexes wind NAM forecast (non-corrected), bias corrected and quantile mapping (QM) corrected for CSNL.

<b>Interval</b>		<b>POD</b>	<b>FAR</b>	<b>BIAS</b>
(-1.5 to -0.5) m/s	NAM forecast	0.182	0.807	0.940
	Simple bias corrected	0.267	0.817	1.460
	QM corrected	0.203	0.807	1.050
(-2.5 to -1.5) m/s	NAM forecast	0.040	0.968	0.940
	Simple bias corrected	0.074	0.936	0.938
	QM corrected	0.059	0.939	1.280
(0.5 to 1.5) m/s	NAM forecast	0.167	0.729	0.615
	Simple bias corrected	0.214	0.743	0.835
	QM corrected	0.205	0.738	0.775
(1.5 to 2.5) m/s	NAM forecast	0.024	0.895	0.289
	Simple bias corrected	0.082	0.908	0.891
	QM corrected	0.071	0.904	0.754